AN EXPERIMENTAL STUDY OF FLOW-INDUCED CRYSTALLIZATION IN HIGH DENSITY POLYETHYLENE AND POLYPROPYLENE

By

MADHAV KAKANI

Bachelor of Technology

Indian Institute of Technology

Kharagpur, India

1992

Submitted to the Faculty of the
Graduate College of the
Oklahoma State University
in partial fulfillment of
the requirements for
the Degree of
MASTER OF SCIENCE
May, 1997

AN EXPERIMENTAL STUDY OF FLOW-INDUCED CRYSTALLIZATION IN HIGH DENSITY POLYETHYLENE AND POLYPROPYLENE

Thesis Approved:

Alan Tree

Thesis Advisor

Karen A. High

Mart S. High

Thomas C. Collins

Dean of the Graduate College

ACKNOWLEDGMENTS

I wish to express my sincere gratitude to my major advisor Dr. D. A. Tree. Dr. Tree has continuously helped me with his invaluable guidance, encouragement, and suggestions. I also would like to thank my wonderful committee members, Dr. M. S High and Dr. K. A. High for their patience and advice.

I would like to take this opportunity to express my sincere thanks to all my friends, specially Tsai, Lindsay, Sheena and Shankar for their help and sense of humor. I dedicate this work to my parents, who have given me love and support and have endured the pain of being away from me.

TABLE OF CONTENTS

Chapter Page

I. INTRODUCTION 1

II.BACKGROUND 4

Flow-Induced Crystallization 4
Crystallization Kinetics 18
Flow Birefringence 22

III. EXPERIMENTAL 25

Crystallization Rheometer 27
Data Logging System 29
Optics and Video Setup 29
Sample Preparation 31
Experimental Technique and Procedure 33
Calculation of the Average Strain Rate and the Average Strain 37
Calculation of the Actual Strain Rate and the Actual Strain 39
Calculation of the Density of the HDPE Samples 41
Calculation of the Percentage Crystallinity of the HDPE Samples 42
Analysis of the Experimental Data 43

IV. RESULTS AND DISCUSSION 44

Pixel Value and Torque Data 44
Optical Retardance 53
Correlation with the Avrami Equation 53
Discussion of the HDPE Data 60
Comparison with Previous Results 80

V. SUMMARY, CONCLUSIONS, AND RECOMMENDATIONS 83

Summary 83
Conclusions 84
Recommendations 85

REFERENCES 87

APPENDIXES 91

APPENDIX A: COMPUMOTOR CONTROL COMMANDS 92
APPENDIX B: DATA LOGGING SYSTEM 94
APPENDIX C: VIDEO IMAGE TECHNIQUE 99
APPENDIX D: EXPERIMENTAL DATA 110

LIST OF TABLES

Table Page

4.1 Avrami Parameters at 124.6 ^{0}C for HDPE 61

4.2 Avrami Exponents Reported in the Literature 64

4.3 Crystallization Rates at 124.6 ^{0}C for HDPE 69

4.4 Density and Percent Crystallinity at 124.6 ^{0}C for HDPE 70

B.1 Connector Pinout 95

LIST OF FIGURES

Figure Page

2.1 Intensity as a Function of Time at 133 ^{0}C, Extensional Rate = 0.032 sec $^{-1}$ 8

2.2 Generalized Light Intensity Behavior After Cessation of Flow 9

2.3 Intensity of Transmitted Light and Fraction of Transmitted Light vs. Time at Extension Rate = 0.03 sec^{-1}, Extensional Strain = 0.6 11

2.4 Intensity of Transmitted Light and Fraction of Transmitted Light vs. Time at Extension Rate = 0.24 sec^{-1}, Extensional Strain = 0.72 12

3.1 Overall View of the Experimental Setup 26

3.2 The Crystallization Rheometer 28

3.3 Optical and Video Setup [5] 30

3.4 Sample Preparation Die (a) Original, (b) Modification 32

3.5 Polymer Sample Covered with Aluminum Foil 35

3.6 Polymer Sample Under Elongational Flow 38

4.1 Pixel Value and Torque vs. Time for HDPE 45

4.2 Region II 47

4.3 Pixel Value vs. Time Under Quiescent Conditions for HDPE 49

4.4 Pixel Value vs. Time for Polystyrene Under Flow 51

4.5 Reduced Retardance vs. Time for HDPE 54

4.6 Correlation with the Avrami Equation for HDPE 56

4.7 Pixel Value vs. Time for Polypropylene Under Flow 58

4.8 Pixel Value vs. Time Under Quiescent Conditions at for PP 59

4.9 Avrami Coefficient (k) vs. Avrami Exponent (n) for HDPE at 124.6 ^{0}C 65

4.10 Reduced Retardance vs. Time for HDPE at 124.6 ^{0}C 67

4.11 Volume Percent Crystallinity vs. Actual Strain Rate for HDPE at 124.6 ^{0}C 71

4.12 Avrami Coefficient vs. Actual Extension Rate for HDPE at 124.6 ^{0}C 72

4.13 Avrami Exponent vs. Actual Extension Rate for HDPE at 124.6 ^{0}C 73

4.14 Pixel Value vs. Time for HDPE at Four Different Locations in the Sample 75

4.15 Reduced Retardance vs. Time for HDPE at Four Different Locations in the Sample77

4.16 Oil Bath Temperature Profile as a Function of Time 79

B.1 Interconnection Diagram of the Analog Interface Card and the Mv/Amplifier/Multiplexer [43] 97

C.1 Camera Calibration Curve 102

D.1(a) Pixel Value vs. Time for HDPE at Extension Rate = 0.76 sec^{-1}, Extensional Strain = 3.8 111

D.1(b) Reduced Retardance vs. Time for HDPE at Extension Rate = 0.76 sec^{-1}, Extensional Strain = 3.8 112

D.1(c) Correlation of Experimental Data with Avrami Equation for HDPE at Extension Rate = 0.76 sec^{-1}, Extensional Strain = 3.8 113

D.2(a) Pixel Value vs. Time for HDPE at Extension Rate = 0.72 sec^{-1}, Extensional Strain = 3.6 114

D.2(b) Reduced Retardance vs. Time for HDPE at Extension Rate = 0.72 sec^{-1}, Extensional Strain = 3.6 115

D.2(c) Correlation of Experimental Data with Avrami Equation for HDPE at Extension Rate = 0.72 sec^{-1}, Extensional Strain = 3.6 116

D.3(a) Pixel Value vs. Time for HDPE at Extension Rate = 0.29 sec^{-1}, Extensional Strain = 2.9 117

D.3(b) Reduced Retardance vs. Time for HDPE at Extension Rate = 0.29 sec^{-1}, Extensional Strain = 2.9 118

D.3(c) Correlation of Experimental Data with Avrami Equation for HDPE at Extension Rate = 0.29 sec^{-1}, Extensional Strain = 2.9 119

D.4(a) Pixel Value vs. Time for HDPE at Extension Rate = 1.7 sec^{-1}, Extensional Strain = 3.4 120

D.4(b) Reduced Retardance vs. Time for HDPE at Extension Rate = 1.7 sec^{-1}, Extensional Strain = 3.4 121

D.4(c) Correlation of Experimental Data with Avrami Equation for HDPE at Extension Rate = 1.7 sec^{-1}, Extensional Strain = 3.4 122

D.5(a) Pixel Value vs. Time for HDPE at Extension Rate = 1.68 sec^{-1}, Extensional Strain = 3.35 123

D.5(b) Reduced Retardance vs. Time for HDPE at Extension Rate = 1.68 sec^{-1}, Extensional Strain = 3.35 124

D.5(c) Correlation of Experimental Data with Avrami Equation for HDPE at Extension Rate = 1.68 sec^{-1}, Extensional Strain = 3.35 125

D.6(a) Pixel Value vs. Time for HDPE at Extension Rate = 0.32 sec^{-1}, Extensional Strain = 3.2 126

D.6(b) Reduced Retardance vs. Time for HDPE at Extension Rate = 0.32 sec^{-1}, Extensional Strain = 3.2 127

D.6(c) Correlation of Experimental Data with Avrami Equation for HDPE at Extension Rate = 0.32 sec^{-1}, Extensional Strain = 3.2 128

D.7(a) Pixel Value vs. Time for HDPE at Extension Rate = 4.0 sec^{-1}, Extensional Strain = 4.0 129

D.7(b) Reduced Retardance vs. Time for HDPE at Extension Rate = 4.0 sec^{-1}, Extensional Strain = 4.0 130

D.7(c) Correlation of Experimental Data with Avrami Equation for HDPE at Extension Rate = 4.0 sec^{-1}, Extensional Strain = 4.0 131

D.8(a) Pixel Value vs. Time for HDPE at Extension Rate = 3.3 sec^{-1}, Extensional Strain = 3.3 132

D.8(b) Reduced Retardance vs. Time for HDPE at Extension Rate = 3.3 sec^{-1}, Extensional Strain = 3.3 133

D.8(c) Correlation of Experimental Data with Avrami Equation for HDPE at Extension Rate = 3.3 sec^{-1}, Extensional Strain = 3.3 134

D.9(a) Pixel Value vs. Time for HDPE at Extension Rate = 0.16 sec^{-1}, Extensional Strain = 3.2 135

D.9(b) Reduced Retardance vs. Time for HDPE at Extension Rate = 0.16 sec^{-1}, Extensional Strain = 3.2 136

D.9(c) Correlation of Experimental Data with Avrami Equation for HDPE at Extension Rate = 0.16 sec^{-1}, Extensional Strain = 3.2 137

D.10(a) Pixel Value vs. Time for HDPE at Extension Rate = 0.21 sec^{-1}, Extensional Strain = 4.06 138

D.10(b) Reduced Retardance vs. Time for HDPE at Extension Rate = 0.21 sec^{-1}, Extensional Strain = 4.06 139

D.10(c) Correlation of Experimental Data with Avrami Equation for HDPE at Extension Rate = 0.21 sec^{-1}, Extensional Strain = 4.06 140

D.11(a) Pixel Value vs. Time for HDPE at Extension Rate = 0.16 sec^{-1}, Extensional Strain = 3.06 141

D.11(b) Reduced Retardance vs. Time for HDPE at Extension Rate = 0.16 sec^{-1}, Extensional Strain = 3.06 142

D.11(c) Correlation of Experimental Data with Avrami Equation for HDPE at Extension Rate = 0.16 sec^{-1}, Extensional Strain = 3.06 143

D.12(a) Pixel Value vs. Time for HDPE at Extension Rate = 3.8 sec^{-1}, Extensional Strain = 3.8 144

D.12(b) Reduced Retardance vs. Time for HDPE at Extension Rate = 3.8 sec^{-1}, Extensional Strain = 3.8 145

D.12(c) Correlation of Experimental Data with Avrami Equation for HDPE at Extension Rate = 3.8 sec^{-1}, Extensional Strain = 3.8 146

D.13(a) Pixel Value vs. Time for HDPE at Extension Rate = 3.36 sec^{-1}, Extensional Strain = 2.47 147

D.13(b) Reduced Retardance vs. Time for HDPE at Extension Rate = 3.36 sec^{-1}, Extensional Strain = 2.47 148

D.13(c) Correlation of Experimental Data with Avrami Equation for HDPE at Extension Rate = 3.36 sec^{-1}, Extensional Strain = 2.47 149

D.14(a) Pixel Value vs. Time for HDPE at Extension Rate = 3.38 sec^{-1}, Extensional Strain = 2.25 150

D.14(b) Reduced Retardance vs. Time for HDPE at Extension Rate = 3.38 sec^{-1}, Extensional Strain = 2.25 151

D.14(c) Correlation of Experimental Data with Avrami Equation for HDPE at Extension Rate = 3.38 sec^{-1}, Extensional Strain = 2.25 152

D.15(a) Pixel Value vs. Time for HDPE at Extension Rate = 4.51 sec^{-1}, Extensional Strain = 3.61 153

D.15(b) Reduced Retardance vs. Time for HDPE at Extension Rate = 4.51 sec^{-1}, Extensional Strain = 3.61 154

D.15(c) Correlation of Experimental Data with Avrami Equation for HDPE at Extension Rate = 4.51 sec^{-1}, Extensional Strain = 3.61 155

D.16(a) Pixel Value vs. Time for HDPE at Extension Rate = 5.97 sec^{-1}, Extensional Strain = 3.0 156

D.16(b) Reduced Retardance vs. Time for HDPE at Extension Rate = 5.97 sec^{-1}, Extensional Strain = 3.0 157

D.16(c) Correlation of Experimental Data with Avrami Equation for HDPE at Extension Rate = 5.97 sec^{-1}, Extensional Strain = 3.0 158

D.17(a) Pixel Value vs. Time for HDPE at Extension Rate = 3.95 sec^{-1}, Extensional Strain = 2.37 159

D.17(b) Reduced Retardance vs. Time for HDPE at Extension Rate = 3.95 sec^{-1}, Extensional Strain = 2.37 160

D.17(c) Correlation of Experimental Data with Avrami Equation for HDPE at Extension Rate = 3.95 sec^{-1}, Extensional Strain = 2.37 161

D.18(a) Pixel Value vs. Time for HDPE at Extension Rate = 6.06 sec^{-1}, Extensional Strain = 3.03 162

D.18(b) Reduced Retardance vs. Time for HDPE at Extension Rate = 6.06 sec^{-1}, Extensional Strain = 3.03 163

D.18(c) Correlation of Experimental Data with Avrami Equation for HDPE at Extension Rate = 6.06 sec^{-1}, Extensional Strain = 3.03 164

D.19(a) Pixel Value vs. Time for HDPE at Extension Rate = 4.06 sec^{-1}, Extensional Strain = 2.44 165

D.19(b) Reduced Retardance vs. Time for HDPE at Extension Rate = 4.06 sec^{-1}, Extensional Strain = 2.44 166

D.19(c) Correlation of Experimental Data with Avrami Equation for HDPE at Extension Rate = 4.06 sec^{-1}, Extensional Strain = 2.44 167

D.20(a) Pixel Value vs. Time for HDPE at Extension Rate = 6.13 sec^{-1}, Extensional Strain = 3.07 168

D.20(b) Reduced Retardance vs. Time for HDPE at Extension Rate = 6.13 sec^{-1}, Extensional Strain = 3.07 169

D.20(c) Correlation of Experimental Data with Avrami Equation for HDPE at Extension Rate = 6.13 sec^{-1}, Extensional Strain = 3.07 170

NOMENCLATURE

A	Cross sectional area of the sample
b	Shear flow parameter
D	Diameter of the roller
HDPE	High density polyethylene
I	Intensity of transmitted light
I_0	Intensity of incident light beam
k	Avrami coefficient
L	Sample thickness
L_i	Initial length of sample
N	Number of non-activated crystallization sites
n	Avrami exponent
PP	Polypropylene
PS	Polystyrene
R	Relative phase difference
r	Radius of roller
T_r	Torque acting on sample
t	Time
V	Rotational velocity of the roller

$\phi(t)$	Volume fraction of crystal at a given time
ϕ_∞	Volume fraction of crystal obtained at infinite time
$\xi(t)$	Relative Crystalline volume fraction
λ	Wave length of light
η_{p1}	First principal refractive index
η_{p2}	Second principal refractive index
χ_M	Principal Axes orientation of the stress tensor
χ_o	Principal Axex orientation of the refractive index tensor
χ	Isoclinic angle
Δ	Birefringence
α	Polarizer orientation angle
ε	Average elongational strain
ε_a	Actual elongational strain
$\dot{\varepsilon}$	Average elongational strain rate
$\dot{\varepsilon}_a$	Actual elongational strain rate
δ_d	Retardation of the amorphous portion of the sample
δ_c	Retardation of crystalline regions of the sample
δ_{tot}	Total test section retardance

CHAPTER I

INTRODUCTION

One of the many important goals of ongoing research in materials science and engineering is to produce high strength, low cost materials. The advent of polymeric materials as substitutes for traditional materials such as metals and glass was a revolution in materials science. Today, polymeric materials continue to replace conventional materials due to a number of useful properties including toughness, flexibility, resistance to corrosion, and low cost. Further improvement in mechanical properties can be achieved by at least four approaches: synthesis of new molecules, blending, manipulation of the molecular structure of existing polymers, and by carefully controlling the microstructure [1].

Semi-crystalline polymers tend to form low-energy helical (LEH) or folded chain crystal (FCC) morphologies. The relatively poor mechanical strength of polymeric materials as compared to materials like steel and drawn silica fibers, can be traced to the LEH and FCC morphologies. The LEH and FCC morphologies consist of highly imperfect structures that contain crystalline and amorphous regions, thus making the flexible-chain polymeric materials mechanically weak [2]. A dramatic increase in mechanical strength can be obtained by orienting the polymer molecules to obtain an extended chain morphology. The polymer molecules can be oriented by applying a stress field, and if crystallization occurs under these conditions, the molecules may form extended chain crystals. The process of inducing crystallinity in a polymer is known as flow-induced crystallization when the stresses are generated by a flow field. As an example, commonly processed polyethylene is a relatively weak material. However, drawn polyethylene shows a one to three order of magnitude increase in tensile modulus, and breaking strength [3, 4]. The drastic increase in mechanical properties is due to the formation of extended chain crystals [3, 4]. Therefore, by carefully processing an inexpensive semi-crystalline polymer such as polyethylene, high strength materials can be produced.

In order to fully exploit the potential of flow-induced crystallization in polymer processing, quantitative data on crystallization kinetics is required. Conventional methods of studying flow-induced crystallization such as gel and melt spinning, and converging flow in polymer dies, suffer from drawbacks such as large temperature gradients, large non-uniform extension rates, flow blockage at the onset of crystallization, and difficulties in crystallization kinetics measurements due to mass transfer of the solvent [4].

The principal aim of this thesis was (1) to generate the much needed kinetic data, and (2) to understand the effect of processing variables such as strain rate, strain, and temperature on the crystallization rate in semi-crystalline polymers. To realize this goal, an efficient experimental technique (described in Chapter III), which overcame most of the previously encountered experimental problems, was used to obtain the kinetic data at different processing conditions. To understand the effect of flow-induced crystallization on polymers with different properties, three polymeric materials namely, high density polyethylene (semi-crystalline), polypropylene (semi-crystalline), and atactic polystyrene (amorphous) were used in the experiments. The experiments with atactic polystyrene were performed to compare and contrast the results obtained for non-crystallizing (PS) and crystallizing materials (HDPE, PP). The experimental data obtained was compared to the Avrami theory. The crystallization kinetics data presented in this thesis are expected to benefit subsequent model development, and optimization of polymer processing operations.

The remainder of this thesis is divided into four chapters. Chapter II presents the relevant background and theoretical development for flow-induced crystallization Chapter III describes the experimental apparatus and the experimental techniques in detail. Chapter IV presents the data and a discussion of the results. Chapter V summarizes the results, presents the conclusions, and gives the recommendations.

CHAPTER II

BACKGROUND

In order to understand the flow-induced crystallization phenomenon in semi-crystalline polymers, knowledge of fundamental concepts such as extensional flow, polymer crystallization kinetics, flow birefringence, and flow-induced crystallization theory is required. A brief description of these concepts is presented in this chapter. A more detailed analysis has been given by Tree [4], Ma [3], and Siddiquee [5]. Only the latest and most relevant developments in flow-induced crystallization and crystallization kinetics are reviewed in detail in this chapter.

Flow-Induced Crystallization

Molecular chain orientation in flexible-chain polymers can be induced either by elongational flow or by shear flow. Significant work has been done to produce extension and shearing flow-fields in order to induce orientation, and crystallization in flexible-chain polymers. Van der Vegt and Smit first reported the flow-induced crystallization phenomenon in pure polymer melts in 1967 [6]. They used a capillary rheometer to measure the viscosities of polymer melts (polypropylene, polyethylene, and polybutadiene). They observed a dramatic increase in the pressure and viscosity when a polypropylene melt was extruded at a temperature just above the melting point. The flow eventually stopped because of the very high pressure drops across the rheometer. X-ray diffraction measurements of the material revealed that the polymer molecules were highly oriented in the direction of flow. Van der Vegt and Smit suggested that the molecules had been oriented in the extensional flow field near the entrance to the capillary, and subsequently crystallized inside the capillary.

Siegloff and O'Leary [7, 8] reported similar results in 1968. For polypropylene extruded through a capillary at temperatures below 195 ^{0}C, X-ray diffraction studies showed orientation of the molecules that was greater at the center than near the walls. Southern and Porter [9, 10] also reported the formation of extended chain crystals of high density polyethylene at the entrance of a capillary die.

In all of the studies done by Van der Vegt and Smit, Siegloff and O'Leary, Southern and Porter, there was no provision for in-situ observation of flow-induced crystallization. Also, die blockage due to polymer crystallization was a problem in most of the experiments involving a capillary die.

Tsebrenko and Vinogradov [11} used a capillary die to study the phenomenon of flow-induced morphology in incompatible (i.e., two phase) polymer blends. Tsebrenko and Vinogradov found that the droplets of the suspended or discreet phase were drawn out into fibrils due to the extensional flow field. Tree and McHugh [4, 12] extended the work of Tsebrenko and Vinogradov by studying the extrusion of two phase polymer blends consisting of a linear low density polyethylene (LLDPE) as the carrier phase, and small amounts of a crystallizable polymer as the suspended phase. Tree and McHugh made the first attempt at in-situ observation by monitoring rheological quantities. Although extended chain crystallinity was induced in the fibrils of the minor phase, rheological measurements were found to be insufficient for detecting crystallization.

The first successful in-situ observation of flow-induced crystallization was made by Sakellarides and McHugh [13]. Sakellarides and McHugh constructed a slit flow die with optical windows. The die was used to extrude two phase polymer blends, and the optical windows enabled in-situ observation. Sakellarides and McHugh demonstrated that in shearing flow, polymer droplets deform by emitting "tails" from the up stream and down stream ends, and that flow-induced crystallization occurred inside the tails.

McHugh, Guy, and Tree [14] reported the first quantitative flow-induced crystallization kinetics data in extensional flow. McHugh et al. studied flow-induced orientation, and crystallization of a high-density polyethylene (HDPE) melt undergoing a planar extensional flow in a four-roll mill. The four-roll mill overcame the die blockage problems associated with capillary dies. The HDPE was suspended as a cylindrical droplet at the flow stagnation point of a linear low density polyethylene (LLDPE) carrier phase. Extensional rates were of the order 0.03 sec^{-1}. Video imaging was used to monitor deformation and crystallization of the HDPE droplet phase in conjunction with measurement of the birefringence and dichroism to quantify the crystallization kinetics.

McHugh et al. [14] found that the flow-induced crystallization rate was higher than the quiescent crystallization rate by several orders of magnitude. Measurements of the initial crystallization rate after flow cessation at 131.5 ^{0}C and 133.2 ^{0}C showed a dependence on initial amorphous phase orientation and the total Hencky strain achieved during flow. However, the dependence on temperature was less drastic than expected for a nucleation-controlled growth mechanism. Also, the melting point elevation model could not account for the crystal growth phenomenon either qualitatively or quantitatively, and suggested the need for alternative explanations for the strong dependence of the crystallization rate on initial orientation [4].

Guy [15] also worked with the 4-Roll Mill and the video image technique to study flow-induced crystallization in a two-phase system of HDPE suspended in a LLDPE carrier phase. Hot stage and dichroism studies revealed that crystallization occurred in the suspended phase at temperatures above which quiescent crystallization would occur. Figure 2.1 shows a typical experimental data set presented by Guy. The experiment was done at 133 ^{0}C, and an extension rate of 0.03 sec^{-1} was applied for 90 seconds. In Figure 2.1, t = 0 corresponds to the onset of flow. Figure 2.1 indicates that the intensity of the transmitted light increased during flow, and decreased rapidly after the cessation of flow. Guy attributed the rapid decrease in the intensity after cessation of flow to stress relaxation in the carrier and droplet phases. At t = 120 seconds, the intensity began to increase due to flow-induced crystallization. A maximum was reached at t = 900 seconds, after which the intensity decayed. Guy also generalized the intensity of transmitted light phenomena for a typical flow-cessation experiment as shown in Figure 2.2. At time equal to zero in Figure 2.2, the crystalline retardation was assumed to be zero. Guy found that the initial crystal growth rate showed a dependence on both the macroscopic orientation

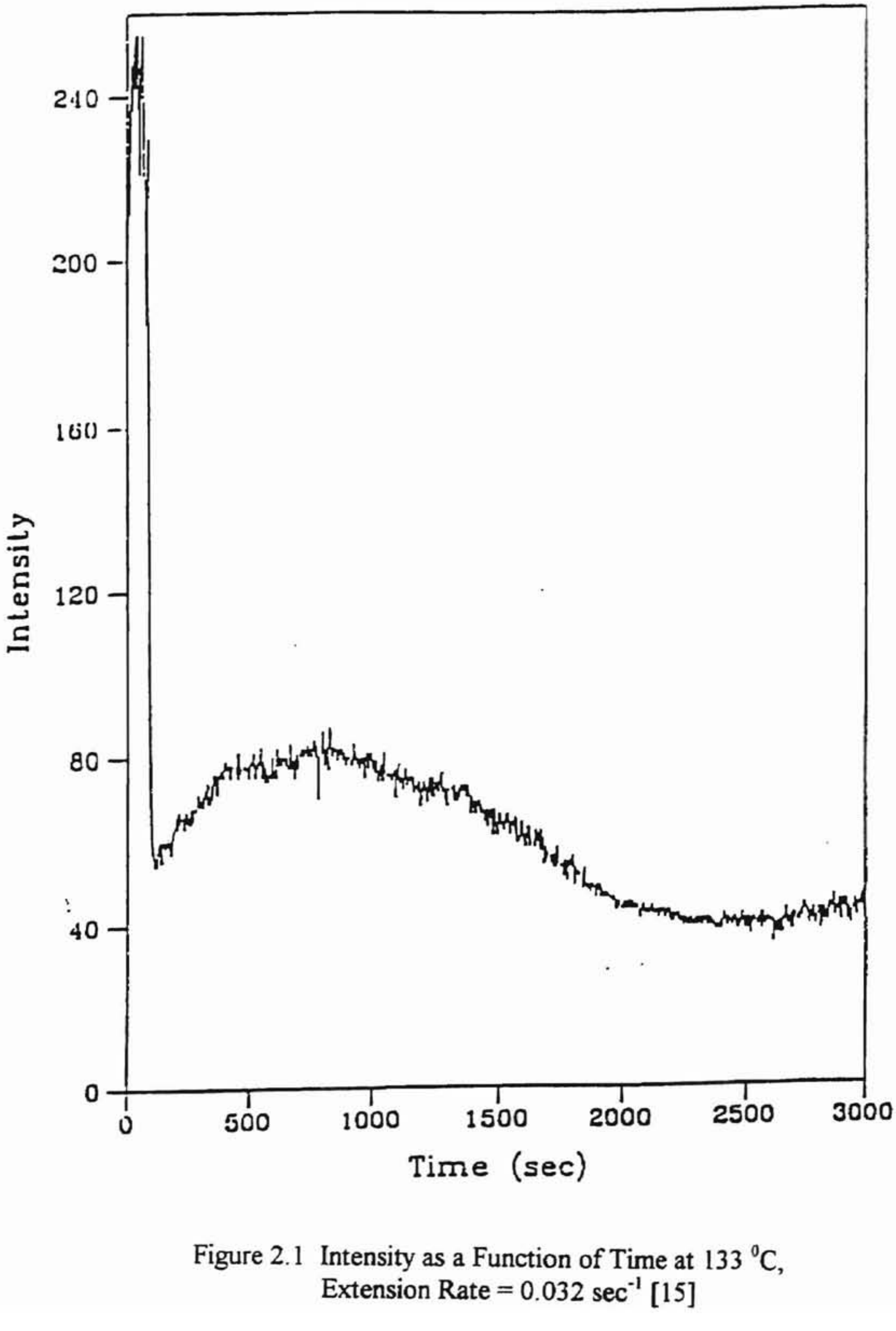

Figure 2.1 Intensity as a Function of Time at 133 ^{0}C,
Extension Rate = 0.032 sec^{-1} [15]

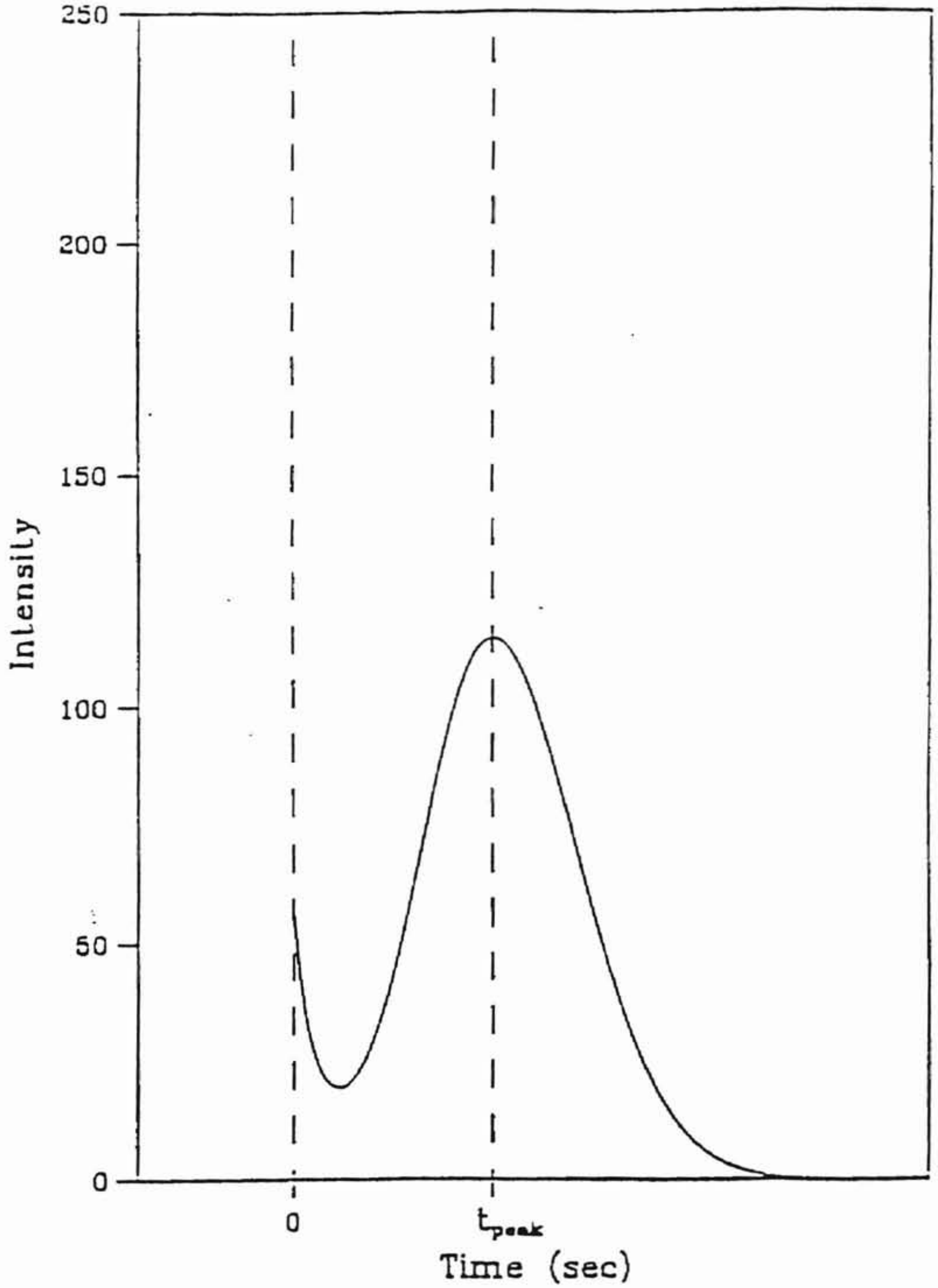

Figure 2.2 Generalized Light Intensity Behavior After Cessation of Flow [15]

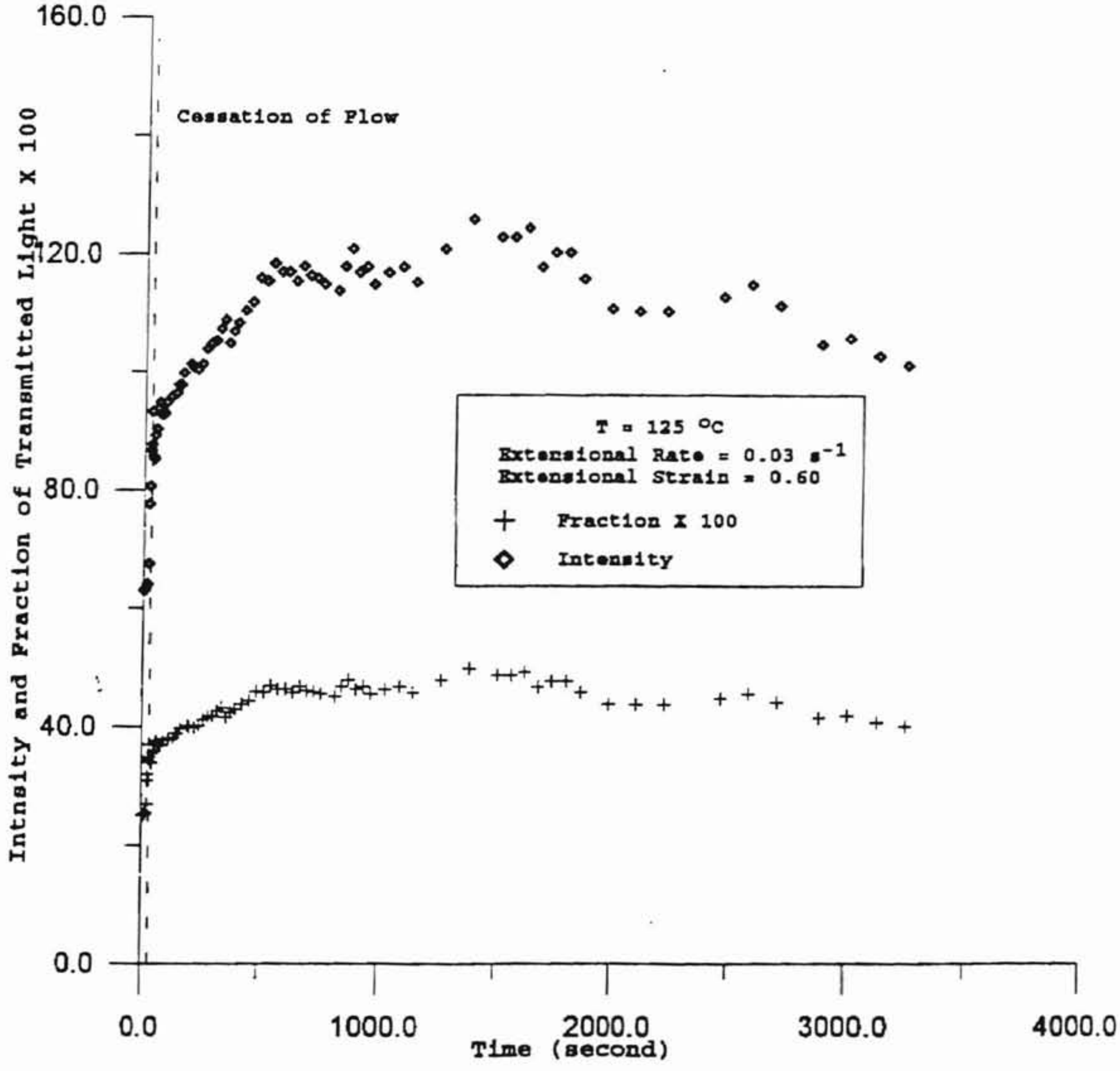

Figure 2.3 Intensity of Transmitted Light and Fraction of Transmitted Light vs. Time at Extension Rate = 0.03 sec^{-1}, Extensional Strain = 0.6 [3]

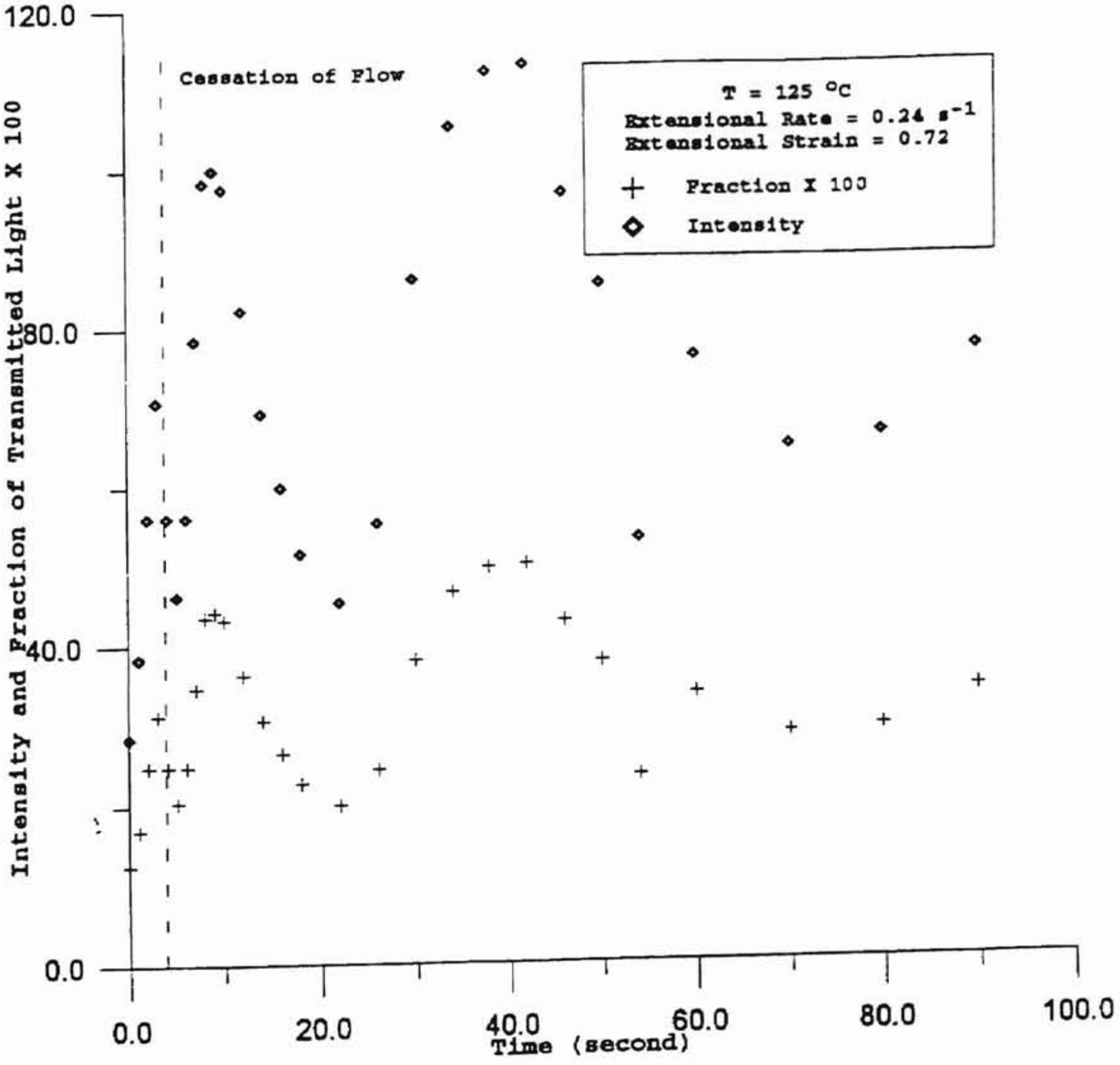

Figure 2.4 Intensity of Transmitted Light and Fraction of Transmitted Light vs. Time at Extension Rate = 0.24 sec^{-1}, Extensional Strain = 0.72 [3]

shear flow. A two-reactor system was used in which the second reactor was designed to give a uniform simple shear flow, and to allow for the measurement of the birefringence during polymerization. Agarwal et al. found that during solution polymerization under shear flow significant orientation of molecules took place once the molecular lengths were large enough. The work of Agarwal et al. seems to indicate that flow-induced crystallization requires some minimum molecular weight.

A new traction machine was developed by Alvarez et al. [18] to simultaneously study the kinetics of crystallization and mechanical behavior under elongational flow. An industrial sample of polyisobutylene (PIB) was dissolved to produce films of suitable dimensions. The machine consisted of two rollers (diameter 35 mm) with rough surfaces, a stepper motor with a reduction gear, and a force transducer. The rollers rotated at a constant rate. The Henky strain could be increased indefinitely, but for PIB samples the maximum value reached was 3. The machine was integrated with an X-ray powder diffraction apparatus, and experiments were performed to observe the onset of crystallization of PIB. Alvarez et al. found that the transient elongational viscosity increased drastically as a function of the applied strain rate. This behavior occurred when the polymer began to crystallize. Also, the onset of PIB crystallization was found to depend on the strain rather than the strain rate.

The conclusions reported by Kobayashi et al. [19] were similar to that of Alvarez et al. [18]. Kobayashi et al. used a Meissner-type uniaxial elongational rheometer to study flow-induced whisker orientation and viscosity of molten composite systems in a uniaxial elongational flow field. The time dependence of flow-induced whisker orientation was analyzed in terms of the average polar angle with respect to the flow direction by wide-angle X-ray diffraction. Kobayashi et al. reported that the orientation of the whiskers was dependent on strain only, and the elongational viscosity was almost independent of the orientational change of the whiskers.

In addition to using the birefringence technique, researchers have used a variety of approaches including: Raman spectroscopy, Meissner rheometry, Nicolet area detector, Differential scanning calorimetry, and Infrared dichroism to study flow-induced crystallization. For example, Citra et al. [20] used polarized Raman spectroscopic measurements on a uniaxially oriented HDPE fiber. Lafrance et al. [21] studied the crystalline orientation in drawn ultra-high molecular weight polyethylene films using wide-angle x-ray diffraction (WAXD). The WAXD scans of the undrawn films showed that the lamellae were oriented in the plane of the films. However, upon drawing at 130 ^{0}C, Lafrance et al. found that the orientation of the molecular chains changed from the direction normal to the film surface and to the elongation direction. Lei and Zhao [22] investigated the effect of mechanical stretching on an immiscible blend using infrared dichroism. Lei and Zhao found that mechanical stretching was an efficient way to induce a rapid orientation of the molecules along the stretching direction.

Goschel et al. [23] and Salem [24] studied the effect of strain rate rather than strain on flow-induced crystallization. By using a Nicolet area detector, Goschel et al. studied the crystallite orientation of uniaxially multi-step drawn poly (ethylene terephthalate) (PET) film strips with draw ratios ranging from 5.4 - 7.3. The orientation parameters were determined from the equatorial wide-angle X-ray studies. Goshel et al.

OKLAHOMA STATE UNIVERSITY

reported that suddenly applied very large drawing stresses on an oriented and non-crystalline structure yielded a perfect crystallite orientation, comparable to those reached by additional drawing treatments.

Salem [24] studied the crystallization of PET during drawing at temperatures of 83, 90 and 96 ^{0}C, and at strain rates in the range 0.01 - 2.1 sec^{-1}. Salem observed that decreasing the strain rate shifted the onset of crystallization to higher draw ratios. Also, decreasing the strain rate reduced the rate at which crystallinity increases with draw ratio. The study also revealed that increasing draw temperature does not necessarily increase the draw ratio for onset of crystallization. At sufficiently high strain rates, the draw ratio decreased with increasing draw temperature.

Ness et al. [25] also investigated the influence of temperature and shear rate on the flow behavior of HDPE melts during extrusion. A Ceast Rheovis 2100 capillary rheometer was used as the test apparatus in the experiments. Ness et al. found that the entry pressure drop for the samples was very low during extrusion. Also, the phenomenon of shear-induced crystallization was easily produced when the temperature was near the melting point of the samples, even though the shear rate was not high.

Liedauer et al. [26] studied shear induced crystallization in melts of isotactic polypropylene at shear rates of 100 - 200 sec^{-1}. In order to study shear induced crystallization in i-PP at 140 - 160 ^{0}C, Liedauer et al. invented a method known as short term shearing. The development of crystallization subsequent to this short term shearing was monitored with the aid of the growing optical retardation. Liedauer et al. observed highly oriented areas in the cross-sections. The time period during which the development of shear induced crystallization took place after cessation of flow was found to be ranging from 600 - 800 seconds.

Considerable work has also being done to understand the effect of crystallization on electrical and mechanical properties of polymers. Pathmanathan and Johari [27] investigated the effect of increased crystallization on the electrical properties of Nylon-12. Pathmanathan and Johari found that crystallinity increased the dc conductivity. Similarly, Boika et al. [1] found that drawn HDPE samples showed significant (over 600 %) improvement in the mechanical properties. Also, specimens with the highest draw ratio exhibited the highest elastic modulus, highest tensile strength, and highest relaxation rates during long-term testing. Elyashevich et al. [2] found that multistage drawing of linear polyethylene succeeded in achieving a higher tensile strength and elastic modulus (1.2 and 35 GPa, respectively) than the orientational crystallization, which gave 0.8 and 15 GPa. However, drawing gave rise to the fracture nuclei in the highly oriented samples, which were not observed in the samples obtained by orientational crystallization. Hsiung and Cakmak [28] studied the effect of injection-molding conditions on the crystallinity, orientation gradients, and mechanical properties of poly (aryl ether ketone) (PAEK). Hsiung and Cakmak found that elongation to break, tensile strength, and impact strength increased with the decrease of injection speed.

In summary, the study of flow-induced crystallization in semi-crystalline polymers has come a long way since the flow-induced crystallization phenomenon was first reported by Van der Vegt and Smit [6] in 1967. Since then, researchers used several techniques viz. Rheometry, DSC, and X-Ray diffraction etc., to study flow-induced crystallization, and reported results similar to that of Van der Vegt and Smit. However, generation of crystallization kinetics data was severly limited due to experimental difficulties. The in-situ observation of flow-induced crystallization was first made possible by Sakellarides and McHugh [13] with the construction of a slit-flow die with optical windows. Tree [4] and Guy [15] generated the first in-situ crystallization kinetics data by using a 4-Roll Mill device.

In addition to reporting the evidence of flow-induced crystallization in crystallizable polymers, researchers have also investigated the influence of temperature, shear and extension rates on the flow-induced crystallization behavior. In general, researchers were unanimous that shearing or extending a crystallizable polymer increased the orientation of the polymer molecules. Also, crystallization was observed to be easily produced at temperatures near the melting point of the sample [25]. Investigators also reported that mechanical and electrical properties improved significantly due to flow-induced crystallization [1, 2, 27]. However, there seems to be some dispute regarding the dominant factors influencing the flow-induced crystallization. Some researchers [18, 19] reported that flow-induced crystallization depended more on strain rather than the strain rate, whereas others [23, 24] observed that strain rate was the dominant factor. Also, little experimental data on crystallization kinetics under extensional flow were reported in the literature. Except for Tree [4], Guy [15], and Ma [3], most of the data presented in the literature were highly qualitative in nature.

OKLAHOMA STATE UNIVERSITY

Crystallization Kinetics

Kinetics is an important aspect of the crystallization process since it provides information that is required in modeling and control of polymer processing operations. Considerable work has been done to understand the crystallization kinetics in flexible-chain polymers. Work done in crystallization kinetics after 1992 is reviewed in this section. Extensive reviews of work done before 1992 were given by Tree [4], and Ma [3].

Crystallization kinetics can be broadly classified in to three categories: "(i) isothermal crystallization kinetics, (ii) constant cooling rate crystallization kinetics, (iii) and crystallization kinetics under arbitrary (non-linear) cooling." [29]. Only isothermal crystallization kinetics is discussed in this section. A detailed discussion of constant cooling rate of crystallization kinetics, and crystallization kinetics under arbitrary cooling can be found in Long et. al. [29]

The following development of the Avrami equation was taken from [29] Isothermal crystallization is usually carried out by rapidly cooling the polymer melt from above the melting temperature of the polymer to the crystallization temperature below the melting point. The polymer is then kept at the crystallization temperature until crystallization has been completed.

The degree of crystallization, *X*, is defined as the time and temperature dependent ratio of the crystallized mass to the original polymer mass.

OKLAHOMA STATE UNIVERSITY

$$X = \frac{\text{mass of crystallized particles}}{\text{total mass of polymer}} = \frac{\rho_c \sum V_i(t)}{\rho_1 V_0} \text{ for i } = 0 \text{ to m},$$

$$\text{at } t = 0 \quad \sum V_i(0) = 0 \qquad \therefore X = 0, \tag{2.1}$$

$$\text{at } t = \infty, \quad \sum V_i(\infty) = V_0 \rho_1 / \rho_c \qquad \therefore X = 1$$

where,

ρ_c = crystal density,

ρ_l = liquid density,

V_0 = total volume of molten polymer,

$V_i(t)$ = volume of each crystallizing particle at time t,

m = number of crystallizing particles.

The process of crystallization is assumed to obey the principle of additivity. The principle of additivity is based on the assumption that the instantaneous rate of transformation is a function of temperature and the amount transformed only, and that it is not dependent on the thermal history of the transformation. The transformation rate is described by the differential equation:

$$\frac{dX}{dt} = \frac{h(T)}{g(X)}, \tag{2.2}$$

where $h(T)$ and $g(X)$ are functions to be determined. Both $h(T)$ and $g(X)$ describe the microscopic kinetics of crystallization. These functions can be obtained from the classical theories of nucleation and growth. Mathematical models for quiescent crystallization at a constant temperature satisfying equation (2.2) can be of the following forms:

(a) A first order kinetic equation:

$$\frac{dX}{dt} = k(T)(1 - X), \tag{2.3}$$

(b) An equation based on a summation of nucleation and growth:

$$\frac{dX}{dt} = f_1(T, X) + f_2(T, X), \tag{2.4}$$

(c) An nth order kinetic equation:

$$\frac{dX}{dt} = nkt^{n-1}(1 - X), \tag{2.5}$$

The general solution to equation (2.5) is given by:

$$-ln[1 - X] = kt^n \tag{2.6}$$

Rewriting equation (2.6) in a slightly different notation leads to the following well-known Avrami equation:

$$-ln[1 - \xi(t)] = kt^n \tag{2.7}$$

where,

$\xi(t) = \frac{\phi(t)}{\phi_\infty}$ = crystalline volume fraction,

$\phi(t)$ = volume fraction of crystal at a given time,

ϕ_∞ = volume fraction of crystal obtained at infinite time,

k = Avrami coefficient,

n = Avrami exponent.

The Avrami equation assumes that the ratio of ρ_c / ρ_l in equation (2.1) is constant and independent of time and temperature. At constant ρ_c / ρ_l, the Avrami exponent, n, in equation (2.7) assumes integer values for given geometrical shapes of the particles. The

OKLAHOMA STATE UNIVERSITY

Avrami equation also assumes that crystallization sites become activated with time and then grow at a constant rate. The total volume of the crystal is then given as the sum of the volume of crystal at each crystallization site.

The flow-induced crystallization process cannot be thoroughly explained by the Avrami theory, since the Avrami theory does not include the stress, strain, and orientation as variables. Tree [4] modified the Avrami theory by incorporating the stress and flow terms in order to explain the effects of stress and elongational flow. The framework developed by Tree assumed that the crystallization process can be a function of stress. Also, a method to account for the flow field in which crystallization occurs was developed. The modifications to the Avrami equation allowed the interpretation of flow-induced crystallization in the same manner as the classical Avrami equation has allowed interpretation of quiescent crystallization.

The Avrami equation was widely used by many investigators to model the isothermal crystallization process in crystallizable polymers. Researches used pure as well as blends to study the crystallization kinetics. Various advanced devices such as differential scanning calorimetry, hot-stage microscopy, and pressure dilatometer etc. were used to measure and analyze the crystallization process in the polymeric materials.

Although the Avrami equation has been widely used, other models to predict crystallization kinetics have also been reported [30, 31]. Also, in general, the Avrami parameters were obtained for quiescent crystallization. Recent reports of Avrami parameters obtained for various materials can be found in [30 - 35]. The reported Avrami exponent values ranged from 1 - 4. For example, He and Zoller [32] reported Avrami

OKLAHOMA STATE UNIVERSITY

exponents between 1.3 and 1.7 for PP. Auer et al. [30] obtained Avrami exponents ranging from 2.1 - 2.7 for fiber-reinforced poly(phenylene sulfide). The low Avrami exponent values were attributed to secondary crystallization. Auer et al. theorized that "the overall crystallization rate describes the overlapping of the (mostly dominant) primary crystallization and the (mostly subjected) secondary crystallization. In polymers the secondary crystallization starts immediately behind the progressing growing front of the spherulites because of the imperfect phase transition. This overlapping decreases the overall Avrami exponent because the exponent of secondary crystallization is relatively low." [30].

Dainelli and Chapoy [33] obtained Avrami exponent values (2 - 2.8) similar to that of Auer et al. [33]. Dainelli and Chapoy found that the rate of crystallization increased with the degree of supercooling. The Avrami exponent varied from 2 - 2.8 depending on the molecular weight distribution of the polymer.

Flow Birefringence

Birefringence can be used to characterize the orientation of crystalline, and semi-crystalline polymers. Birefringence is the difference in the refractive indices along the two principal axes of a material. The process can be thought of as splitting a beam of polarized light into two beams (the ordinary, and the extraordinary beams) which travel along the axes at different speeds. The birefringence of a crystallizable polymer undergoing elongational flow increases due to chain orientation and the formation of extended chain crystals in the direction of the flow field. Birefringence is often preferred to mechanical methods because the birefringence techniques have better compliance times and do not interfere with the flow [4].

The relative phase difference, R, due to the different rate of propagation of the emerging beams is given by [4]:

$$R = \frac{L}{\lambda}[\eta_{p1} - \eta_{p2}] \tag{2.8}$$

where,

η_{p1} = first principal refractive index,

η_{p2} = second principal refractive index,

η_{p1} - η_{p2} = birefringence = Δ

Closely related to the phase difference, R, is the retardance δ_{tot}, which is given by [4]:

$$\delta_{tot} = 2\pi R \tag{2.9}$$

The total retardance of the system is also equal to:

$$\delta_{tot} = \delta_{da} + \delta_{c} + \delta_{f} \tag{2.10}$$

where,

δ_{da} = retardation of the amorphous sample phase,

δ_{c} = retardation of the crystalline regions of the sample,

δ_{f} = form retardance of the sample.

The fraction of transmitted light, T, as a function of birefringence, Δ, and isoclinic angle, χ, is given by [4]:

$$T = \frac{1}{4}\sin^2\left(\frac{\pi L\Delta}{\lambda}\right)[1 - \cos 4(\chi - \alpha)] \tag{2.11}$$

where,

L = sample thickness,

λ = wave length of light,

α = polarizer orientation angle.

In the experiment, the reference direction was taken as $\chi = 0$, and $\alpha = 45^0$. Therefore, equation (2.11) was simplified to:

$$T = \frac{1}{2} sin^2 (\frac{\pi L \Delta}{\lambda}) \tag{2.12}$$

Combining equation (2.12) with equation (2.9) we get:

$$T = \frac{1}{2} sin^2 (\frac{\delta_{tot}}{2}) \tag{2.13}$$

Since T is equal to I / I_0, equation (2.13) could be inverted to:

$$\delta_{tot} = N\pi \pm 2 \sin^{-1}\left[\left(\frac{2I}{I_0}\right)^{\frac{1}{2}}\right] \tag{2.14}$$

where,

δ_{tot} = total test section retardance,

I = intensity of the transmitted light,

I_0 = intensity of the incident light beam,

N = fringe order to which transmittance is closest.

Equation (2.14) was used to calculate the retardance throughout this thesis.

CHAPTER III

EXPERIMENTAL

The principal aim of the experimental work in this thesis was to measure the crystallization kinetics of a polymer in an extensional flow field. This goal was accomplished by using the crystallization rheometer. A detailed description of the experimental setup and techniques has been given by Siddiquee [5] and Ma [3], and has been freely adopted in this chapter. However, emphasis has been placed on the recent modifications made to the experimental techniques and procedures.

The overall experimental setup is shown in Figure 3.1. The principal components of the experimental setup shown in Figure 3.1 are: the crystallization rheometer, the data logging system, and the video-optic setup. The necessary extensional flow field was generated by the crystallization rheometer. The data logging system was used to record the torque acting on the polymer sample. The optical train in the crystallization rheometer allowed observation of the birefringence patterns in the polymer samples. The birefringence behavior was recorded by the video camera, and the images were digitized using a computer program. The components of the experimental setup shown in Figure 3.1 are described in more detail later in this chapter.

OKLAHOMA STATE UNIVERSITY

Crystallization Rheometer

The most important part of the experimental setup was the crystallization rheometer, shown in Figure 3.2. The rheometer consisted of two pairs of rotary clamps (labeled A and B) made from stainless steel. The clamps were connected via stainless steel shafts to the rotation mechanism. The rotation mechanism consisted of pulleys, idler shafts, and timing belts (D, E, F, and G). One of the pulleys was driven by a computer controlled motor (H). The arrangement kept each roller at the same rotation rate.

The polymer sample (19.4 cm by 2.54 cm by 0.3 cm) was clamped in place as shown in Figure 3.2. The clamps with the polymer sample were then immersed in an insulated, temperature controlled oil bath with a stainless steel liner. There were two round optical windows (2.5 cm I.D.) located at the front and back of the bath, through which the birefringence pattern was observed.

Silicon oil was used as the heating medium in the temperature bath, and a temperature controller from Techne (Model TU-16A) was used to maintain a uniform temperature to within ± 0.2 ^{0}C.

The motor was connected to the computer, and programmed to a desired velocity through X-language commands. A discussion of the program with sample X-language commands is given in APPENDIX A.

OKLAHOMA STATE UNIVERSITY

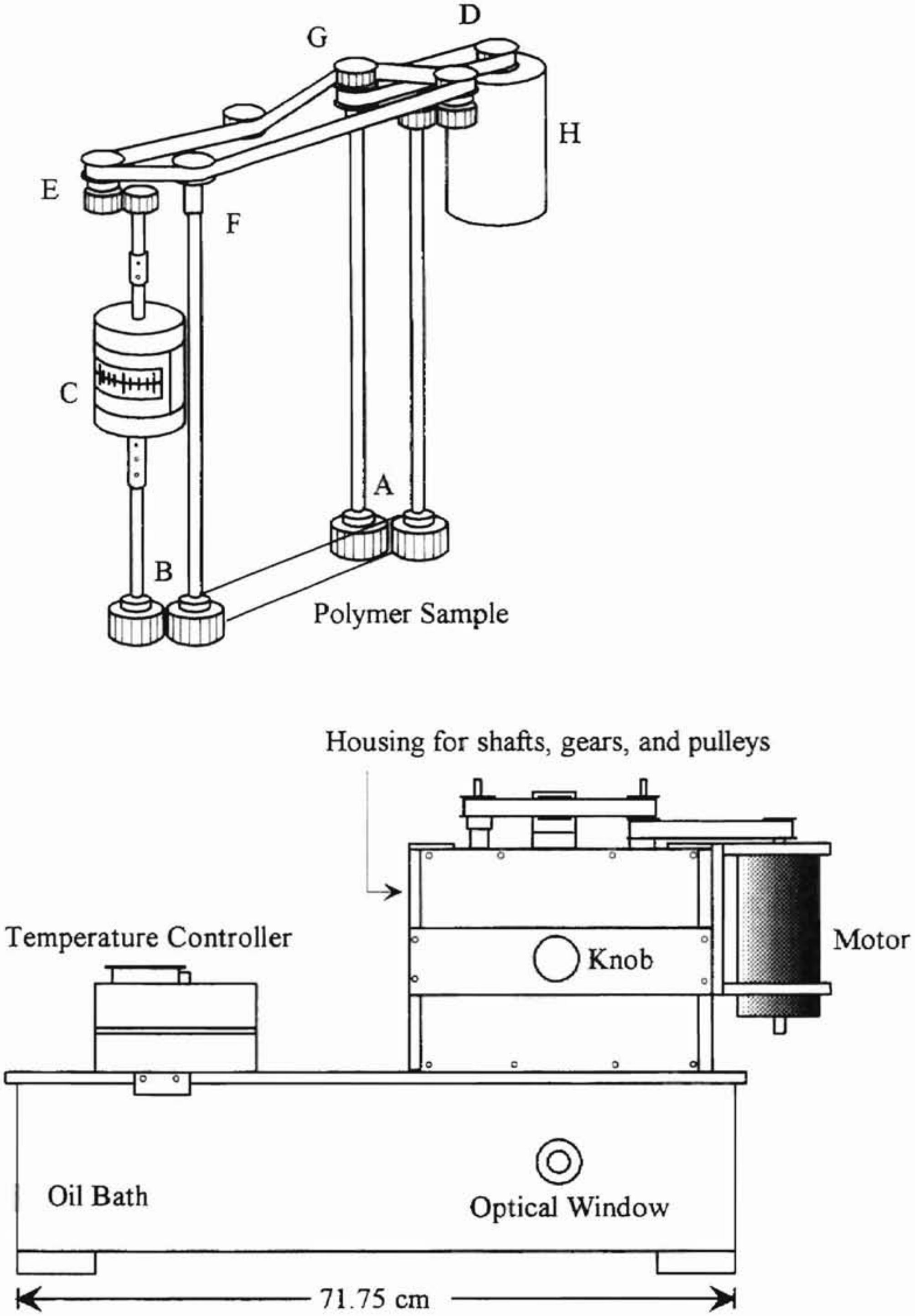
D
G
H
E
F
C
A
B
Polymer Sample
Housing for shafts, gears, and pulleys
Temperature Controller
Knob
Motor
Oil Bath
Optical Window
71.75 cm

Figure 3.2 The Crystallization Rheometer

Data Logging System

A data logging system was used to record the torque acting on the polymer sample during, and after the cessation of flow. The data logging system included a Cole-Parmer #08109-25 (model 14C) analog interface card which enabled an IBM PC to digitize analog voltages at the rate of 3 data points per second, and a Cole-Parmer #08109-32 (PC64) general purpose data acquisition software package. The torque acting on the sample was measured by an inline torque meter (C in Figure 3.2) installed in the crystallization rheometer. The analog data from the torque meter were converted into digital values by the data logging system, and the results were shown directly on the computer screen.

Optics and Video Setup

The optical and video setup shown in Figure 3.3 was used to observe, and record the birefringence data as described by Ma [3].

> "The optical train consisted of a light source, a collimating lens, a light filter, a polarizer, the polymer sample, and an analyzer. The light source was an Ealing Fiber Optics System with a light pipe. The emission end of the pipe was covered with foil, and pricked with a needle to give a good approximation of a point source of light. The light filter had maximum transmission at 488 nm (blue light). The polarizer, and analyzer had a clear aperture of 9.6 cm when mounted. All of the elements of the optical train were mounted in their respective holders except for the polymer sample

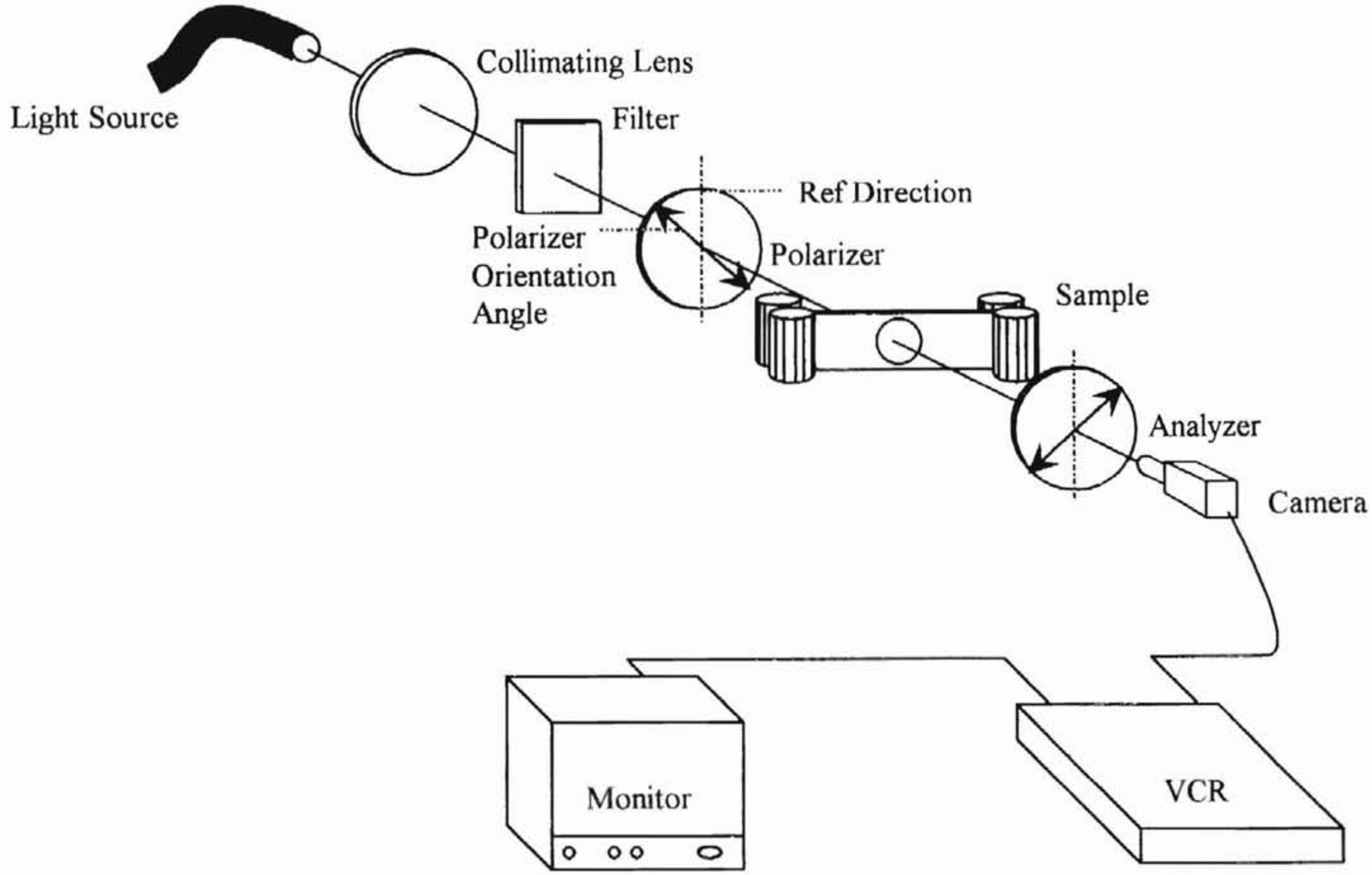
Light Source
Collimating Lens
Filter
Ref Direction
Polarizer
Polarizer Orientation Angle
Sample
Analyzer
Camera
Monitor
VCR

Figure 3.3 Optical and Video Setup [5]

which was immersed in the silicon oil. The optical holders were clamped to a aluminum optical rail.

The video setup consisted of a black and white monitor, a video camera (30 frames/sec.), and a VCR. The video camera and VCR were used to record the birefringence behavior. The black and white monitor was used to view the birefringence pattern during the experiment, and also to analyze the data. The video camera was set on a tripod in front of the equipment, and set at the same height as the optical window of the temperature bath." [3].

Sample Preparation

To obtain the best results, smooth, homogeneous samples were required. Ma [3] used an aluminum die, shown in Figure 3.4 (a), to prepare the polymer samples. The die was filled with HDPE resin in the form of pellets, and heated to 160 ^{0}C in a vacuum oven to remove any air bubbles. After six hours, the die was removed from the oven, and placed in a Carver Laboratory Press for 30 minutes. Then the die was allowed to cool, and the sample was removed. Only those samples which did not have imperfections (air bubbles, waviness etc.) were used in experiments. All other samples were rejected.

Although the samples obtained by Ma's technique were smooth and homogeneous, removing the sample from the die was difficult because the bottom surface of the sample adhered to the die. Coating the surface of the die with silicon oil before placing the polymer resin in the die cavity did not completely solve the adhesion problem. Therefore, modifications were made to the die as indicated in Figure 3.4 (b). In the new design, the

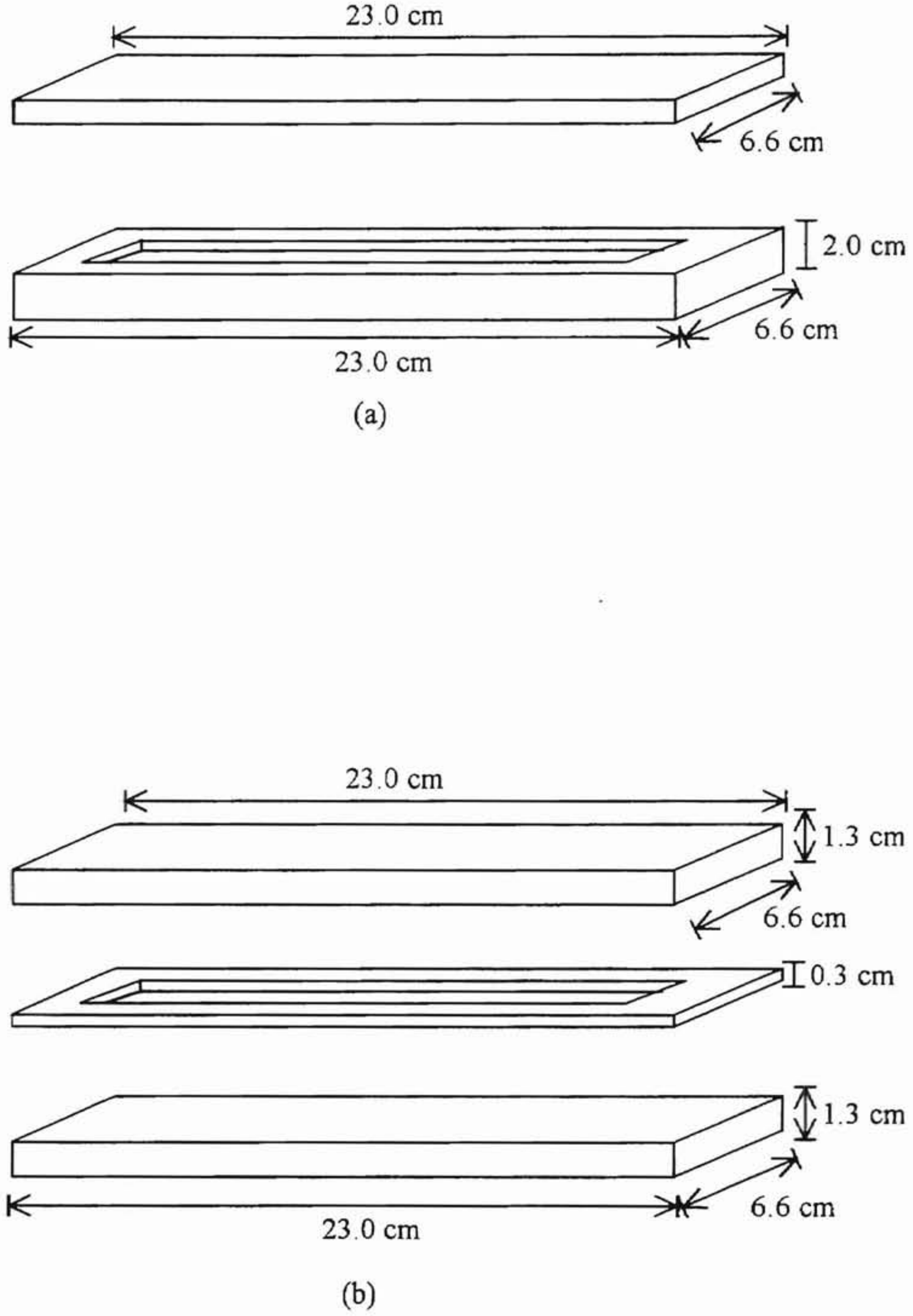
23.0 cm
6.6 cm
2.0 cm
6.6 cm
23.0 cm
(a)
23.0 cm
1.3 cm
6.6 cm
0.3 cm
1.3 cm
6.6 cm
23.0 cm
(b)

Figure 3.4 Sample Preparation Die (a) Original, (b) Modification

die cavity and the base of the die were divided into two independent pieces. The base of the die was covered with aluminum foil before being mated to the die cavity. The modifications completely solved the problem of the sample adhering to the die, and made removal of the sample from the cavity very easy. Also, Ma's technique involved heating the die in a vacuum oven for six hours, and then pressing the die for 30 minutes. In order to reduce the preparation time, Ma's technique was modified by directly placing the die in the press, and applying pressure for 30 minutes at a temperature slightly above the melting point of the polymer resin. The total time required to prepare a sample was thus reduced from 8 hours to 1 hour. The samples obtained were smooth and without air bubbles, which obviated the usage of the vacuum oven to remove air bubbles in the samples.

Experimental Techniques and Procedure

The experimental procedure involved the following steps: (1) calibration of the data logging system; (2) calibration of the optical train; (3) placing the polymer sample in the optical path; (4) heating the sample to destroy all order, orientation, and crystallinity; (5) cooling the sample to the desired run temperature; (6) applying the extensional flow field; and (7) recording the birefringence pattern.

The data logging system was calibrated before it was used in the experiment. The data logging system was calibrated in such that the torque value showed by the data logging software on the computer screen was the same as the analog torque value indicated by the inline torque meter (C in Figure 3.2). The calibration procedure of the data logging system is described in detail in APPENDIX B.

The optical train consisting of a light source, a collimating lens, a light filter, a polarizer, and an analyzer was calibrated before the polymer sample was placed in the optical path. To assure that the light through the crystallization rheometer windows was horizontal, the oil bath and the optical rail were leveled with a spirit level. Also. the light source and the video camera were adjusted in such a way that the light source image appeared at the center of the black and white monitor

The polymer sample (2.54 cm by 19.4 cm by 0.3 cm) was held in the optical path by the immersed rollers. In order to secure the sample, the rollers were first elevated above the surface of the oil with hydraulic jacks. The sample was then slid between the rollers. Then the roller gap adjustment knob was tightened to hold the sample in place. The hydraulic jacks were then released to allow the rollers and the sample to be immersed in the oil. At elevated temperatures, the sample tended to float up to the surface of the oil because of the difference between the density of the oil and the sample. To prevent floating, the samples were covered with aluminum foil, except for the region where birefringence was to be measured. The region of observation was rectangular in shape (2 cm by 1 cm) as shown in Figure 3.5. Covering the sample with aluminum foil sufficiently held the sample in place.

After the polymer sample was placed correctly in the optical train, the sample was heated to a temperature typically 2 - 5 ^{0}C above the melting point. For example, HDPE samples were typically heated to 135 ^{0}C. Then the polarizer, which was initially parallel to

OKLAHOMA STATE UNIVERSITY

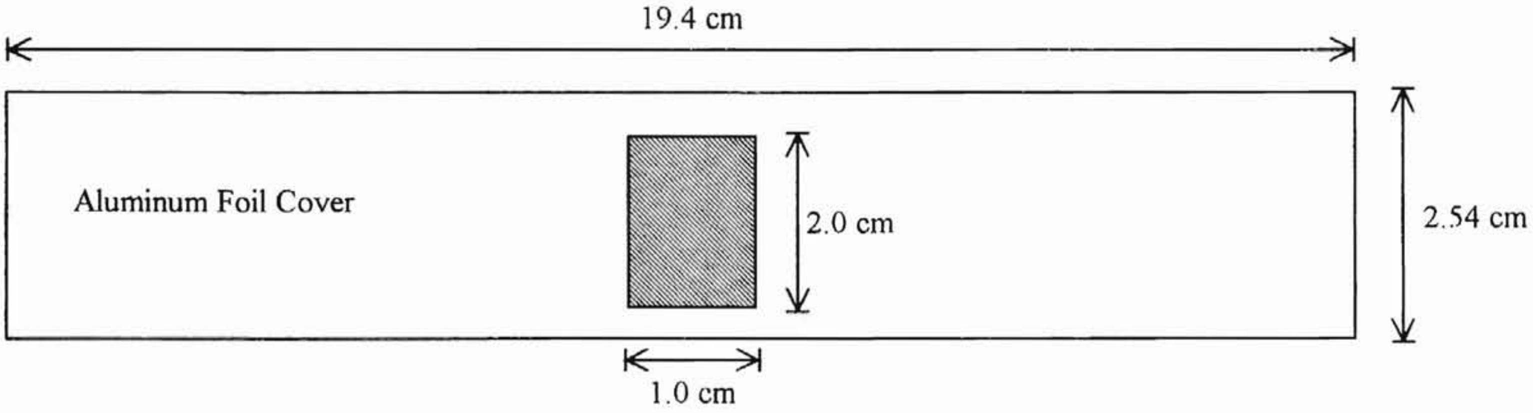
19.4 cm
Aluminum Foil Cover
2.0 cm
2.54 cm
1.0 cm

Figure 3.5 Polymer Sample Covered with Aluminum Foil

the analyzer, was rotated 45^0 counter clockwise, and the analyzer was set perpendicular to the polarizer. The sample was assumed completely molten when no birefringence was observed for 5 minutes. Then the temperature was set to the desired run temperature, which was usually less than the melting point of the sample, and the VCR was set to record the birefringence behavior on the videotape. In some of the initial experiments, no special effort was made to cool the oil bath. In all the later experiments, the quenching process was hastened by a cooling coil immersed in the silicon oil. The coolant used was tap water. The process of quenching the sample in order to attain equilibrium at the desired run temperature typically required 20 minutes.

A Compumotor, controlled by a computer program, was used to produce the flow field. In the program, commands were given to rotate the rollers such that the sample experienced the desired average strain rate, and average total strain. A description of the program, and the commands to run the Compumotor are given in APPENDIX A. The average strain rate, and the average total strain were then calculated from the values input to the computer program. Note should be made that the actual strain rate experienced by the polymer sample at any given point was usually different from the average strain rate because the deformation of the sample was not uniform. The methods to calculate the average and actual strain rates are given below:

Calculation of the Average Strain Rate and the Average Strain

The velocity field in a shear free flow shown in Figure 3.6 is given by [36, p.101]:

$$v_x = -\frac{1}{2}\varepsilon(1+b)x \tag{3.1}$$

$$v_y = -\frac{1}{2}\dot{\varepsilon}(1-b)y \tag{3.2}$$

$$v_z = \dot{\varepsilon}z \tag{3.3}$$

where,

$\dot{\varepsilon}$ = average elongation rate (sec^{-1}),

b = shear flow parameter, $0 \leq b \leq 1$

In an elongational flow field, $b = 0$, and elongation rate, $\dot{\varepsilon} > 0$. Rearranging equation (3.3), we get:

$$\varepsilon = \frac{v_z}{z} \tag{3.4}$$

The velocity of the sample in the direction of the flow field is given by:

$$v_z = 2\pi rV = \pi DV \tag{3.5}$$

where,

D = diameter of the roller = 5.715 cm, and

V = rotational velocity of the roller (rotations per second).

The elongational flow field on the sample was generated by the rollers. The rollers held the two ends of the sample. An assumption was made that the total elongational flow

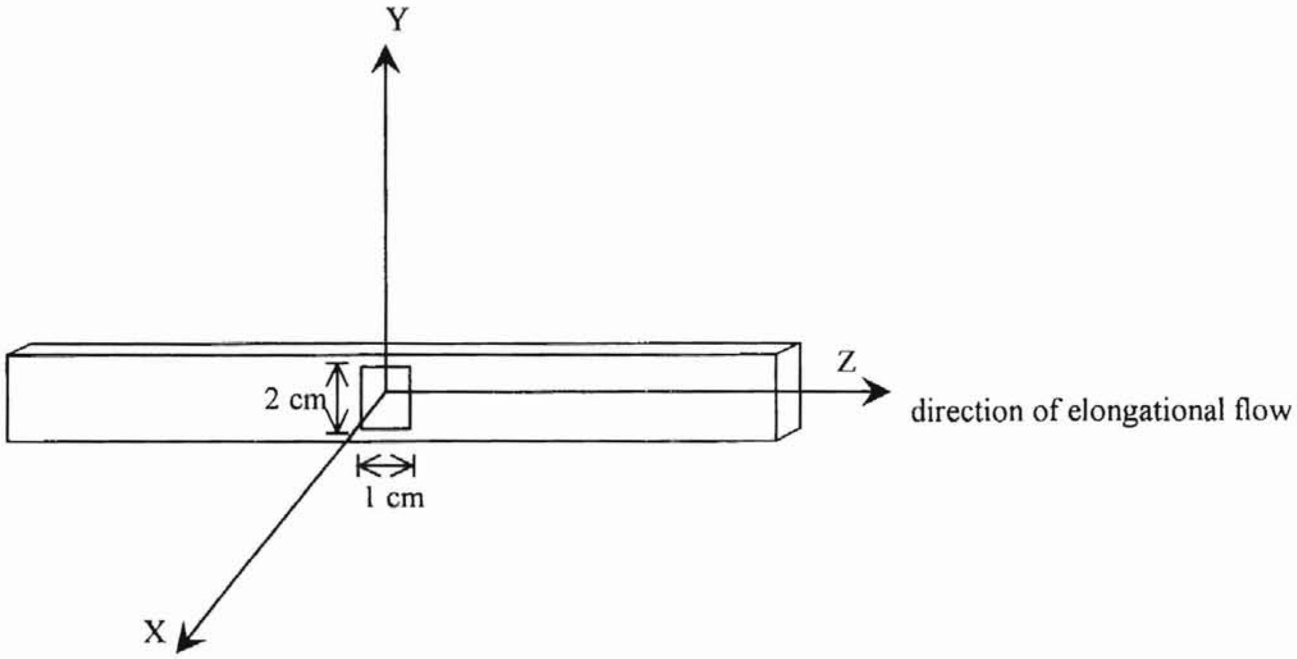
Y
Z
direction of elongational flow
2 cm
1 cm
X

Figure 3.6 Polymer Sample Under Elongational Flow

experienced by the sample was generated equally by each roller. Hence, the effective initial length of the sample elongated by a roller is taken as:

$$z = L_i/2 \tag{3.6}$$

where,

$L_i =$ initial length of the sample = 1 cm.

Note should be made that the entire sample (length 19.5 cm) was covered with aluminum foil except the region of interest which was a rectangular area of length 1 cm., and height 2 cm. Therefore, the total length of the sample before deformation was taken as 1 cm. After substituting equation (3.5) and equation (3.6) in equation (3.4), we get

$$\varepsilon = \frac{2\pi DV}{L_i} = 35.9V \sec^{-1} \tag{3.7}$$

The average total strain of the sample is then given as:

$$\varepsilon = \varepsilon t \tag{3.8}$$

where,

$t =$ elongation time.

Calculation of the Actual Strain Rate and the Actual Strain

The average strain rate calculated by equation (3.7) was valid only when the deformation of the sample in the rectangular region was uniform. However, the actual strain rate experienced by the sample was found to be different from the average strain rate obtained from equation (3.7). For example, if two experiments were performed with the same average strain rates and average strains, observation of the samples during the experiments showed that the actual strains experienced by the samples were often different. Therefore, a new method was developed to determine the actual strain rate, and actual strain experienced by the sample. In the new method, the length of the sample before, and after deformation was measured directly from the monitor in pixel units. The actual strain experienced by the sample was then computed by :

$$\varepsilon_a = \frac{L_f - L_i}{L_i} \tag{3.9}$$

where,

ε_a = actual strain,

L_i = initial length of the rectangular region of the sample in pixel units before deformation.

L_f = final length of the sample in pixel units after deformation.

The values of L_i and L_f were obtained by measuring the lengths of the sample displayed on the monitor before and after deformation, respectively.

The actual strain rate experienced by the sample is given by:

$$\varepsilon_a = \frac{\varepsilon_a}{t} \tag{3.10}$$

The torque acting on the sample was recorded by the data logging software. The motor would stop rotating the rollers after the desired average Hencky strain was obtained. The VCR continued recording for approximately 6 hours. The birefringence pattern and the torque data were analyzed later.

Calculation of the Density of the HDPE Samples

The densities of the samples were determined by using a density gradient column. The density gradient was prepared by using a constructed column and the PACE™ gradient maker. The constructed column consists of a 15 cm (I.D.), 70 cm tall Plexiglass™ water bath on an aluminum stand and a 5 cm (I.D.) glass tube that is secured inside the bath. Tubing was used to deliver a constant flow of water to the top of the water bath from a constant temperature water source, while another length of tubing took water out of the bottom of the column.

The column operates on the basis that the float (or specimen) will descend in the column until $\rho_{liquid} = \rho_{specimen}$. The accuracy achieved in using this method can be as great as four-digit accuracy, with the calibrated floats being known to ±0.0001 g/cm3 and the heights of floatation of the specimens being measured to ±0.05 cm. Two miscible liquids were used to make the density gradient. Distilled water was the high density fluid and isopropyl alcohol was the lower density fluid. At 23 ^{0}C, distilled water has a density of 0.9954g/cm^3 and isopropyl alcohol has a density of 0.7965 g/cm^3. Three ASTM density floats of known densities, 0.9250 g/cm^3, 0.9625 g/cm^3, and 0.9750 g/cm^3 were placed into the density gradient column and allowed to settle completely. A linear equation describing the density gradient in the column was calculated by using the densities of the beads relative to their positions in the column. The linear equation to calculate the density of a sample from the sample's position in the density gradient column was obtained as:

$$\rho = -0.001133x + 1.017 \qquad (3.11)$$

where,

x = position of the sample in the gradient column (cm), and

ρ = density of the sample (g/cm^3)

Note should be made that equation (3.11) is valid only for the density gradient created in our experiment. The coefficients (slope and intercept) of equation (3.11) assume different values for each new density gradient prepared, because the beads in the column occupy different equilibrium positions.

A polymer sample (0.5 cm by 0.5 cm) whose density needed to be calculated was dropped into the density gradient column. The sample was allowed to attain the an equilibrium position (x). The equilibrium position of the sample was then used in equation (3.11) to calculate the density of the sample.

Calculation of the Percentage Crystallinity of the HDPE Samples

The percentage crystallinity was calculated by [37, p.385-386]:

$$v^c = 100 \times \left(\frac{\rho - \rho_a}{\rho_c - \rho_a} \right) \tag{3.12}$$

where,

v^c = percentage volume fraction crystallinity (%),

ρ = density of HDPE (g/cc),

ρ_a = density of amorphous HDPE, and

ρ_c = density of perfectly crystalline HDPE.

The densities of amorphous (0% crystallinity) and perfectly crystalline (100% crystallinity) HDPE were taken as 0.854 g/cc and 0.997 g/cc respectively [38, Table IV.1, p.388-389].

Analysis of the Experimental Data

The experimental data were used to quantify the flow-induced crystallization kinetics. The total retardance in the crystallizing system was given by:

$$\delta_{tot} = 2N\pi \pm 2\,sin^{-1}\left[\left(\frac{2I}{I_0}\right)^{\frac{1}{2}}\right] \qquad (2.14)$$

The development of equation (2.14) was described in Chapter II.

In order to determine the total retardance, intensities of the transmitted light were required. The intensities of the transmitted light were obtained by using a video image technique. Ma [3] used a computer software package to digitize the experimental data recorded on a video tape into pixel values, and the pixel values were then converted into light intensities. The computer software package required continuous user interaction and acquiring huge amounts of data by using the software became very tedious. Hence, a computer program was developed to automate the entire data acquisition process. The computer program is described in detail in APPENDIX C.

Equation (2.14) was used to calculate the total retardance as a function of time, and the Avrami parameters were then determined by plotting $ln(-ln[1-\xi(t)])$ vs. $ln(t)$. The slope of the best fit straight line was taken as the Avrami exponent, n, and the intercept was set equal to $ln(k)$.

CHAPTER IV

RESULTS AND DISCUSSION

The experimental setup described in Chapter III was used to observe and record the flow-induced crystallization phenomena shown by high density polyethylene (HDPE), polystyrene (PS), and polypropylene (PP). The experimental data obtained were converted to crystallization kinetics data and then correlated with the Avrami equation. HDPE samples were used to study flow-induced crystallization over a wide range of extension rates. Experiments with PP and PS were performed to corroborate the results obtained from the HDPE.

Pixel Value and Torque Data

Figure 4.1 shows a typical plot of pixel value and torque as a function of time for a HDPE sample. The sample was subjected to a strain of 3.6 at a rate of 0.72 sec^{-1}. The flow field was applied at 124.6 ^{0}C. The time t = 0 seconds in Figure 4.1 corresponds to the time at which the heater was set to the desired run temperature of 124.6 ^{0}C. Pixel value data from HDPE at other extension rates are given in APPENDIX D.

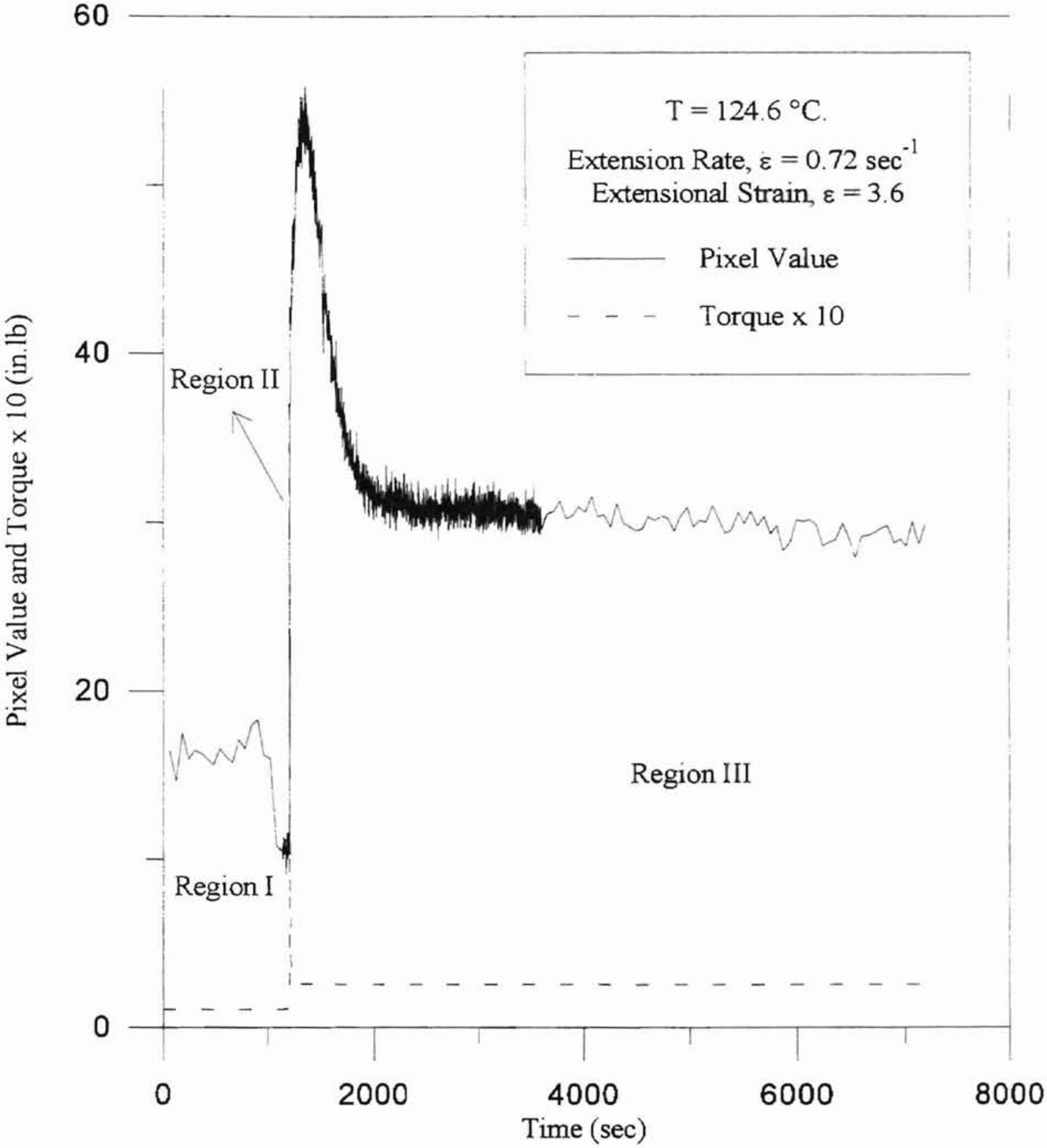

Figure 4.1 Pixel Value and Torque vs. Time for HDPE

The plot in Figure 4.1 can be divided into three regions, labeled I, II, and III. Region I includes the first 20 minutes of the experiment. In Region I, the molten polymer sample was quenched from 135 ^{0}C to the desired run temperature of 124.6 ^{0}C. The pixel value at $0 < t < 1100$ seconds was approximately 18. At $t \cong 1100$ seconds, the pixel value dropped suddenly to ~10 and remained constant until the flow field was applied at $t = 1200$ seconds. The sudden drop in the pixel value at $t \cong 1100$ seconds was attributed to the formation of nucleation sites. Ma [3] observed similar pixel value behavior in his experiments with HDPE at 125 ^{0}C.

The run temperature of 124.6 ^{0}C was attained approximately 18 minutes after the experiment began. Even though the sample reached the run temperature before $t = 20$ minutes, the sample was left undisturbed until $t = 20$ minutes in order to stabilize the run temperature and to keep the quenching period uniform for all of the experiments.

Region II began at $t = 20$ minutes. An extension rate of 0.72 sec^{-1} was applied for 5 seconds. Region II is shown on a different time scale in Figure 4.2. The intensity of the transmitted light and the torque both spiked. The pixel value attained a local maximum of 32 at approximately the same time as the extensional flow stopped. The pixel value and torque then rapidly decreased. The pixel value decreased to approximately 16. The torque decreased for approximately 20 seconds and then remained constant.

Region III begins at the cessation of flow and continues to the end of the data set. The pixel value started to increase almost immediately after the cessation of flow. The pixel value reached a new peak after approximately 1400 seconds at a value of

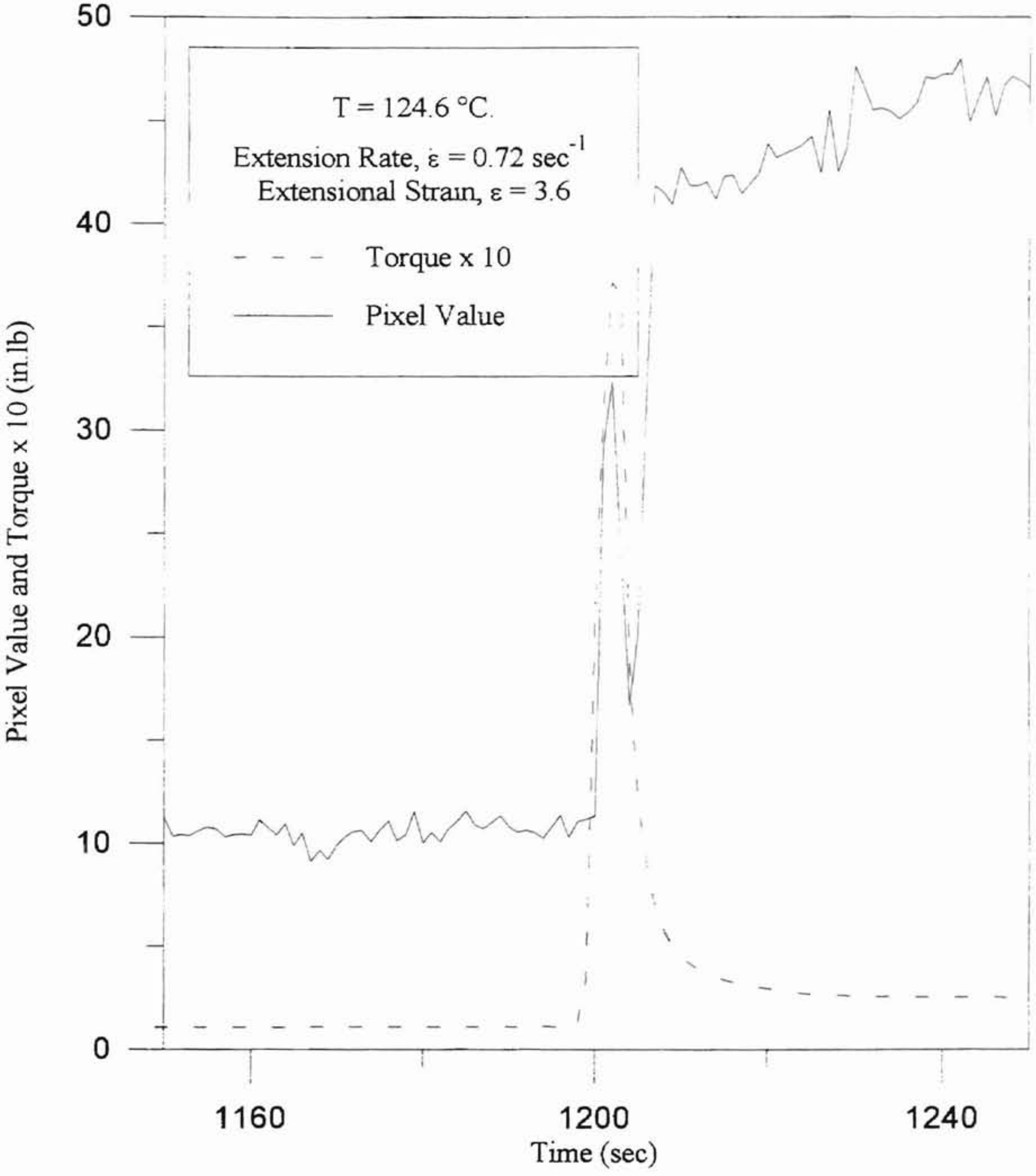

Figure 4.2 Region II

approximately 55. The pixel value then decreased to eventually attain a value of 30 at t ≅ 3000 seconds. The pixel value remained constant at 30 for the duration of the experiment.

In order to understand the data shown in Figure 4.1, the results of additional experiments as well as equation (2.14) need to be considered. Figure 4.3 shows the pixel value data obtained from a separate experiment with HDPE performed under the same thermal history as in Figure 4.1, but with no extensional flow field (i.e. quiescent conditions). Figure 4.3 shows the same type of pixel value behavior as can be seen in Region I of Figure 4.1. Specifically, the pixel value drops off suddenly as the sample cooled. The drop off in pixel value was attributed to the onset of nucleation. The nucleation sites scattered the light resulting in an intensity decrease. The similarity of the data in Region I of Figure 4.1 and the data in Figure 4.3 lead to the conclusion that the pixel value profile in Region I is not indicative of flow-induced crystallization.

The increase in the intensity of light during the flow (Region II) was attributed primarily to the polymer molecules orienting under the applied stress field, and not due to crystallization. This hypothesis was confirmed by running the experiment with a non-crystallizing polymeric material. An atactic polystyrene (PS) was selected. The experimental procedure using PS samples was similar to that involving HDPE samples. However, the HDPE sample was heated to 135 ^{0}C (3 ^{0}C above the melting point of HDPE) in order to destroy all order, orientation, and crystallinity before the sample was cooled to the run temperature. Since PS does not have a melting point, the PS sample was heated to 190 ^{0}C, a temperature far above its glass transition temperature of 100 - 120 ^{0}C. The PS sample was heated to 190 ^{0}C, which was the maximum temperature

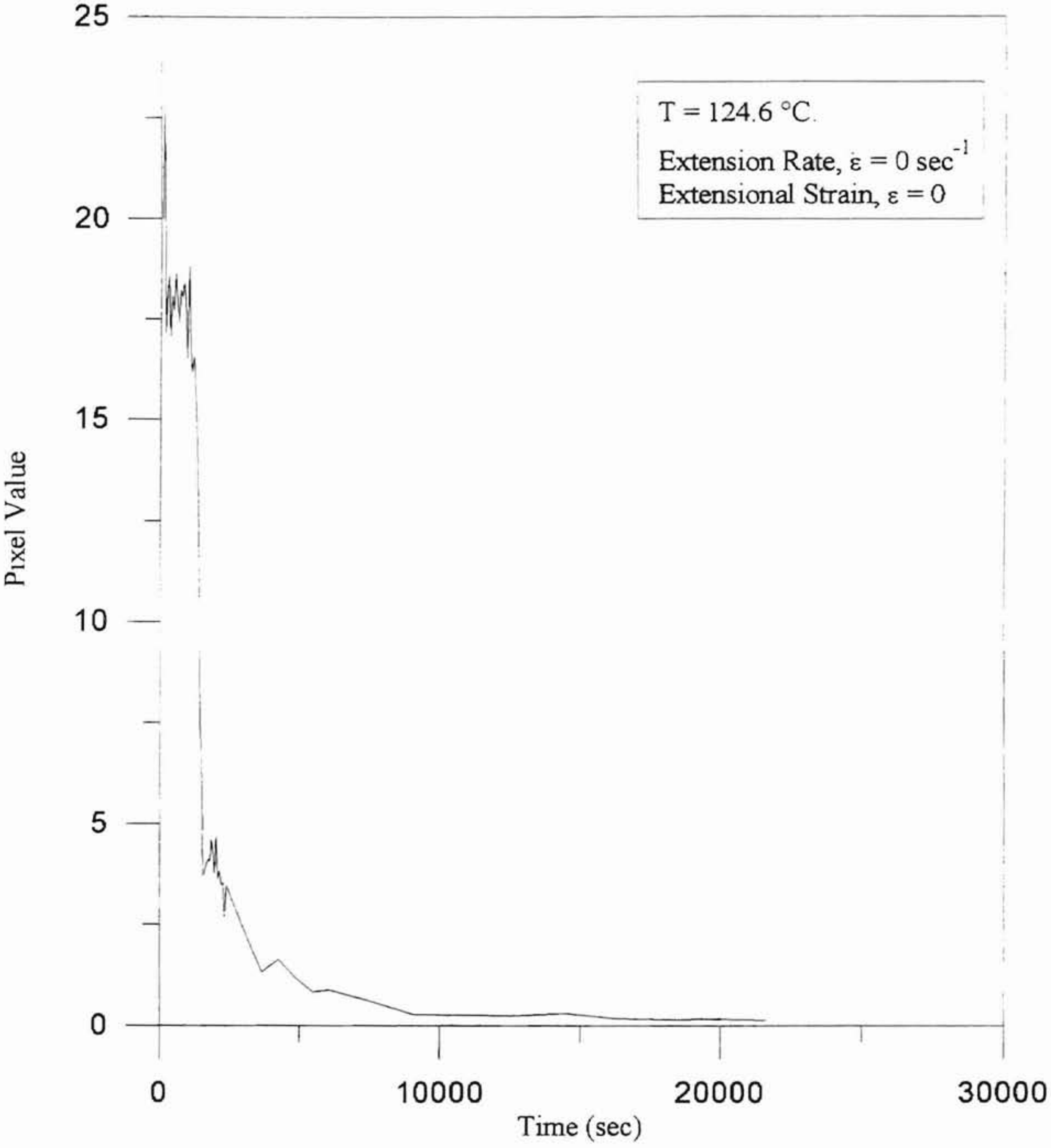

Figure 4.3 Pixel Value vs Time Under Quiescent Conditions for HDPE

attainable by the heating equipment used in the experiment. The PS sample was rubbery at 190 ^{0}C. The sample was cooled to a run temperature of 160.5 ^{0}C in 20 minutes.

Figure 4.4 shows the pixel value data obtained for PS at 160.5 ^{0}C. The applied extension rate was 0.36 sec^{-1} and the total strain was 3.6. The low pixel value at $t = 0$ seconds indicates that the PS sample was devoid of any order. Figure 4.4 shows that when the flow field was applied at $t = 20$ minutes, the intensity of the transmitted light increased to a maximum, and when the flow field stopped after 10 seconds, the intensity rapidly decreased to a minimum value. The light intensity then stayed at the minimum value for the duration of the experiment. The decrease in the pixel value in Region II immediately after the cessation of flow was attributed to the relaxation of the amorphous phase. The fact that the pixel value in Figure 4.1 did not decrease to zero can be attributed to the formation of a small amount of crystal in the sample during the flow period. McHugh, Guy and Tree [14], and Ma [3] reported similar pixel value behavior. Therefore, the spike in the pixel value in Region II of Figure 4.1 was caused by the flow field, and was not due to crystallization.

The increase in the intensity of the transmitted light in Region III can be attributed either to crystallization in the sample or to amorphous orientation of the sample. The only way to induce orientation of the sample in our experiment was by applying stress [3]. However as shown in Figure 4.1, the torque remained constant after the cessation of the flow field. The change in the pixel value could not have been caused by stress. Therefore, the increase in the intensity of light in Region III was attributed to the formation of flow-induced crystallization.

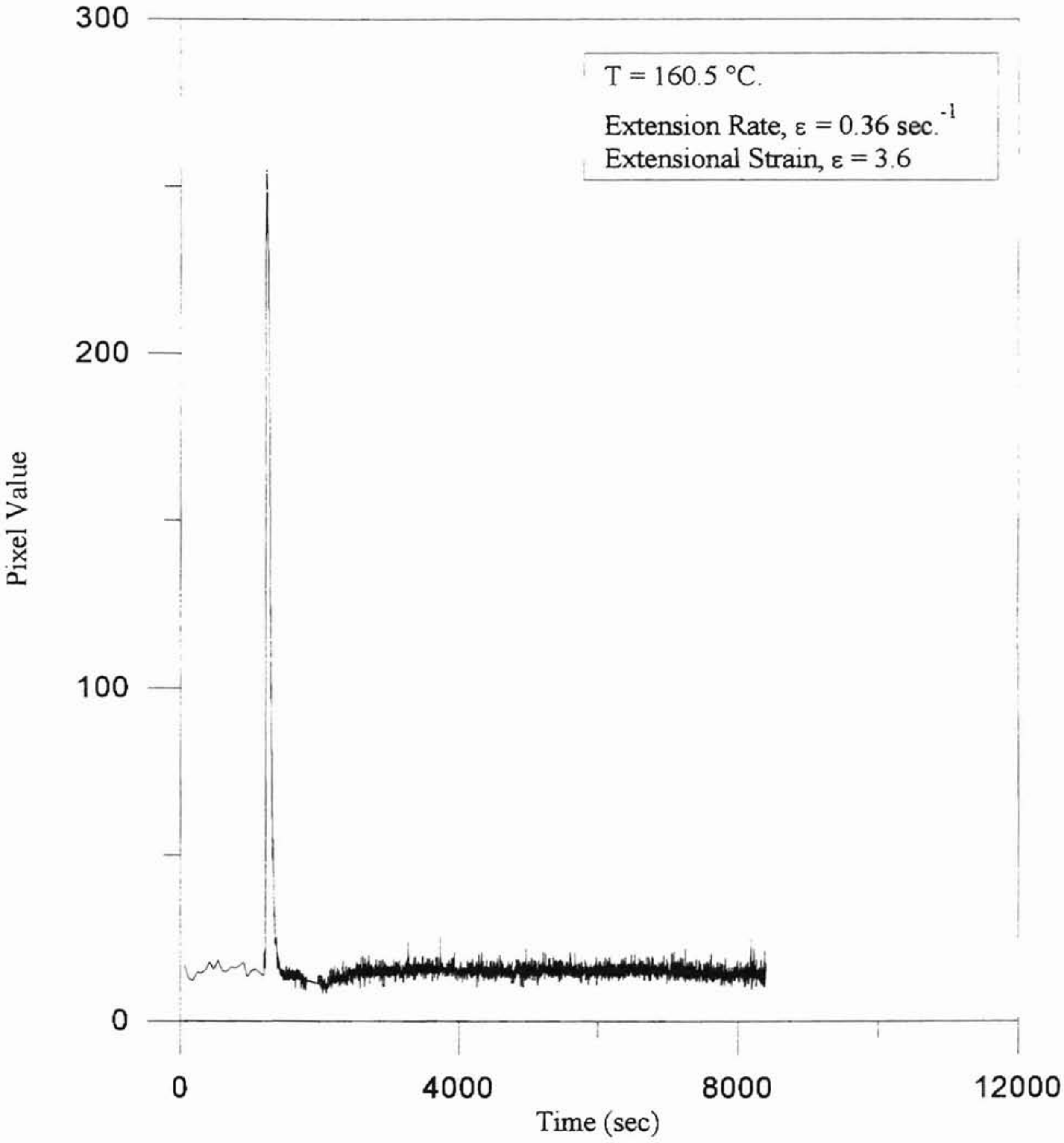

Figure 4.4 Pixel Value vs. Time for Polystyrene Under Flow

The generalized profile of intensity of transmitted light given by Guy [15] in Figure 2.2 indicates that the pixel value repeatedly increases and decreases in a sinusoidal fashion until the flow-induced crystallization process in the polymer system is complete. Also, note should be made that a decrease in intensity does not mean a decrease in retardance. In the calculation of retardance from equation (2.14), the positive sign is used when starting at a fringe and the pixel value is increasing toward the maximum between fringes. Once this maximum has been passed, the fringe order is increased by one and the negative sign is used as the next fringe is approached [15]. Hence, retardance continues to increase until the pixel value becomes constant. The constant pixel value of 30 in Region III of Figure 4.1 suggests that the polymer sample might have experienced rapid initial flow-induced crystal growth and attained the maximum possible crystallization in a short period of time. Another reason for the decrease in the pixel value in Region III could be the onset of quiescent crystallization in addition to flow-induced crystallization. The folded-chain crystals formed due to quiescent crystallization might have scattered the light passing through the sample thus decreasing the intensity of transmitted light. However, the possibility of quiescent crystallization is remote in Region III of Figure 4.1. The experiment with the HDPE sample at 124.6 ^{0}C under quiescent conditions (Figure 4.3) indicated that the sample did not show crystallization as the pixel value decreased through out the duration of the experiment.

Optical Retardance

In order to quantify the flow-induced crystallization, the pixel value data shown in Figure 4.1 were converted to retardance by the method described in Chapter III. Reduced retardance vs. time for the pixel value data of Figure 4.1 is shown in Figure 4.5. In Figure 4.5, note should be made that t = 0 corresponds to the cessation of flow, where as in Figure 4.1, t = 0 marked the beginning of the quenching process. Figure 4.5 reveals that the reduced retardance initially increased with time rapidly, and asymptotically approached a value of 1.0 at large values of time. The increase in reduced retardance with time after the cessation of the flow field is an indication of the development of flow-induced crystallization in the polymer sample, and is in agreement with the results presented by Tree [4], Guy [15], Ma [3], and Desai et al. [38, 39]. The reduced retardance is directly proportional to the relative crystallinity ($\xi(t)$ in the Avrami equation (2.7)) of the polymer system. The increasing reduced retardance with time in Figure 4.5 after cessation of flow implies that relative crystallinity is increasing with time. Hence Figure 4.5 is indicative of nucleation and growth mechanisms occurring in the HDPE polymer sample.

Correlation with the Avrami Equation

The Avrami equation is not strictly applicable to model the flow-induced crystallization in a crystallizable polymer. Nevertheless, the Avrami theory models very well the nucleation and growth mechanisms at the early stages of crystallization [4].

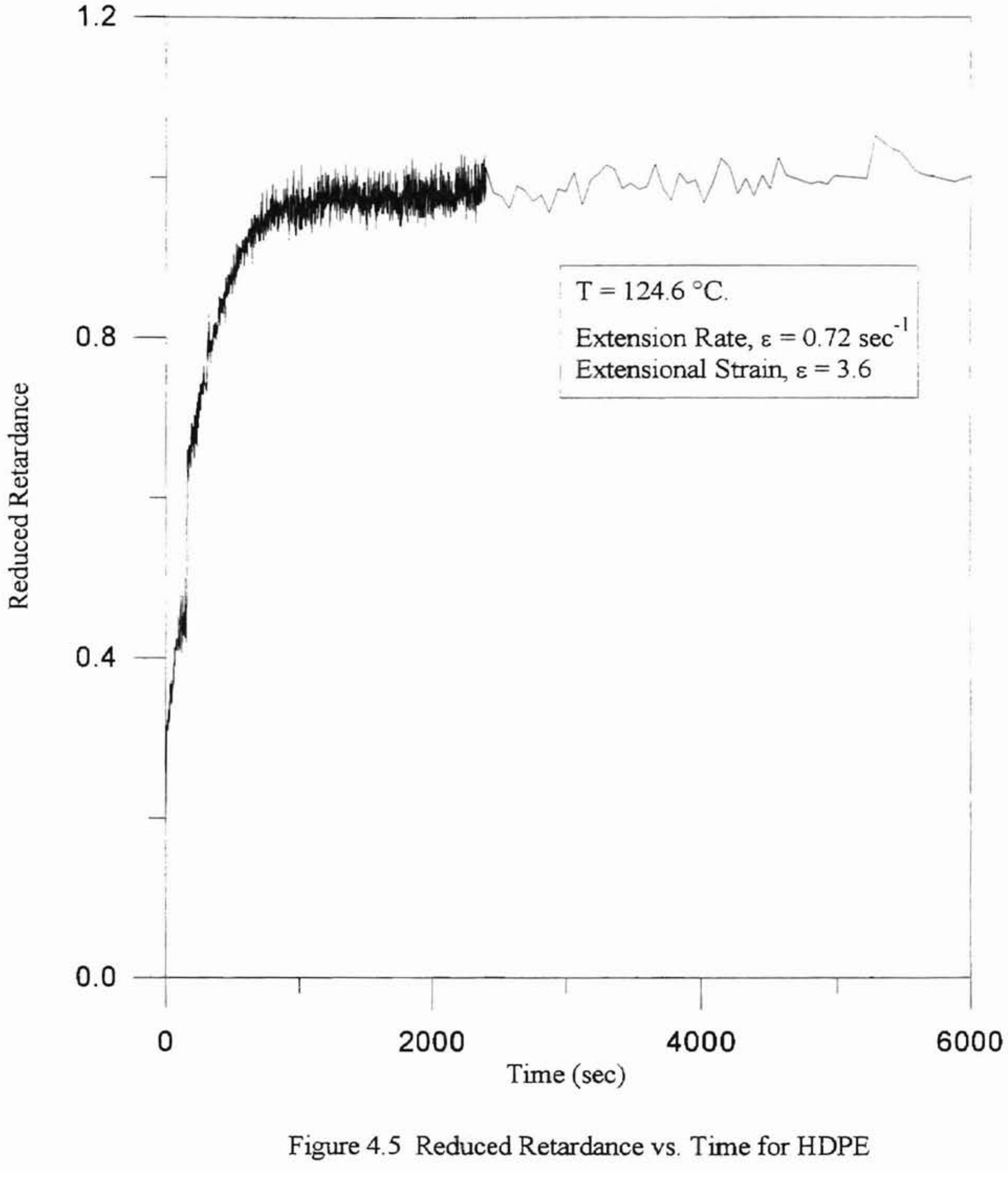

Figure 4.5 Reduced Retardance vs. Time for HDPE

Hence, the Avrami equation was assumed to be suitable for the experimental data reported in this thesis.

The Avrami parameters were determined by fitting the retardance data shown in Figure 4.5 to the Avrami equation. Figure 4.6 shows the plot of $ln(-ln[1- \xi(t)])$ vs. $ln(t)$, and the best fit straight line. The slope of the line is the Avrami exponent, n, and the intercept of the line with the y-axis is $ln(k)$, where k is the Avrami coefficient. Figure 4.6 indicates that the data are well correlated by the Avrami equation. Experiments done at other extension rates (0.29 sec^{-1} - 6.13 sec^{-1}) were also well correlated by the Avrami equation. In general, the Avrami exponent was found to be 0.5 ± 0.2 for HDPE. Plots of pixel and retardance data along with the correlations by the Avrami equation at different experimental conditions can be seen in APPENDIX D.

In our effort to study flow-induced crystallization in different semi-crystalline polymers, polypropylene (PP) was also used to generate kinetic data in addition to HDPE. Experiments with PP were performed to demonstrate that HDPE is a good model system for semi-crystalline polymers.

The PP samples were of the same size and shape as the HDPE samples. The thermal history was similar to that of HDPE except that the PP samples were heated to 175 ^{0}C (3 ^{0}C above the melting point of PP) and then cooled to a run temperature of 150 ^{0}C in 20 minutes. PP samples showed rapid quiescent crystallization at temperatures below 150 ^{0}C. At temperatures above 150 ^{0}C, the PP samples either floated or were torned apart when the extensional flow field was applied, even at very low extension rates. Therefore, 150 ^{0}C was selected as the ideal run temperature.

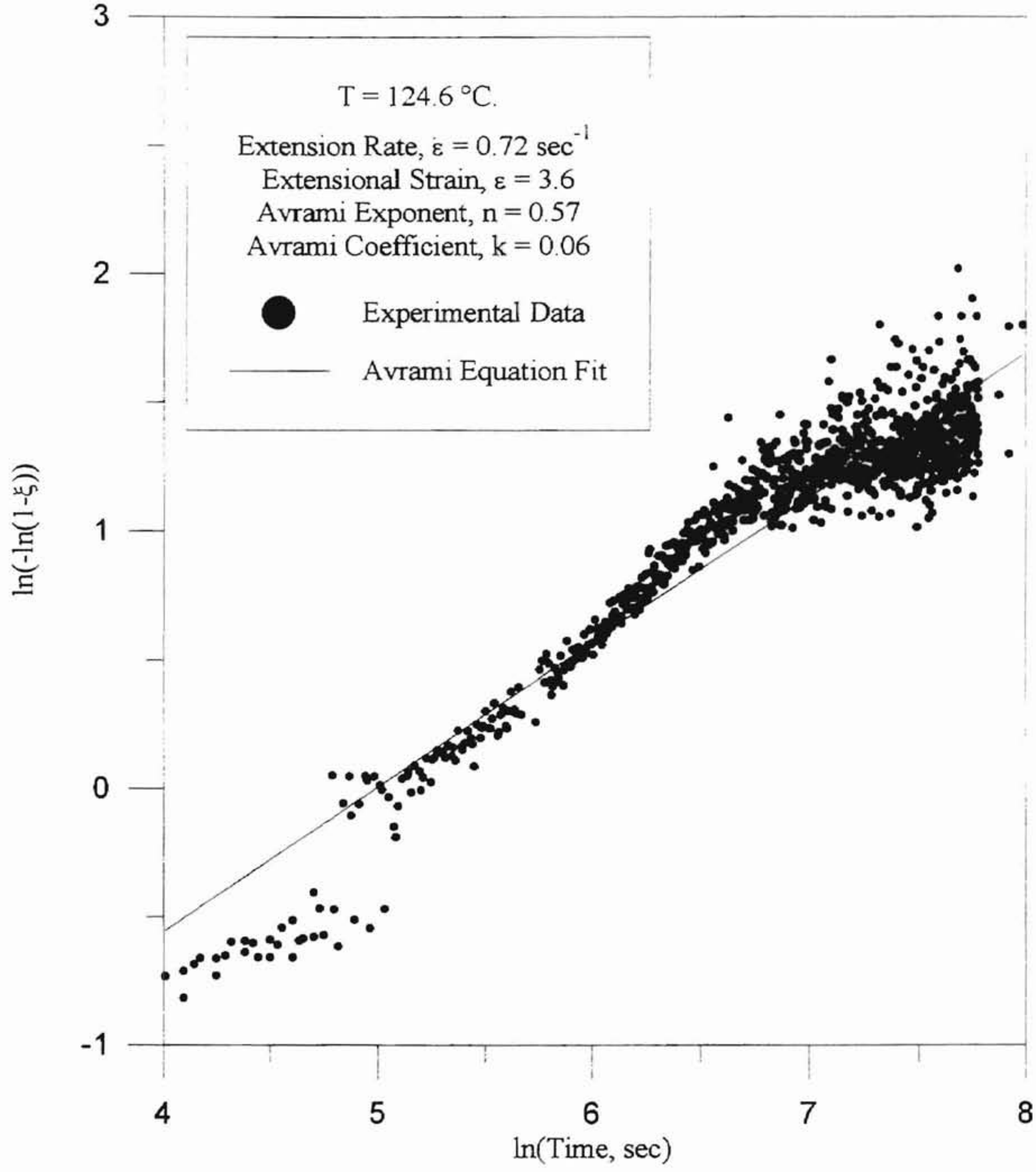

Figure 4.6 Correlation with the Avrami Equation for HDPE

Figure 4.7 shows the pixel value data obtained for PP at 150 ^{0}C. The extensional flow field was applied at t = 20 minutes, at the rate of 0.72 sec^{-1} for a total strain of 3.6. Figure 4.8 shows the pixel value data obtained for PP at 150 ^{0}C under quiescent conditions (no extensional flow field). Examination of Figure 4.7 and Figure 4.8 show that there are regions of Figure 4.7 that correspond to the three regions of Figure 4.1. Region I includes the time before the deformation in which no flow-induced crystallization occurred. Region II is characterized by a spike that marks the deformation. Region III shows the evidence of flow-induced crystallization. Interestingly, under shear flow conditions, Liedauer et al. [26] reported that the time span during which the development of the flow-induced crystallization took place after cessation of flow was found to be 600 - 800 seconds. The polymer sample used by Liedauer et al. in their experiments was PP. The time span during which the flow-induced crystallization took place for the PP sample (Figure 4.7) was ~5000 seconds whereas that for the HDPE sample (Figure 4.1) was ~2000 seconds.

The comparison of the pixel value data of PP and HDPE under both extensional flow and quiescent conditions reveals that the trend in the pixel value behavior was similar for both the materials, although the absolute pixel values were different. This is a very significant result, demonstrating that at least two semi-crystalline polymers (HDPE and PP) show flow-induced crystallization after the cessation of an extensional flow-field. However, the induction times were different for HDPE and PP. The induction time for the HDPE sample in Figure 4.1 was zero where as that for the PP sample in Figure 4.7

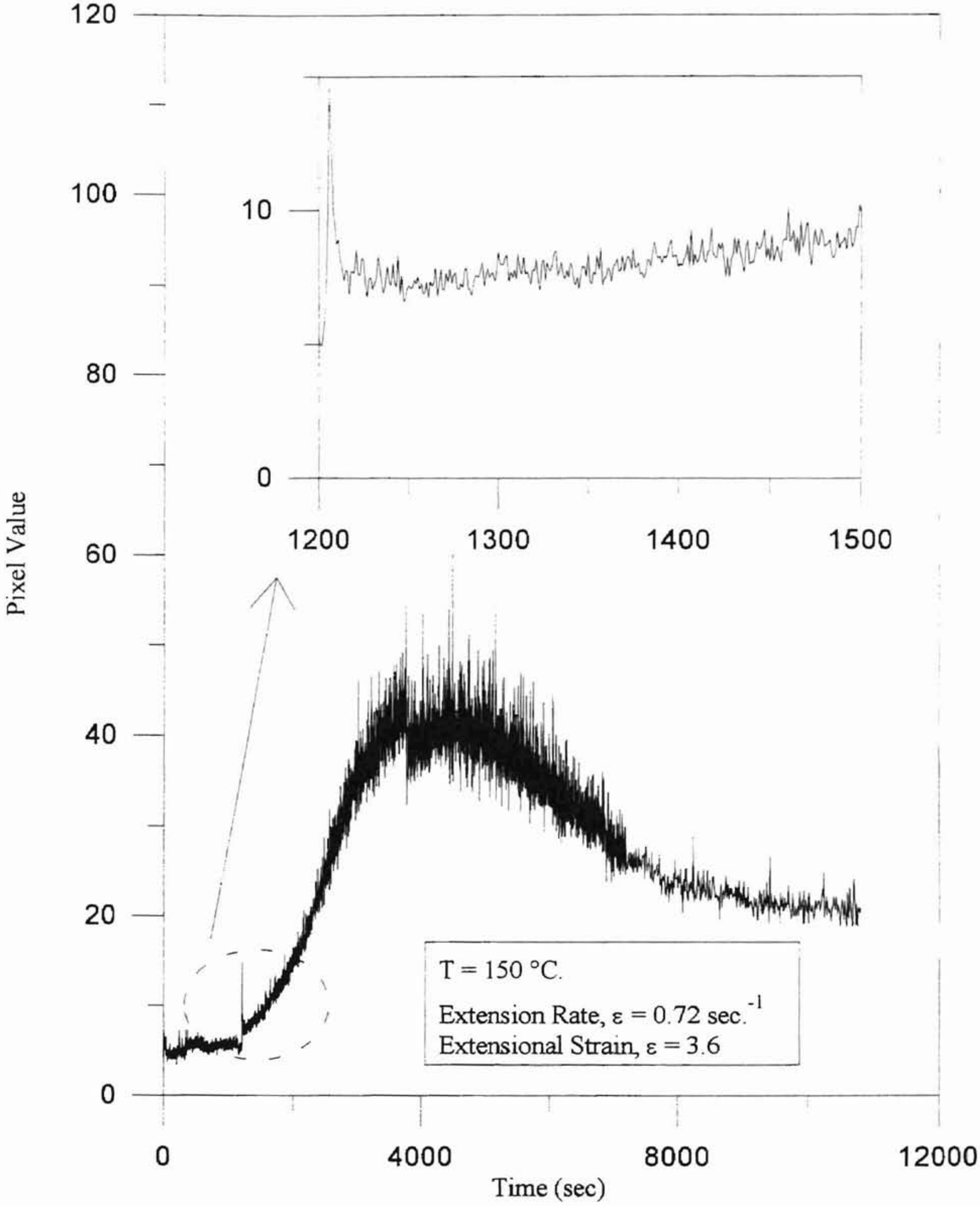

Figure 4.7 Pixel Value vs. Time for Polypropylene Under Flow

was approximately 100 seconds. The higher induction time for PP suggests that the crystal growth in the PP sample was slower as compared to the HDPE sample.

Discussion of the HDPE Data

The principal aim of the experiments was to study the effect of different extension rates on flow-induced crystallization at a constant average extensional strain. Table 4.1 summarizes all of the experiments performed with HDPE samples, including: actual extension rates, extensional strains, and the Avrami parameters. The run temperature of all the experiments was 124.6 ± 0.2 ^{0}C. Examination of the actual strain values shown in Table 4.1 indicate that the actual strain was not the same for of all the experiments. However, the actual strain values were close to 3 in most of the experiments.

The value of Avrami exponent was found to be near 0.5 for all the experimental runs. Also, the value of the Avrami coefficient was found to be between 0 and 1. Similar non-integer Avrami exponent values were reported in the literature.

Tree [4] used a blend of HDPE (minor phase) and LLDPE (carrier phase) to study flow-induced crystallization under extensional flow at ~132 ^{0}C. Tree reported Avrami exponents ranging from 2 - 4.5, but mostly the Avrami exponents were close to 2. Tree suggested that an Avrami exponent of 2 signified one dimensional crystal growth under extensional flow. Tree used the HDPE sample in the form of small cylindrical droplets whereas rectangular HDPE samples were used in the experiments reported in this thesis. Also the run temperatures were different (~132 ^{0}C and 124.6 ^{0}C respectively). Hence, the

Serial #	Actual Strain Rate (sec^{-1})	Actual Total Strain	Avrami Exponent, *n*	Avrami Coefft., *k*	Figure # (Appendix D)
1	0.76	3.8	0.94	0.006	D.1
2	0.72	3.6	0.57	0.06	D.2
3	0.29	2.9	0.37	0.22	D.3
4	1.7	3.4	0.27	0.48	D.4
5	1.68	3.35	0.5	0.06	D.5
6	0.32	3.2	0.67	0.02	D.6
7	4.0	4.0	0.19	0.74	D.7
8	3.3	3.3	0.19	0.77	D.8
9	0.16	3.2	0.46	0.09	D.9
10	0.21	4.06	0.42	0.16	D.10
11	0.16	3.06	0.69	0.015	D.11
12	3.8	3.8	0.84	0.014	D.12
13	3.36	2.47	0.79	0.017	D.13
14	3.38	2.25	0.47	0.12	D.14
15	4.51	3.61	0.29	0.46	D.15
16	5.97	3.0	0.24	0.78	D.16
17	3.95	2.37	0.45	0.16	D.17
18	6.06	3.03	0.22	0.95	D.18
19	4.06	2.44	0.76	0.015	D.19
20	6.13	3.07	0.32	0.6	D.20

Table 4.1 Avrami Parameters at 124.6 ^{0}C for HDPE

different experimental conditions seem to have been reflected in the Avrami parameters.

Auer et al. [30] reported non-integer Avrami exponents (2.1 - 2.7) for experiments under quiescent conditions. Auer et al. considered the reported Avrami exponents low. Auer et al. theorized that the low and non-integer values of Avrami exponent was due to the overlapping of primary and secondary crystallization. The overlapping reduced the overall Avrami exponent because the exponent of the secondary crystallization was relatively low.

Long et al. [29] also gave probable causes for non-integer values of the Avrami exponent obtained under quiescent conditions. The Avrami equation assumes that the value of ρ_c / ρ_l in equation (2.1) is constant during the crystallization process. The Avrami exponent, n is then uniquely related to the nucleation rate and the growth morphology of the crystallizing particles, and should assume integer values for given geometrical shapes of the particles [29]. Long et al. explained that the non-integer values of Avrami exponent may result due to the changes in ρ_c / ρ_l, nucleation rate, crystal growth rate, and morphology of growth during the crystallization process. Also, the Avrami exponent decreases if any of ρ_c / ρ_l , nucleation rate, or crystal growth rate decreases.

Figure 4.5 indicates that the crystallization rate initially increased rapidly with time and then decreased to zero. This variation in the crystal growth rate may probably have caused the Avrami exponents to assume low non-integer values.

Desai and Abhiraman [38, 39] observed significant deviations when they correlated the experimental data with the Avrami equation. The experimental data were obtained from PET filaments under shear-flow conditions. Desai and Abhiraman suggested that the deviations could be due to: (1) the transients in the heating process; (2) the framework of Avrami analysis being inconsistent with the material response; (3) the changing orientation distribution of the uncrystallized fraction during the course of crystallization. In cases in which the experimental data correlated well with the Avrami equation, the Avrami exponent values obtained by Desai and Abhiraman were consistently less than one (no quantitative values of Avrami exponents were reported). Desai and Abhiraman theorized that the Avrami exponent decreases with an increase in the precursor orientation prior to crystallization. Also, the authors suggested that the changing orientation of the uncrystallized fraction during crystallization decreased the Avrami exponent. Although the experimental data in this thesis were generated under extensional flow, the Avrami exponents obtained seem to be in qualitative agreement with those of Desai and Abhiraman. However, the experimental data in this thesis seem to be better correlated with the Avrami equation than that of Desai and Abhiraman. Table 4.2 summarizes some recent Avrami exponents reported in the literature.

Figure 4.9 shows the Avrami coefficient vs. the Avrami exponent plot. The Avrami coefficient seems inversely proportional to Avrami exponent. Figure 4.9 suggests an exponential relationship between k and n. An exponential fit to the data shown in Figure 4.9 yielded the following relationship between k and n:

$$k = 3.24e^{-7n} \tag{4.1}$$

Equation 4.1 implies that one can predict the value of Avrami coefficient for a given Avrami exponent, or vice-versa for HDPE at 124.6 ^{0}C. Hence, either of the two Avrami

Author	Experimental Conditions	Materials Used	Avrami Exponents	Comments
Tree [4]	Extensional Flow, 132 ^{0}C	HDPE (minor phase), LLDPE (carrier phase)	2 - 4.5	Mostly Avrami exponents were close to 2. One dimensional growth suggested
Auer et al. [30]	Quiescent conditions, 220 - 250 ^{0}C	Aramid fibre-reinforced poly (phenylene sulfide) (PPS)	2.1 - 2.7	The low Avrami exponent values were due to overlapping of primary and secondary crystallization
Gupta et al. [35]	extrusion, nonisothermal, 160 - 210 ^{0}C	HDPE / LLDPE blend	2 - 3	HDPE forms tridimensional and LLDPE forms two dimensional crystallites
Dainelli et al. [33]	quiescent conditions, 319 - 325 ^{0}C	phenylethyl hydroquinone	2 - 2.8	Avrami exponent depended on molecular weight distribution
He et al. [32]	quiescent conditions, 130 - 190 ^{0}C	PP	1.3 - 1.7	Avrami exponents were independent of crystallization pressure and temperature
Hammami et al. [31]	quiescent conditions, 107 - 117 ^{0}C	i-PP	~3	heterogeneous nucleation, three dimensional spherulitic growth
Desai and Abhiraman [38, 39]	Shear-Flow, 150 ^{0}C	PET filaments	< 1.0	Low Avrami exponent values attributed to changing orientation of uncrystallized fraction during crystallization

Table 4.2 Avrami Exponents Reported in the Literature

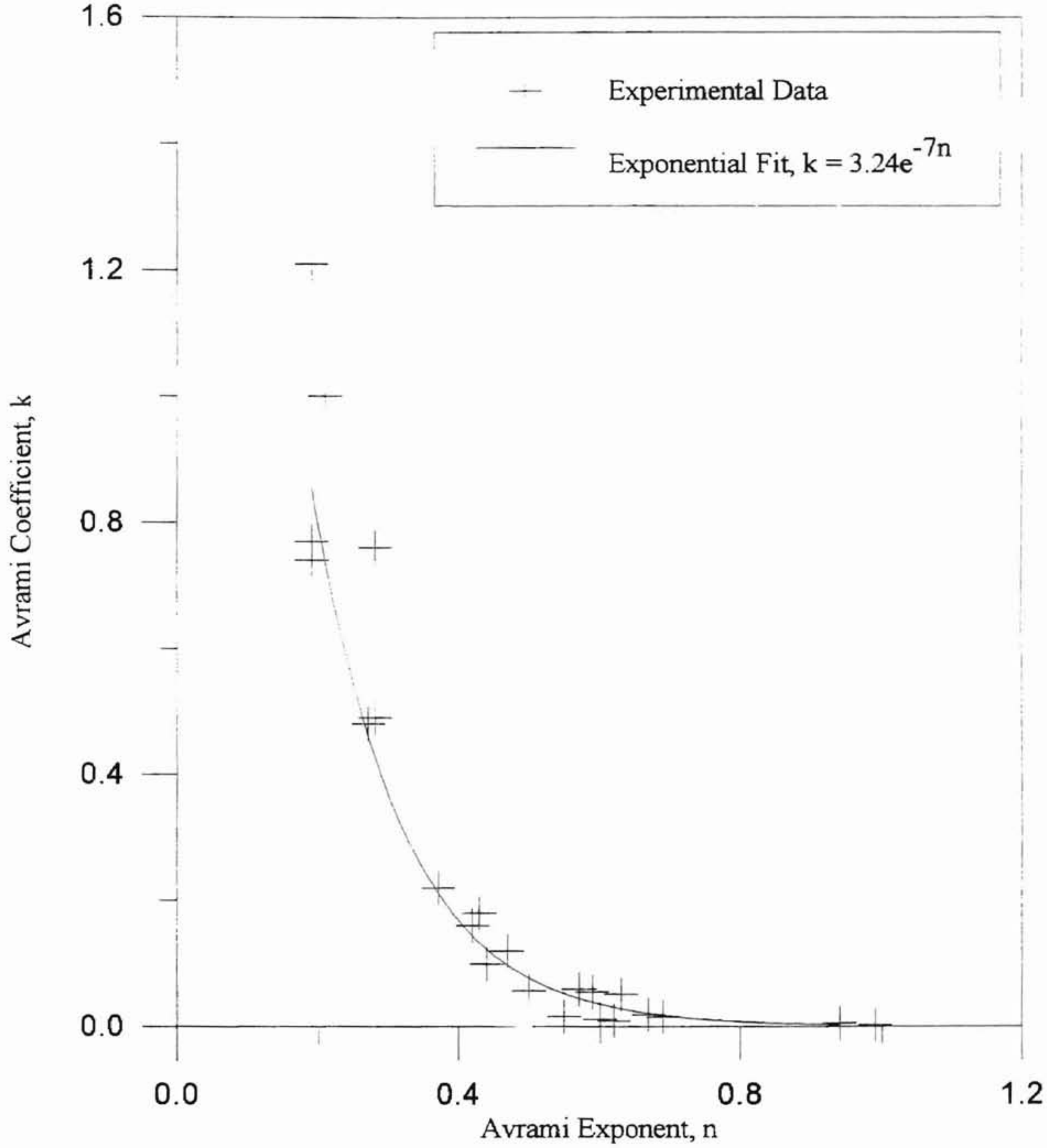

Figure 4.9 Avrami Coefficient (k) vs. Avrami Exponent (n) for HDPE at 124.6 °C

parameters seem to be adequate to characterize the crystallization kinetics of HDPE at 124.6 ^{0}C.

Figure 4.10 shows the relative retardance curves for all of the data sets given in Table 4.1. Figure 4.10 demonstrates that in all cases the relative retardance (relative crystallinity) rose rapidly at small values of time. At large values of time, the relative retardance rate (crystallization rate) slowed and gradually dropped to zero. This trend in retardance is in general agreement with the results presented by Tree [4], Guy [15], Ma [3], and Desai and Abhiraman [38, 39].

Careful examination of Figure 4.10 also shows that the curves fall into three groupings. The groupings are shown by the color coding. In general the upper group had the highest extension rates and the lower group had the lowest extension rates. This result was expected [3, 39, and 40]. However, the correlation between the rate of strain and crystallization rate was far from perfect. Specifically, the middle group of curves in Figure 4.10 did not always have extension rates in between the lower and higher grouping of curves. The lack of perfect correlation between the extension rate and the crystallization rate suggests that the experimental procedure may have some drawbacks. The probable problems associated with the experiment are discussed later in this chapter.

The slope of the relative retardance curve extrapolated to zero gives the initial crystallization or growth rate. The slope was calculated by considering the relative retardance data from the time at which the pixel value died down immediately after the cessation of flow to the time at which the pixel value attained the peak. For example, in Figure 4.5, relative retardance data from $t = 0$ seconds to $t \cong 200$ seconds would be

OKLAHOMA STATE UNIVERSITY

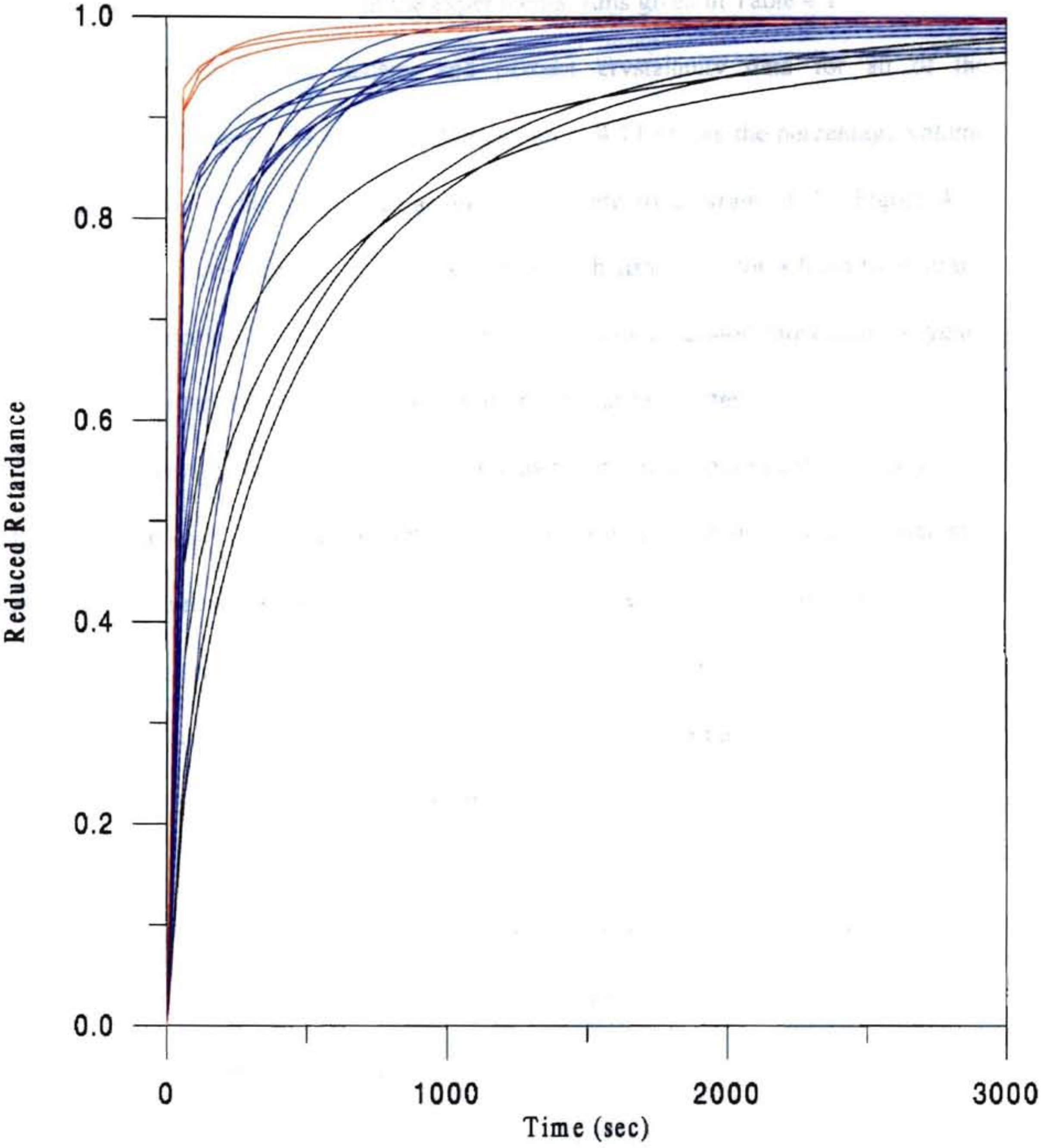

Figure 4.10 Reduced Retardance vs. Time for HDPE at 124.6 °C

OKLAHOMA STATE UNIVERSITY

considered to calculate the slope. The relative retardance at $t \cong 200$ seconds corresponds to the pixel value peak in Figure 4.1 at $t \cong 1400$ seconds. Table 4.3 summarizes the initial crystallization rates calculated for all the experimental runs given in Table 4.1.

Table 4.4 shows the density and percent crystallinity data for all of the experimental runs done at 124.6 ^{0}C for HDPE. Figure 4.11 shows the percentage volume crystallinity vs. the actual strain rate at an approximate total strain of 3. Figure 4.11 indicates that the percentage crystallinity decreases with strain rate for a fixed total strain, implying that stretching the sample for longer times at low extension rates induces higher crystallinity than stretching the sample for shorter times at high extension rates

The density of the sample used in the experiment under quiescent conditions was measured by the density gradient column to be 0.9536 g/cc. The percentage crystallinity value obtained from equation (3.9) for $\rho = 0.9536$ g/cc was: $\nu^c = 69.23\%$. Figure 4.11 indicates that for an extension rate of approximately 4 sec^{-1} and above, the percentage crystallinity obtained under extensional flow is lower than the percent crystallinity obtained under quiescent conditions. This observation tends to suggest that there may be an optimum extension rate range.

The Avrami coefficients and the Avrami exponents are shown as a function of actual strain rates in Figure 4.12 and Figure 4.13 respectively. The error bars associated with the Avrami parameters are also shown in the Figure 4.12 and Figure 4.13. The error bars were obtained from the regression analysis of the experimental data used in obtaining the Avrami parameters. The regression analysis was done using Microsoft Excel™ software.

Serial #	Avrami Exponent, n	Avrami Coefft., k	Initial Crystallization Rates x 100 (sec^{-1})
1	0.94	0.006	0.19
2	0.57	0.06	0.48
3	0.37	0.22	1.98
4	0.27	0.48	3.17
5	0.5	0.06	0.31
6	0.67	0.02	0.21
7	0.19	0.74	8.2
8	0.19	0.77	1.1
9	0.46	0.09	0.42
10	0.42	0.16	1.21
11	0.69	0.015	0.19
12	0.84	0.014	0.75
13	0.79	0.017	0.78
14	0.47	0.12	9.1
15	0.29	0.46	10.4
16	0.24	0.78	26.2
17	0.45	0.16	2.8
18	0.22	0.95	12.92
19	0.76	0.015	0.17
20	0.32	0.6	11.7

Table 4.3 Crystallization Rates at 124.6 ^{0}C for HDPE

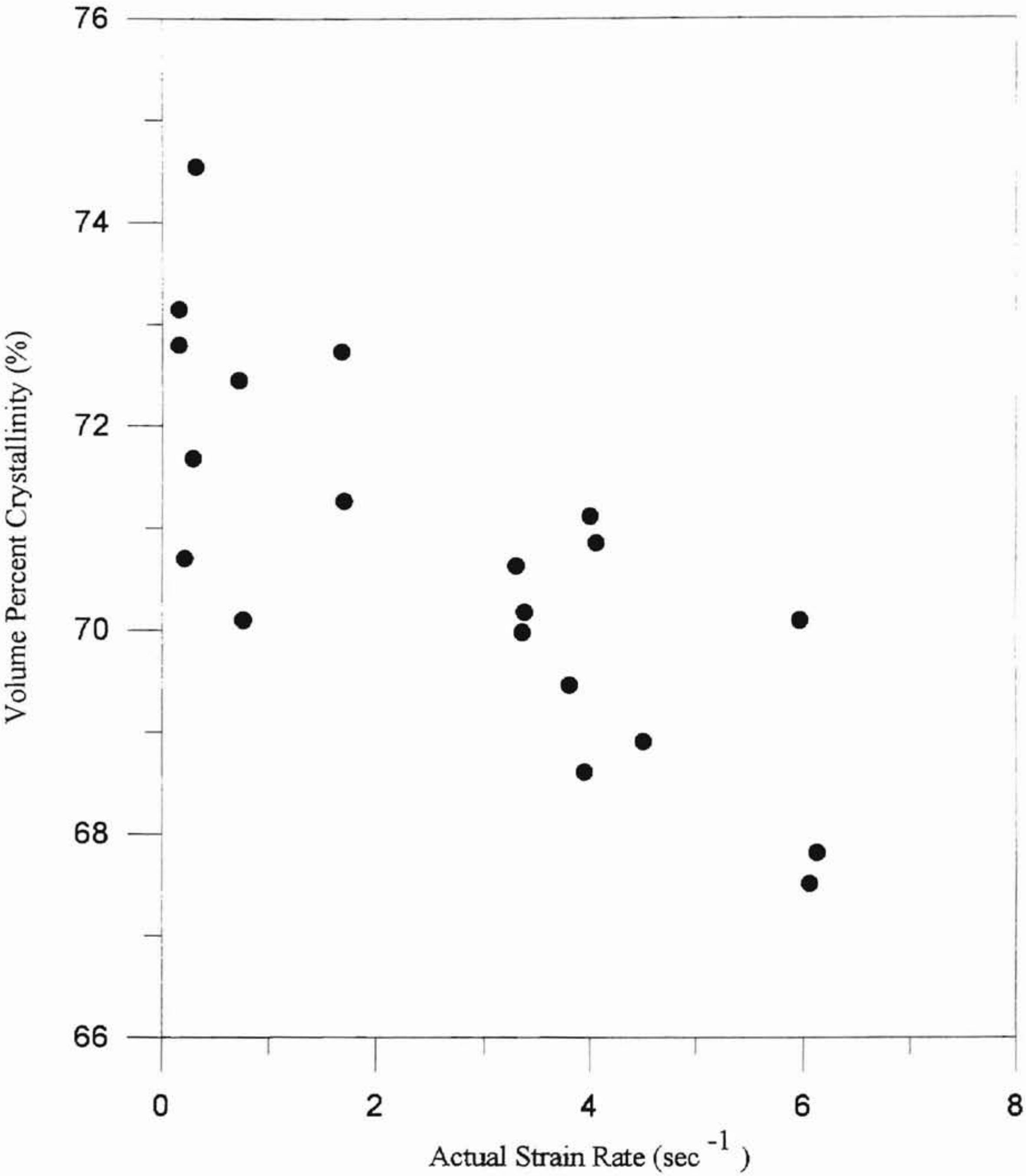

Figure 4.11 Volume Percent Crystallinity vs. Actual Strain Rate for HDPE at 124.6 °C

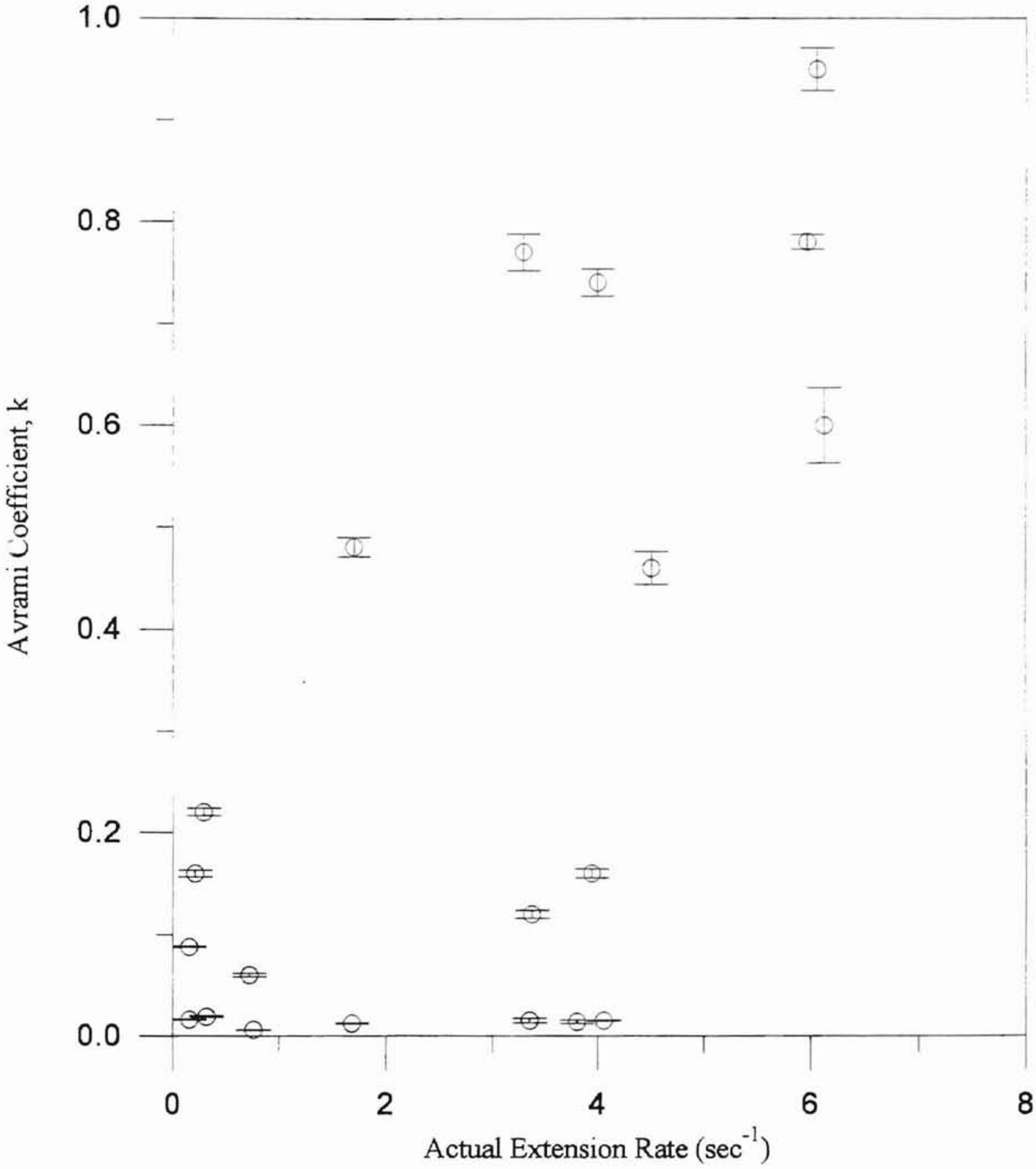

Figure 4.12 Avrami Coefficient vs. Actual Extension Rate for HDPE at 124.6 °C

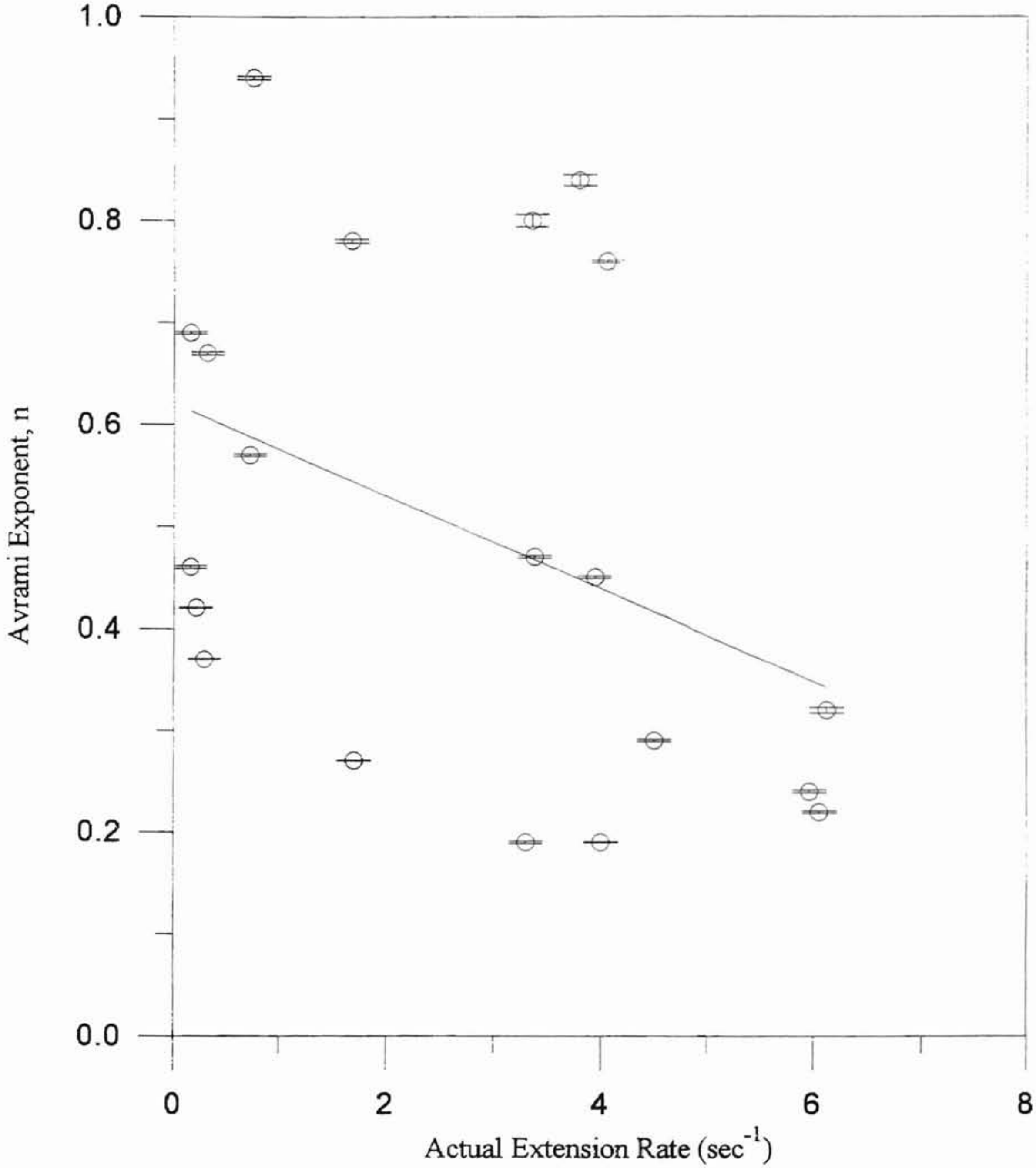

Figure 4.13 Avrami Exponent vs. Actual Extension Rate for HDPE at 124.6 °C

OKLAHOMA STATE UNIVERSITY

Figure 4.12 indicates that higher values of Avrami coefficients have larger errors associated with them. Although in many cases the Avrami coefficient seems to have higher values at higher actual strain rates, the Avrami coefficient does not seem to be vary with actual strain rate in a predictable fashion.

The plot of Avrami exponent vs. actual strain rate shown in Figure 4.13 indicates that the error associated with the Avrami exponent is small and uniform. The Avrami exponent, like the Avrami coefficient, does not seem to be a simple function of the actual strain rate. Also, Figure 4.12 and Figure 4.13 show random variation in the values of Avrami parameters. For example, at an actual strain rate of around 4 $\sec^{-1}$, the Avrami coefficients vary from 0.02 to 0.75. Similarly, the Avrami exponents vary from 0.2 to 0.8 at the actual strain rate of 4 $\sec^{-1}$.

The random variation in the Avrami parameters, and the error values associated with the Avrami parameters suggest that the Avrami parameters, and the polymer morphology in general, may be very sensitive to experimental conditions like temperature fluctuations, rate of quenching, and quenching period. The experiments were assumed to be performed under similar experimental conditions. However, the variations in the values of Avrami parameters suggest that the assumption of invariant experimental conditions may not be entirely true.

In order to narrow down the possible sources of error in the Avrami parameters, the reproducibility of the experimental data was examined. First, reproducibility within the same experiment was checked by taking data from four randomly chosen points on the sample. Figure 4.14 shows the pixel value data as a function of time at the four different

OKLAHOMA STATE UNIVERSITY

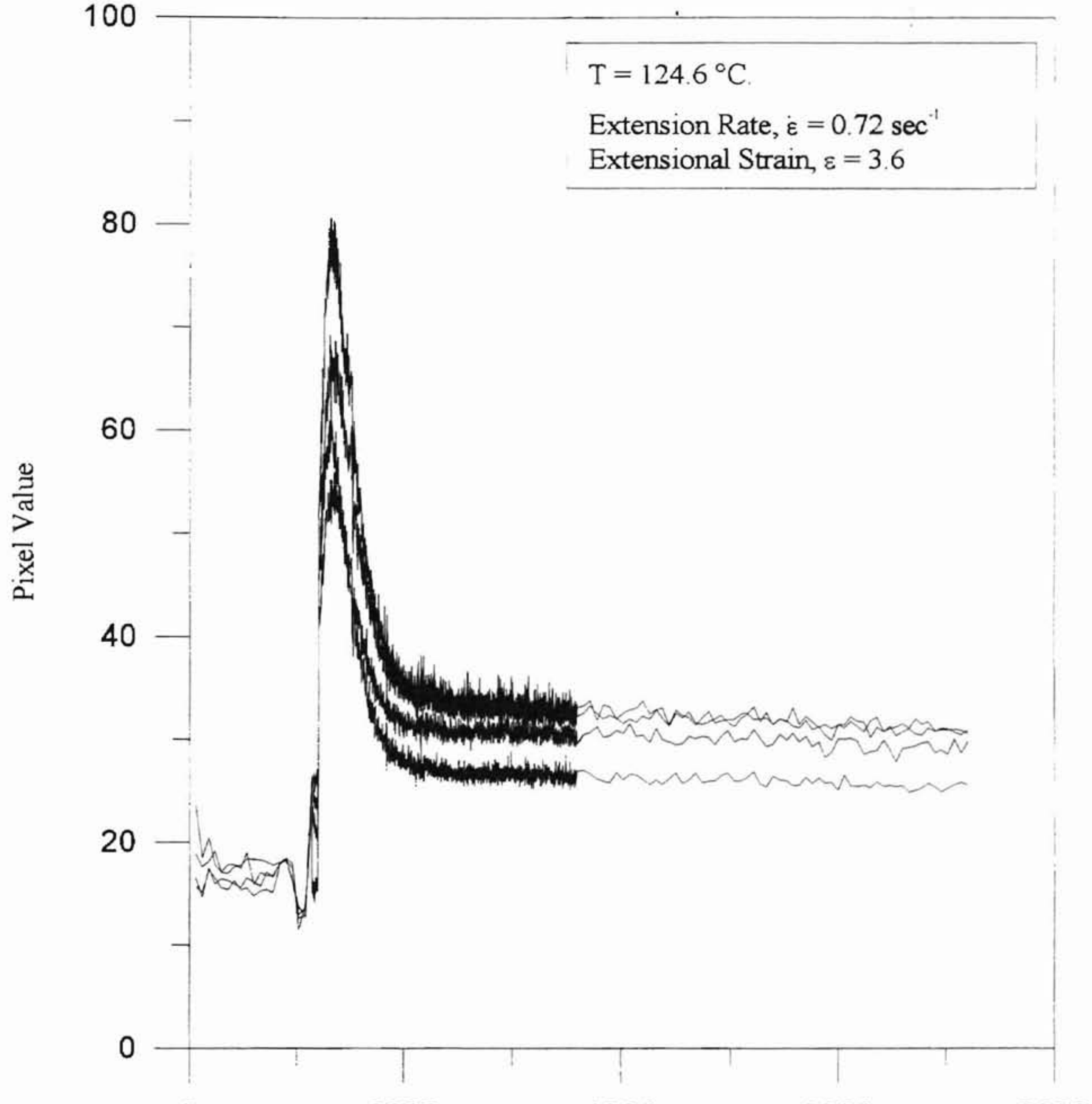

Figure 4.14 Pixel Value vs. Time for HDPE at Four Different Locations in the Sample

locations. The HDPE sample was subjected to an extension rate of 0.72 sec^{-1} for 5 seconds at 124.6 ^{0}C. The pixel values at different locations follow the same trend although the magnitudes are different. Figure 4.15 shows the corresponding reduced retardance curves. The superimposing curves indicate that the trend in retardance behavior was similar through out the sample. The pixel value and reduced retardance curves given in APPENDIX D for all the experimental runs show excellent reproducibility within a sample.

A close look at Table 4.1 reveals that there are no two experiments with exactly the same actual strains and actual strain rates. In order to check reproducibility between two experiments, one needs to have similar actual strains and actual strain rates. As stated in Chapter III, the actual extension rate experienced by the sample was different from the applied extension rate. Since the actual strain rates were measured only after the samples were stretched, it was not possible to have a prior knowledge of actual extension rates experienced by the samples. However, an attempt was made to compare two experiments with approximately the same actual strain and actual strain rates.

Table 4.1 shows that there were a few experiments with nearly the same actual strain rates and actual strains. For example, the experiments with serial numbers 1 and 2 in Table 4.1 have similar extension rates and extensional strains but the Avrami parameters were different, especially the Avrami coefficient. The Avrami coefficient of experiment 1 was 0.006 and that of experiment 2 was 0.06, which is an order of magnitude higher than that of experiment 1. The experiments with serial numbers 4 and 5, 9 and 11, 13 and 14, '8 and 20 in Table 4.1 exhibit similar variations in Avrami parameters. Note that the

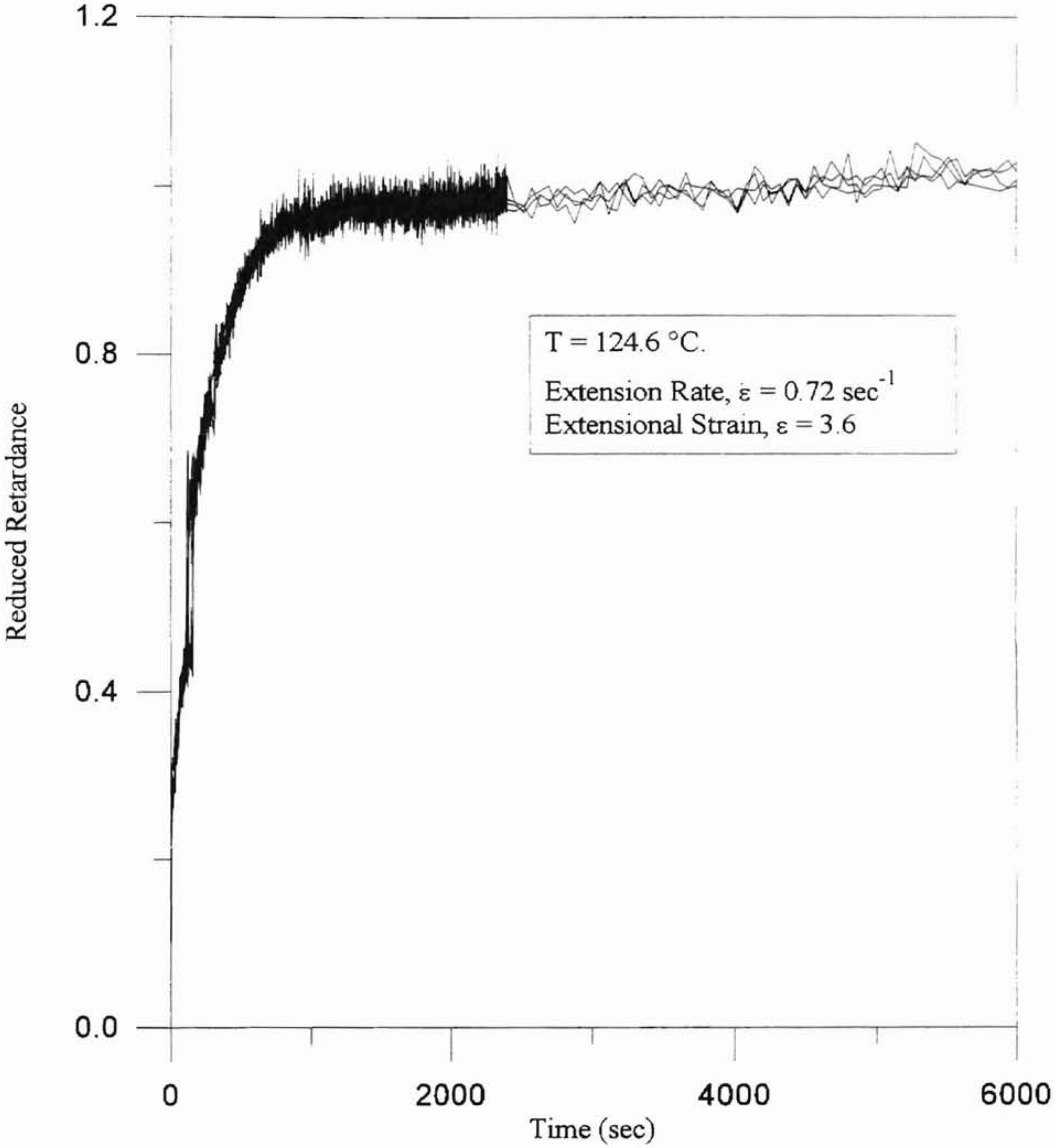

Figure 4.15 Reduced Retardance vs. Time for HDPE at Four Different Locations in the Sample

Avrami coefficients seem to vary more than the Avrami exponents between two similar experiments.

Hence, the data in Table 4.1 indicates that the reproducibility between two experiments under apparently similar conditions was not very good although reproducibility within a sample at different locations was excellent.

The oil bath temperature profile was studied in order to check whether the fluctuations in the temperature were responsible for the error in the data. Figure 4.16 shows the oil bath temperature profile as a function of time for two different set point temperatures, namely, 124.5 ^{0}C and 124.7 ^{0}C. The temperature was reduced from 135 ^{0}C to the desired set point temperature within 20 minutes, and was maintained at the set point for the rest of the experiment. For both of the experiments, the temperature fluctuation about the set point was found to be around ± 0.2 ^{0}C. Also, from Figure 4.16, it is clear that the cooling rates for both the experiments were almost identical. The negligible temperature fluctuations about the set point, and similar cooling rates between different experiments implies that the random variation in Avrami parameters may be due to some other variable(s) not taken in to account either in the experimental procedure, or in the calculations, or both.

The birefringence technique used in the experiment gave information about the phase change in the light transmitted through the polymer sample. The relative change in the amplitude of the transmitted light cannot be obtained through birefringence. One possible way to completely characterize the flow-induced crystallization phenomena

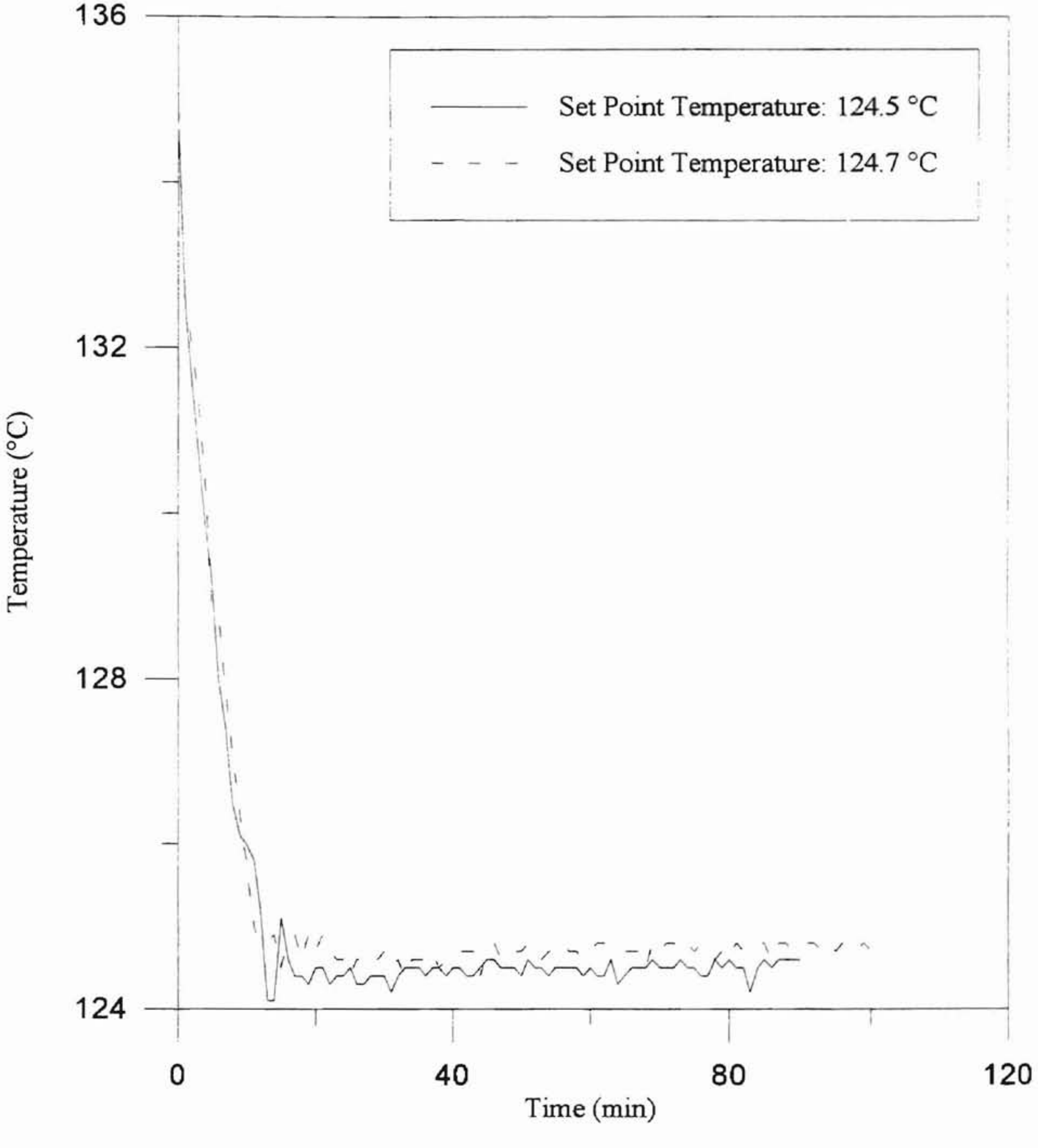

Figure 4.16 Oil Bath Temperature Profile as a Function of Time

OKLAHOMA STATE UNIVERSITY

occurring in the polymer sample is to interpret the experimental data by obtaining both the phase change and amplitude change information of the transmitted light.

The relative change in amplitude of the transmitted light is defined as dichroism [15]. Dichroism is typically several orders of magnitude smaller than birefringence [15], and was ignored in the experiments presented in this chapter. The experimental data presented in this chapter indicated that the pixel value was very small before the extensional flow-field was applied at t = 20 minutes. The low pixel value indicates the formation of nucleation sites in the sample. The pixel value obtained during the quenching period and before the application of the extensional flow-field may not be yielding complete information about the transformations occurring in the sample. Dichroism and birefringence measurements during the quenching period (t = 0 - 20 minutes) and after the cessation of flow may give the critical information needed to fully characterize the flow-induced crystallization phenomenon in the sample. Also, combined studies of dichroism and birefringence data may explain the inconsistencies shown in the experimental data. Hence, combined measurements of dichroism and birefringence are strongly recommended to be incorporated in the experimental setup. Also, experiments at different quenching periods (10 min., 15 min., 25 min. etc.) are suggested to be performed in order to study the effect of quenching period on the pixel value behavior shown by the polymer sample.

OKLAHOMA STATE UNIVERSITY

Comparion with Previous Results

The extensional flow-induced crystallization kinetics data generated by the current experimental technique were compared with the results presented by Guy [15] and Ma [3].

For example, Figure 2.1 shows the experimental data presented by Guy at 133 ^{0}C, and at an extension rate of 0.03 sec^{-1}. Figure 2.1 indicates that the intensity of the transmitted light increased during flow, and decreased rapidly after the cessation of flow-field. The intensity again increased afterwards to a maximum value due to flow-induced crystallization, and then reduced. This behavior is consistent with our experimental data shown in Figure 4.1. Both data sets are also in agreement with the generalized intensity of the transmitted light for a typical flow-cessation experiment presented by Guy in Figure 2.2.

Figure 2.3 shows the experimental data obtained by Ma. The experiment was done at 125 ^{0}C under an extension rate of 0.03 sec^{-1}, and a total extensional strain of 0.60. Figure 2.3 indicates that the intensity of transmitted light reduced after the cessation of flow, and then increased to a maximum, and then decreased. The experimental data shown in Figure 4.1 shows the same behavior. However, experiments done by Ma at higher extension rates showed a repeated increase and decrease in the intensity of transmitted light after the cessation of flow. For example, Figure 2.4 shows the data obtained by Ma at 125 ^{0}C under an extension rate of 0.24 sec^{-1}, and a total strain of 0.72. This behavior in the intensity of transmitted light was not seen in the experimental data presented in this thesis at either low or high extension rates.

Both Alvarez [18] and Kobayashi [19] reported that crystallization was a function of strain. Alvarez used a traction machine to study crystallization in polyisobutylene (PIB) at different Hencky strains. Kobayashi used a Meissner type rheometer to study crystallization in composite systems. The experimental data presented in this thesis were

OKLAHOMA STATE UNIVERSITY

obtained at various strain rates, but the average strain was kept constant. In order to compare the data with that of Alvarez and Kobayashi, experimental data at different strains are required. The experimental data presented in this thesis suggests that for a fixed average strain, the relative crystallinity increases with time for all strain rates in the range 0.29 - 6.13 sec^{-1}. Hence, the data presented in this thesis are not adequate enough to either support or contradict the observations made by Alvarez and Kobayashi.

Ness et al. [25] carried out extrusion experiments with the HDPE samples at temperatures ranging from 160-200 ^{0}C and at shear rates ranging from 50 - 1000 sec^{-1} Ness et al. observed that shear-induced crystallization was easily produced at temperatures near the melting point of the samples, even though the shear rate was not high. The experiments with HDPE presented in this thesis were done at a temperature of 124.6 ± 0.2 ^{0}C, which is near the melting point of HDPE (132 ^{0}C). The lowest extension rate reported in this thesis was 0.29 sec^{-1}. Interestingly, the HDPE samples exhibited flow-induced crystallization at the extension rate of 0.29 sec^{-1}. As experiments with extension rates lower than 0.29 sec^{-1} were not performed, one is not clear whether flow-induced crystallization in the HDPE samples can be observed at extension rates lower than 0.29 sec^{-1}. Nevertheless, the experimental data are in qualitative agreement with the observation of Ness et al. that crystallization can be produced at low shear rates at a temperature near the melting point of the sample.

CHAPTER V

SUMMARY, CONCLUSIONS AND RECOMMENDATIONS

Summary

A new and efficient experimental technique was used to generate considerable amount of kinetic data in order to study flow-induced crystallization in semi-crystalline polymers under extensional flow field. HDPE, PP, and PS were used in the experiments to generate the kinetic data. The experimental setup involved a crystallization rheometer, a video-optic technique, and a data logging system. The crystallization rheometer was used to induce an extensional flow field on the polymer sample, the video-optic technique was used to observe and record the birefringence behavior of the sample, and the data logging system was used to record the torque acting on the sample. The experimental data were compared to the Avrami theory. The experimental data presented in this thesis are expected to benefit flow-induced crystallization model development and the optimization of polymer processing operations.

Conclusions

1. A faster and more efficient method to prepare samples has been developed. The sample preparation time has been reduced from 8 hours to 1 hour.
2. Floatation of the sample during the experiment has been arrested to a large extent. The samples were covered with aluminum foil, except for the region where birefringence was to be measured. Covering the sample with aluminum foil sufficiently held the sample in place.
3. The data acquisition process has been automated by means of a computer program and large amounts of data has been collected for various extension strain rates and strains with less effort.
4. The experimental technique was used successfully to generate birefringence data for HDPE, PP, and PS. The birefringence data were then converted to crystallization kinetics data.
5. Under quiescent conditions, HDPE, PP, and PS did not show flow-induced crystallization. This important result indicates that stress field is required to observe flow-induced crystallization in crystallizable polymers.
6. PS, which is a non-crystallizing material, did not show flow-induced crystallization in an extensional flow field. The experiments with the PS samples proved that the increase in the pixel value during extensional flow was due to polymer molecules orienting under the applied stress, and not due to crystallization.

OKLAHOMA STATE UNIVERSITY

7. The experimental data obtained for HDPE and PP were in qualitative agreement with that presented by Tree [4], Guy [15], and Ma [3]. HDPE and PP showed similar birefringence behavior under extensional and quiescent conditions. This significant result demonstrates that at least two semi-crystalline polymers (HDPE and PP) show flow-induced crystallization after the cessation of an extensional flow-field.
8. The experimental data obtained from the HDPE samples under extensional flow correlated very well with the Avrami equation. The Avrami exponent was found to be around 0.5 ± 0.2, and the Avrami coefficient was < 1 for HDPE at 124.6 ^{0}C. However, the Avrami parameters failed to give any physical insights.
9. The reduced retardance (relative crystallinity) increased rapidly with time at small values of time. At large values of time, the crystallization rate slowed and gradually dropped to zero.
10. The data obtained in an experiment at different locations on the HDPE sample were reasonably reproducible. However, data obtained from two experiments performed under similar conditions for a polymeric material were not consistent.

Recommendations

1. The crystallization rheometer and the video-optic technique can be used to further study flow-induced crystallization in semi-crystalline polymers such as HDPE, PP, and other crystallizable polymers.

OKLAHOMA STATE UNIVERSITY

2. The kinetic data generated for HDPE were at 124.6 ^{0}C. Data generation at other temperatures is recommended to understand the effect of temperature on flow-induced crystallization kinetics.
3. The sample quenching period was fixed at 20 minutes. Experiments at different quenching periods, for example, 15, 25, and 30 minutes are recommended in order to understand the effect of quenching period on flow-induced crystallization.
4. As crystallization kinetics data of PP obtained in this thesis were limited, more experiments need to be done with PP and other crystallizable resins in order to study flow-induced crystallization in materials in addition to HDPE.
5. Combined studies of dichroism and birefringence need to be done to fully estimate the extent of flow-induced crystallization in a crystallizable polymer sample.
6. The problems associated with reproducibility of the data need to be addressed. One possible way to overcome the reproducibility problems could be by identifying an appropriate set of experimental conditions at which data from different runs would be consistent.

OKLAHOMA STATE UNIVERSITY

REFERENCES

1 Boiko, Y. M., Brostow W., Goldman, A. Y., and Ramamurthy, A. C., "Tensile, Stress Relaxation and Dynamic Mechanical Behavior of Polyethylene Crystallized from Highly Deformed Melts", Polymer, 36, 7 (1995).

2 Elyashevich, G. K., Karpov, E. A., Rosova, E. Y., and Streltses, B. V., "Orientational Crystallization and Orientational Drawing as Strengthening Methods for Polyethylene", Polymer Engineering and Science, 33, 20 (1993).

3 Ma, Sheng, "The Crystallization Kinetics of Polyethylene in Extensional Deformation", M.S Thesis (Chemical Engineering), Oklahoma State University, Stillwater, Oklahoma (1994).

4 Tree, D. A, "Crystallization Kinetics of Polymer Melts in Extensional Flow", Ph.D. Thesis (Chemical Engineering), University of Illinois, Urbana, Illinois (1990).

5 Siddiquee, M.S Thesis (Chemical Engineering), Oklahoma State University, Stillwater, Oklahoma (1992).

6 Van der Vegt, A. K., and Smit, P. P. A., "Crystallization Phenomena in Flowing Polymers", S. C. I. Monograph, 26, 313 (1967).

7 Seiglaff, C. I., and O'leary, K. J., "Rheological Phase Transitions in Polypropylene", J. Macromol. Sci. Phy., B2(4), 793 (1968).

8 Seiglaff, C. I., and O'leary, K. J., "Melting Transitions of Polypropylene", Trans. Soc. Rheol., 14:1, 49 (1970).

9 Southern, J. H., and Porter, R. S., "The Properties of Polyethylene Crystallized Under the orientation and Pressure Effects of a Pressure Capillary Viscometer", J. Appl. Polym. Sci., 14, 2305 (1970).

10 Southern, J. H., and Porter, R. S., "Melting Behavior of Polyethylene Crystallized in a Pressure Capillary Viscometer", J. Polym. Sci., A-2, 10, 1135 (1972).

OKLAHOMA STATE UNIVERSITY

11 Tsebrenko, M. V., Reganova, N. M., and Vinogradov, G. V., "Rheology of Molten Blends of Polyoxymethylene and Ethylene-Vinyl Acetate Copolymer and the Microstructure of Extrudates as a Function of Their Melt Viscosities", Polym. Eng. Sci., 20, 1023 (1980).

12 McHugh, A. J., and Tree, D. A., "Fiber Formation During Capillary Flow of Crystallizable Blends", Int. Polym. Process., II:3/4, 223 (1988).

13 Sakellarides, S. L., and McHugh, A. J., "Structure Formation During Polymer Blend Flows", Polym. Eng. Sci., 27(22), 1662 (1987).

14 McHugh, A. J., Guy, R. K., Tree, D. A., "Extensional Flow-Induced Crystallization of a Polyethylene Melt", Colloid and Polymer Science, 271, 629 (1993).

15 Guy, R. Kirk, "A Study of Flow-Induced Crystallization in Two-Phase Polymer Melts", Ph.D. Thesis (Chemical Engineering), University of Illinois, Urbana, Illinois (1992).

16 Meissner, J., Raible, T., and Stephenson, S. E., J. Rheology, 25, 1 (1981).

17 Agarwal, U. S., Khakhar, D. V., "Shear Flow Induced Orientation Development during Homogeneous Solution Polymerization of Rigid Rodlike Molecules", Macromolecules, 26, 3960 (1993).

18 Alvarez, A. G., Assenza, G., Legrand, J. F., and Piau, J. M., "Elongational Viscosity and Flow Crystallization of Polymer Melts", C. R. Acad. Sci. Paris, t. 320, Series II, 23 (1995).

19 Kobayashi, M., Takahashi, T., Takimoto, J., and Koyama, K., "Flow-Induced Whisker Orientation and Viscosity for Molten Composite Systems in a Uniaxial Elongational Flow Field", Polymer, 36, 3927 (1995).

20 Citra, M. J., Chase, D. B., Ikeda, R. M., and Gardner, K. H., "Molecular Orientation of High-Density Polyethylene Fibers Characterized by Polarized Raman Spectroscopy", Macromolecules, 28, 4007 (1995).

21 Lafrance, C. P., Debrigare, J., and Prud'Homme, R. E., "Study of Crystalline Orientation in Drawn Ultra-High Molecular Weight Polyethylene Films", Journal of Polymer Science: Part B: Polymer Physics, 31, 255 (1993).

22 Lei, H., and Zhao, Y., "Stress-induced Orientation in Polymer Blends Containing a Side-chain Liquid Crystalline Polymer", Polymer, 35, 104, (1994).

OKLAHOMA STATE UNIVERSITY

23 Goschel, U., Deutscher, K., and Abetz, V., "Wide-angle X-ray Scattering Studies Using an Area Detector: Crystallite Orientation in Semicrystalline PET structures", Polymer, 37, 1 (1996).

24 Salem, D. R., "Crystallization During Hot-Drawing of Poly(ethylene terephthalate) Film: Influence of Temperature on Strain-rate/Draw-time Superposition", Polymer, 35, 771 (1994).

25 Ness, J. N., Liang, J. Z., "A Study of Rheological Properties and Crystallization Behavior for HDPE Melts During Extrusion", Journal of Applied Polymer Science, 48, 557 (1993).

26 Liedauer, S., Eder, G., and Janeschitz-Kriegl, H., "On the Limitations of Shear Induced Crystallization in Polypropylene Melts", International Polymer Processing X, 3, 243 (1995).

27 Pathmanathan, K., and Johari, G. P., "The Effect of Increased Crystallization on the Electrical Properties of Nylon-12", Journal of Polymer Science: Part B: Polymer Physics, 31, 265 (1993).

28 Hsiung, C. M., and Cakmak, M., "Effect of Injection-Molding Conditions on the Crystallinity, Orientation Gradients, and Mechanical Properties of Poly(aryl ether ketone). II. Large Dumbbell Parts", Journal of Applied Polymer Science, 47, 149 (1993).

29 Long, Y., Shanks, R. A., and Stachurski, Z. H., "Kinetics of Polymer Crystallization", Progress in Polymer Science, 20, 651 (1995).

30 Auer, C., Kalinka, G., Krause, T., and Hinrichsen, G., "Crystallization Kinetics of Pure and Fiber-Reinforced Poly(phenylene sulfide)", Journal of Applied Polymer Science, 51, 407 (1994).

31 Hammami, A., and Spruiell, J. E., "Quiescent Nonisothermal Crystallization Kinetics of Isotactic Polypropylenes", Polymer Engineering and Science, 35, 797 (1995).

32 He, J., and Zoller, P., "Crystallization of Polypropylene, Nylon-66 and Poly(ethylene terephthalate) at Pressures to 200 MPa: Kinetics and Characterization of Products", Journal of Polymer Science: Part B: Polymer Physics, 32, 1049 (1994).

33 Dainelli, D., and Chapoy, L. L., "Morphology and Crystallization Kinetics of a Rigid Rod, Fully Aromatic, Liquid Crystalline Copolyester", Macromolecules, 26, 385 (1993).

34 Hieber, C. A., "Correlations for the Quiescent Crystallization Kinetics of Isotactic Polypropylene and Poly(ethylene terephthalate)", Polymer, 36, 1455 (1995).

OKLAHOMA STATE UNIVERSITY

35 Gupta, A. K., Rana, S. K., and Deopura, B. L., "Crystallization Kinetics of High-Density Polyethylene/Linear Low-Density Polyethylene Blend", Journal of Applied Polymer Science, 51, 231 (1994).

36 Bird, R. B., Armstrong, R. C., Hassager, O., "Dynamics of Polymeric Liquids, Volume 1, Fluid Mechanics", Second Edition, John Wiley and Sons, (1987).

37 Wunderlich, B., "Macromolecular Physics", Volume 1, Academic Press (1973).

38 Desai, P., Abhiraman, A. S., "Fundamental Aspects of Stress, Deformation, and Phase Transitions in Crystallizable Polymers: Experiments with Poly(ethylene terephthalate) in Uniaxial Stress Fields", J. Polym. Sci.: Part B: Polymer Physics, 26, 1657-1675 (1988).

39 Desai, P., Abhiraman, A. S., "Crystallization in Oriented Poly(ethylene terephthalate) Fibers. I. Fundamental Aspects", J. Polym. Sci. Polym. Phys. Ed., 23, 653-674 (1985).

40 "Compumotor User Guide", Compumotor Division, Parker Hannifin Corporation, USA, (1991).

41 "Compumotor Software Reference Guide", Compumotor Division, Parker Hannifin Corporation, USA, (1991).

42 "Model #08109-25 15-bit A/D Card", Cole-Parmer Instrument Company, USA, (1993).

43 "Model #08109-35 Mv/Amplifier/Multiplexer", Cole-Parmer Instrument Company, USA, (1993).

44 "Model #08109-32 Data Logging Software Package", Cole-Parmer Instrument Company, USA, (1993).

45 "DT2853 User Manual", Data Translation, Inc. USA, (1991).

OKLAHOMA STATE UNIVERSITY

APPENDIXES

OKLAHOMA STATE UNIVERSITY

APPENDIX A:

COMPUMOTOR CONTROL COMMANDS

The Compumotor was used to generate the required extensional flow field in the experiment. The Compumotor was controlled by means of a software in the C:\WARE sub-directory. High-level programming commands in X-language can be given to move the rollers in the desired direction at a given rotational speed and duration of rotation. The software was run by typing "RUN" at the system prompt and the "Terminal Emulator" menu option was selected to program the motor. The most commonly used X-language commands are illustrated below with comments :

Command	Comment
>LD2	disable the hardware limits
>1LD	check the state of the hardware limits
> H-	move the rollers in the counter-clockwise direction
> V0.5	set the rotational speed to 0.5 rotations per sec.
>D2500	set the distance to 2500 steps
>T60	wait for 60 sec. before executing the next command in the buffer

OKLAHOMA STATE UNIVERSITY

>G run the motor

A more detailed description along with other commands and programming techniques can be found in [40, 41].

OKLAHOMA STATE UNIVERSITY

APPENDIX B:

DATA LOGGING SYSTEM

The torque acting on the polymer sample during the experiment was recorded by a Cole-Parmer's data logging system. The data logging system consists of a #08109-25 (Model 14C) Analog Interface card, a #08109-35 (Model 20A) Mv/Amplifier/Multiplexer, and a #08109-32 Data Logging software package.

"The #08109-25 (Model 14C) Analog Interface card enables an IBM PC computer to translate continuously variable analog voltages into their digital equivalents of ones and zeros. The interface card also provides a means for the computer to turn external equipment on and off. There are four small switches in the upper left corner of the card. The switch 4 should be in the "ON" position and the other switches should be in the "OFF" position. This will map the Analog Interface into input locations 772 through 775. The connector pinout is shown in Table B.1." [42].

"The #08109-35 (Model 20A) Mv/Amplifier/Multiplexer in combination with the Model #08109-25 (Model 14C) A/D card allows a personal computer to be used as a multi-channel millivoltmeter. The Mv/Amplifier/Multiplexer delivers highly accurate and

OKLAHOMA STATE UNIVERSITY

PIN 8 . . . CHANNEL 1+

PIN 7 . . CHANNEL 2+

PIN 6 . . . CHANNEL 0+

PIN 5 . . . CHANNEL 3+

PIN 4 . . . GROUND

PIN 3 . . . GUARD

PIN 2 . . . OUTPUT D

PIN 1 . . . OUTPUT A

PIN 15 . . . CHANNEL 1-

PIN 14 . . . CHANNEL 2-

PIN 13 . . . CHANNEL 0-

PIN 12 . . . CHANNEL 3-

PIN 11 . . . DIGITAL INPUT

PIN 10 . . . OUTPUT C

PIN 9 . . . OUTPUT B

Table B.1 Connector Pinout [43]

OKLAHOMA STATE UNIVERSITY

stable data when properly applied. The Mv/Amplifier/Multiplexer is connected to the A/D card as shown in Figure B.1." [43].

The Data Logging software package is a menu driven user-friendly data acquisition package. The software package can acquire torque data at a maximum rate of 3 data points per second. The data can be continuously displayed on the screen as well as stored in a file or charted on a printer. The software package can accept analog input from a maximum of 64 channels and up to 4 multiplexers can be used. The description of the software and the commands is detailed in [44].

The Data Logging System was calibrated before it was used in the experiment. First the software was run by typing "LOG_SRCA" at the system prompt and "Configure System" menu option was selected from the main menu of the program. Then "define the data point" menu option was selected. Then the following steps were taken :

1. The offset factor was set to zero and the scaling factor was set to one on the screen.
2. The dial was set to zero on the torque meter installed on the crystallization rheometer.
3. The corresponding digital value from the "Formatted reading " location on the screen was noted.
4. The dial was set to various other positions and the corresponding values from the "Formatted reading" location were noted.

The digital value vs. torque was plotted on the Y - X axes and the slope and intercept of the line were then determined. The digital value displayed on the screen varies as:

$$V = m.x + c \qquad \text{(B1)}$$

OKLAHOMA STATE UNIVERSITY

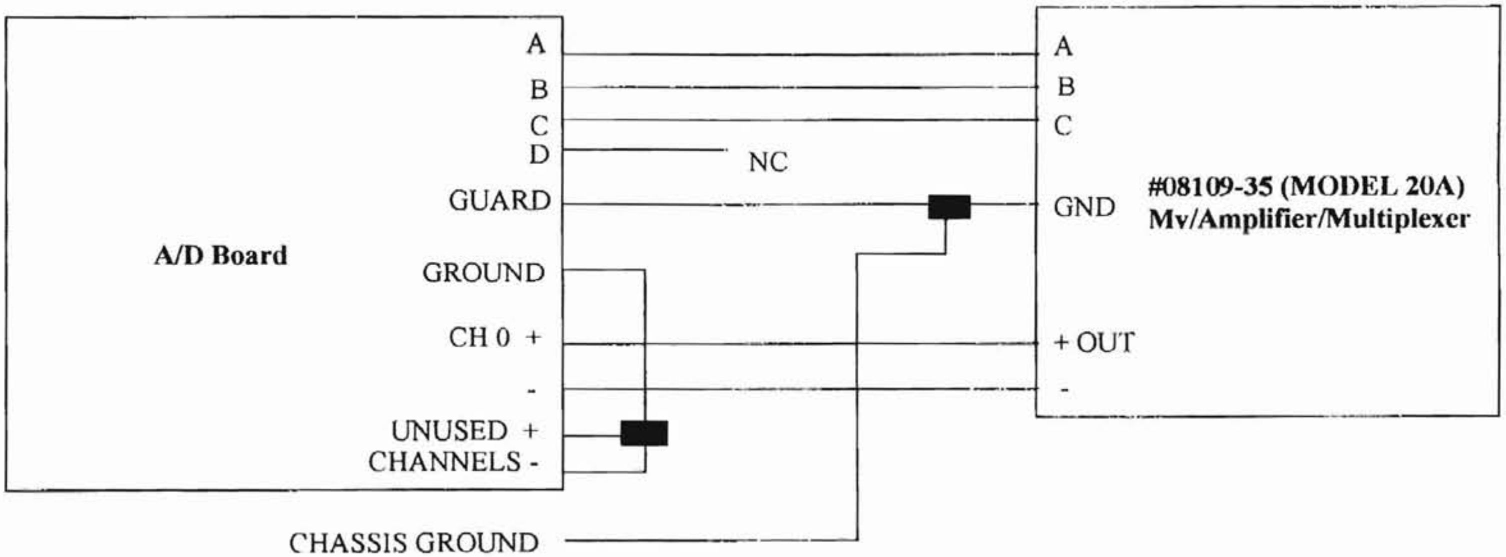
A/D Board
A
B
C
D
GUARD
GROUND
CH 0 +
-
UNUSED +
CHANNELS -
NC
CHASSIS GROUND
A
B
C
GND
+ OUT
-
#08109-35 (MODEL 20A)
Mv/Amplifier/Multiplexer

Figure B.1 Interconnection Diagram of the Analog Interface Card and the Mv/Amplifier/Multiplexer [43]

OKLAHOMA STATE UNIVERSITY

where

x = dial position on the torque meter,

V = voltage equivalent shown on the screen,

m = slope of the line,

c = intercept on the Y-axis.

In order to display the value of torque on the screen instead of its voltage equivalent, Equation (B1) was rewritten as:

$$x = (1/m).(V - c) = S.(V + O) \qquad \text{(B2)}$$

where

S = scaling factor = $1/m$

O = offset factor = $-c$.

These new values of the scaling factor and the offset factor were then incorporated into the software.

OKLAHOMA STATE UNIVERSITY

APPENDIX C:

VIDEO IMAGE TECHNIQUE

A DT2853 Frame Grabber installed in the computer was used to digitize the experimental data recorded on the video tape into pixel values. The VCR and the monitor can be connected to the DT2853 Frame Grabber by following the directions and the wiring connection diagrams given in [45].

A sophisticated image processing software package in the C:\IRIS-T sub-directory was used to obtain the pixel values. The software digitizes the video input signals and displays them on the monitor in the form of pixels. A pixel value of 0 corresponds to zero light intensity and a pixel value of 255 corresponds to maximum light intensity. By updating the videotape frame by frame and by placing the cursor at different locations on the video image, pixel values were obtained. A complete description of all the commands to operate and program the DT2853 Frame Grabber is given in DT2853 User Manual [45].

Data acquisition by using this software package was tedious because of the continuous user interaction required to obtain the pixel values. Therefore, a computer program was written to automate the data acquisition process. The program is listed at

OKLAHOMA STATE UNIVERSITY

the end of APPENDIX C. The program can be used to get the pixel values simultaneously at various locations on the flow field and the values obtained can be stored in a file. The location can be a single point or a rectangular area in which case the pixel value is the average of all the pixel values in the area. Also, the pixel values can be obtained at a given time interval. For example, one can specify that the first 1 hour of the recording be used to get pixel values at every 1 second and the next 2 hours of recording be used to obtain pixel values at every 60 seconds, etc.. In order to use the program, an input data file must be created with the desired pixel locations and time intervals specified. A sample input data file may look something like this:

2	no. of time slices
3	no. of locations at which pixel values are required
60 1.0	time slice 1 : 60 min. duration at 1 sec time intervals
100 200 10 10	location 1 : 10 x 10 rectangular area with top left corner at (100,200)
250 135 10 10	location 2
350 250 10 10	location 3
120 60.0	time slice 2 : 120 min. duration at 60 sec. time intervals
150 200 10 10	location 1 for second time slice
320 135 10 10	location 2 " " "
340 230 10 10	location 3 " " "

The program generates the output data file with the pixel values obtained at the specified locations. Although the program automated the data acquisition process, the main drawback of the program was that one cannot get the pixel values at time intervals less than 1 second, whereas by using the DT2853 Image Processing software one can get pixel values every 1/30 th of a second. Therefore, both of the programs were used as the demands of the project required.

OKLAHOMA STATE UNIVERSITY

The pixel value obtained was not the same as the intensity of light required in the calculation of the total retardance because the signals produced by the video camera were not proportional to the intensity of the incident light. The outgoing gray scale vs. the estimated incident gray scale is shown in Figure C.1. In order to produce a linear response to the video signals, the camera was calibrated according to a method described by Guy [15]. The intensity of the transmitted light with no sample was taken to be:

$$I = \frac{I_0}{2} cos^2 \alpha \qquad \text{(C1)}$$

where

I = the intensity of the incident light,

I_0 = the intensity of the light source,

α = the angle between the polarizers.

The polarizers were initially kept parallel and the light intensity of the source was adjusted such that the outgoing signal from the camera had a pixel value of 255 (saturation point). Then α was changed gradually from 0 to 90^0 and the output signal from the camera was recorded by the digitizing equipment. Equation (C1) was then used to estimate the corresponding transmitted light intensity.

Figure C.1 clearly shows that the pixel value varies linearly with the incident light at low light intensities and the pixel value varies non-linearly at higher light intensities. At low light intensities, the slope of the straight line is greater than 1, implying that the video camera tends to produce an output signal that is too great. Exactly the opposite behavior is indicated at higher intensities of incident light as the camera tends to reduce the output signal intensity. The calibration curve shown in Figure C.1 can be placed in the look-up

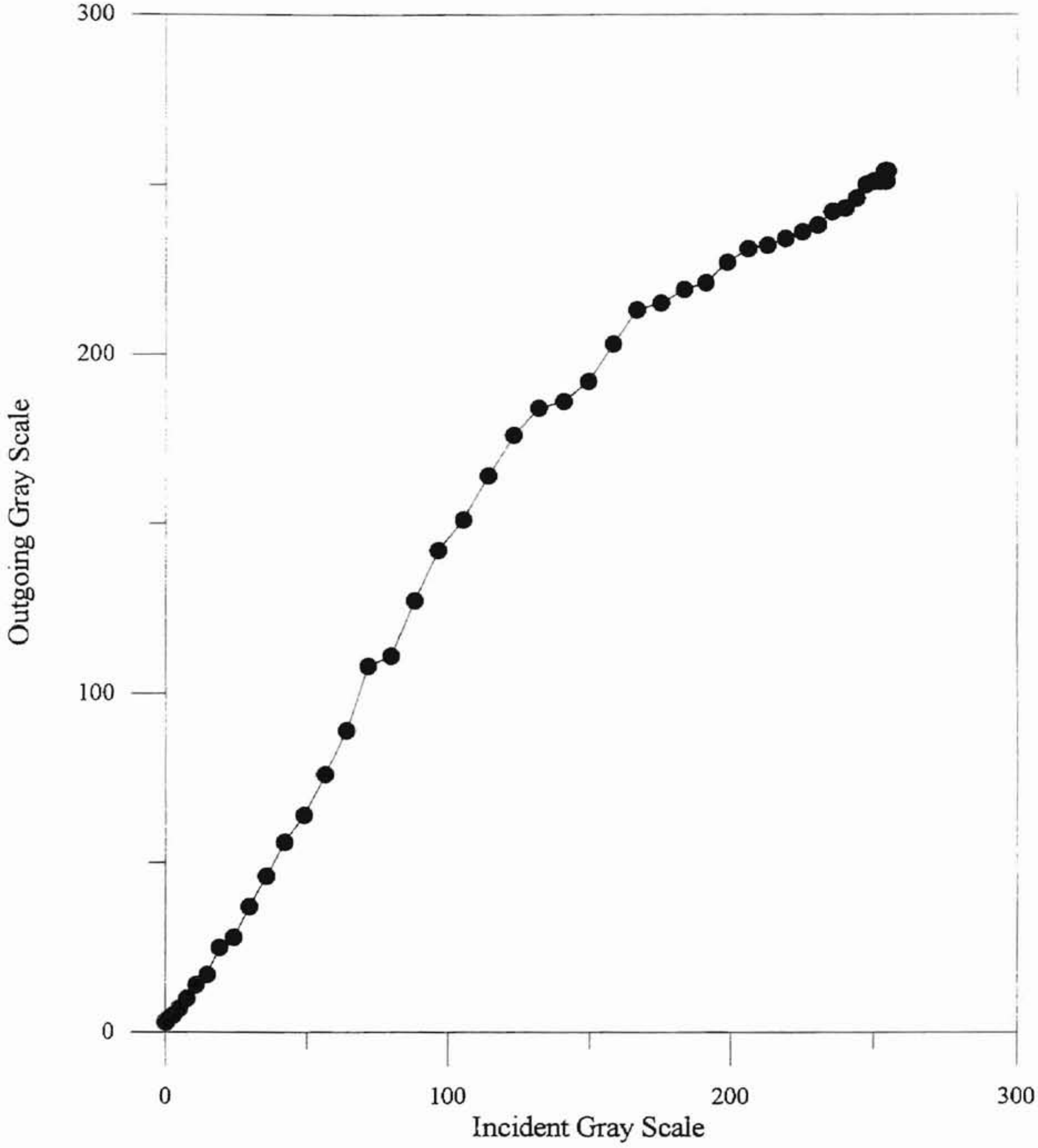

Figure C.1 Camera Calibration Curve

OKLAHOMA STATE UNIVERSITY

table of the digitizing equipment such that a linear response to the video signals could be obtained.

The following is the listing of the computer program used to digitize the experimental data recorded on the video tape. The program was divided into two files, namely, dt.h (header file) and dt.cpp (source file). The computer program requires an input data file specifying the locations at which pixel values need to be obtained. The program generates an output file based on the data given in the input file.

```
************************ Header File -dt.h************************
#ifndef DT_H
#define DT_H

#include<dos.h>
#include<iostream.h>
#include<fstream.h>
#include<time.h>
#include<stdlib.h>
#include<conio.h>

#define BASE         0x230        // i/o register base address
#define INCSR1       BASE         // video input control/status register 1
#define INCSR2       BASE+2       // video input control/status register 2
#define OUTCSR       BASE+4       // video output control/status register
#define CURSOR       BASE+6       // cursor register address
#define INDEX        BASE+8       // index register address
#define INLUT        BASE+0xA     // input look-up table entry
#define REDGRN       BASE+0xC     // red-green output look-up table register
#define BLUE         BASE+0xE     // blue output look-up table register
#define DISP         0xF          // display bit
#define ENDSTOP      0x8          // bit 3 of input control/status register
#define BUSY         0x80         // bit 7 of input control/status register
#define ON  1
#define OFF 0
#define BASE0     0x0A00000       // memory base address of buffer0
#define BASE1     0x0A40000       // memory base address of buffer1
typedef unsigned long ULONG;
typedef struct _window
```

```
{
    int  row;
    int  col;
    int  width;
    int  height;
} Window;
// function prototypes
void InitBoard(void);
void Acquire(void);
void Display(void);
void Sync(void);
void HighCopy(ULONG Source,ULONG Dest);
void DoIt(void);

#endif


************************** Source File - dt.cpp *******************
#include "dt.h"

// global variables
int             buffer =   0;          // acquire to buffer 0
char            gdt[6][8];             // global descriptor table
unsigned char   data[2][512];          // pixel data array
union REGS      regs;
union REGS      ret;
struct SREGS    sregs;

int             period;         // time period of each frame
double          interval;       // interval at which data is acquired
ofstream        output;         // output file
double          dTime;          // total time
int             nWindows;       // no. of windows
Window*         pWind;          // array of window structures

main(int argc,char** argv)
{
        if(argc != 3)
        {
                cout << "Usage : dt input_file output_file\n";
                exit(1);
        }
        ifstream input(argv[1]);        // open the input data file
        output.open(argv[2]);           // open the output data file
        InitBoard();                    // initialize the board
    Sync();                         // external sync

    int n;
    input >> n;                                 // no. of differnt time frames
    input >> nWindows;                          // read no. of windows
    pWind =    new Window[nWindows];            // window structure array
    cout << "--------------Start the V.C.R and press any key-----------\n";
    getch();
    clrscr();                                   // clear the screen
    cout << "-------------------------------------------------------\n";
    cout << "|      Program running. Don't turn off the computer,   |\n";
    cout << "|              T.V and the V.C.R                       |\n";
    cout << "-------------------------------------------------------\n";

    dTime =    0.0;
    for( int i = 0 ; i < n ; i++ )
    {
        input >> period;        // input the time period(min) of each frame
        input >> interval;              // input the time interval(sec)
        period    *=   60;              // convert to seconds
        // read the window coordinates
        for( int j = 0 ; j < nWindows ; j++ )
        {
            input >> pWind[j].row;          // read the row number
            input >> pWind[j].col;          // read the column number
            input >> pWind[j].width; // read the width of the window
            input >> pWind[j].height; // read the height of the window
        }
        DoIt();                 // acquire the data and store it in the file
    }
    input.close();              // close the input file
    output.close();             // close the output file
    delete pWind;
    return 0;                   // exit
}

// Function to acquire and store the data in a file at the time intervals specified
void DoIt(void)
{
    double        avg;
    ULONG         high,s;
    int      N;
    long     counter=   0;
    long     max  =    period/interval;  // max no. of samples
    time_t  t1,t2;
    s   =   (ULONG)FP_OFF(data) + ((ULONG)FP_SEG(data) <<4);
    time(&t1);
    time(&t2);
    while( counter < max )
    {
        Acquire();       // acquire the image
        Display();       // display the image on the monitor
        if( difftime(t2,t1) >= interval )
        {
            dTime +=   interval;  // increment the total time
            output << dTime;        // print the time
            t1   =    t2;
            counter++;              // increment the counter
            for( int nWin = 0 ; nWin < nWindows ; nWin++ )
            {
                high = (ULONG)BASE0;
                N    =    pWind[nWin}.width * pWind[nWin].height;
                for( int m = 0 ; m < pWind[nWin].row ; m+=2)
                                                //dummy read
                {
                    HighCopy(high,s);
                    high  +=   (ULONG)1024;
                }
                avg   =    0.0;
                for( int k = 0 ; k < pWind[nWin].height ; k+=2 )
                {
                    HighCopy(high,s);
                    for( int i = 0 ; i < 2 ; i++ )
                    {
                        for( int j = pWind[nWin].col ; j <
            pWind[nWin].col+pWind[nWin].width ; j++ )
                            avg   +=   (double)data[i][j];
                    }
                    high  +=   (ULONG)1024;
                }
                output << "\t" << avg/N;     // print the pixel value
            }    // end of for loop
            output << "\n";
        }    // end of if loop
        time(&t2);
    }    // end of while loop
}

//   function to initialize the board
```

```
void InitBoard(void)
{
        outport(OUTCSR,OFF);    // initialize OUTSCR,dusplay off
        outport(INCSR1,inport(INCSR1) | ENDSTOP);//writeINCSR1 to set bit 3
        // write INCSR1 to clear BUSY (bit 7). This stops the board
        outport(INCSR1,inport(INCSR1) & ~BUSY);
        // program the input look-up tables
        // save the values of INCSR1 and INCSR2
        int  inr1  =    inport(INCSR1);
        int  inr2  =    inport(INCSR2);
        while(inport(INCSR1) & BUSY); // check the BUSY bit. it must be clear
                                        to proceed.
        // write to INCSR2,setting the board to Load LUT mode( MODE = 100)
        outport(INCSR2,0x40);
        for( int i = 0 ; i < 256 ; i++ )
        {
        // set the ISEL bits to select the input look-up table to be programmed.
                outport(INCSR1,inport(INCSR1) & 0xfff8); // lut 0
                // write the appropriate value to INDEX
                outport(INDEX,i);
                // write INLUT with the appropriate input lut value in the low byte
                outport(INLUT,i);
        }
        // restore the INCSR1 and INCSR2 to their original values
        outport(INCSR1,inr1);
        while( inport(INCSR1) & BUSY );
        outport(INCSR2,inr2);
        // program the output look-up tables
        // save the values of INCSR2 and OUTCSR
        inr2 = inport(INCSR2);
        int outr    =    inport(OUTCSR);
        while( inport(INCSR1) & BUSY );
        // write to INCSR2, setting the mode bits to Load LUT( MODE = 100 )
        outport(INCSR2,0x40);   // 6,5 and 4 bits to 100
        for( i = 0 ; i < 256 ; i++ )
        {
                // write the apropriate value to the OSEL bits in OUTCSR
                outport(OUTCSR,inport(OUTCSR) & 0xfff0);  // select LUT 0
                outport(INDEX,i);
                // red in low byte, green in high byte to REDGRN register
                outport( REDGRN,i+(i<<8) );
                outport(BLUE,i);  // blue in low byte
        }
        // restore the original values  of INCSR2 and OUTCSR
        while( inport(INCSR1) & BUSY );
        outport(INCSR2,inr2);
        outport(OUTCSR,outr);
        while( inport(INCSR1) & BUSY );
        // initialize INCSR2, anything except Load LUT mode
        outport(INCSR2,0x20);
}

//  function to acquire the image to board
void Acquire(void)
{
        while( inport(INCSR1) & BUSY );    // wait
        // write INCSR2 to set mode bits(4-6) for video in operation,
        // (001 binary), to select which frame-store memory buffer
        // (BUFSEL, bit 7) to use, and to set WP0,..WP3 to the desired
        // level of write protection
        outport( INCSR2, (inport(INCSR2) & 0xff00) + 0x10 + (buffer << 7) );
        // write INCSR1 to set the ISEL bits( 0-3) to select the  input
        // look-up table and to set BUSY(bit 7) to start the operation
        // ENDSTOP(bit 3) should be set
        outport(INCSR1,(inport(INCSR1) & 0x60) + 0x88 );
        while( inport(INCSR1) & BUSY );
}

//  function to display the buffer on the monitor
void Display(void)
{
        int tmp = buffer;
        outport(OUTCSR,(inport(OUTCSR) & 0xff6f) + 0x0080 + (tmp << 4) );
}

//  function to set syncronization source
void Sync(void)
{
        int sync = 1;    // external
        outport(OUTCSR,(inport(OUTCSR) & 0xffdf) + (sync << 5) );
}

//  function to copy 1KB(2 rows)of data from high memory  to a buffer
void HighCopy(ULONG Source,ULONG Dest)
{
        // initialize gdt
        for(int i = 0 ; i < 6 ; i++ )
                for( int j = 0 ; j < 8 ; j++ )
                        gdt[i][j]  =   0;
        // third entry( source address descriptor )
        gdt[2][1]  =   0x4;
        gdt[2][2]  =   (char)Source;
        Source >>= 8;
        gdt[2][3]  =   (char)Source;
        Source >>= 8;
        gdt[2][4]  =   (char)Source;
        gdt[2][5]  =   0x93;
        // fourth entry( destination address descriptor )
        gdt[3][1]  =   gdt[2][1];
        gdt[3][2]  =   (char)Dest;
        Dest >>= 8;
        gdt[3][3]  =   (char)Dest;
        Dest >>= 8;
        gdt[3][4]  =   (char)Dest;
        gdt[3][5]  =   gdt[2][5];
        // interrupt 15H,function 87H
        regs.h.ah  =   0x87;
        regs.x.cx  =   0x200;     // unit words(block size t be moved in words.
                                  // 1 word = 2bytes
        regs.x.si  =   FP_OFF(gdt);
        sregs.es   =   FP_SEG(gdt);
        int86x(0x15,&regs,&ret,&sregs);
}
```

APPENDIX D:

EXPERIMENTAL RESULTS

This appendix consists all of the experimental data presented in Table 4.1 of Chapter IV. Each experimental run is presented in the form of three plots describing pixel value vs. time, reduced retardance vs. time, and correlation of the experimental data with the Avrami equation. Each plot shows four data sets. The data sets were obtained at four randomly chosen points on the sample in order to check reproduciblility within a sample. Experimental conditions such as strain rate, strain, and temperature are also provided on each plot.

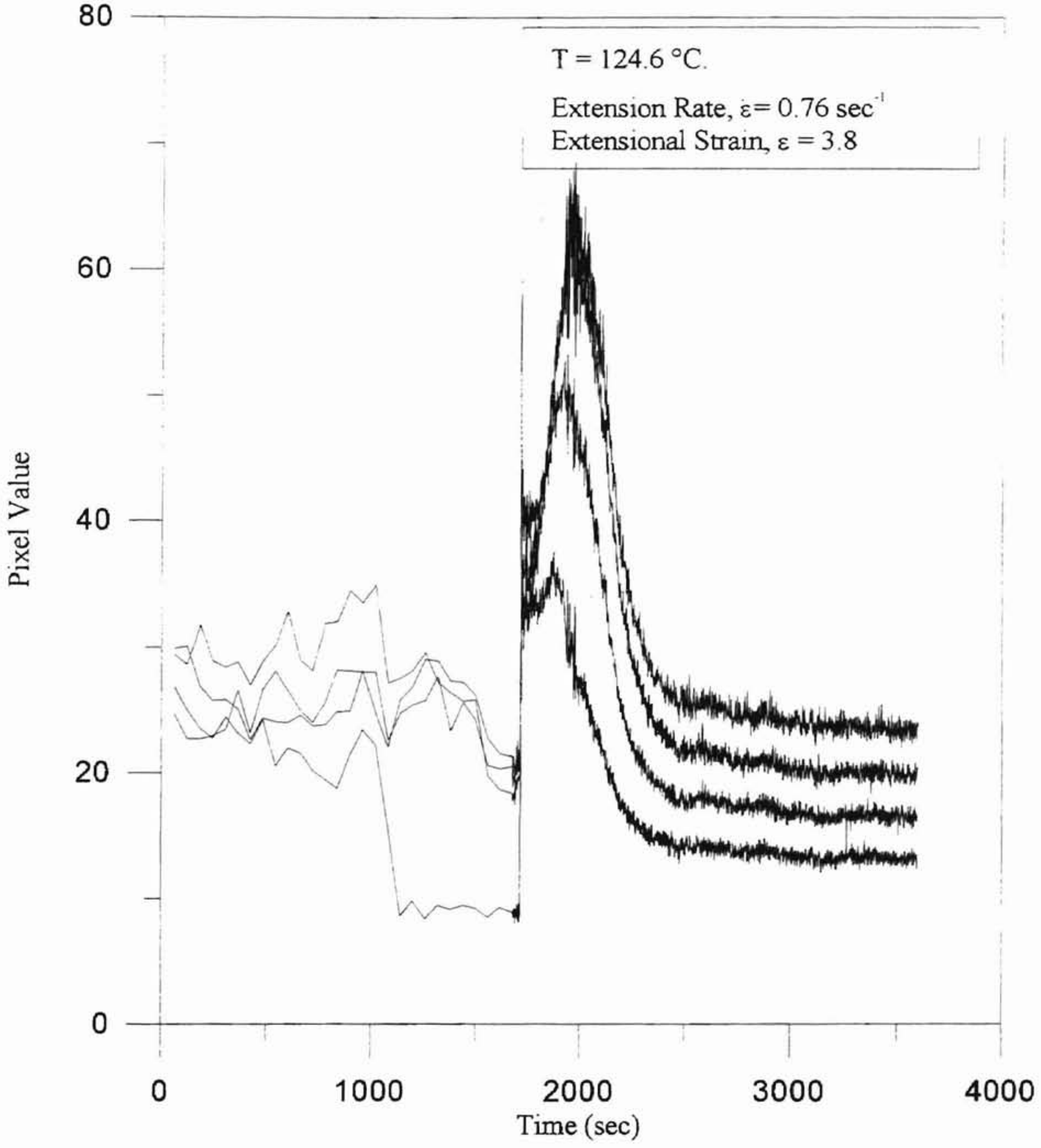

Figure D.1 (a) Pixel Value vs. Time for HDPE at Extension Rate = 0.76 sec^{-1}, Extensional Strain = 3.8

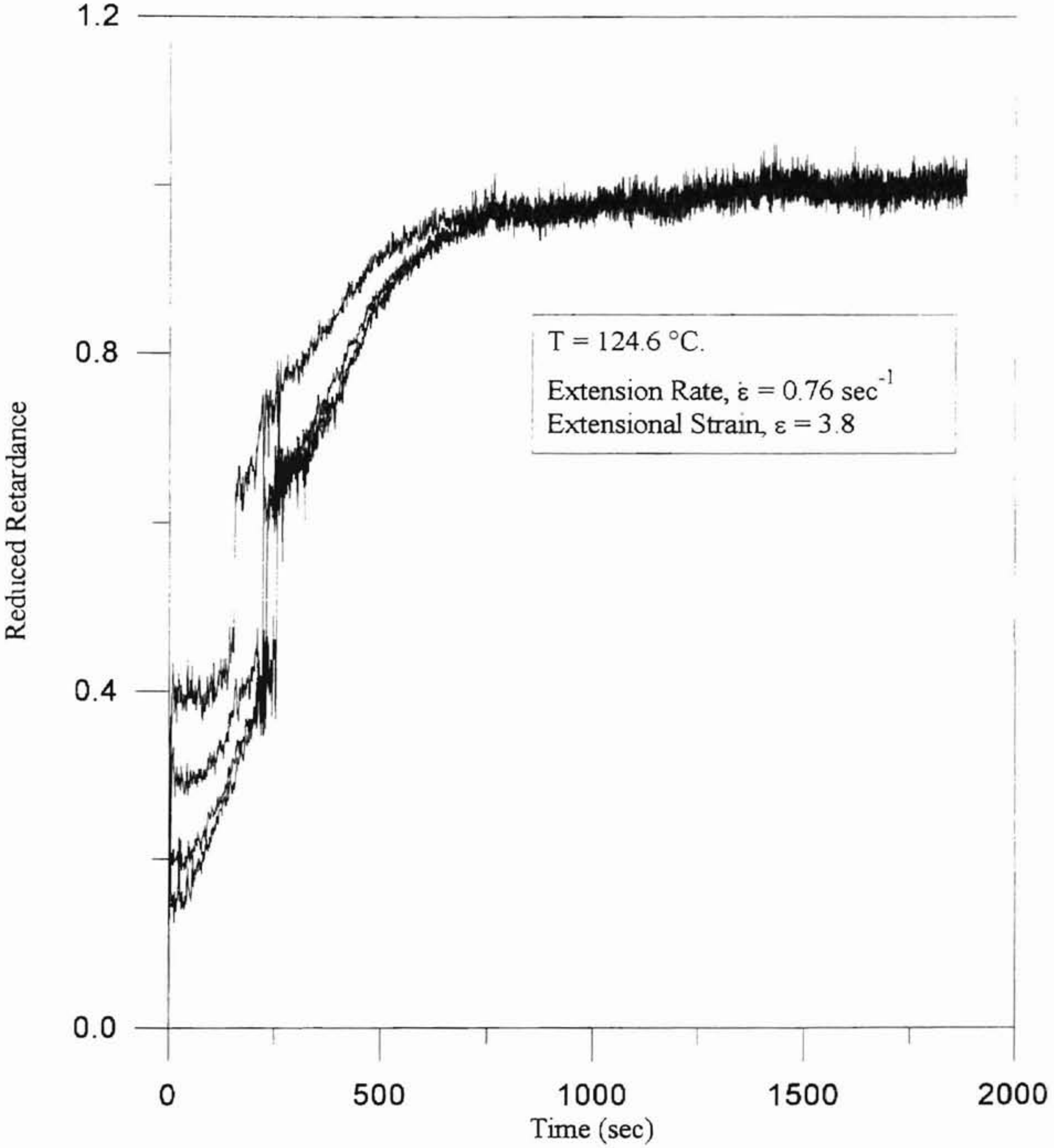

Figure D.1 (b) Reduced Retardance vs. Time for HDPE at Extension Rate = 0.76 sec^{-1}, Extensional Strain = 3.8

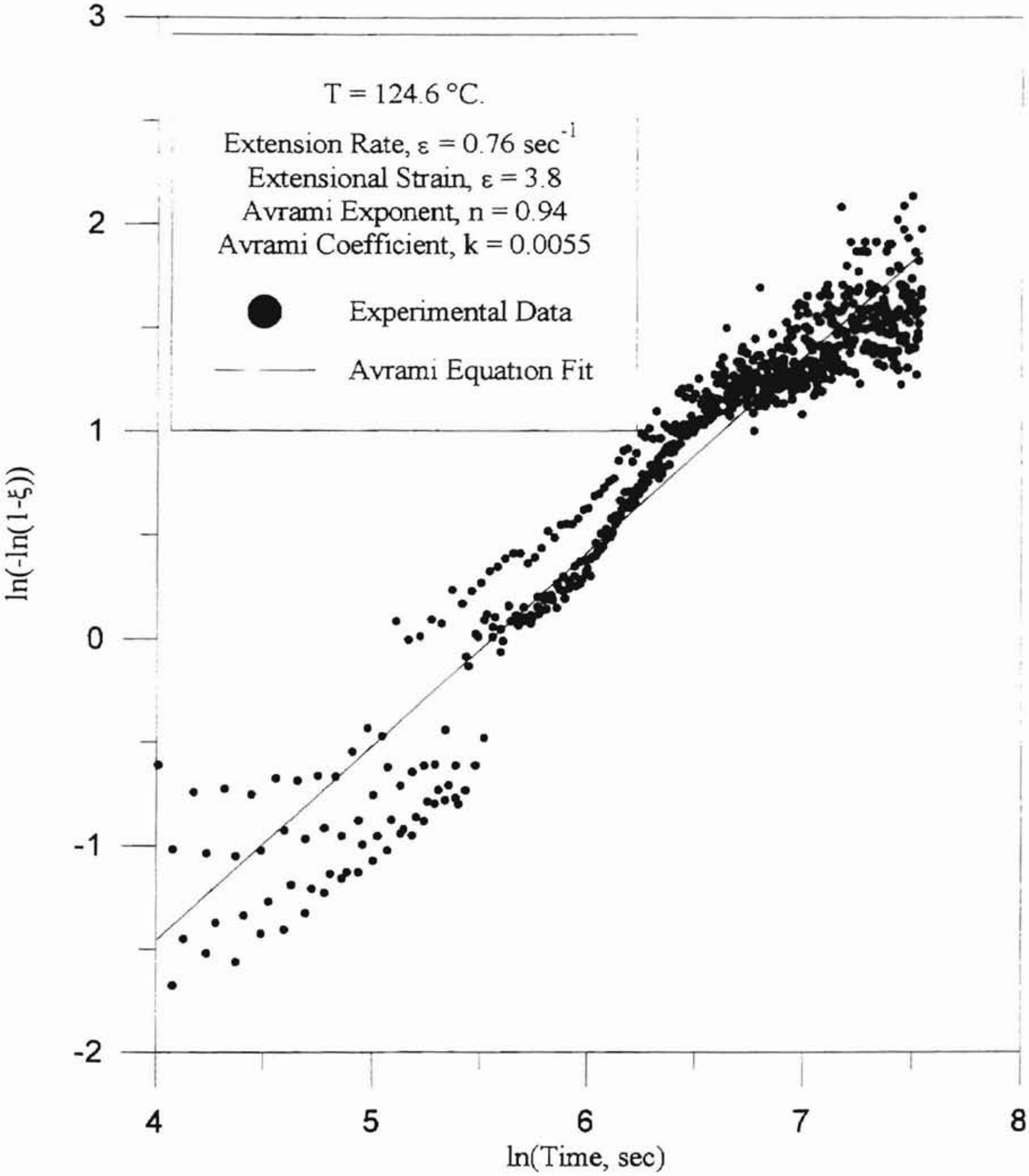

Figure D.1 (c) Correlation of Experimental Data With Avrami Equation for HDPE at Extension Rate = 0.76 sec $^{-1}$, Extensional Strain = 3.8

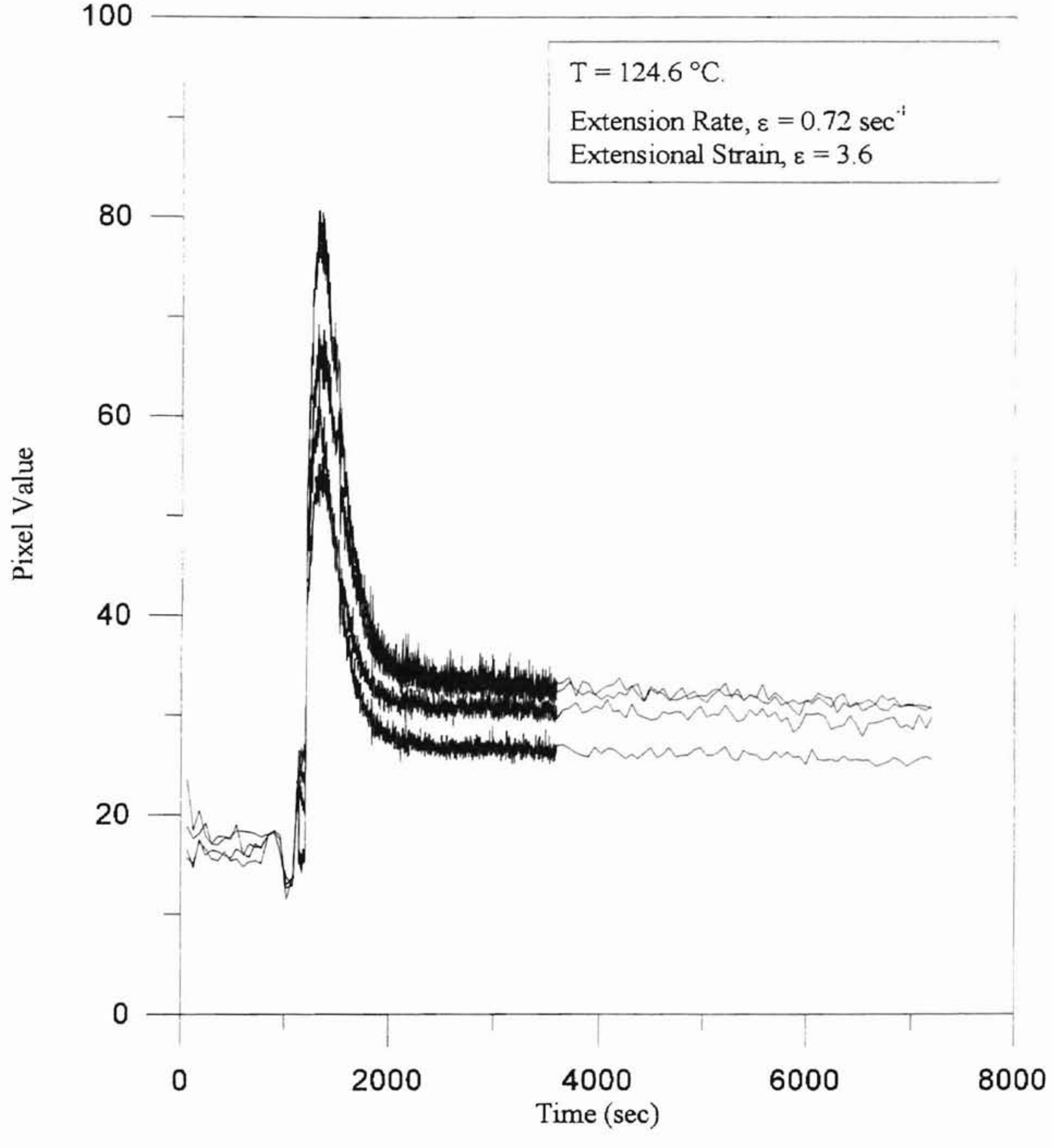

Figure D.2 (a) Pixel Value vs. Time for HDPE at
Extension Rate = 0.72 sec^{-1},
Extensional Strain = 3.6

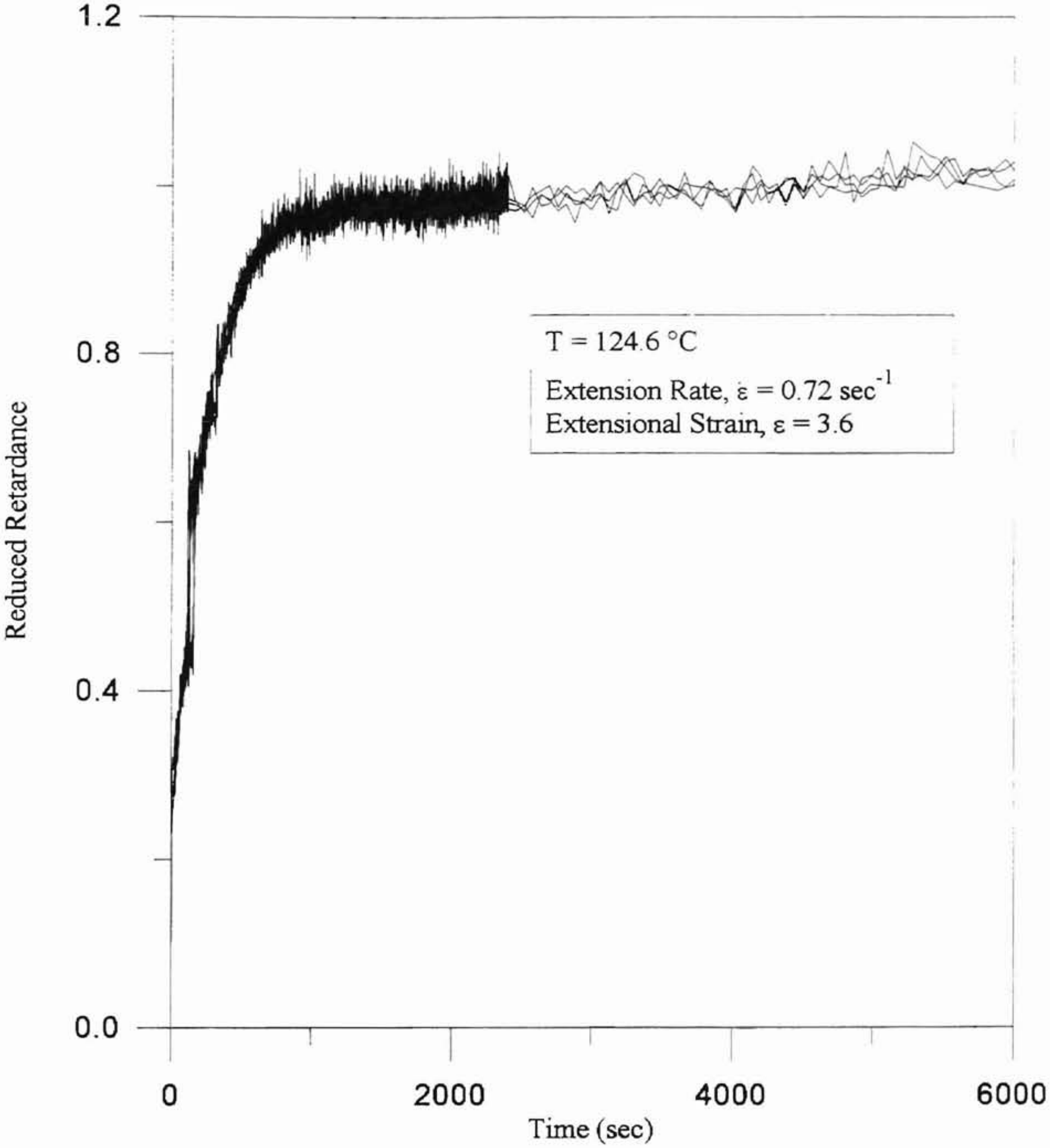

Figure D.2 (b) Reduced Retardance vs. Time for HDPE at Extension Rate = 0.72 sec^{-1}, Extensional Strain = 3.6

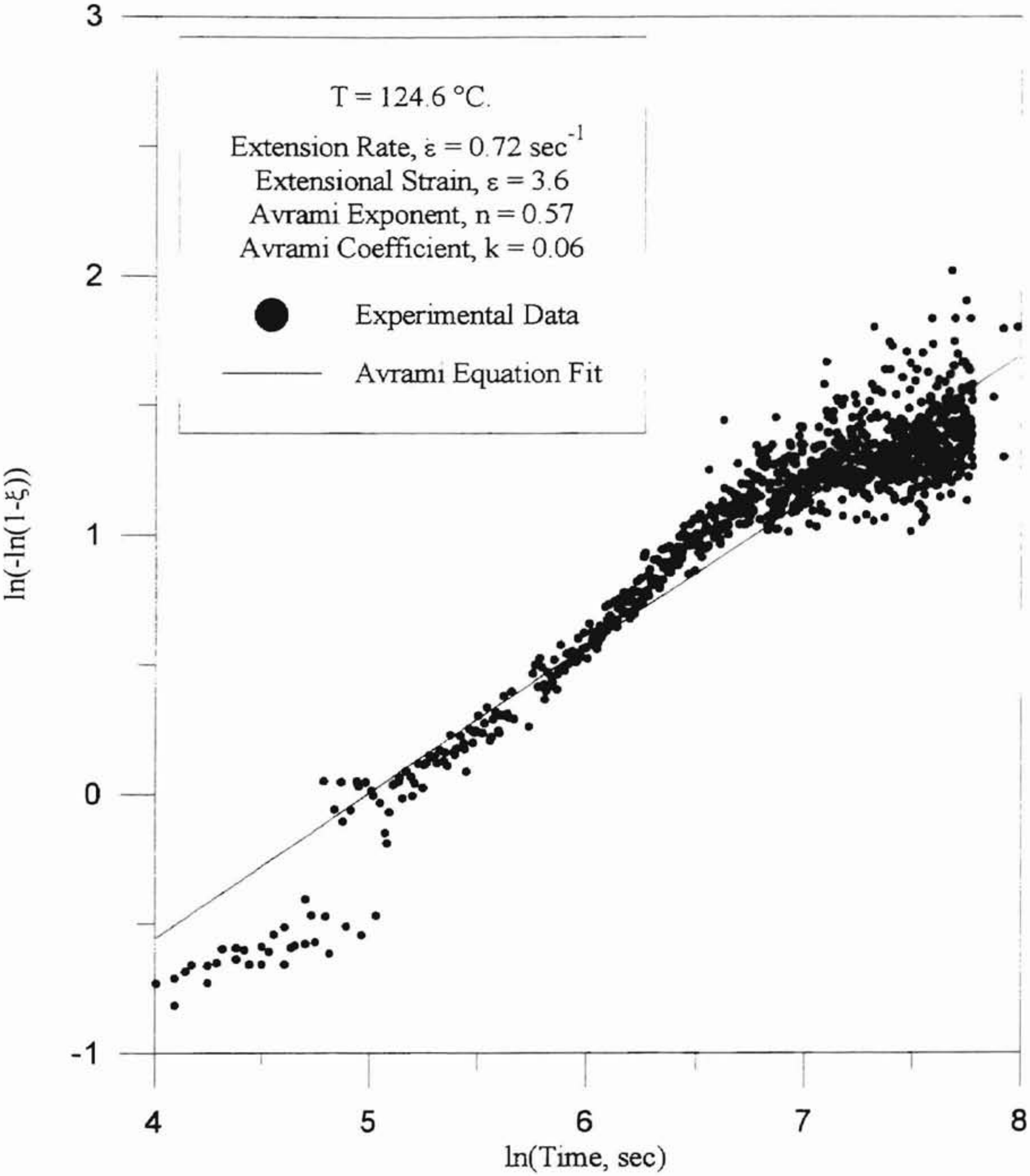

Figure D.2 (c) Correlation of Experimental Data With Avrami Equation for HDPE at Extension Rate = 0.72 sec $^{-1}$, Extensional Strain = 3.6

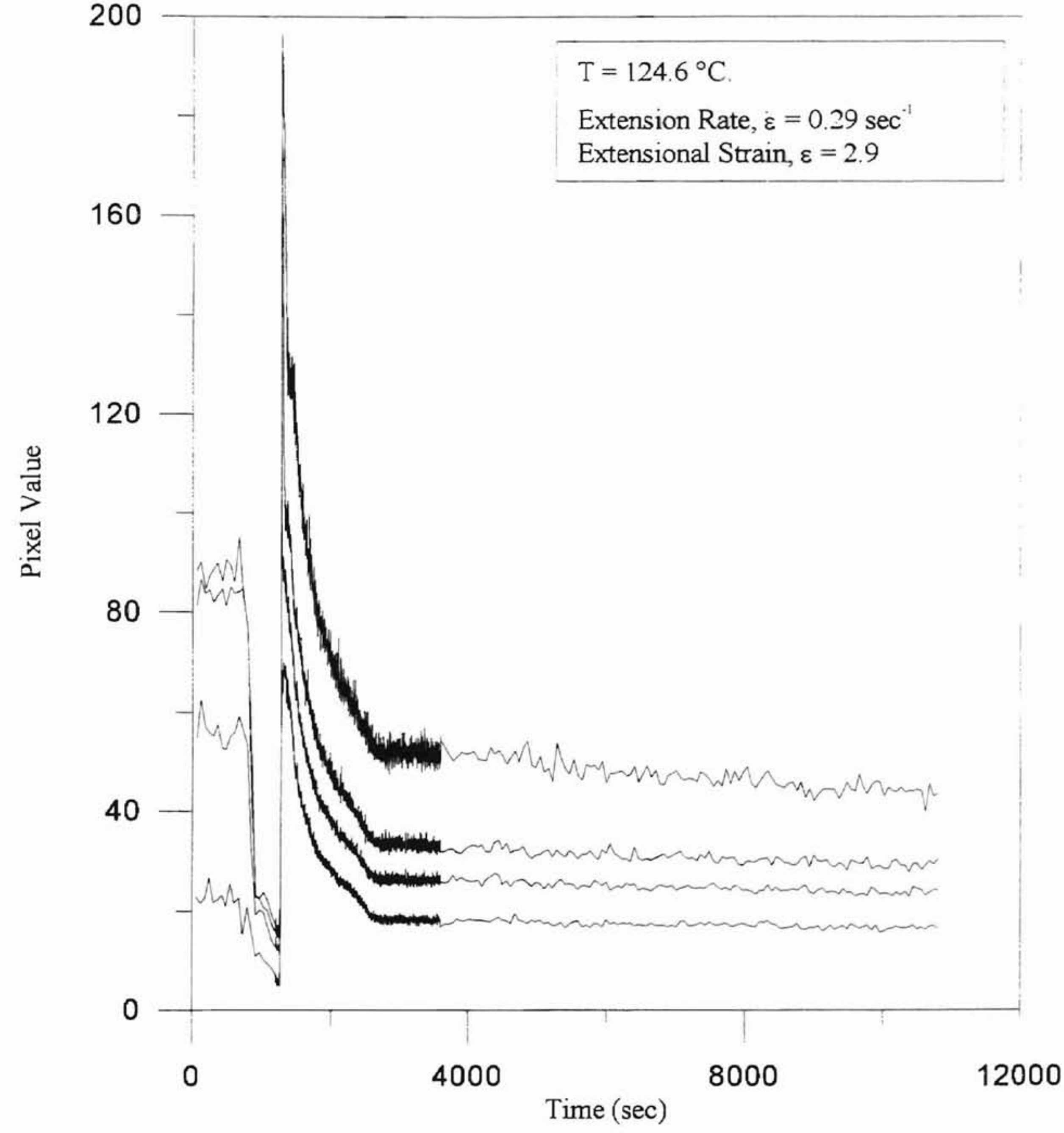

Figure D.3 (a) Pixel Value vs. Time for HDPE at Extension Rate = 0.29 sec^{-1}, Extensional Strain = 2.9

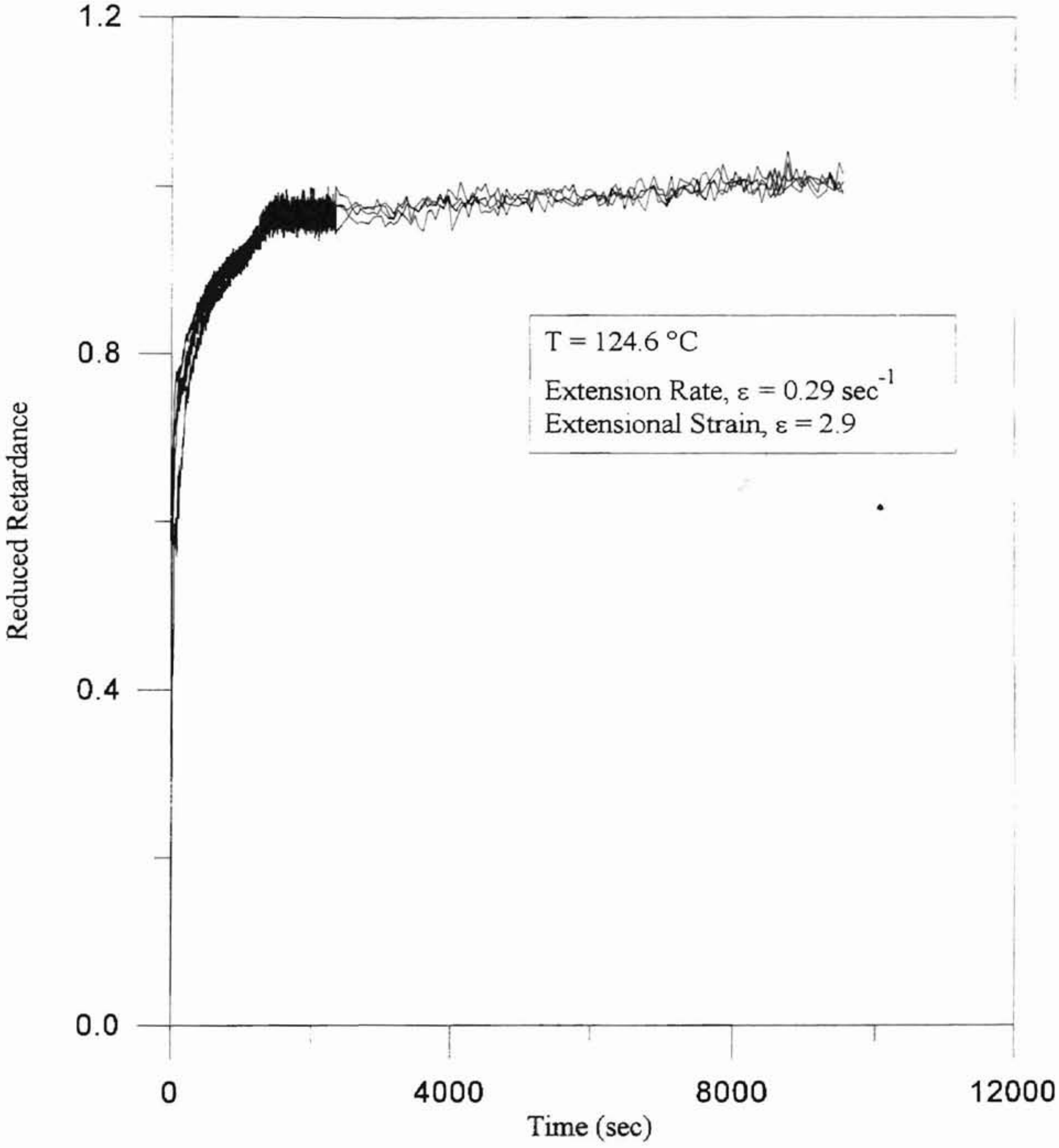

Figure D.3 (b) Reduced Retardance vs. Time for HDPE at Extension Rate = 0.29 sec^{-1}, Extensional Strain = 2.9

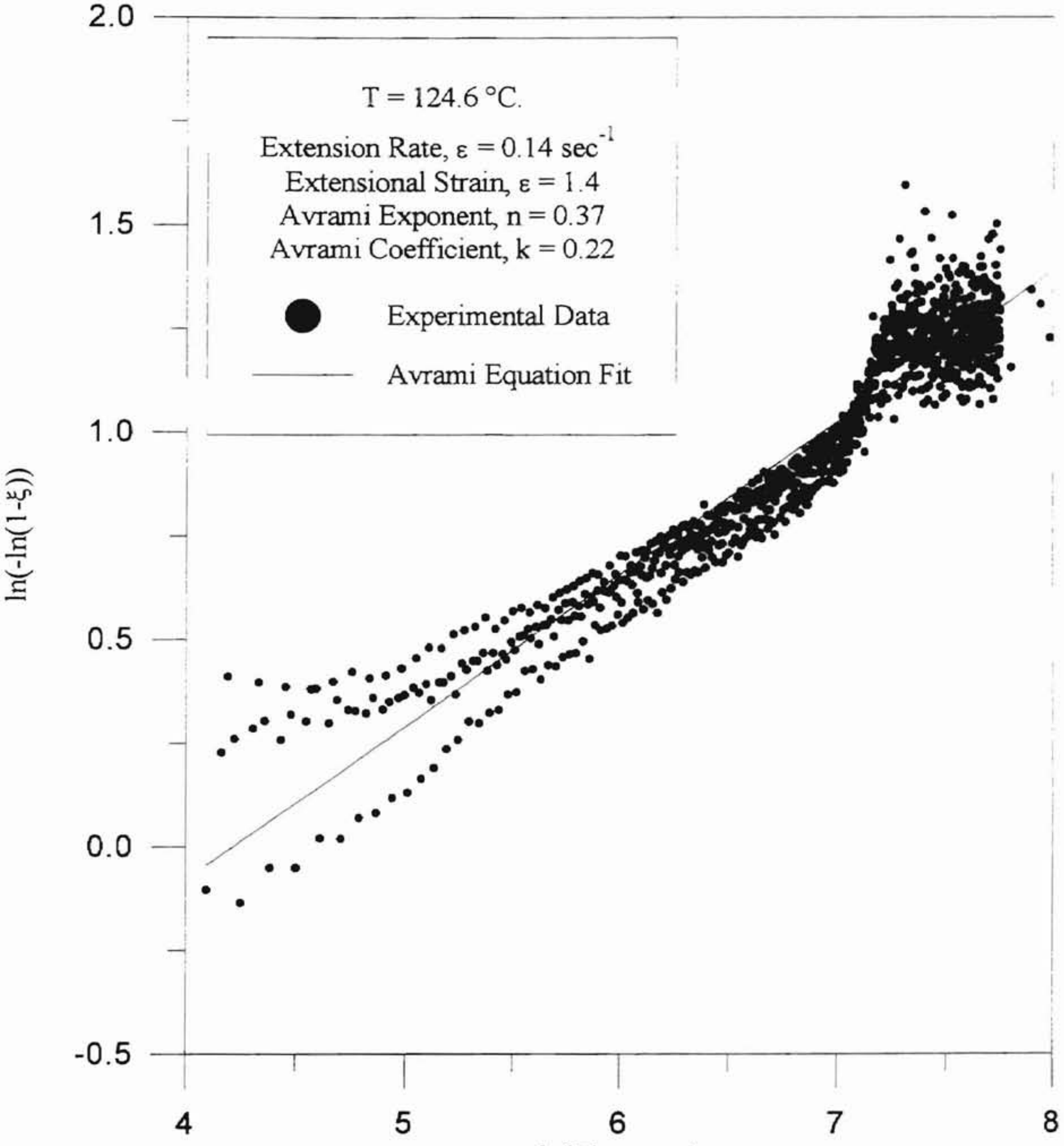

Figure D.3 (c) Correlation of Experimental Data With Avrami Equation for HDPE at Extension Rate = 0.14 sec^{-1}, Extensional Strain = 1.4

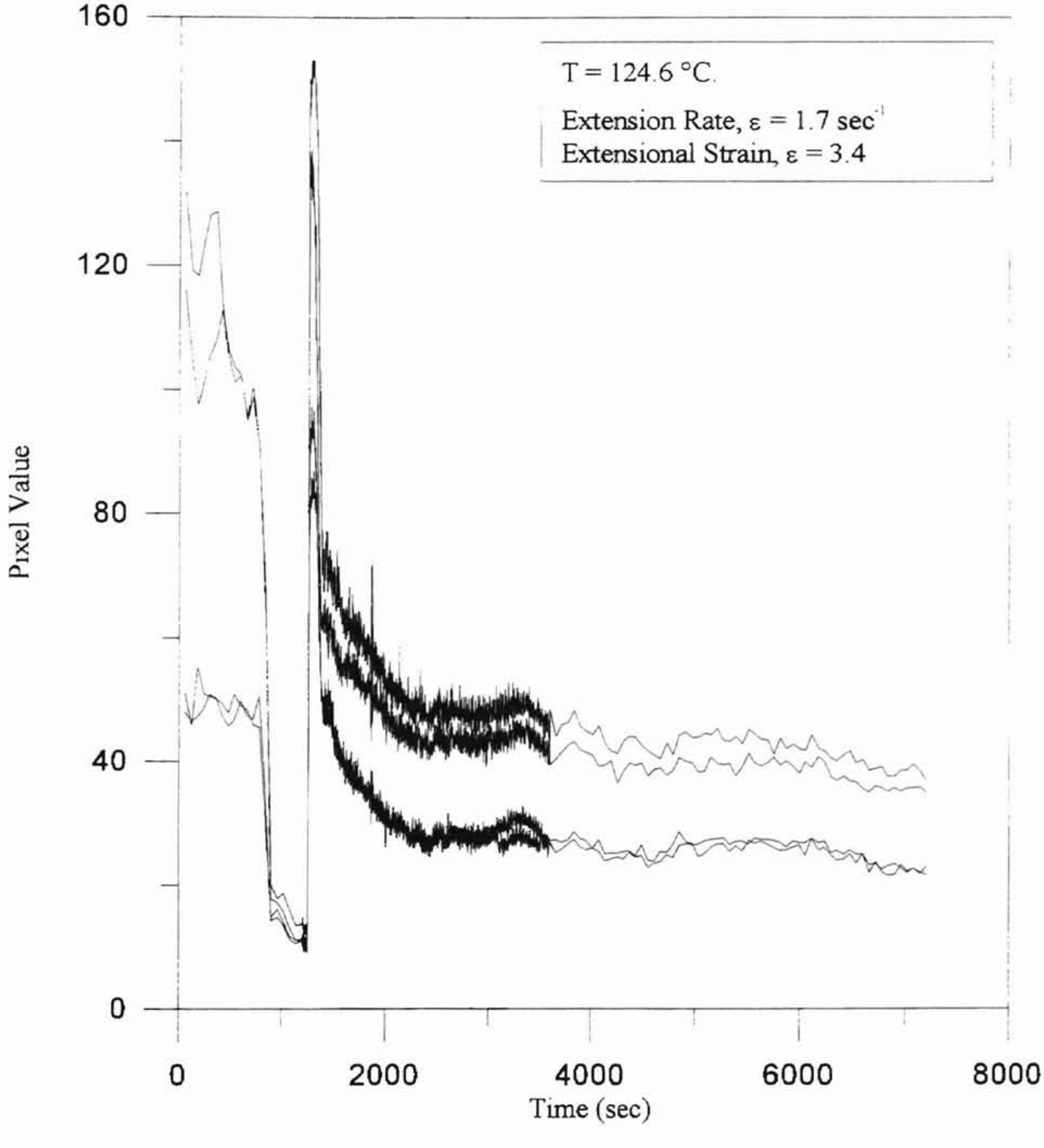

Figure D.4 (a) Pixel Value vs. Time for HDPE at Extension Rate = 1.7 sec^{-1}, Extensional Strain = 3.4

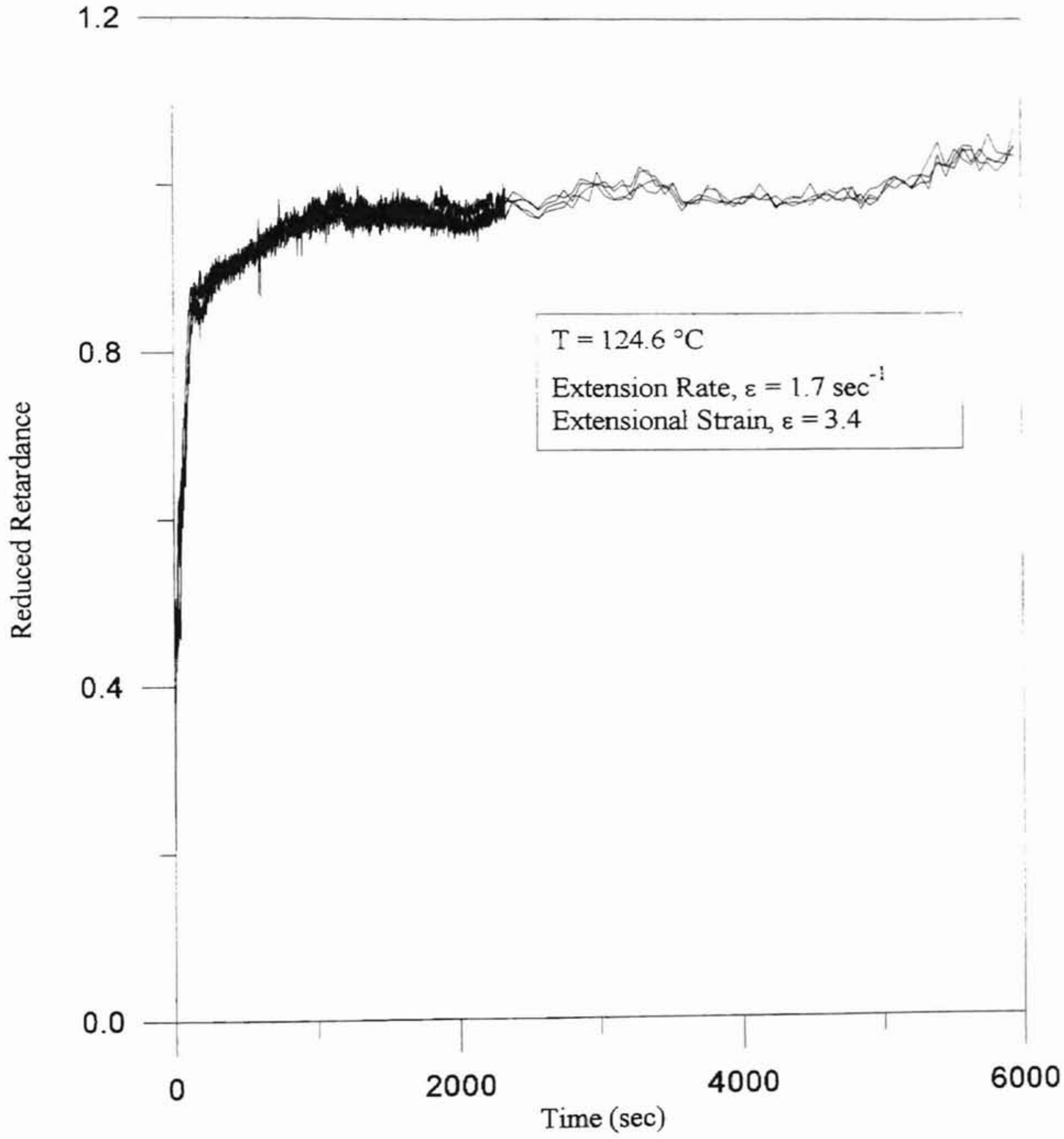

Figure D.4 (b) Reduced Retardance vs. Time for HDPE at Extension Rate = 1.7 sec^{-1}, Extensional Strain = 3.4

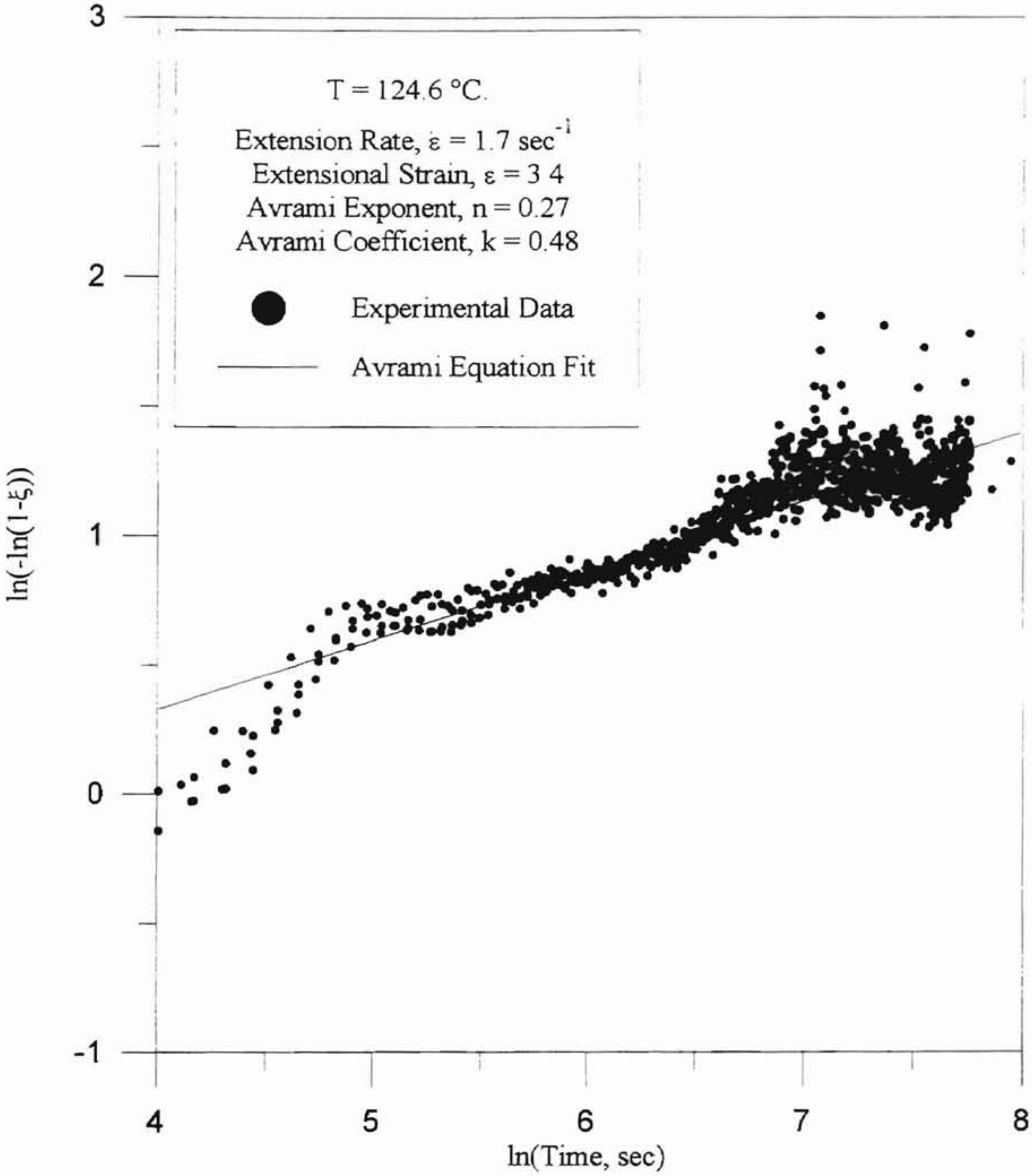

Figure D.4 (c) Correlation of Experimental Data With Avrami Equation for HDPE at Extension Rate = 1.7 sec $^{-1}$, Extensional Strain = 3.4

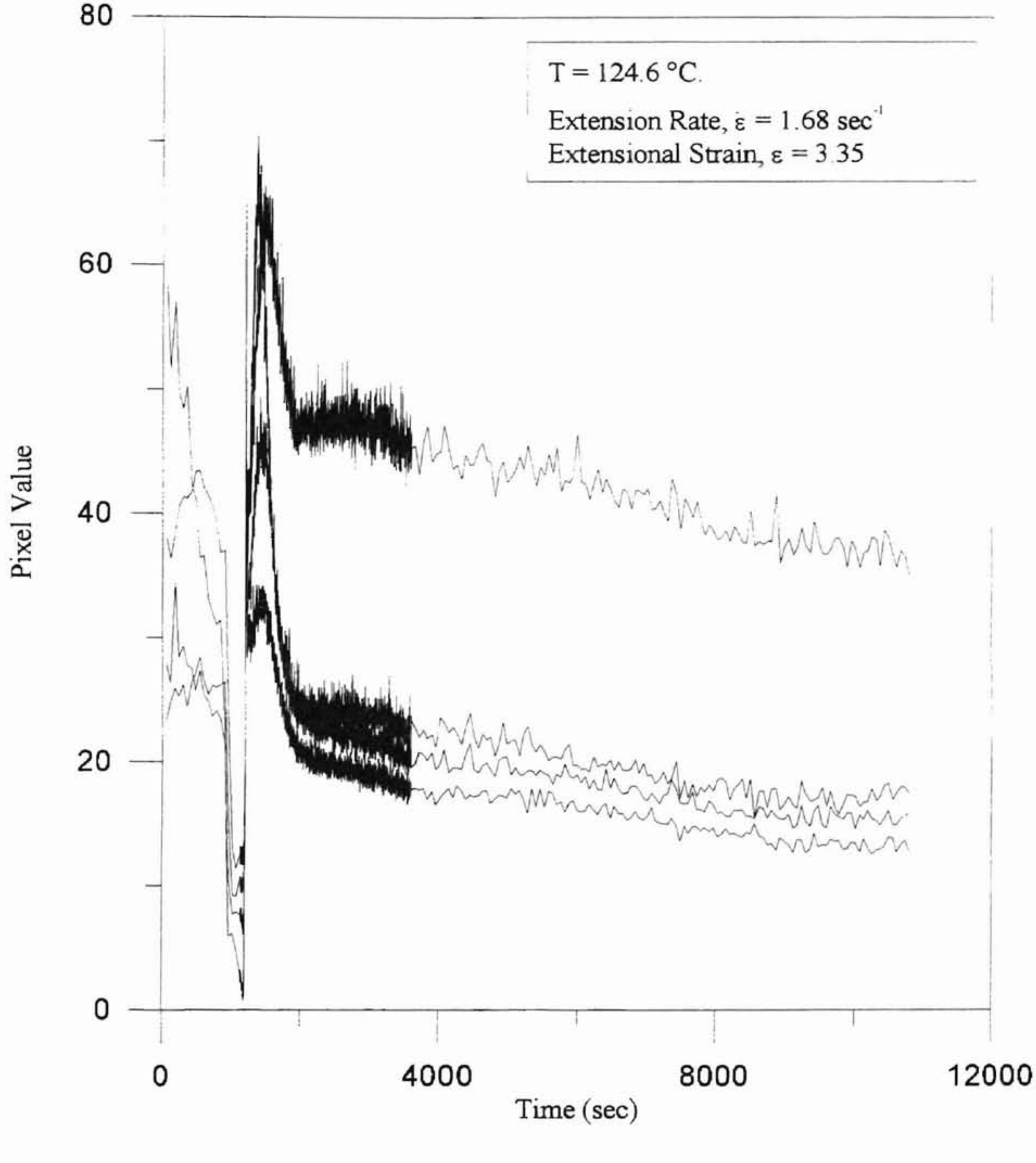

Figure D.5 (a) Pixel Value vs. Time for HDPE at Extension Rate = 1.68 sec^{-1}, Extensional Strain = 3.35

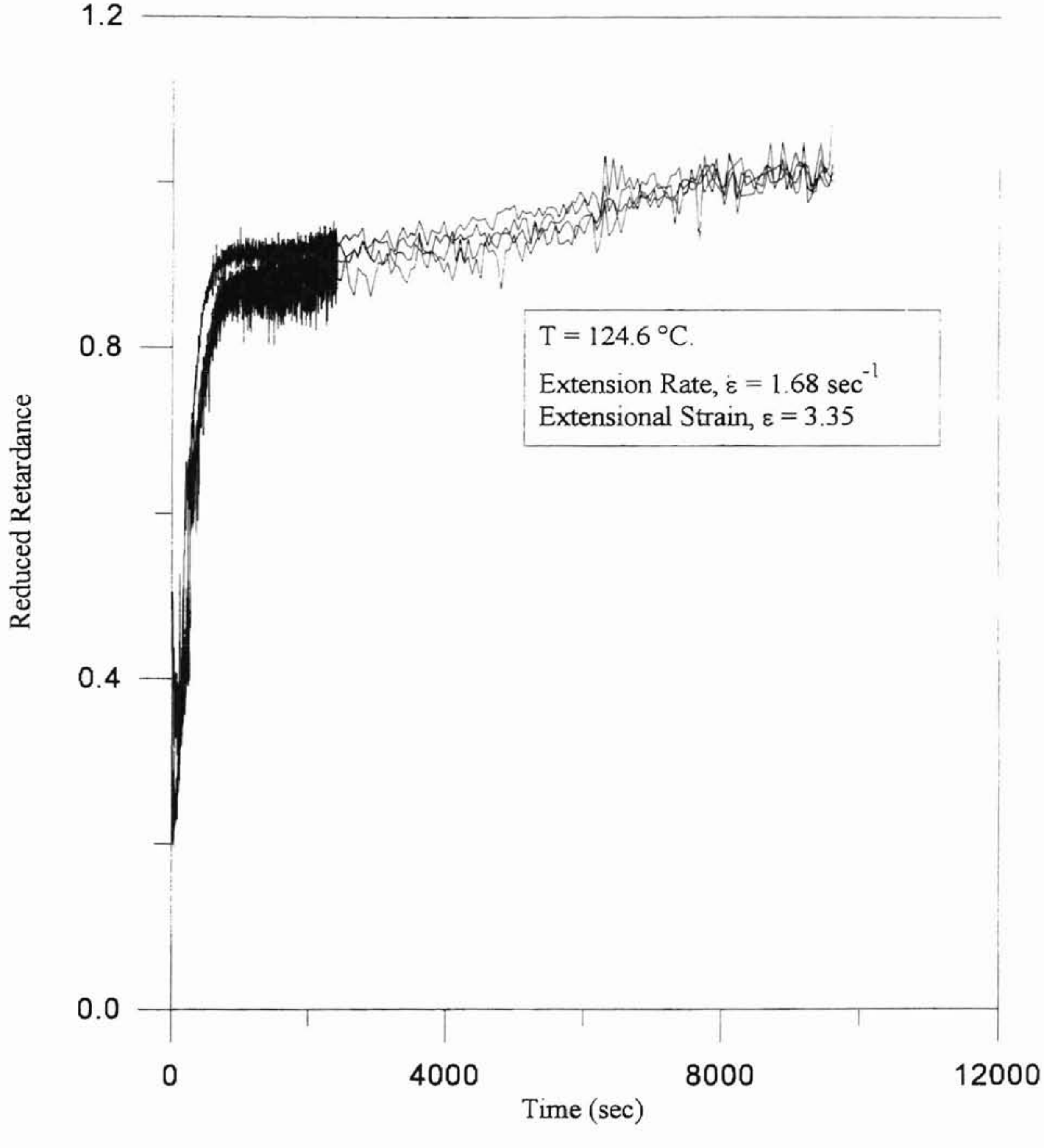

Figure D.5 (b) Reduced Retardance vs. Time for HDPE at Extension Rate = 1.68 sec^{-1}, Extensional Strain = 3.35

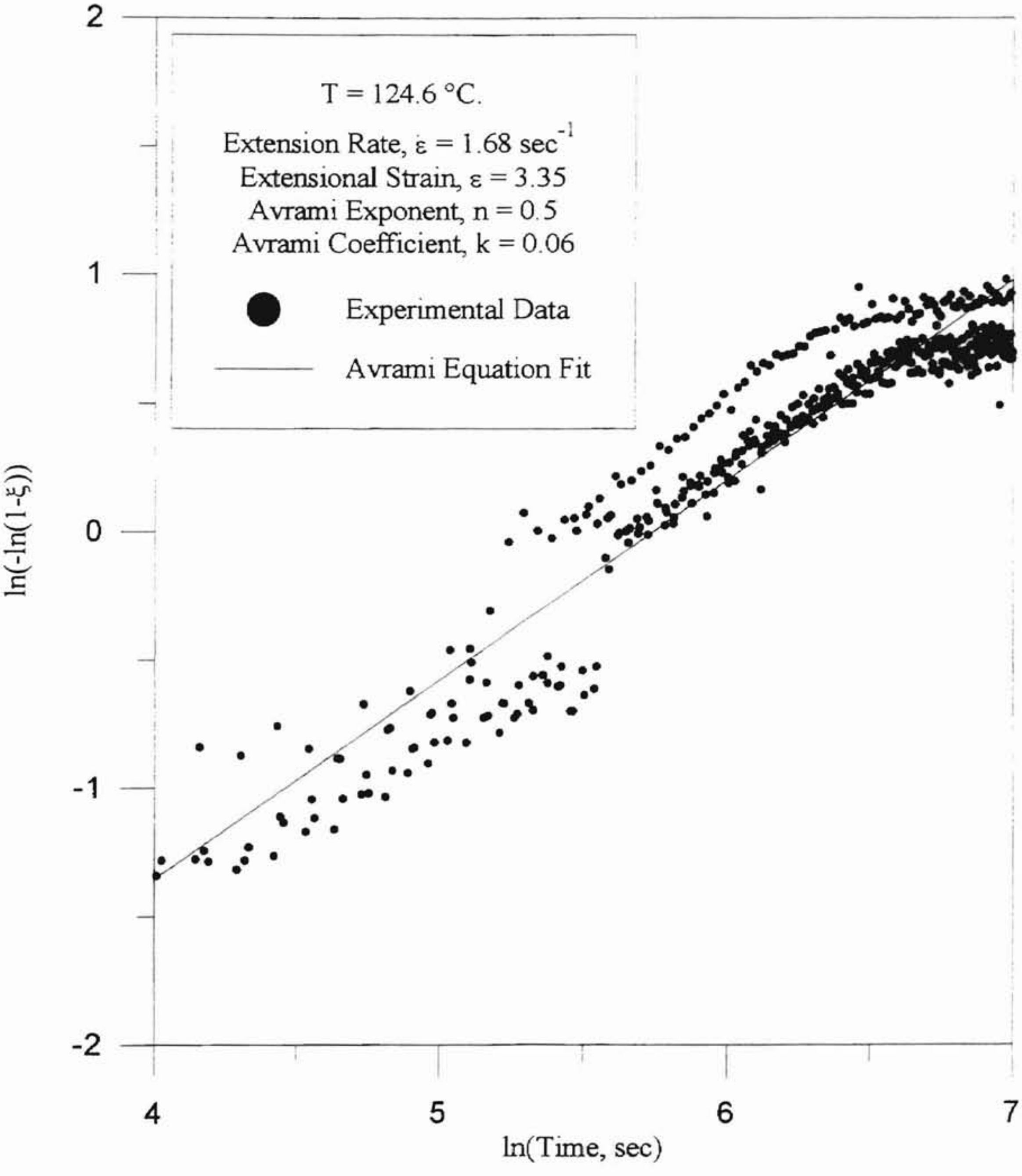

Figure D.5 (c) Correlation of Experimental Data With Avrami Equation for HDPE at Extension Rate = 1.68 sec $^{-1}$, Extensional Strain = 3.35

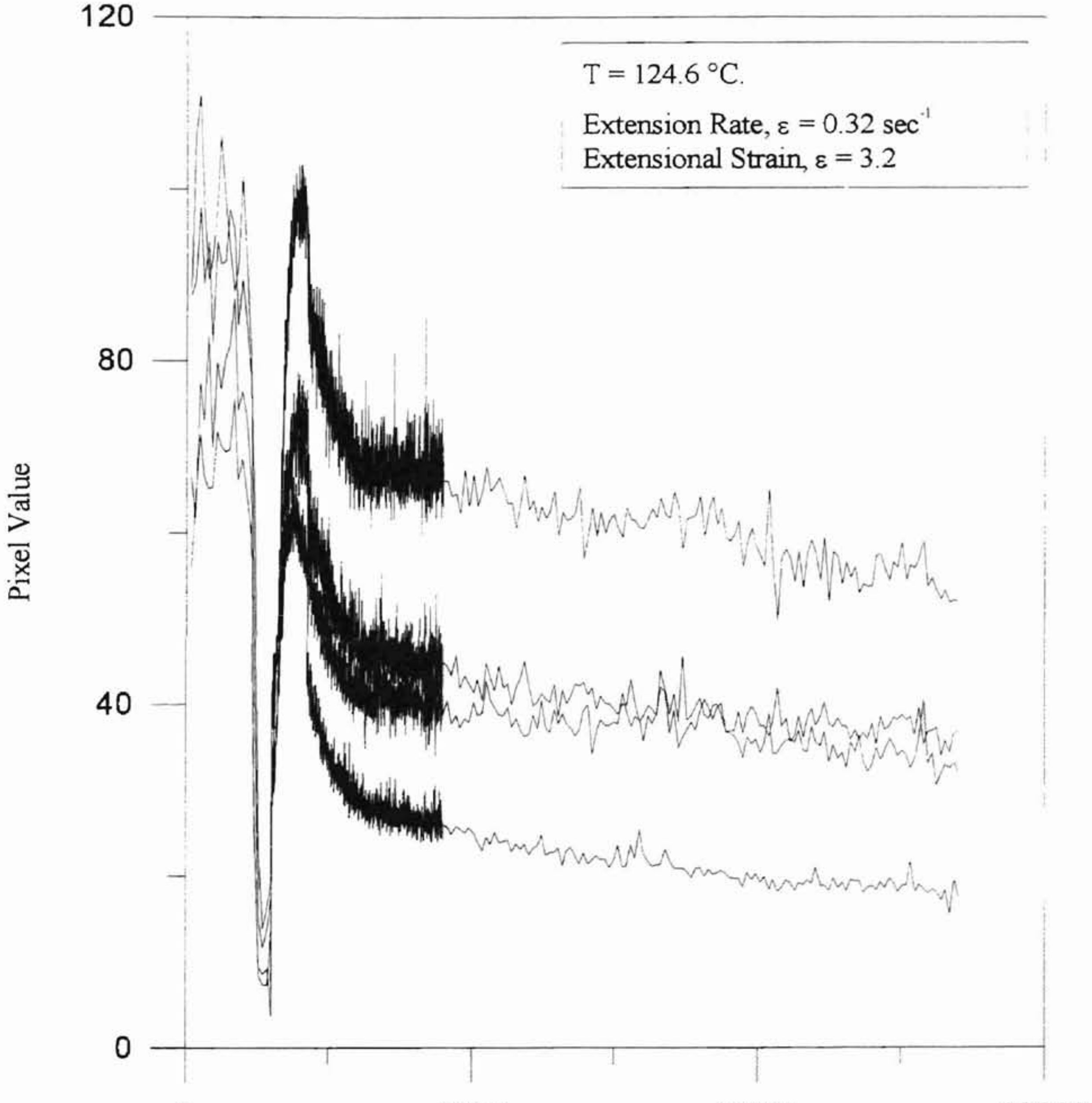

Figure D.6 (a) Pixel Value vs. Time for HDPE at Extension Rate = 0.32 sec^{-1}, Extensional Strain = 3.2

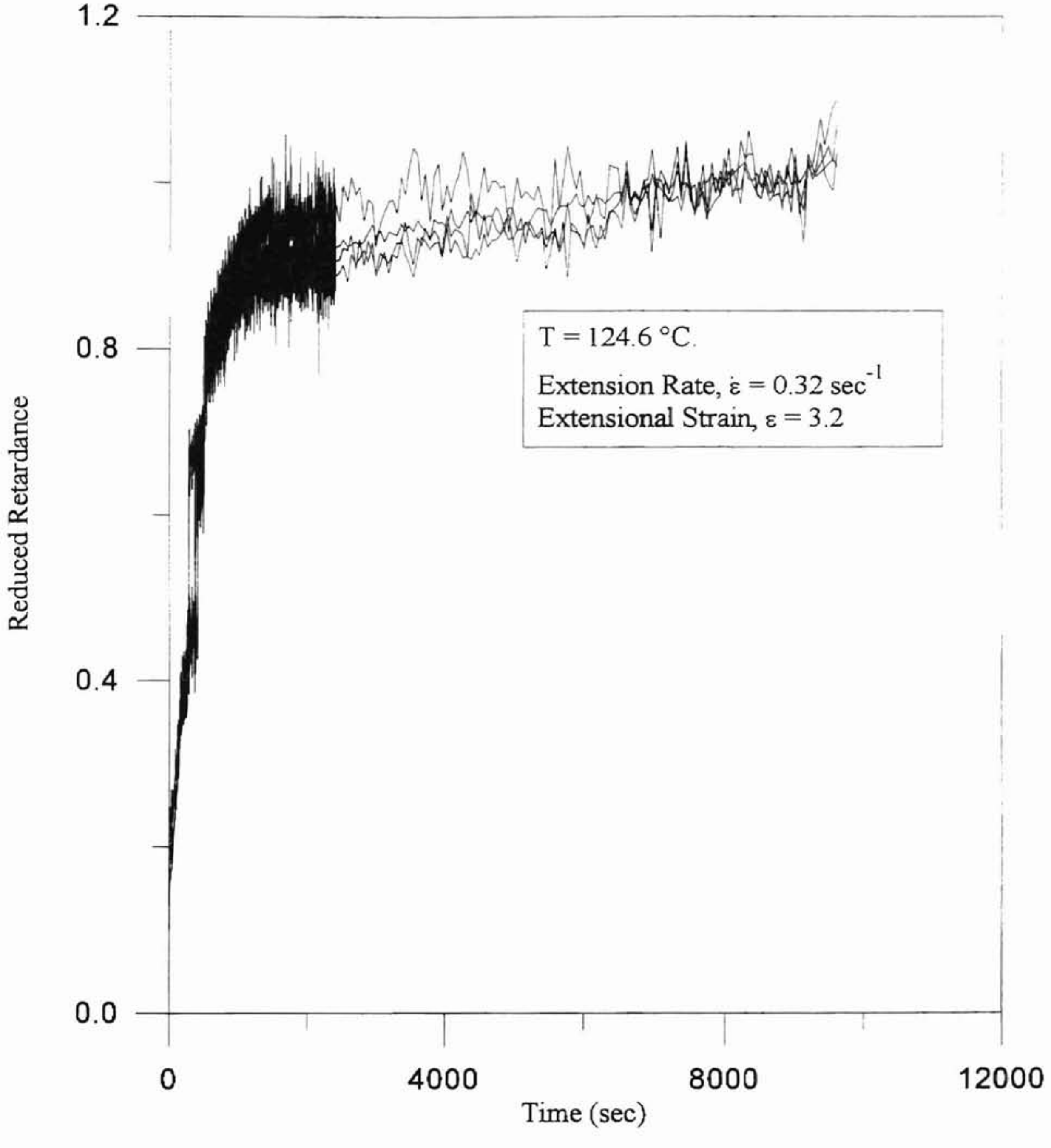

Figure D.6 (b) Reduced Retardance vs. Time for HDPE at Extension Rate = 0.32 sec^{-1}, Extensional Strain = 3.2

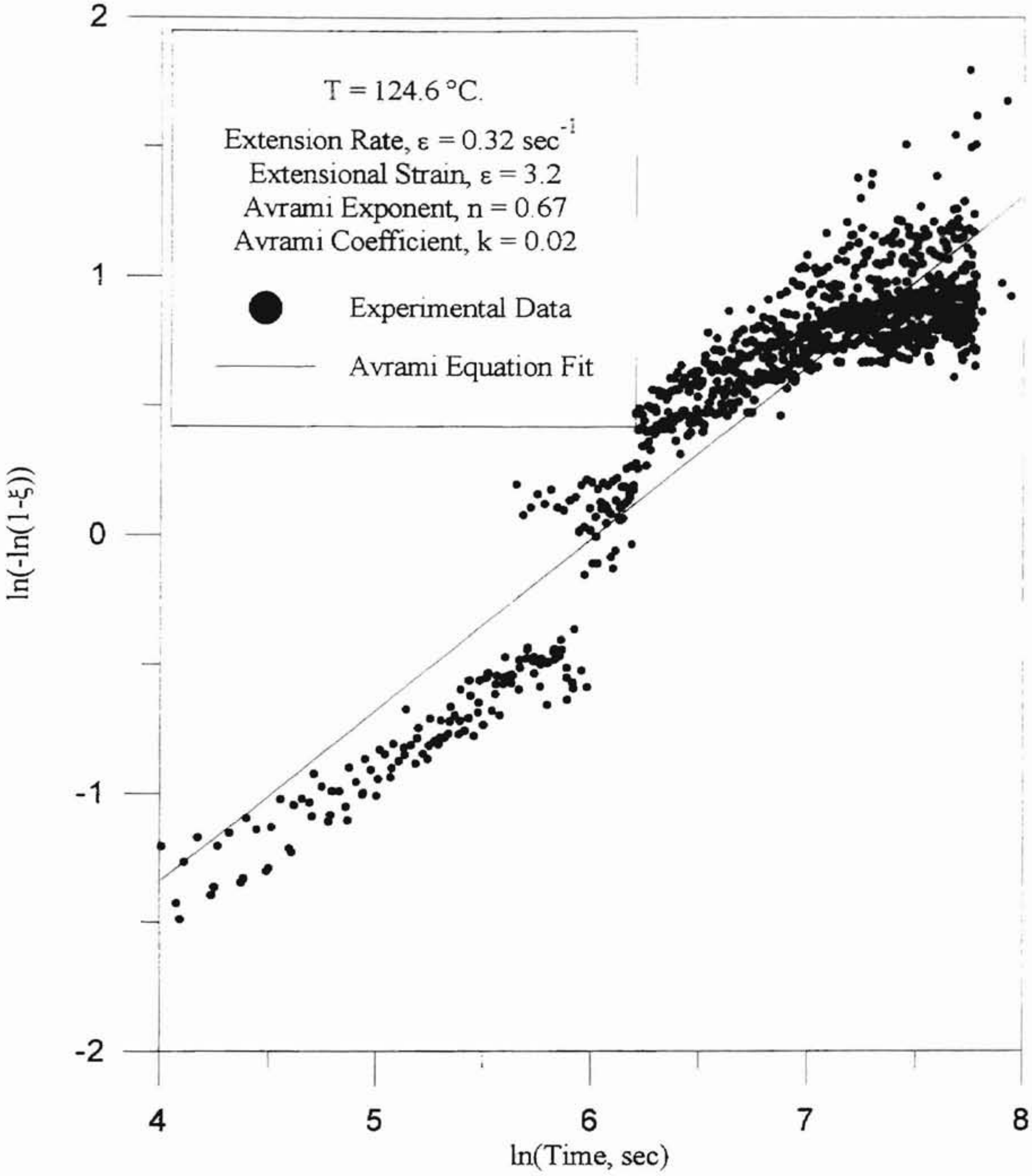

Figure D.6 (c) Correlation of Experimental Data With Avrami Equation for HDPE at Extension Rate = 0.32 sec $^{-1}$, Extensional Strain = 3.2

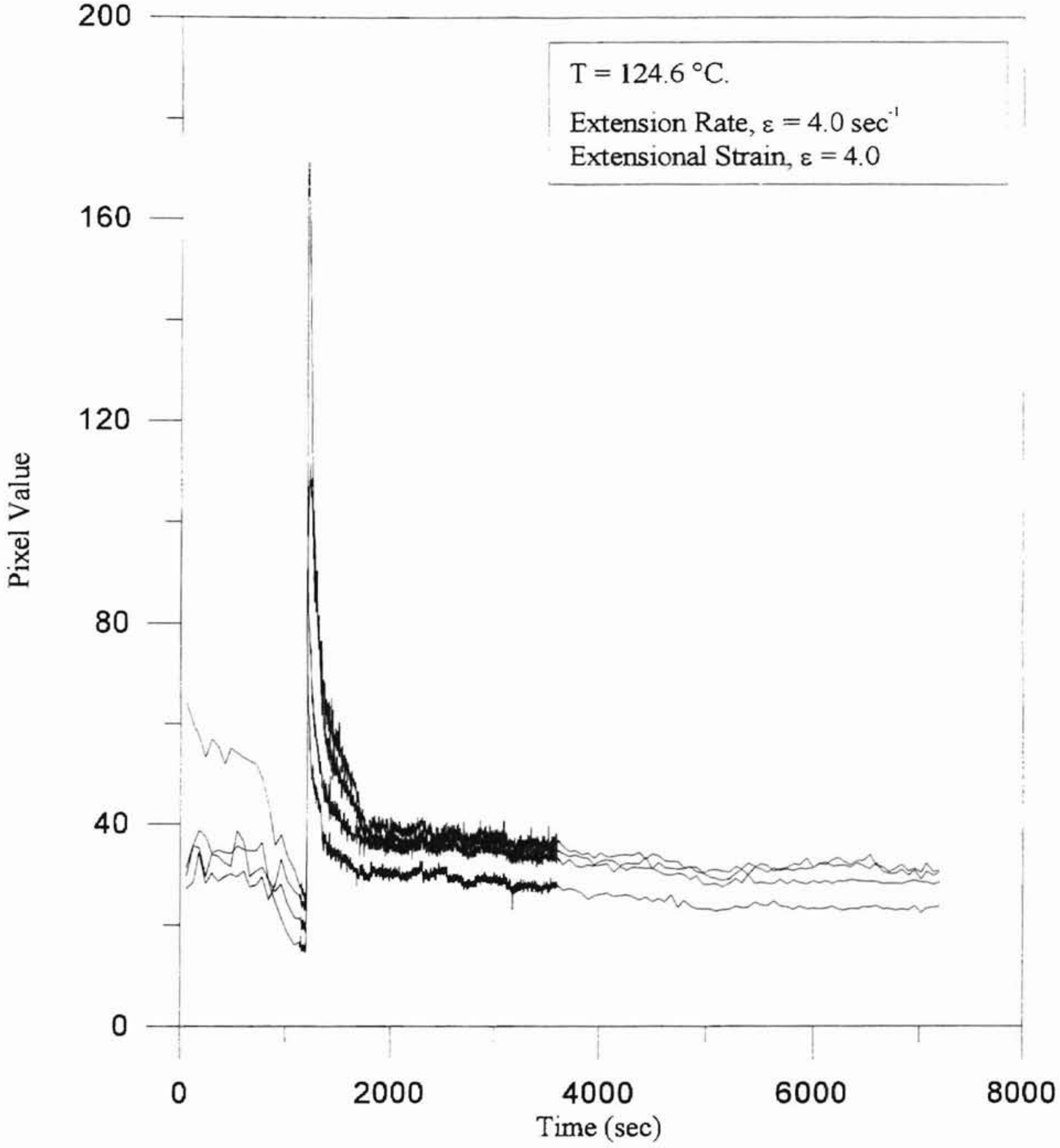

Figure D.7 (a) Pixel Value vs. Time for HDPE at Extension Rate = 4.0 sec^{-1}, Extensional Strain = 4.0

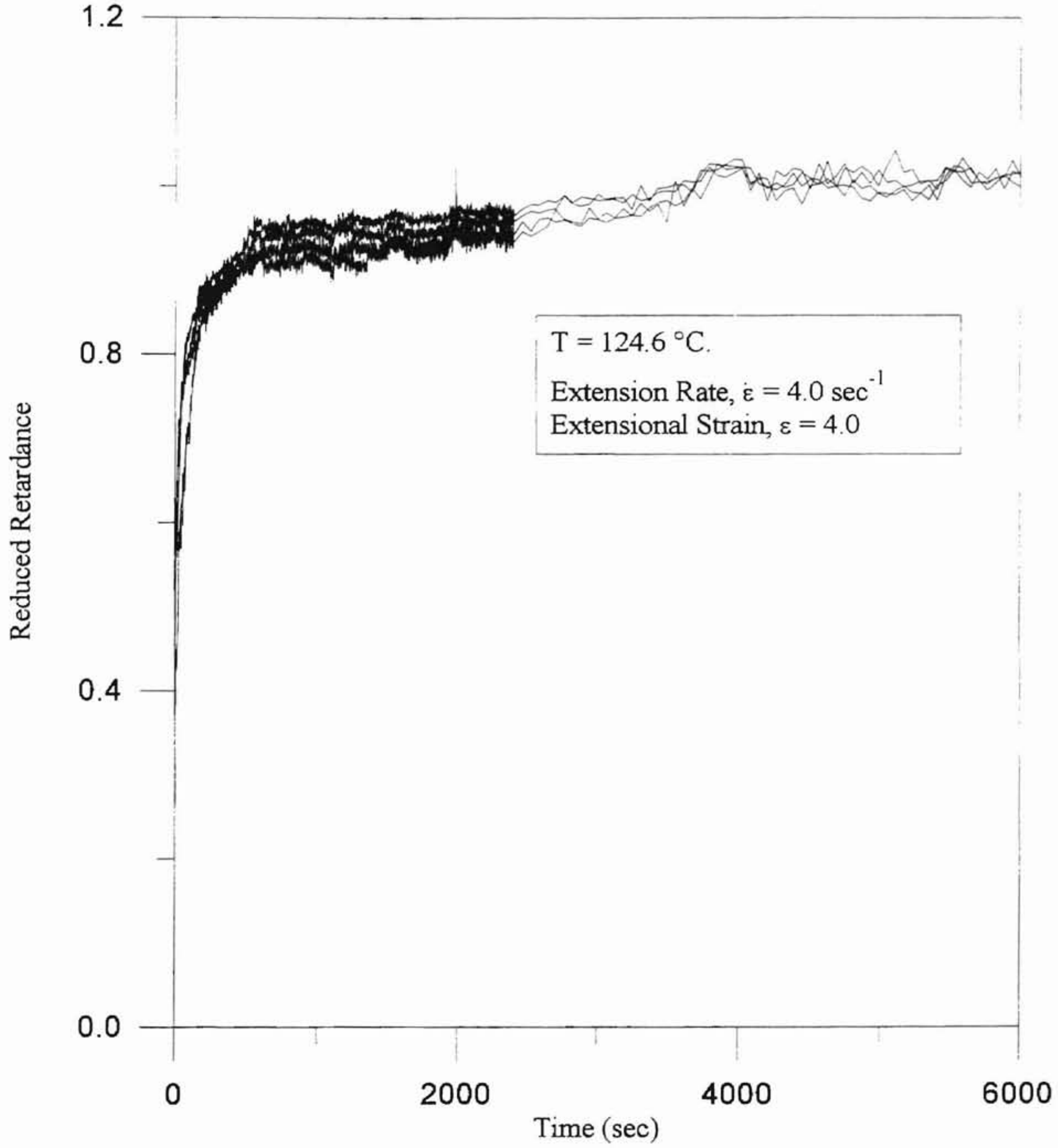

Figure D.7 (b) Reduced Retardance vs. Time for HDPE at Extension Rate = 4.0 sec^{-1}, Extensional Strain = 4.0

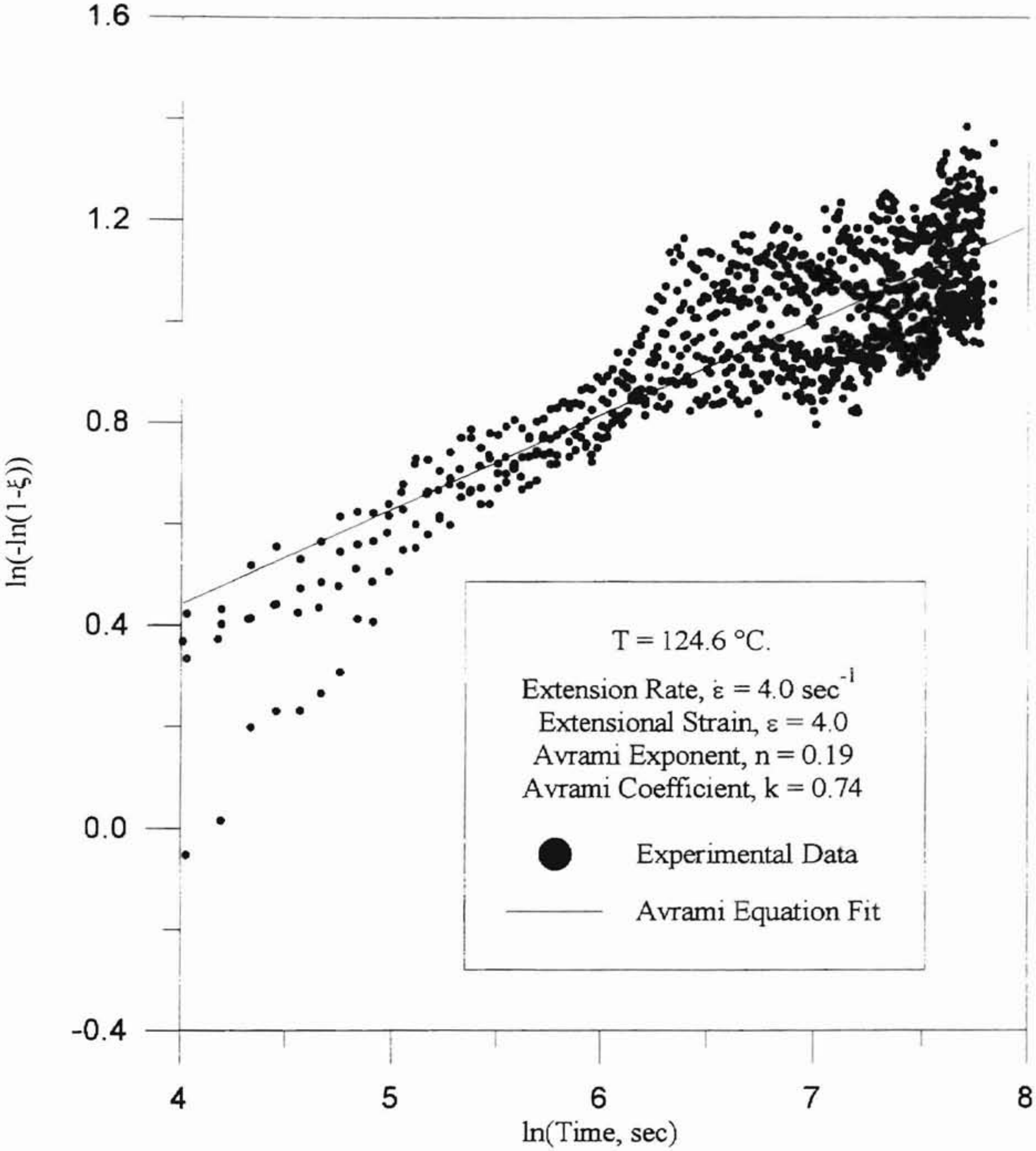

Figure D.7 (c) Correlation of Experimental Data With Avrami Equation for HDPE at Extension Rate = 4.0 sec $^{-1}$, Extensional Strain = 4.0

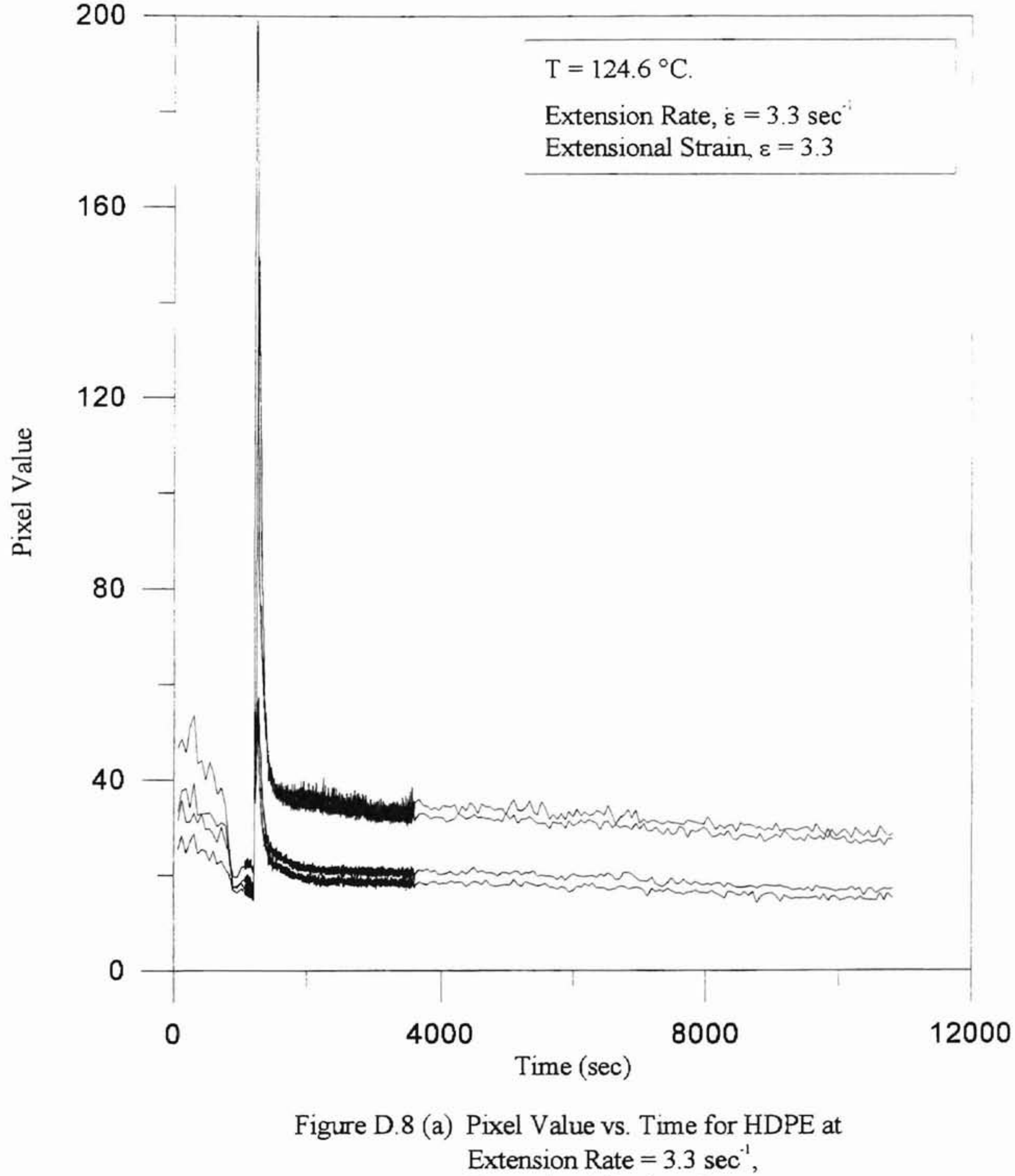

Figure D.8 (a) Pixel Value vs. Time for HDPE at Extension Rate = 3.3 sec^{-1}, Extensional Strain = 3.3

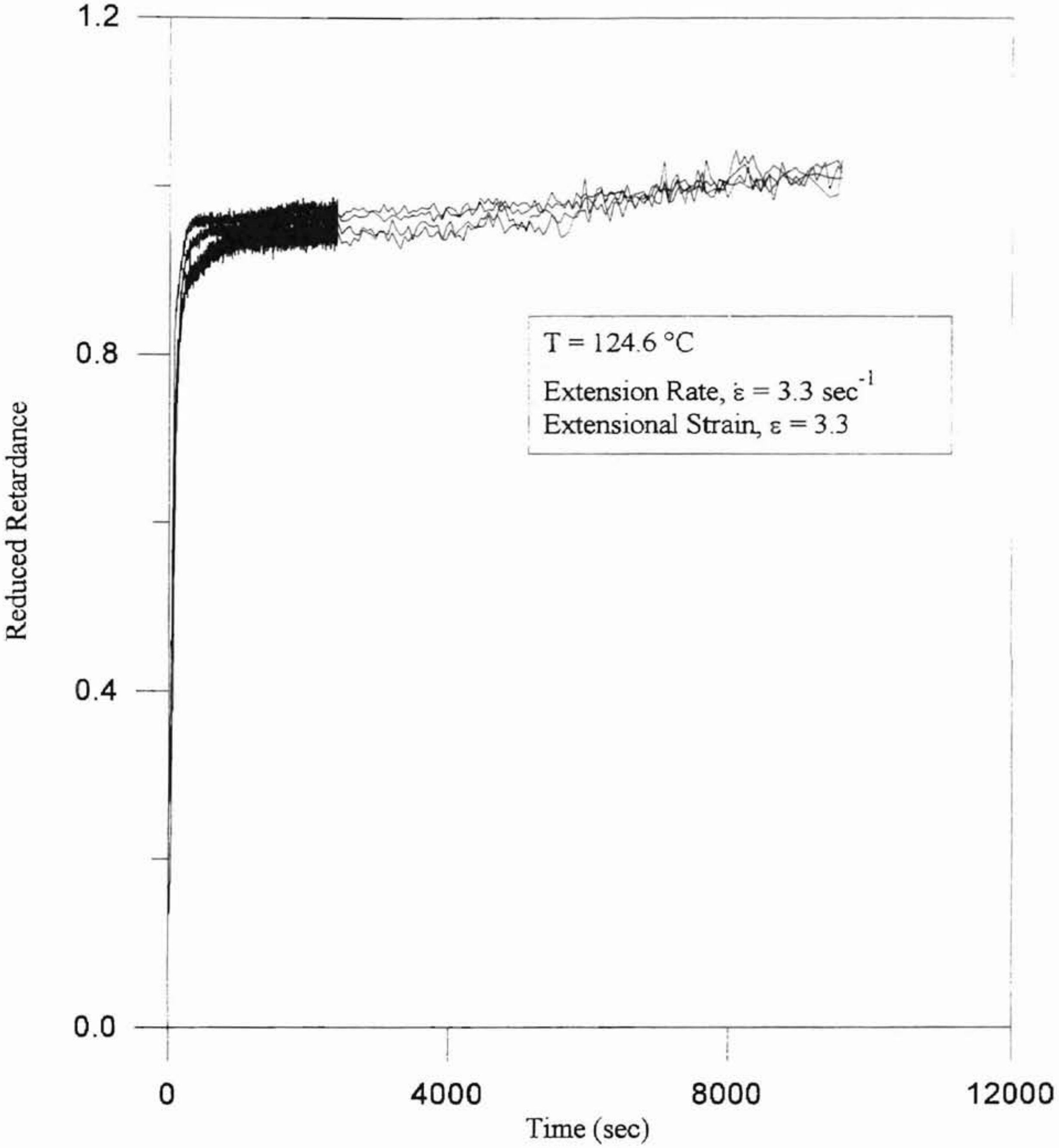

Figure D.8 (b) Reduced Retardance vs. Time for HDPE at Extension Rate = 3.3 sec^{-1}, Extensional Strain = 3.3

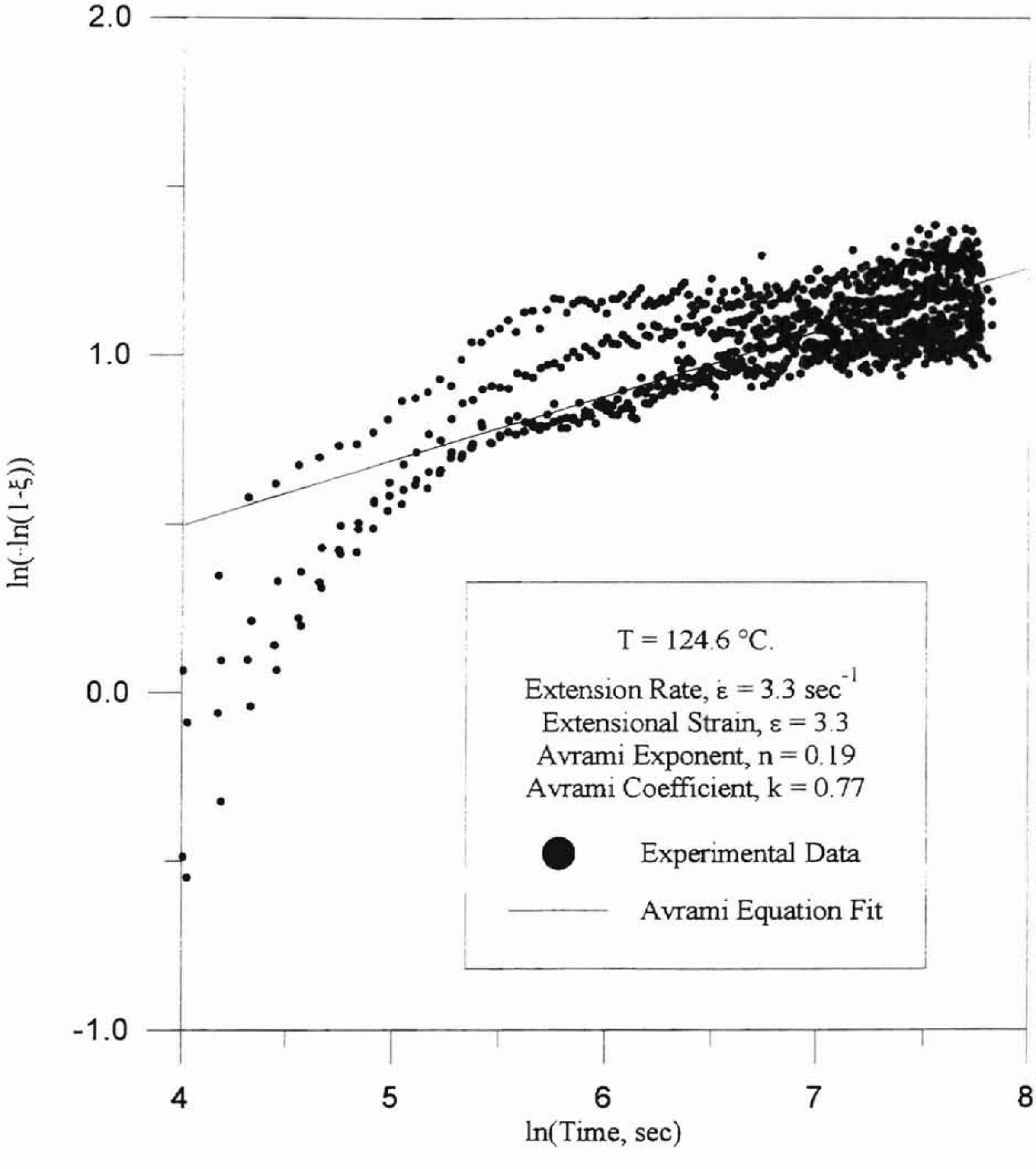

Figure D.8 (c) Correlation of Experimental Data With Avrami Equation for HDPE at Extension Rate = 3.3 sec $^{-1}$, Extensional Strain = 3.3

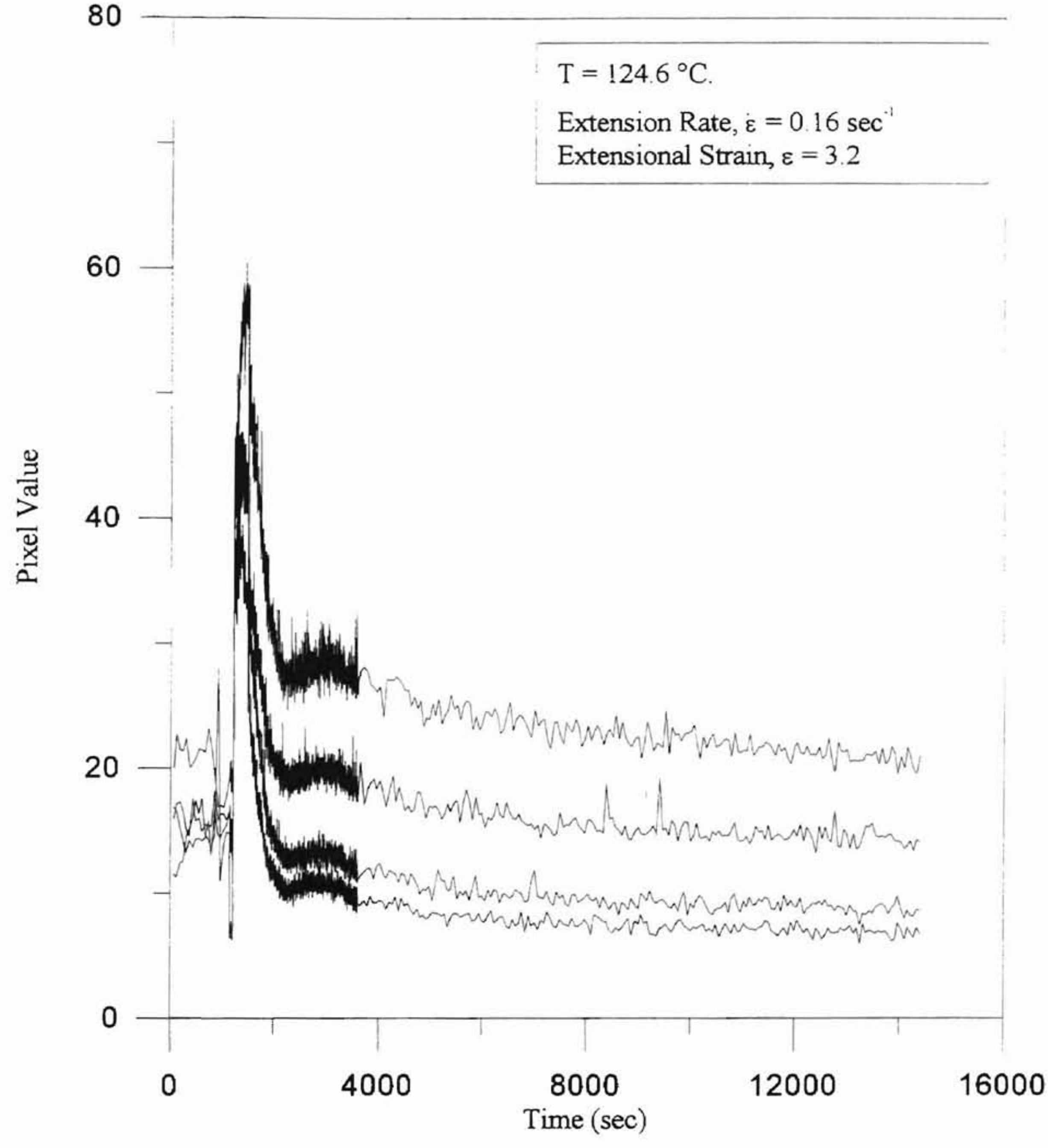

Figure D.9 (a) Pixel Value vs. Time for HDPE at Extension Rate = 0.16 sec^{-1}, Extensional Strain = 3.2

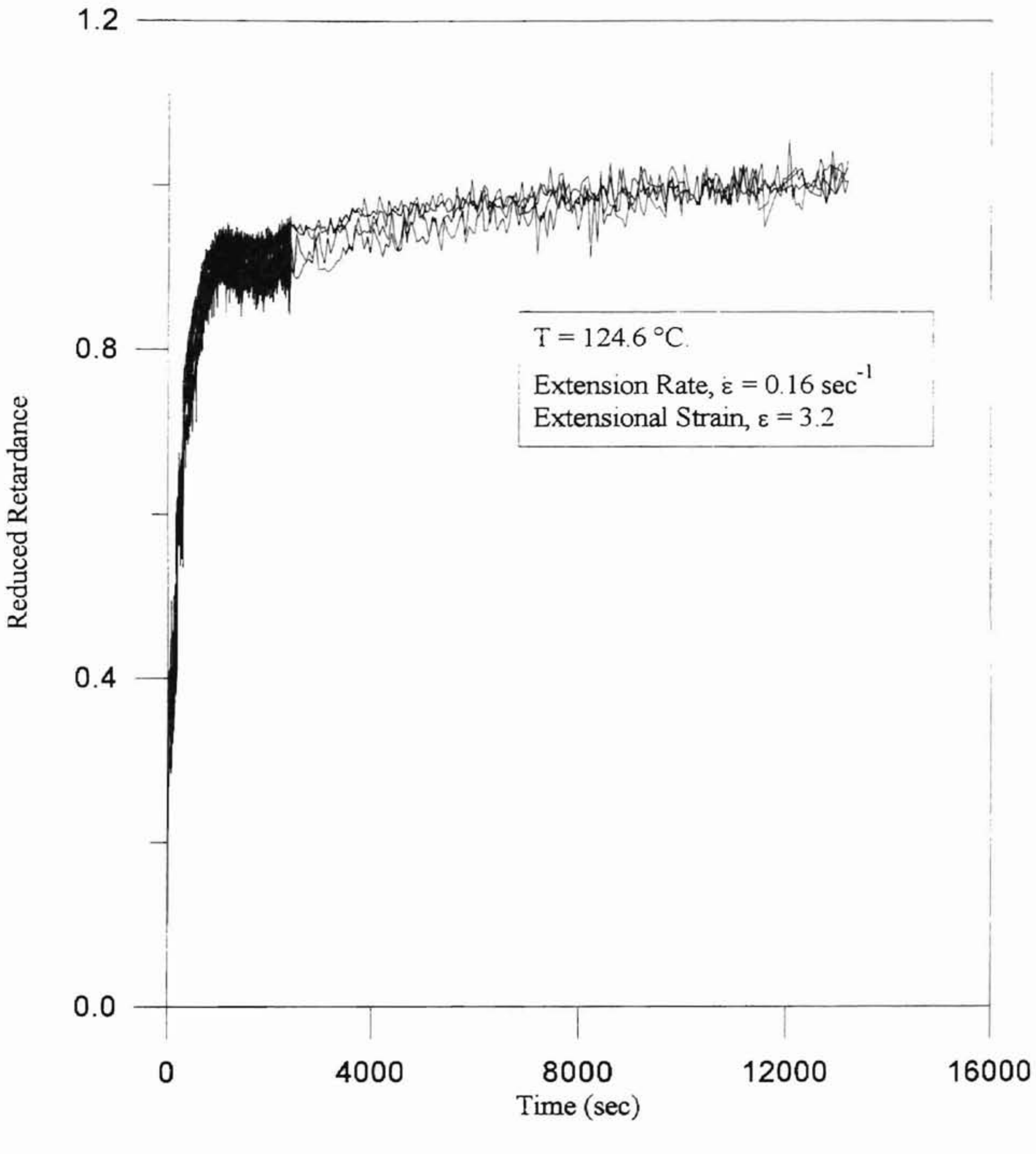

Figure D.9 (b) Reduced Retardance vs. Time for HDPE at Extension Rate = 0.16 sec^{-1}, Extensional Strain = 3.2

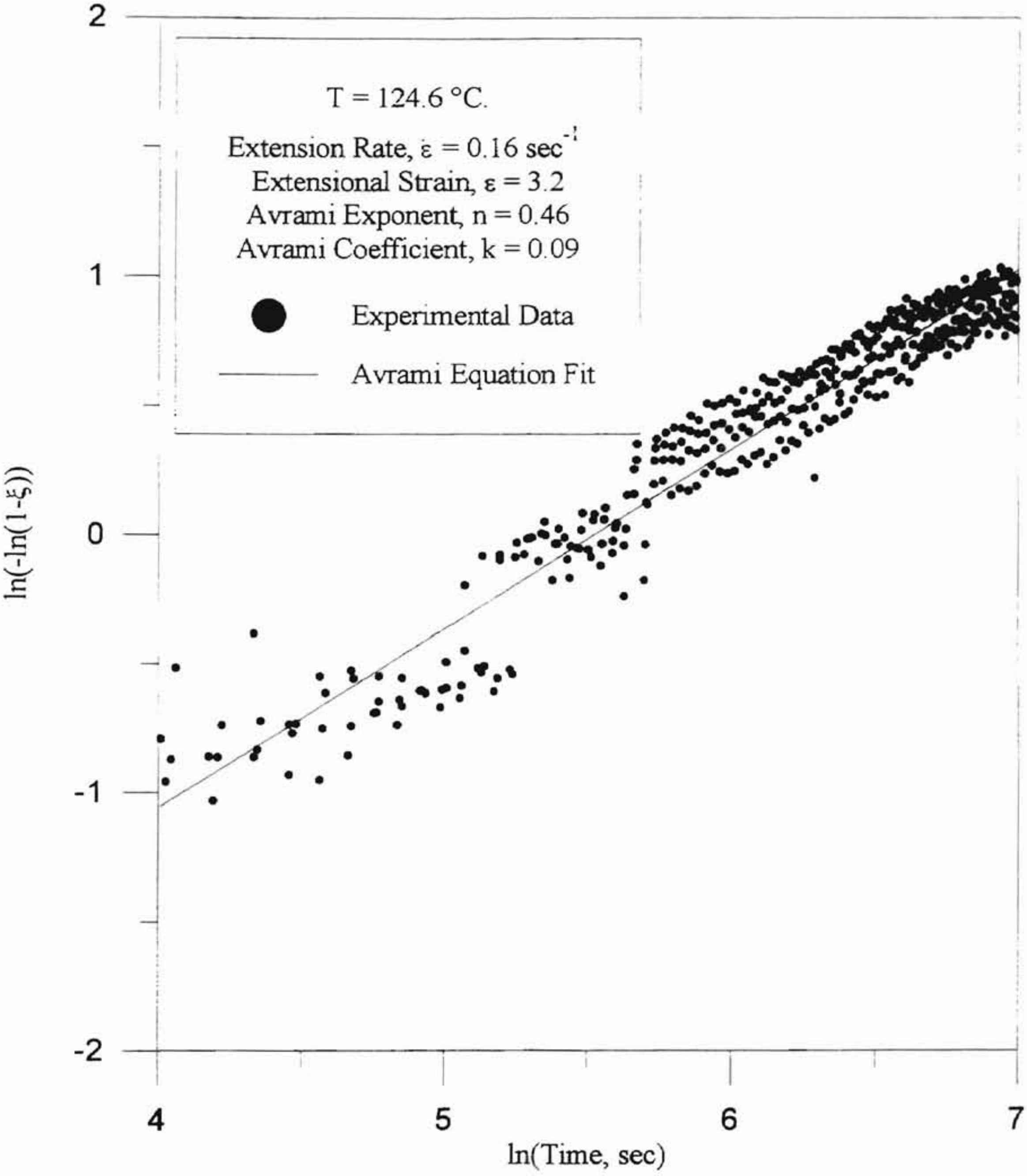

Figure D.9 (c) Correlation of Experimental Data With Avrami Equation for HDPE at Extension Rate = 0.16 sec $^{-1}$, Extensional Strain = 3.2

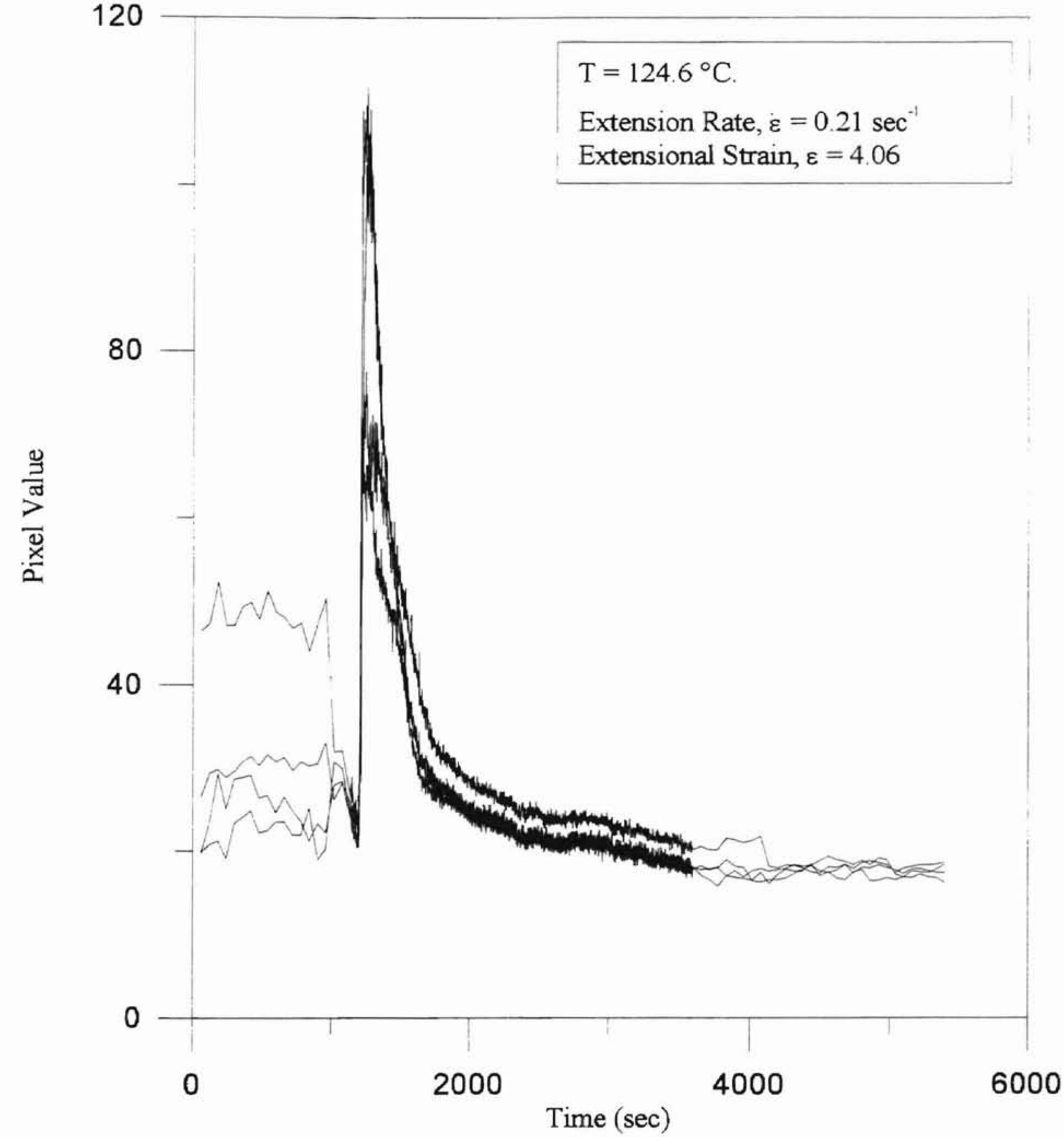

Figure D.10 (a) Pixel Value vs. Time for HDPE at Extension Rate = 0.21 sec^{-1}, Extensional Strain = 4.06

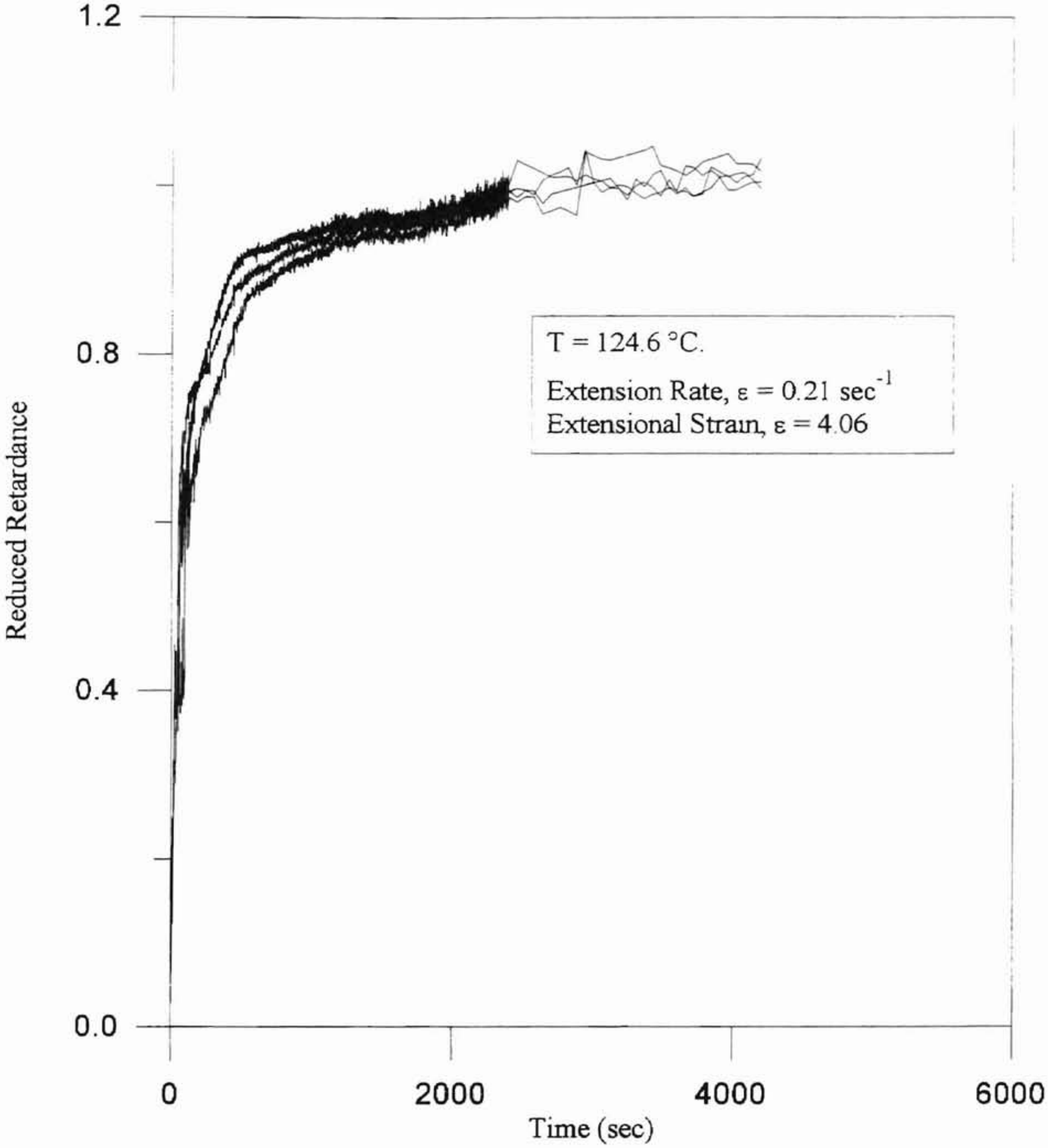

Figure D.10 (b) Reduced Retardance vs. Time for HDPE at
Extension Rate = 0.21 sec^{-1},
Extensional Strain = 4.06

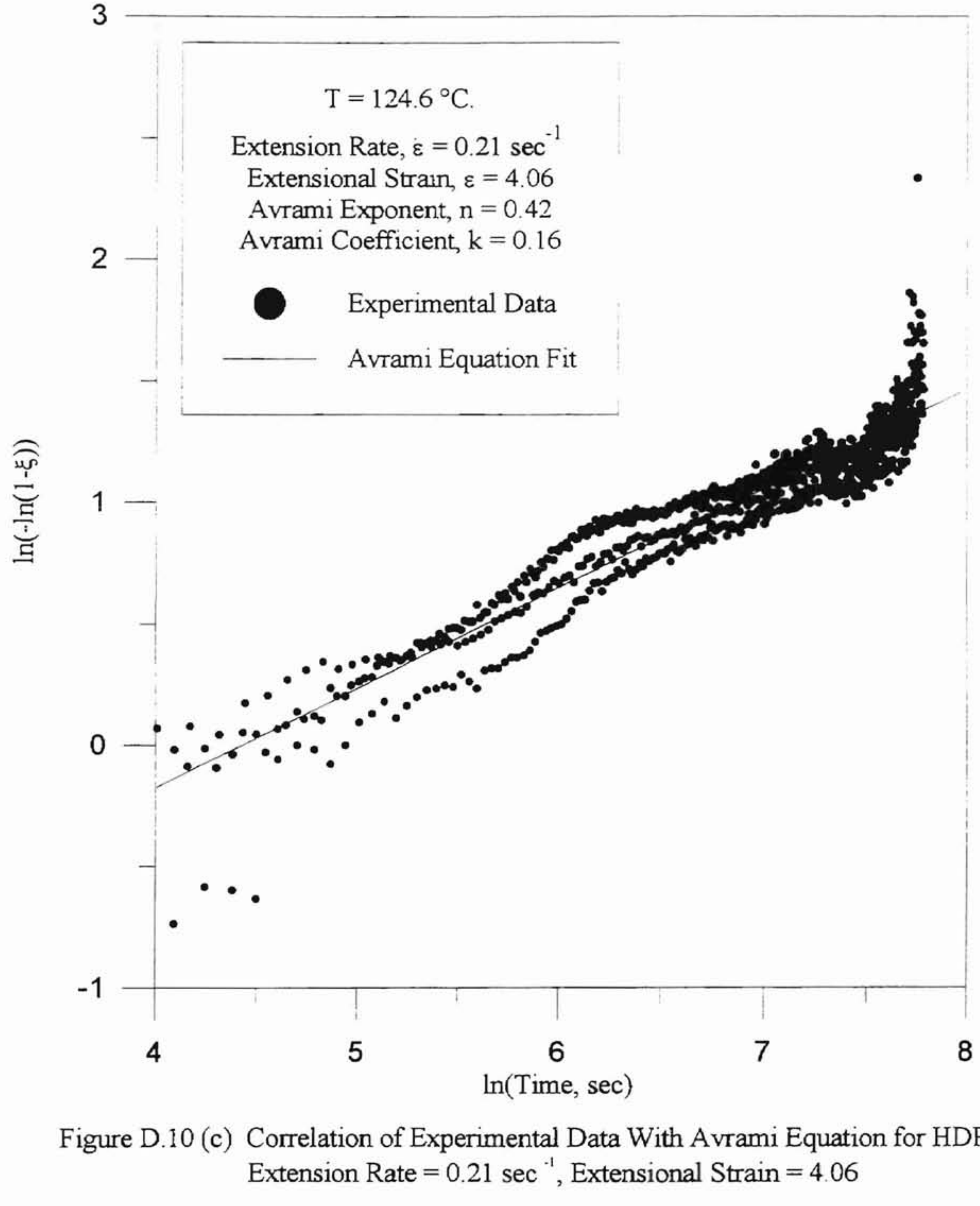

Figure D.10 (c) Correlation of Experimental Data With Avrami Equation for HDPE at Extension Rate = 0.21 sec^{-1}, Extensional Strain = 4.06

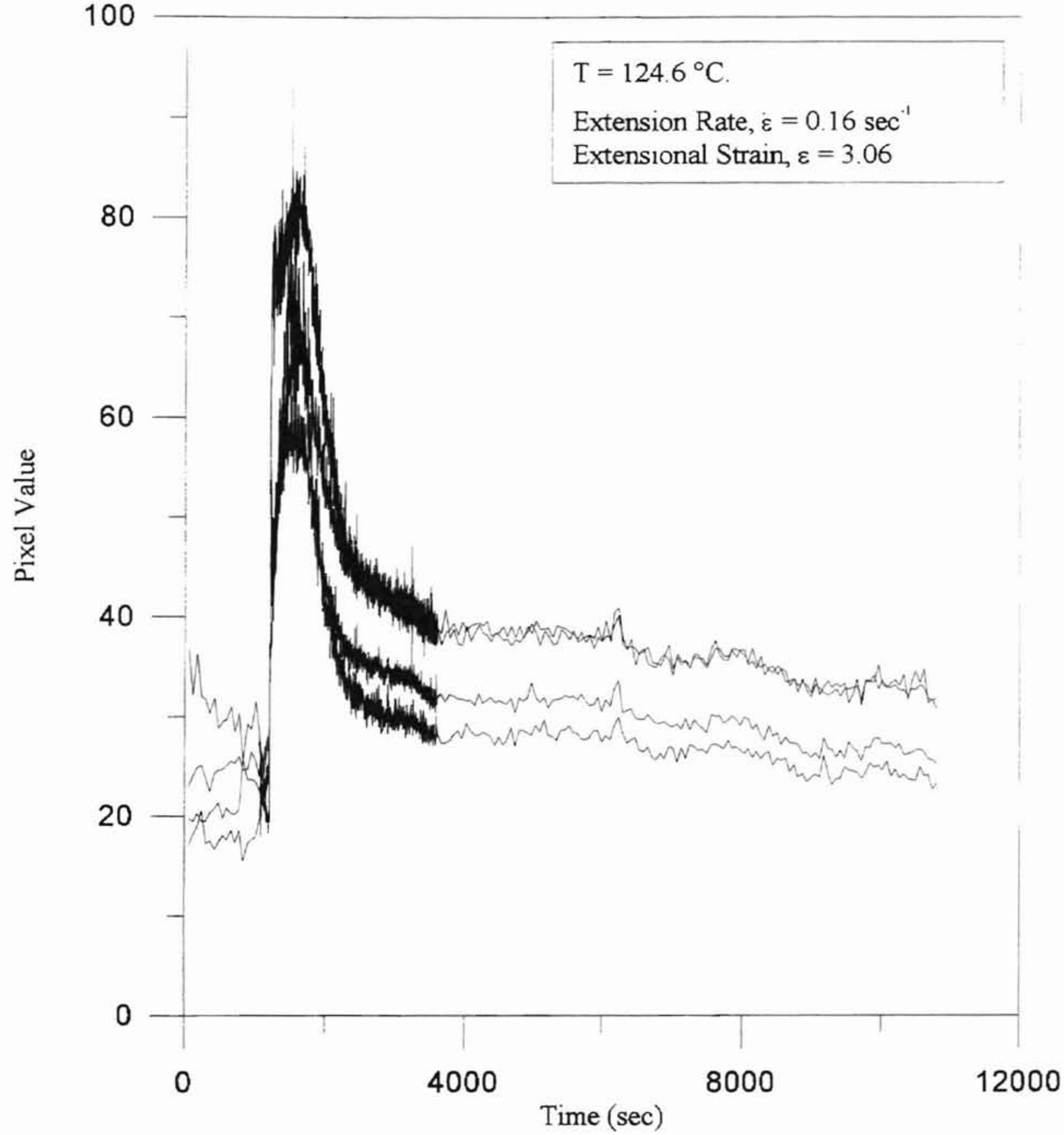

Figure D.11 (a) Pixel Value vs. Time for HDPE at Extension Rate = 0.16 sec^{-1}, Extensional Strain = 3.06

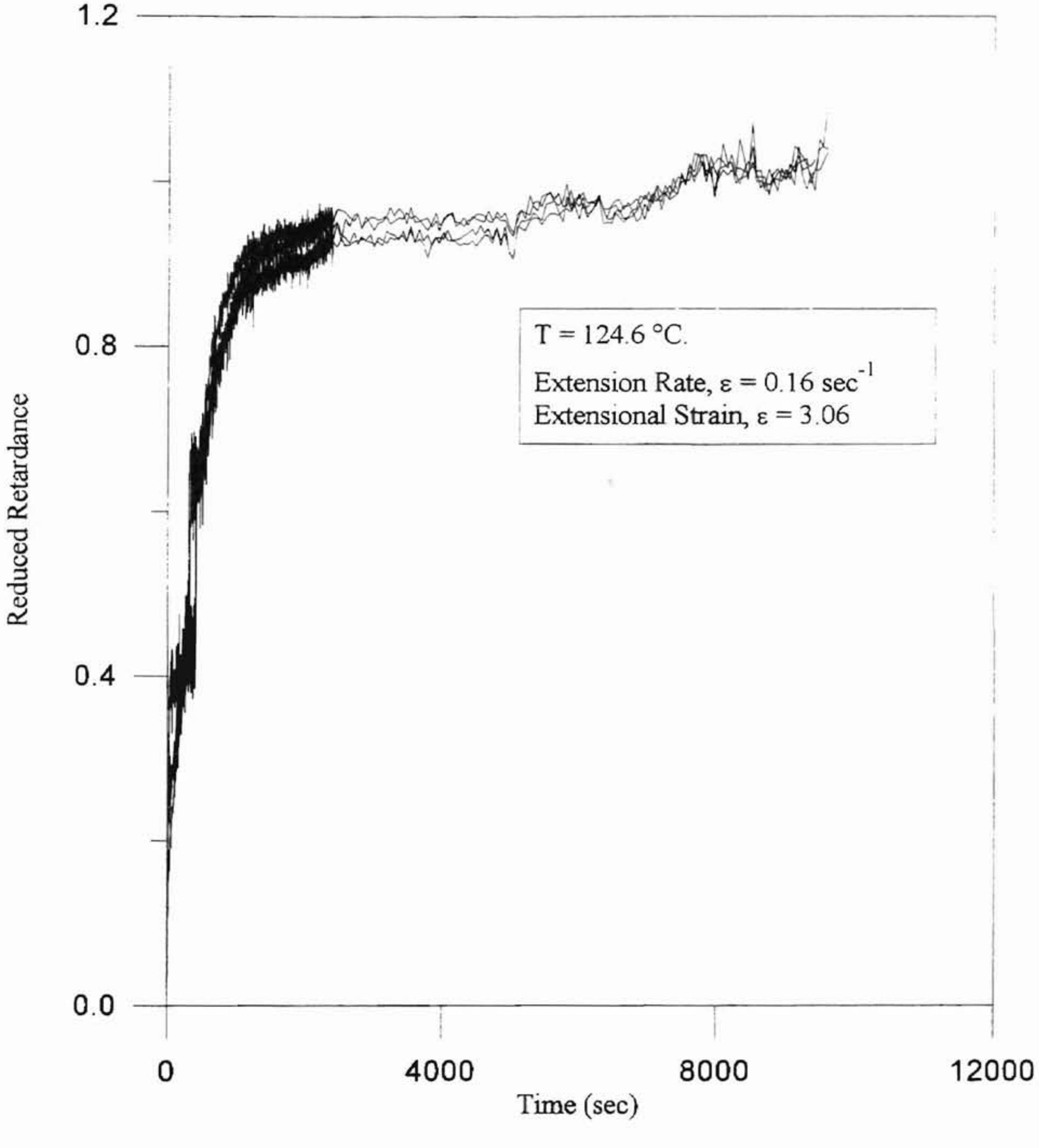

Figure D.11 (b) Reduced Retardance vs. Time for HDPE at Extension Rate = 0.16 sec^{-1}, Extensional Strain = 3.06

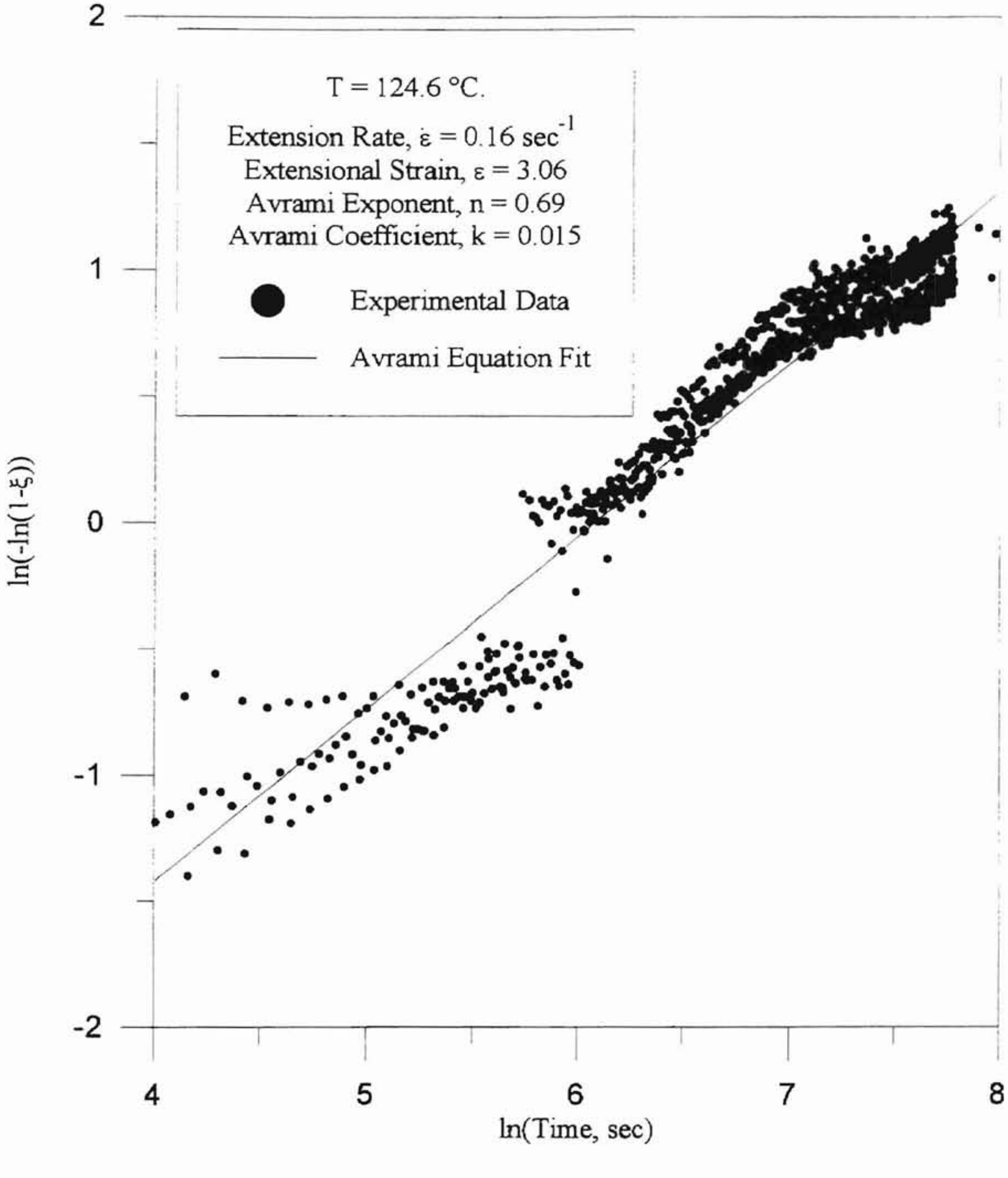

Figure D.11 (c) Correlation of Experimental Data With Avrami Equation for HDPE at Extension Rate = 0.16 sec $^{-1}$, Extensional Strain = 3.06

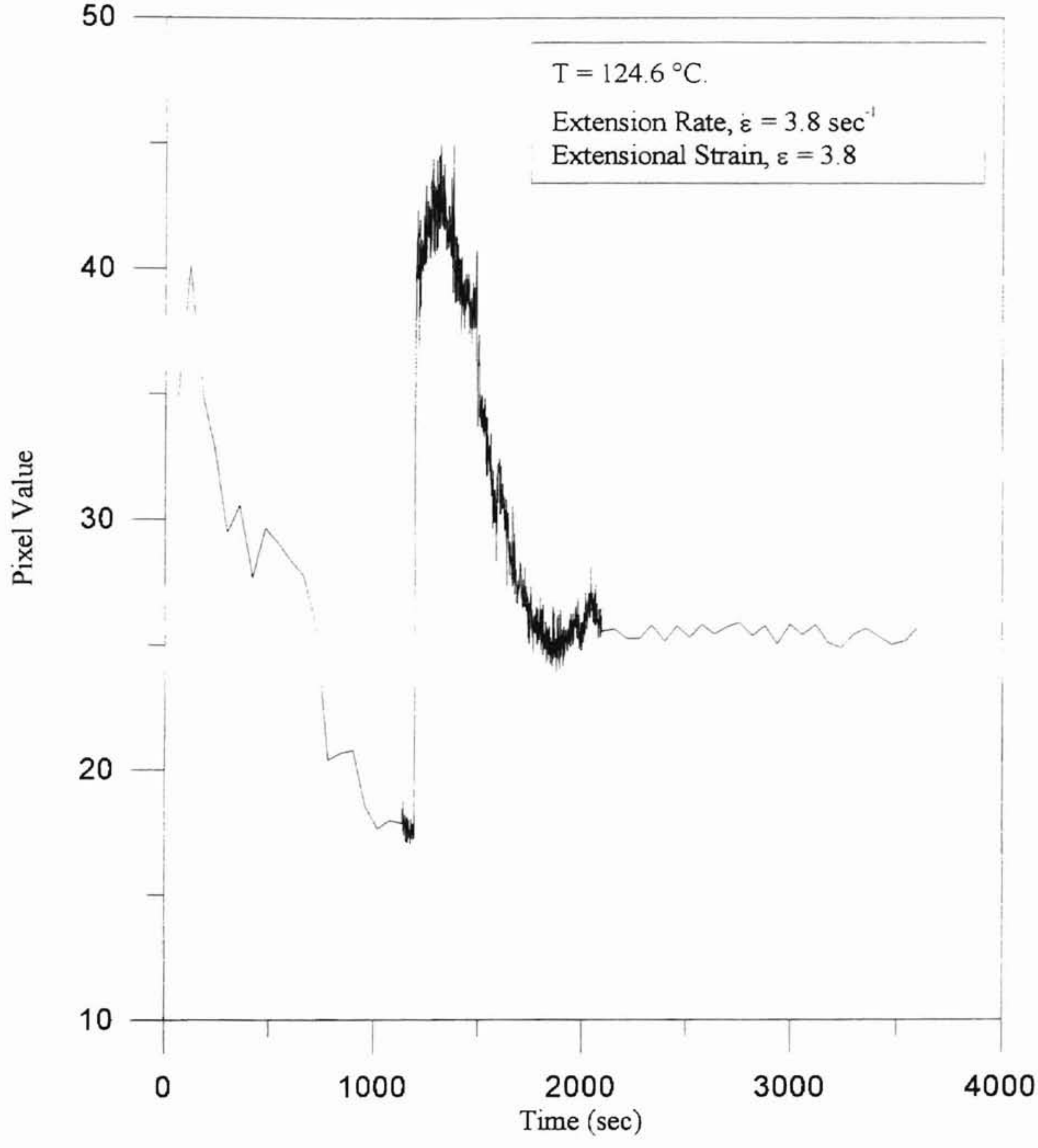

Figure D.12 (a) Pixel Value vs. Time for HDPE at Extension Rate = 3.8 sec^{-1}, Extensional Strain = 3.8

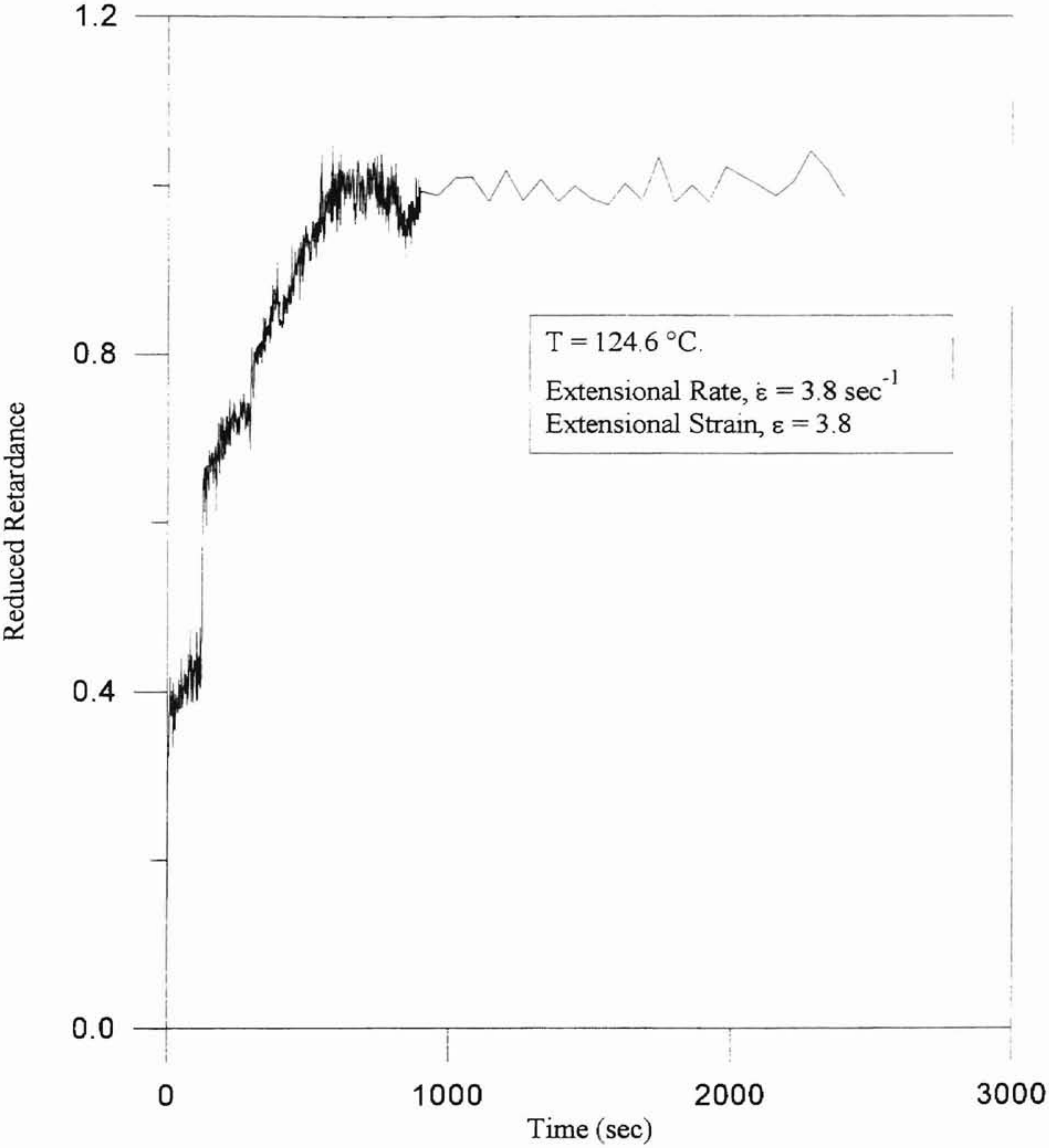

Figure D.12 (b) Reduced Retardance vs. Time for HDPE at Extension Rate = 3.8 sec^{-1}, Extensional Strain = 3.8

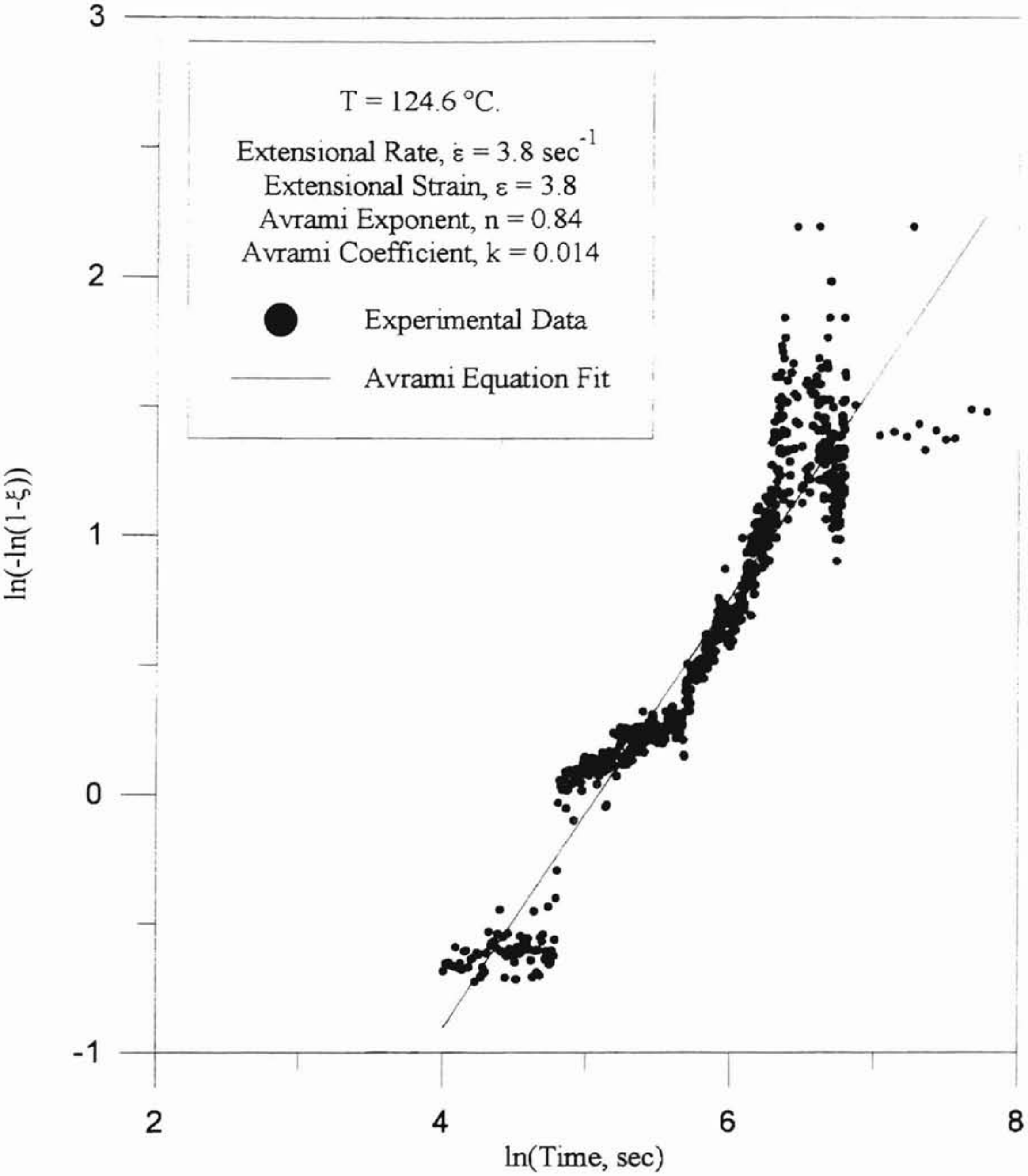

Figure D.12 (c) Correlation of Experimental Data With Avrami Equation for HDPE at Extension Rate = 3.8 sec $^{-1}$, Extensional Strain = 3.8

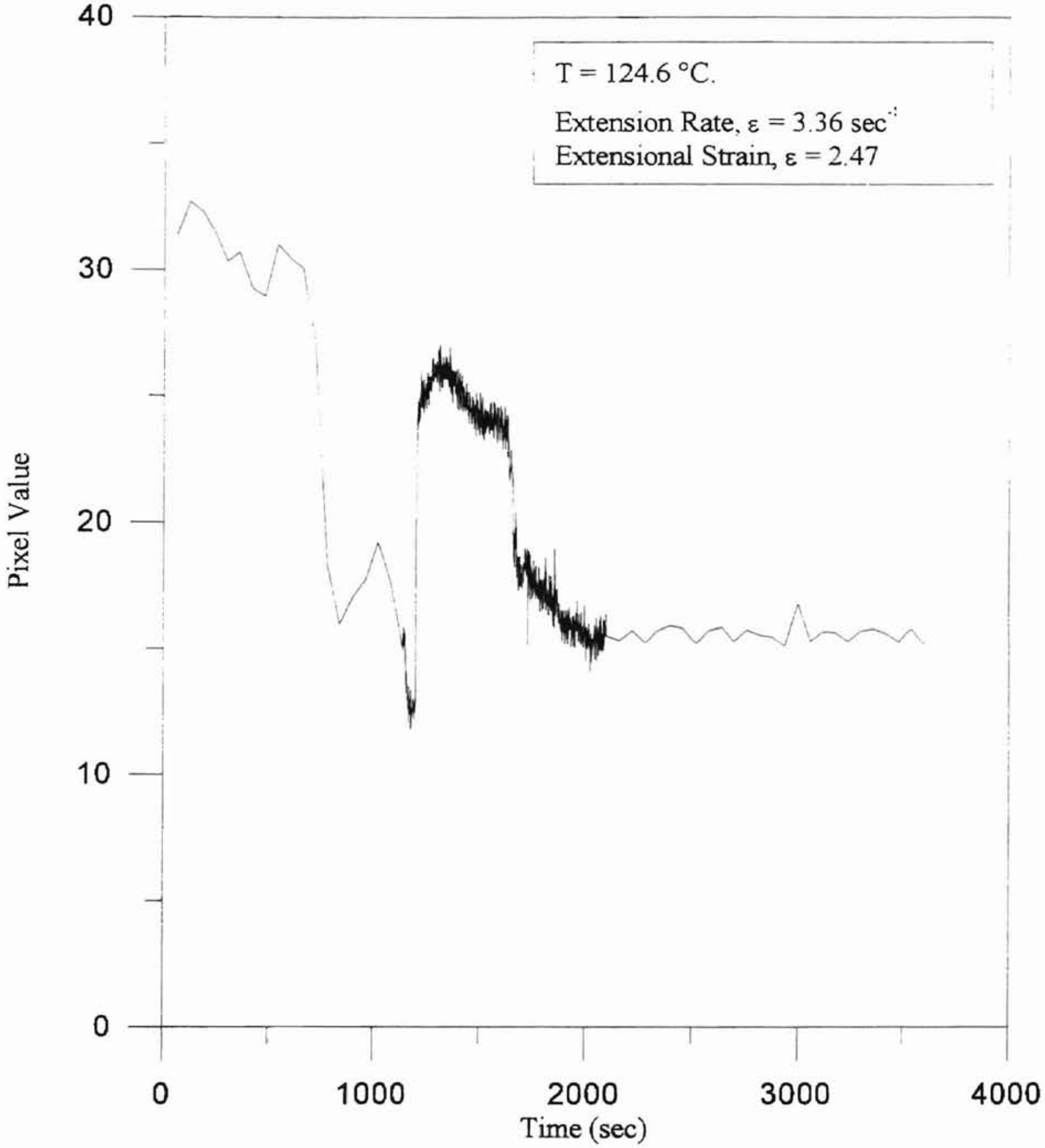

Figure D.13 (a) Pixel Value vs. Time for HDPE at Extension Rate = 3.36 sec^{-1}, Extensional Strain = 2.47

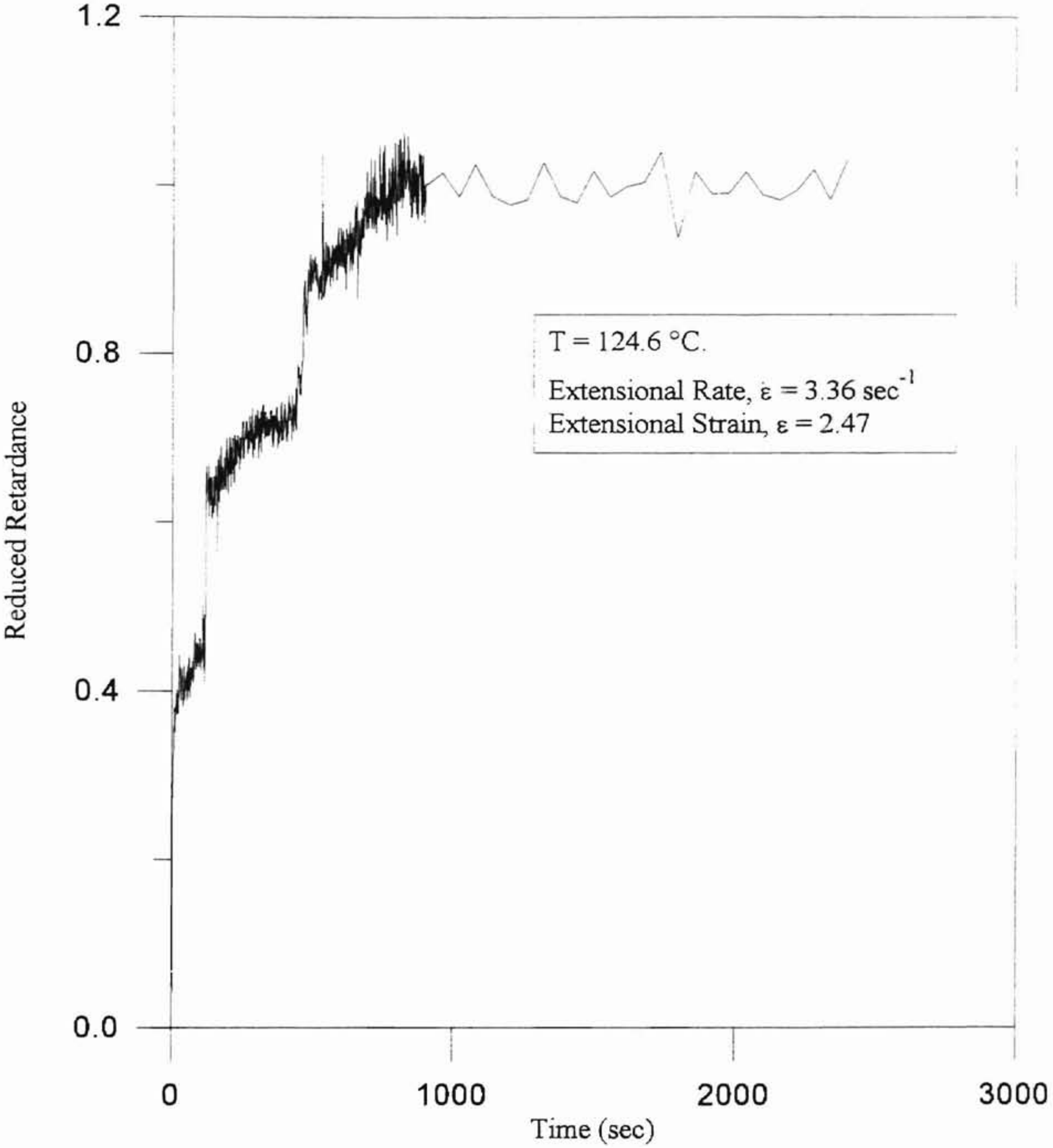

Figure D.13 (b) Reduced Retardance vs. Time for HDPE at Extension Rate = 3.36 sec^{-1}, Extensional Strain = 2.47

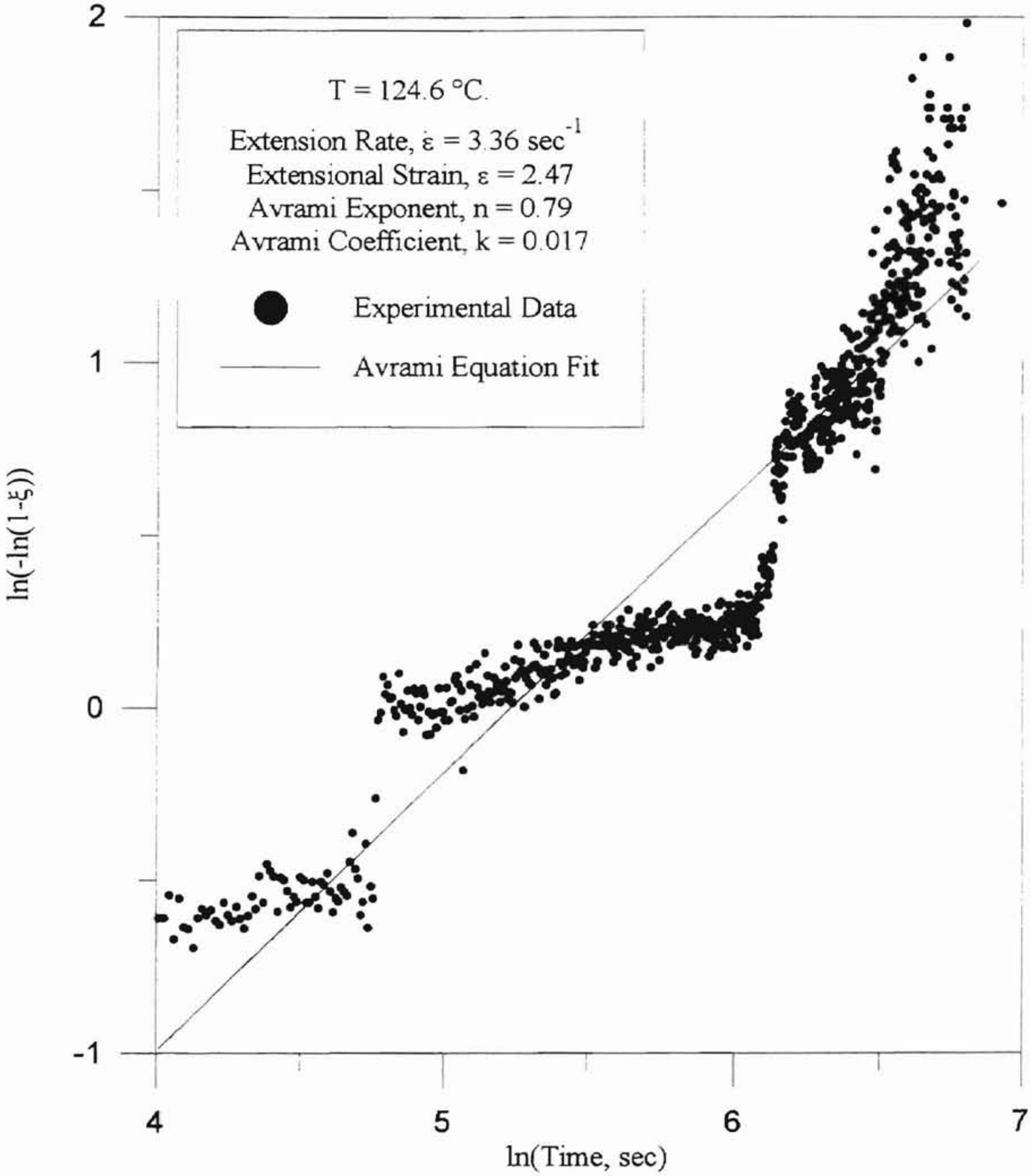

Figure D.13 (c) Correlation of Experimental Data With Avrami Equation for HDPE at Extension Rate = 3.36 sec^{-1}, Extensional Strain = 2.47

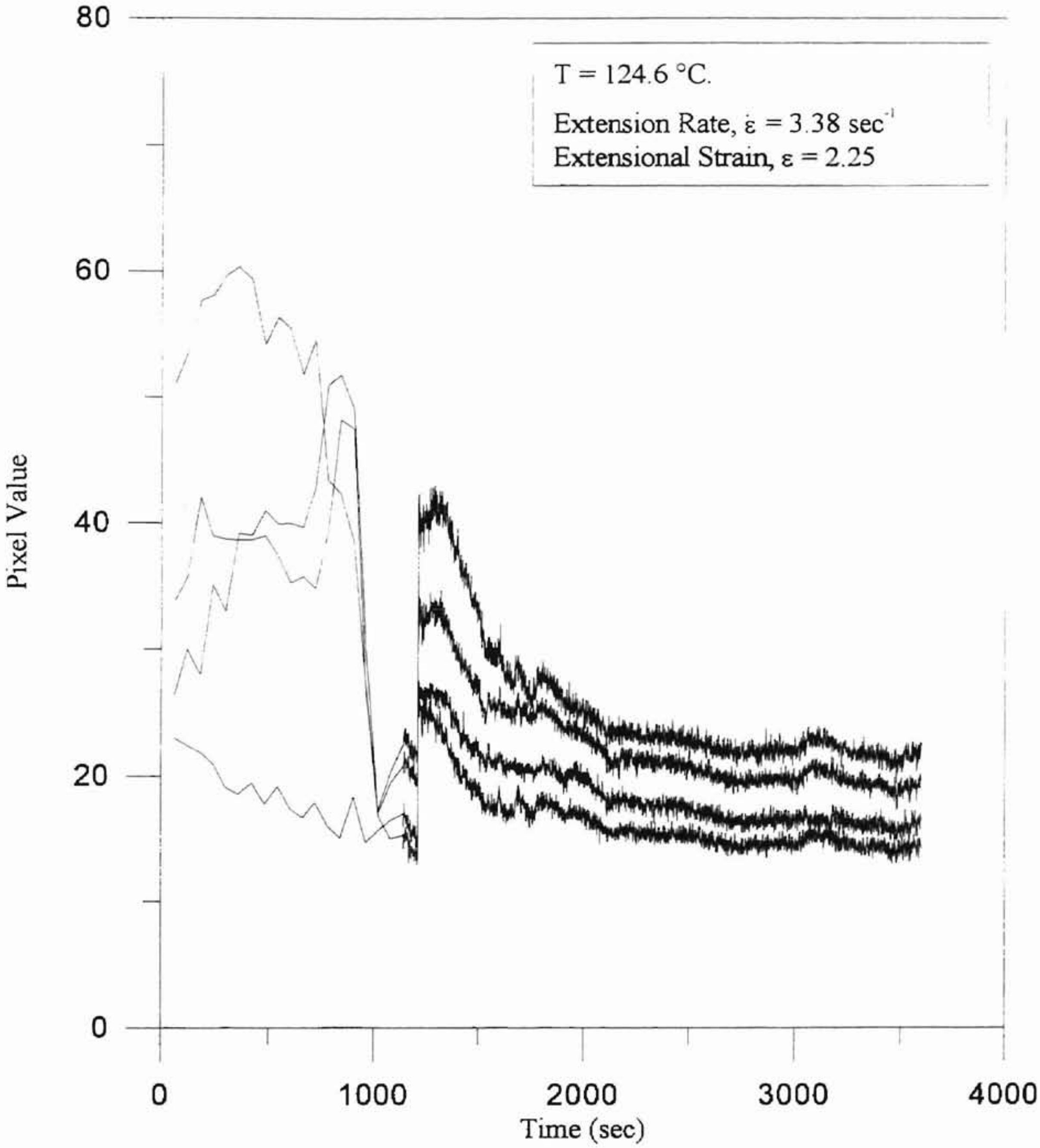

Figure D.14 (a) Pixel Value vs. Time for HDPE at
Extension Rate = 3.38 sec^{-1},
Extensional Strain = 2.25

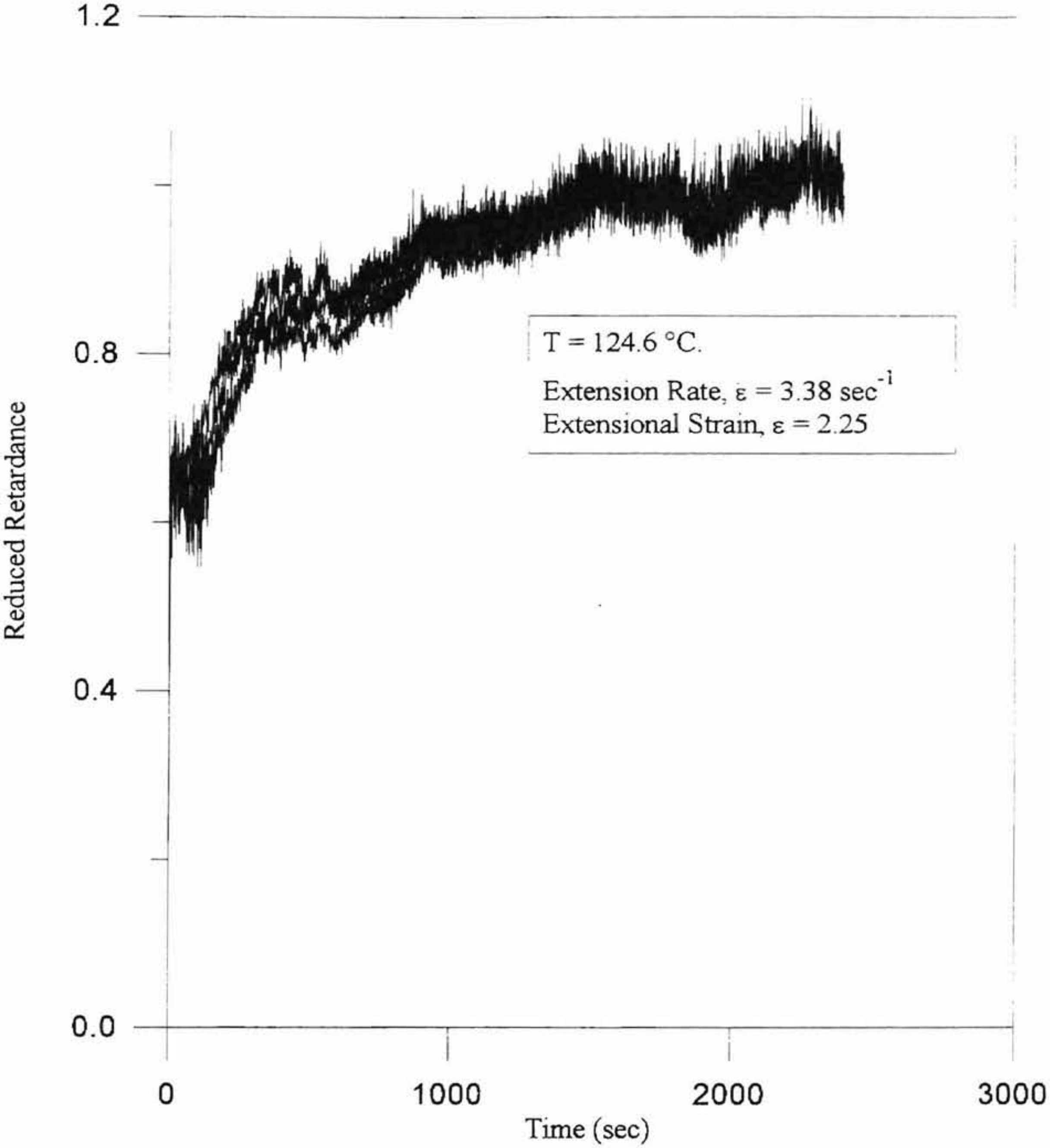

Figure D.14 (b) Reduced Retardance vs. Time for HDPE at Extension Rate = 3.38 sec^{-1}, Extensional Strain = 2.25

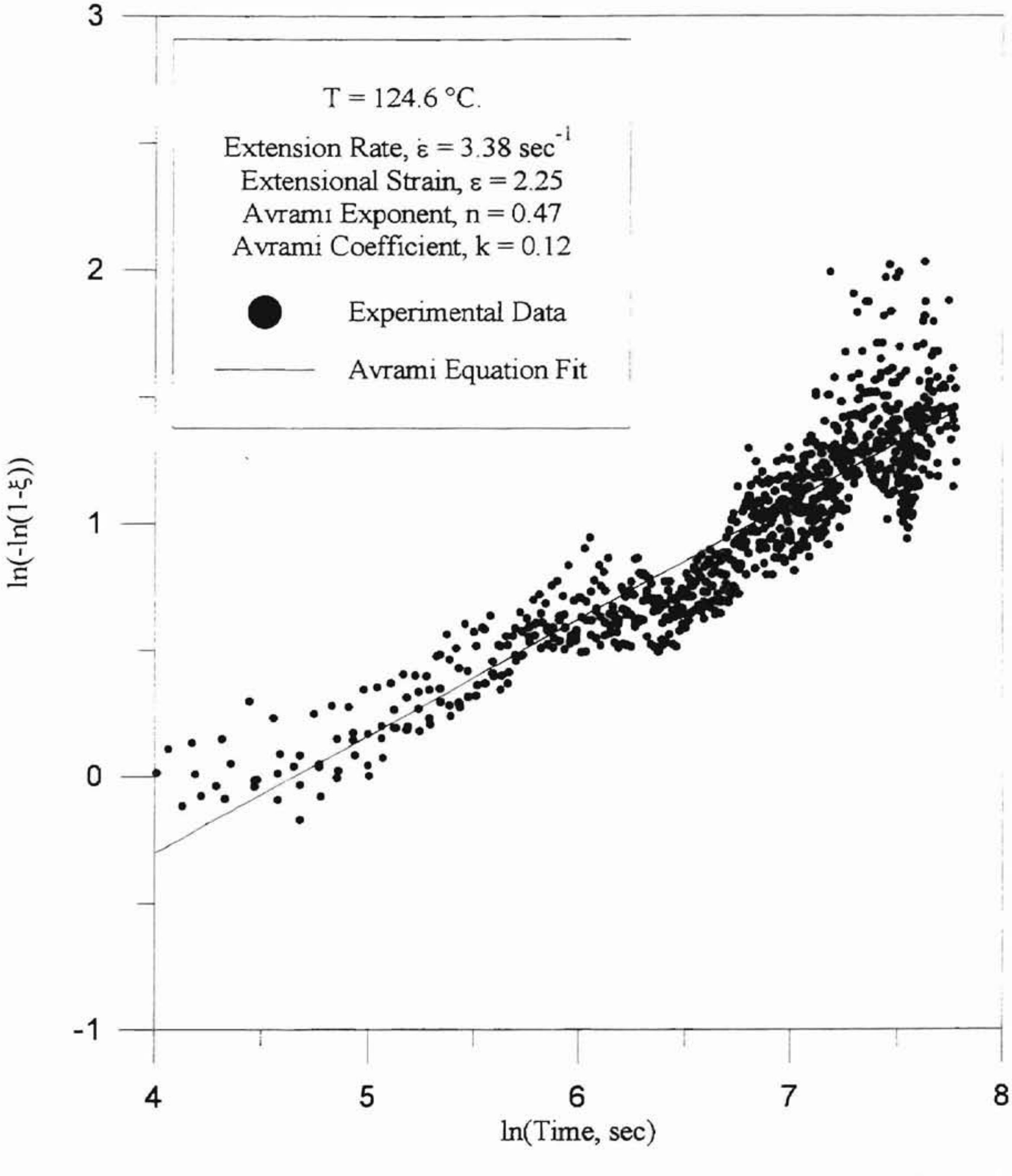

Figure D.14 (c) Correlation of Experimental Data With Avrami Equation for HDPE at Extension Rate = 3.38 sec $^{-1}$, Extensional Strain = 2.25

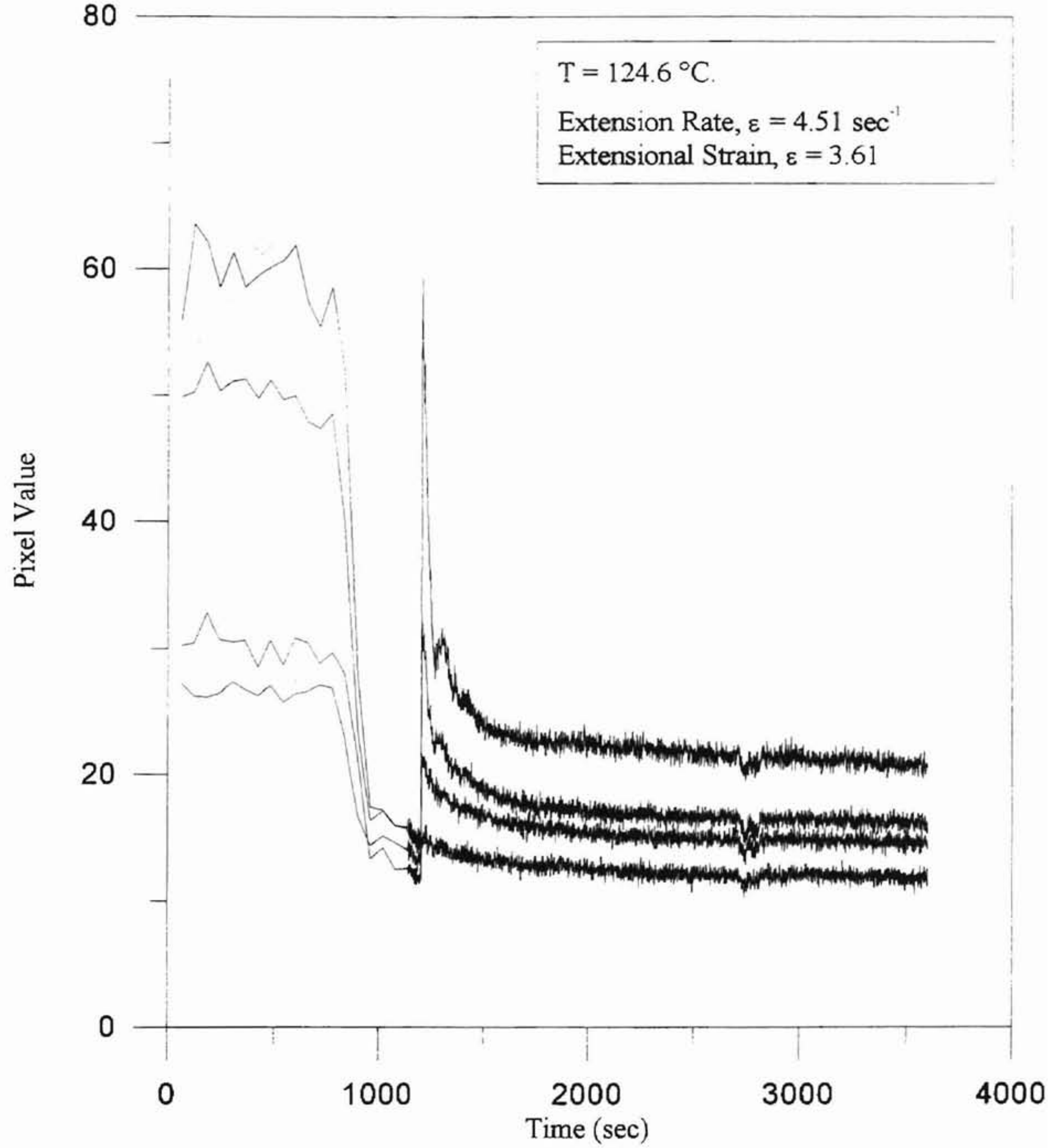

Figure D.15 (a) Pixel Value vs. Time for HDPE at Extension Rate = 4.51 sec^{-1}, Extensional Strain = 3.61

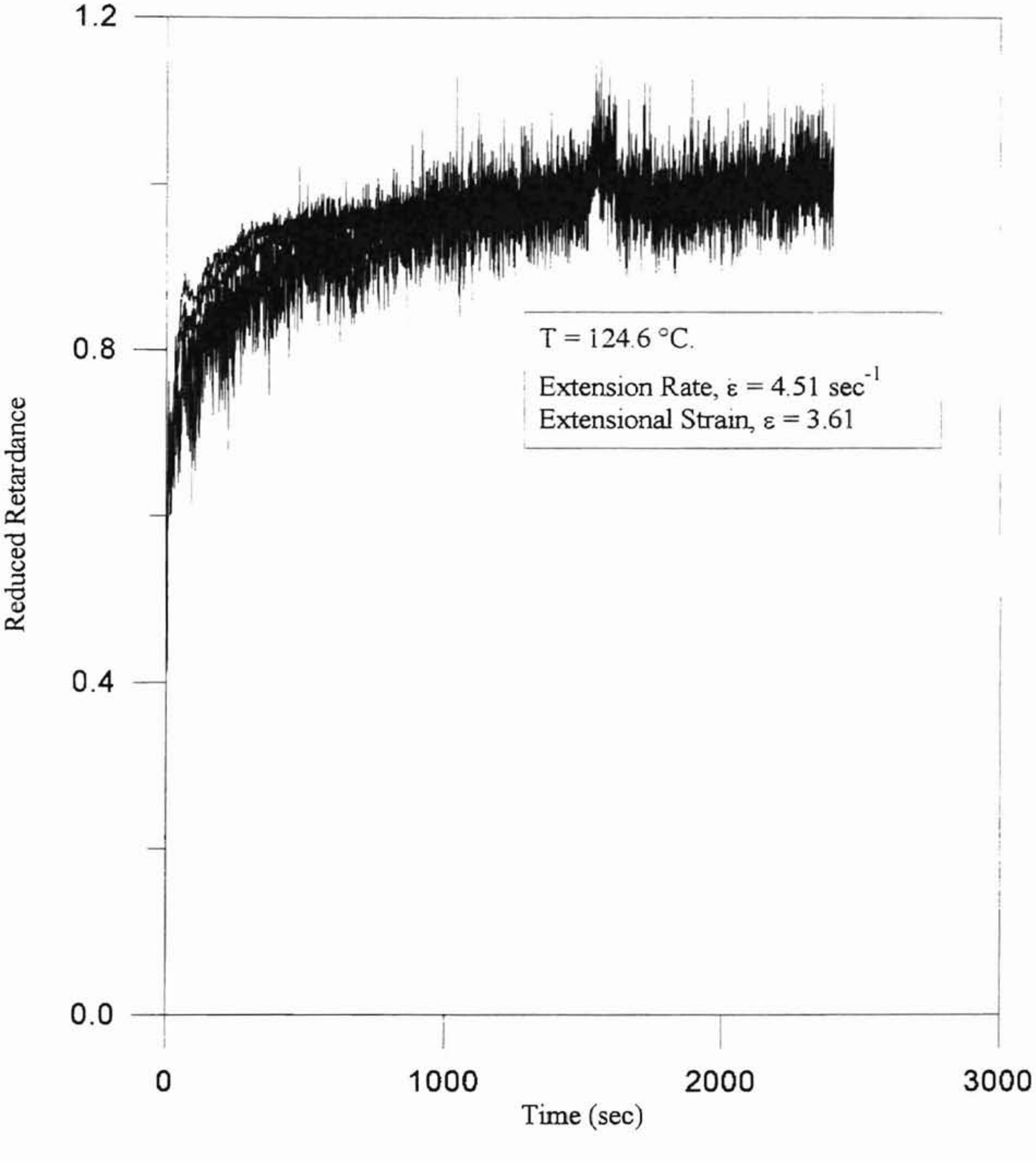

Figure D.15 (b) Reduced Retardance vs. Time for HDPE at Extension Rate = 4.51 sec^{-1}, Extensional Strain = 3.61

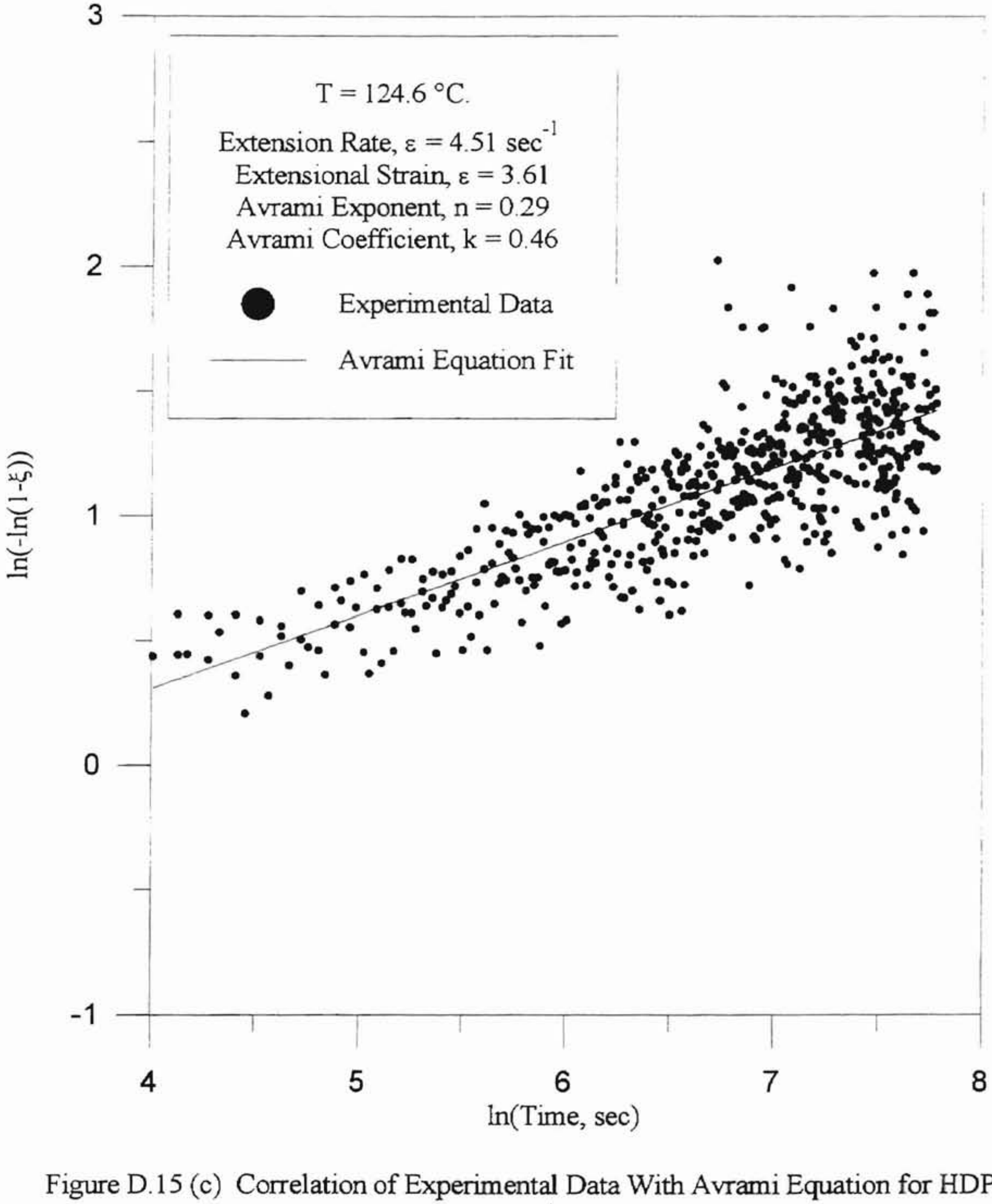

Figure D.15 (c) Correlation of Experimental Data With Avrami Equation for HDPE at Extension Rate = 4.51 sec $^{-1}$, Extensional Strain = 3.61

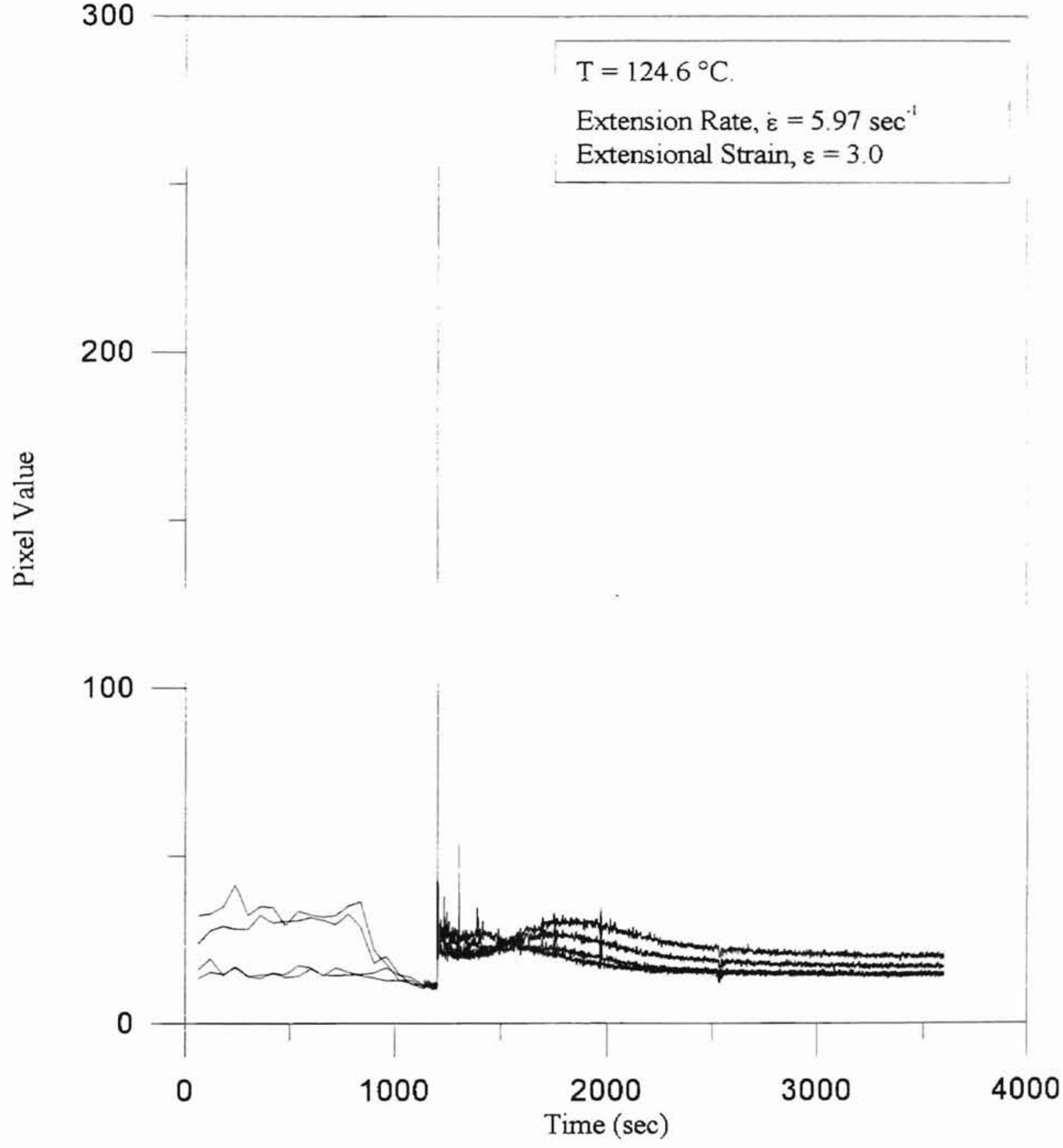

Figure D.16 (a) Pixel Value vs. Time for HDPE at Extension Rate = 5.97 sec^{-1}, Extensional Strain = 3.0

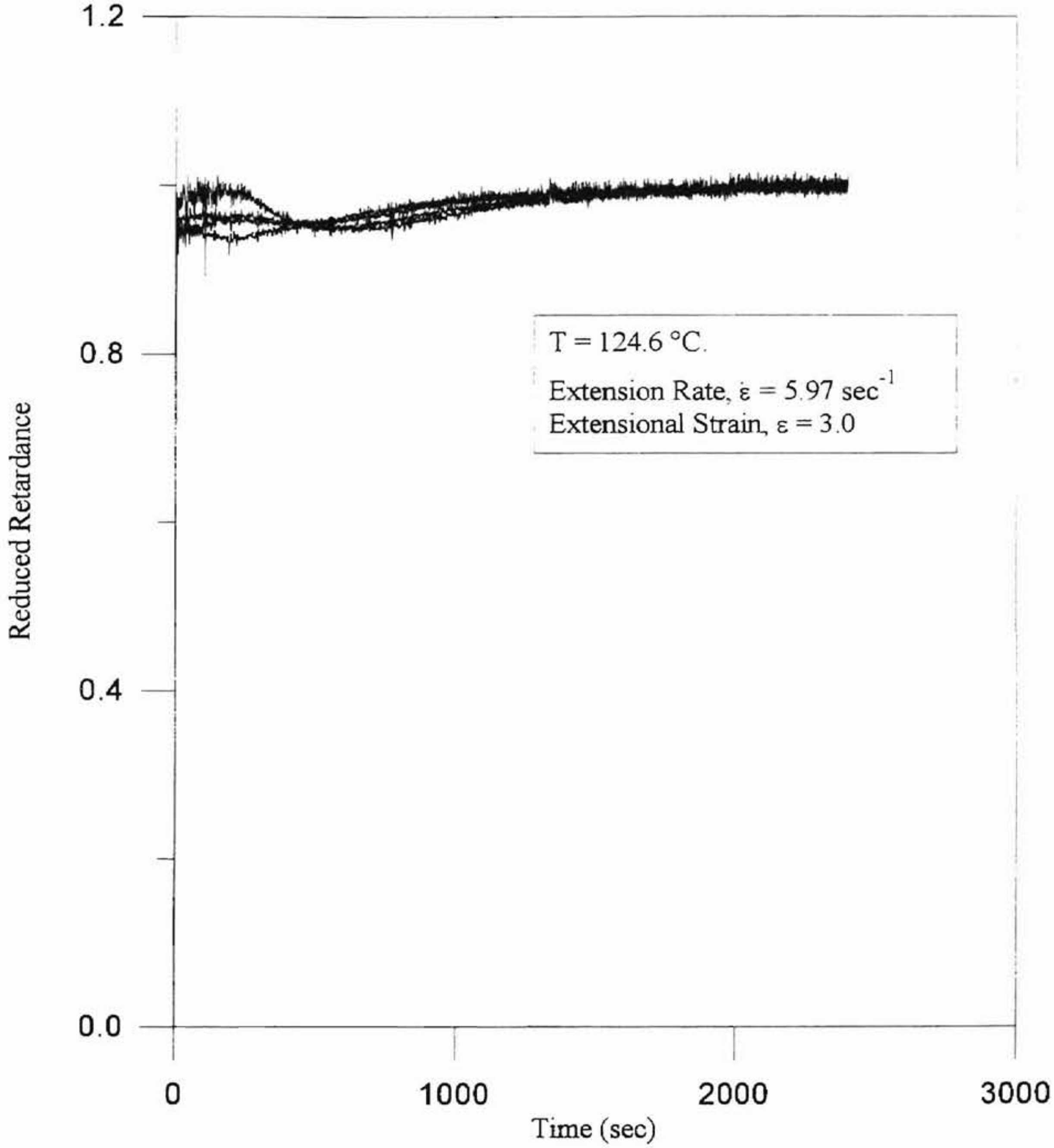

Figure D.16 (b) Reduced Retardance vs. Time for HDPE at Extension Rate = $5.97\ \mathrm{sec}^{-1}$, Extensional Strain = 3.0

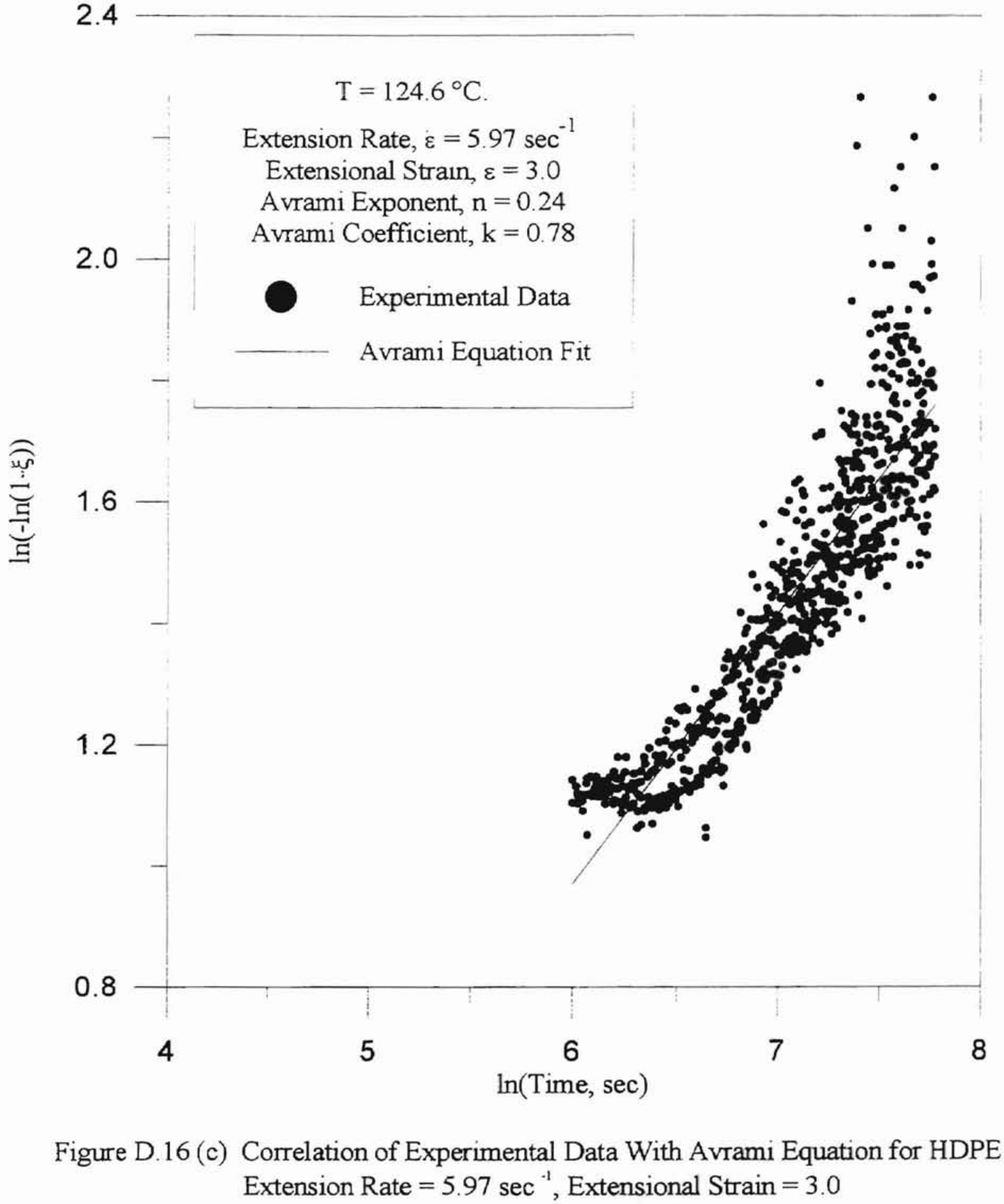

Figure D.16 (c) Correlation of Experimental Data With Avrami Equation for HDPE at Extension Rate = 5.97 sec $^{-1}$, Extensional Strain = 3.0

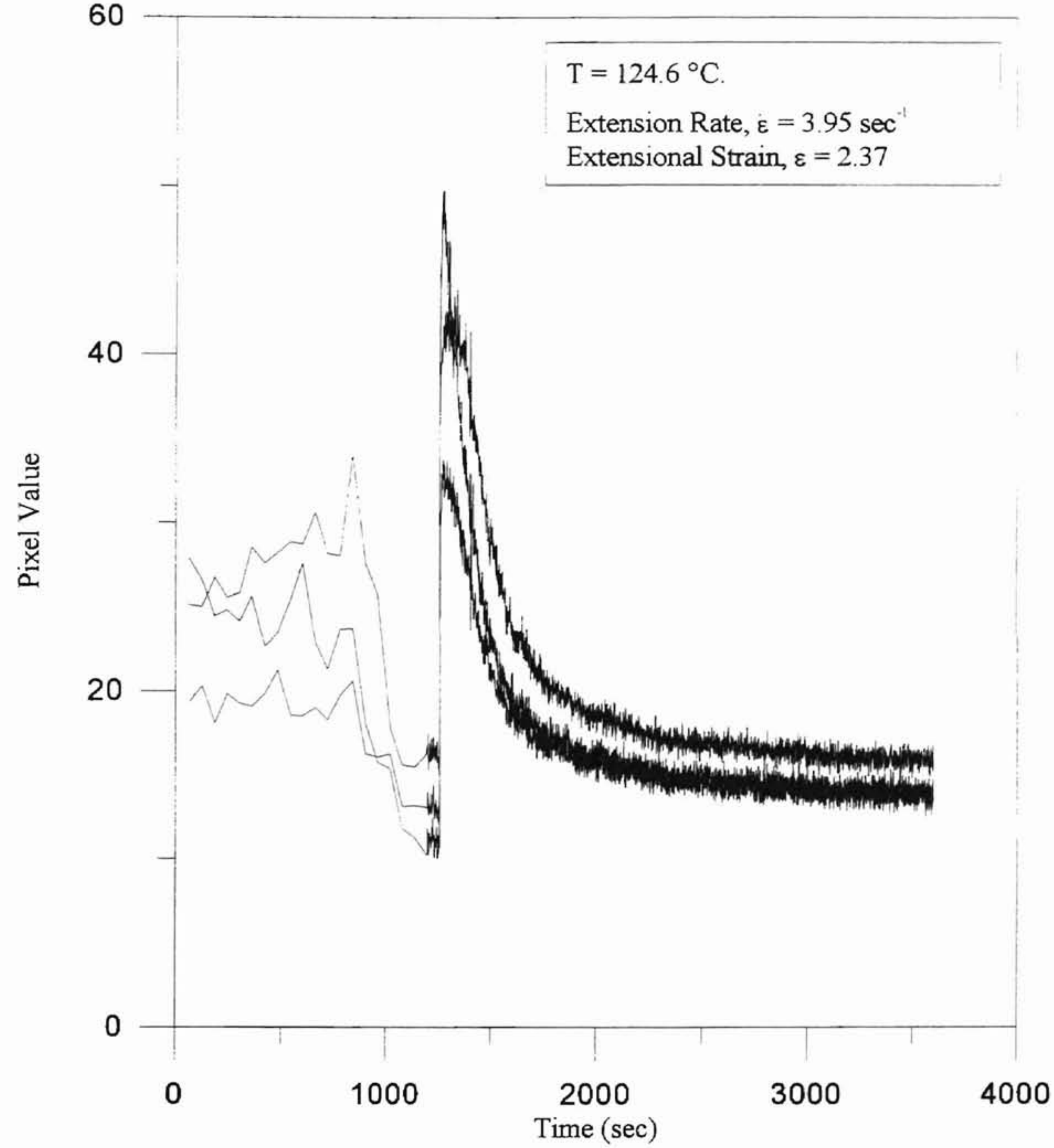

Figure D.17 (a) Pixel Value vs. Time for HDPE at Extension Rate = 3.95 sec^{-1}, Extensional Strain = 2.37

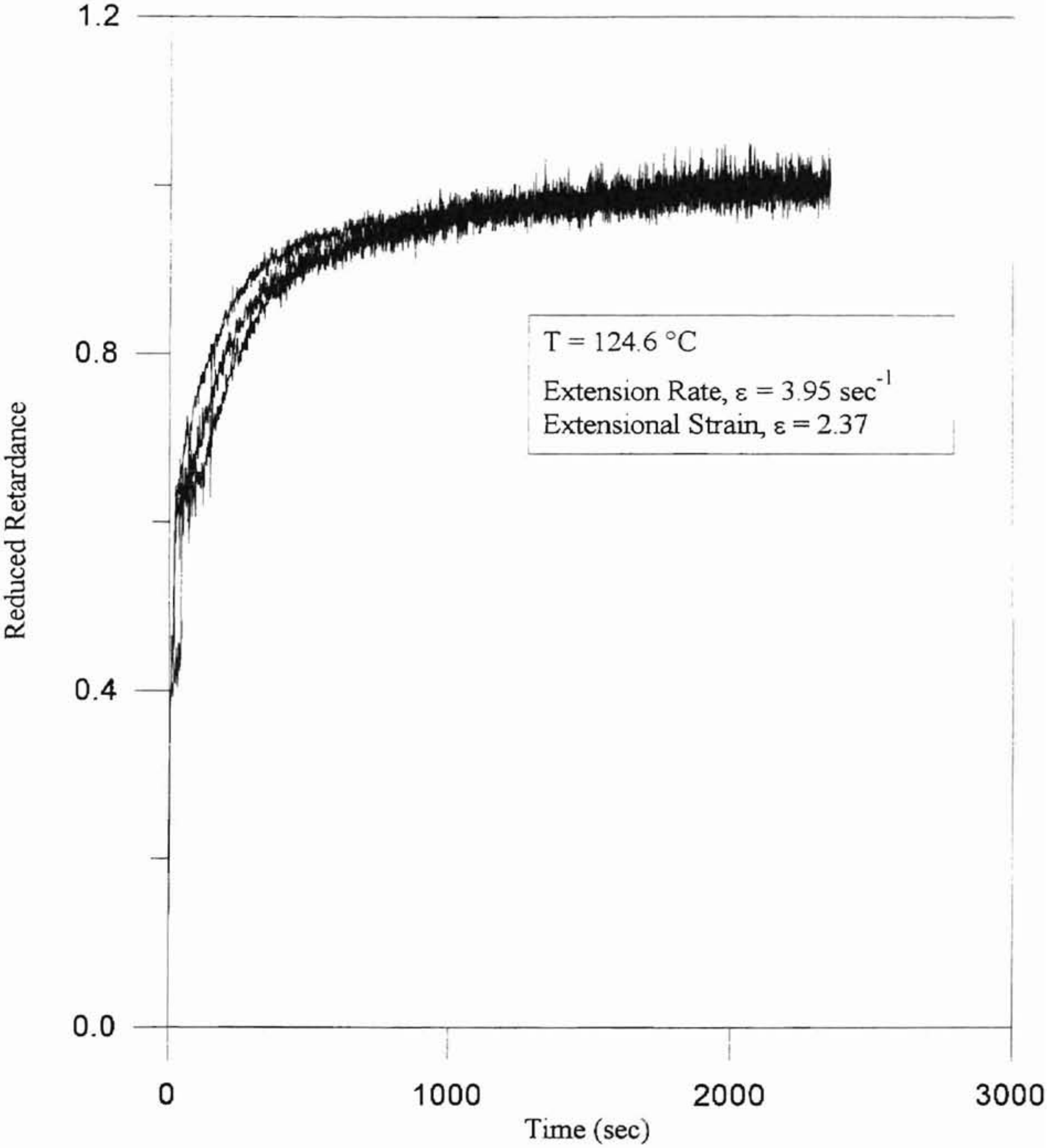

Figure D.17 (b) Reduced Retardance vs. Time for HDPE at Extension Rate = $3.95\ sec^{-1}$, Extensional Strain = 2.37

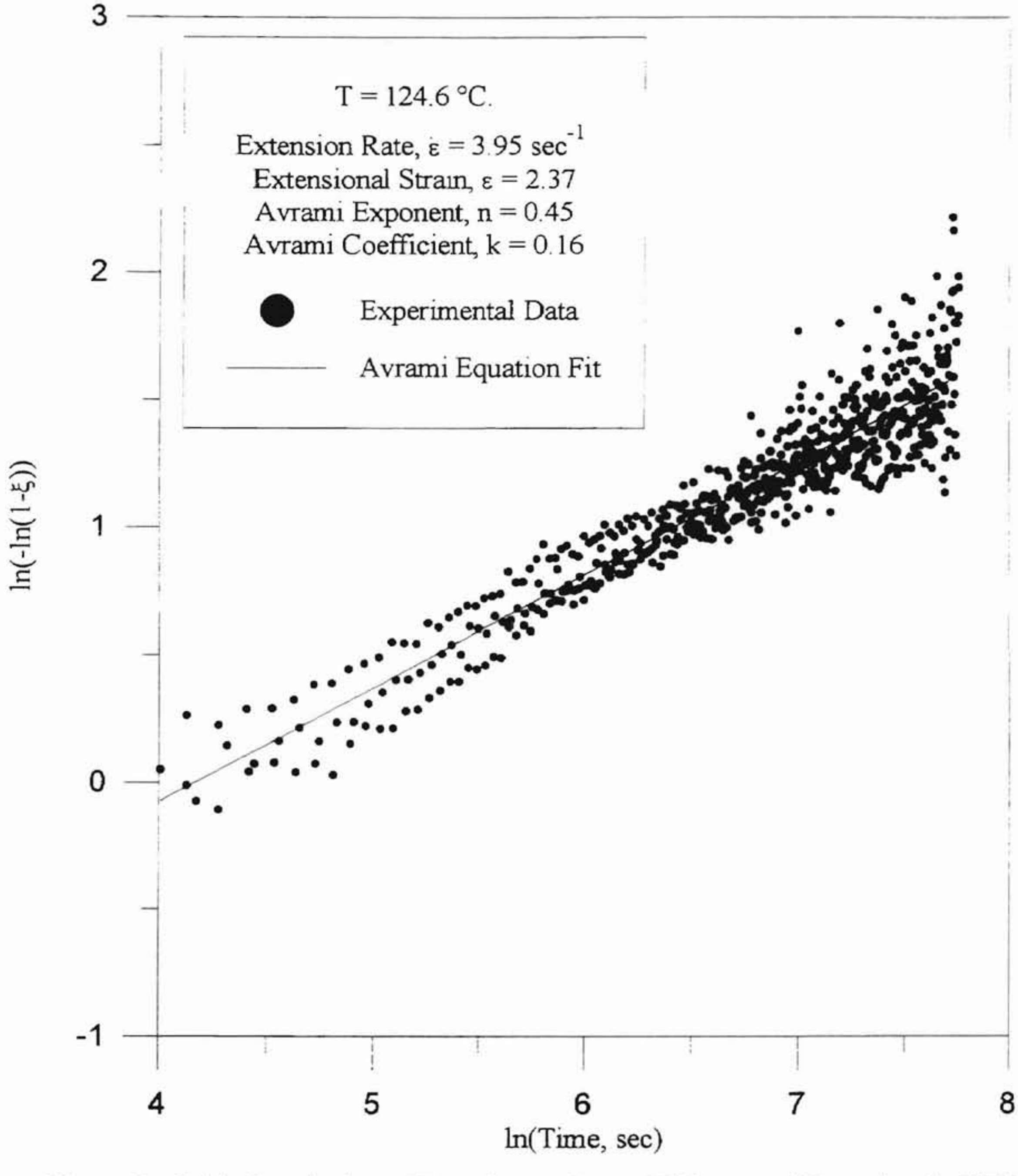

Figure D.17 (c) Correlation of Experimental Data With Avrami Equation for HDPE at Extension Rate = 3.95 sec $^{-1}$, Extensional Strain = 2.37

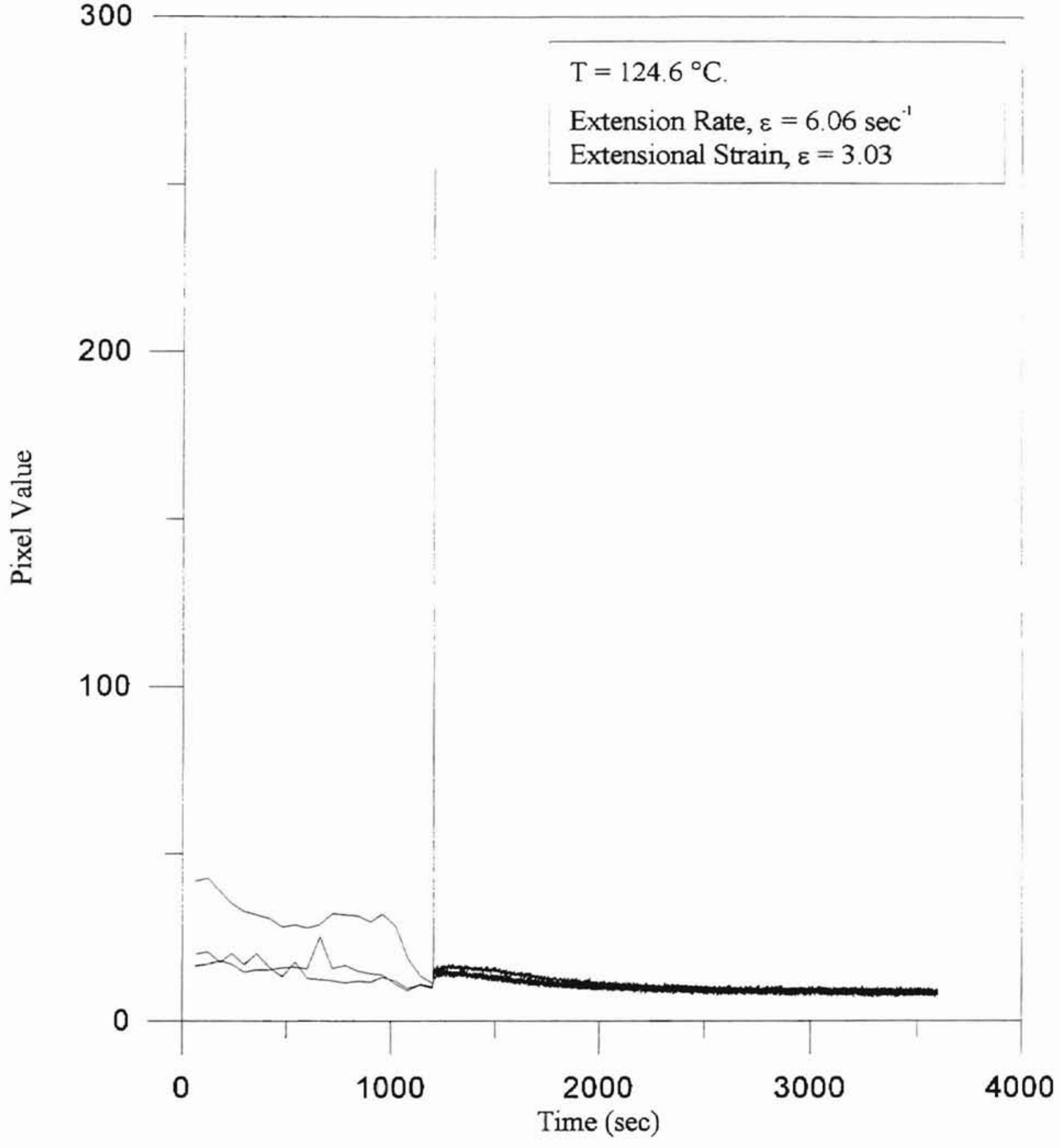

Figure D.18 (a) Pixel Value vs. Time for HDPE at Extension Rate = 6.06 sec^{-1}, Extensional Strain = 3.03

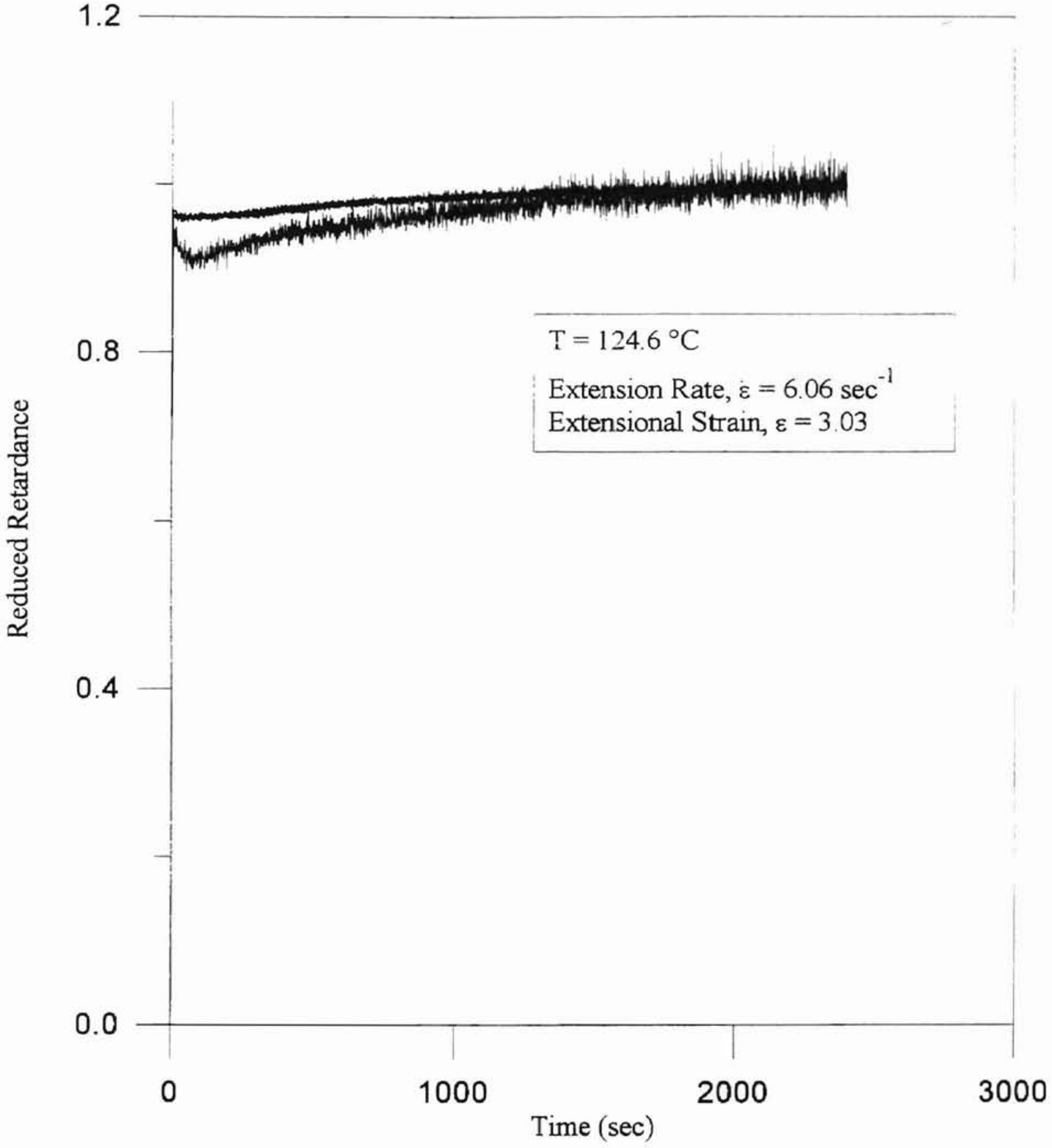

Figure D.18 (b) Reduced Retardance vs. Time for HDPE at Extension Rate = 6.06 sec^{-1}, Extensional Strain = 3.03

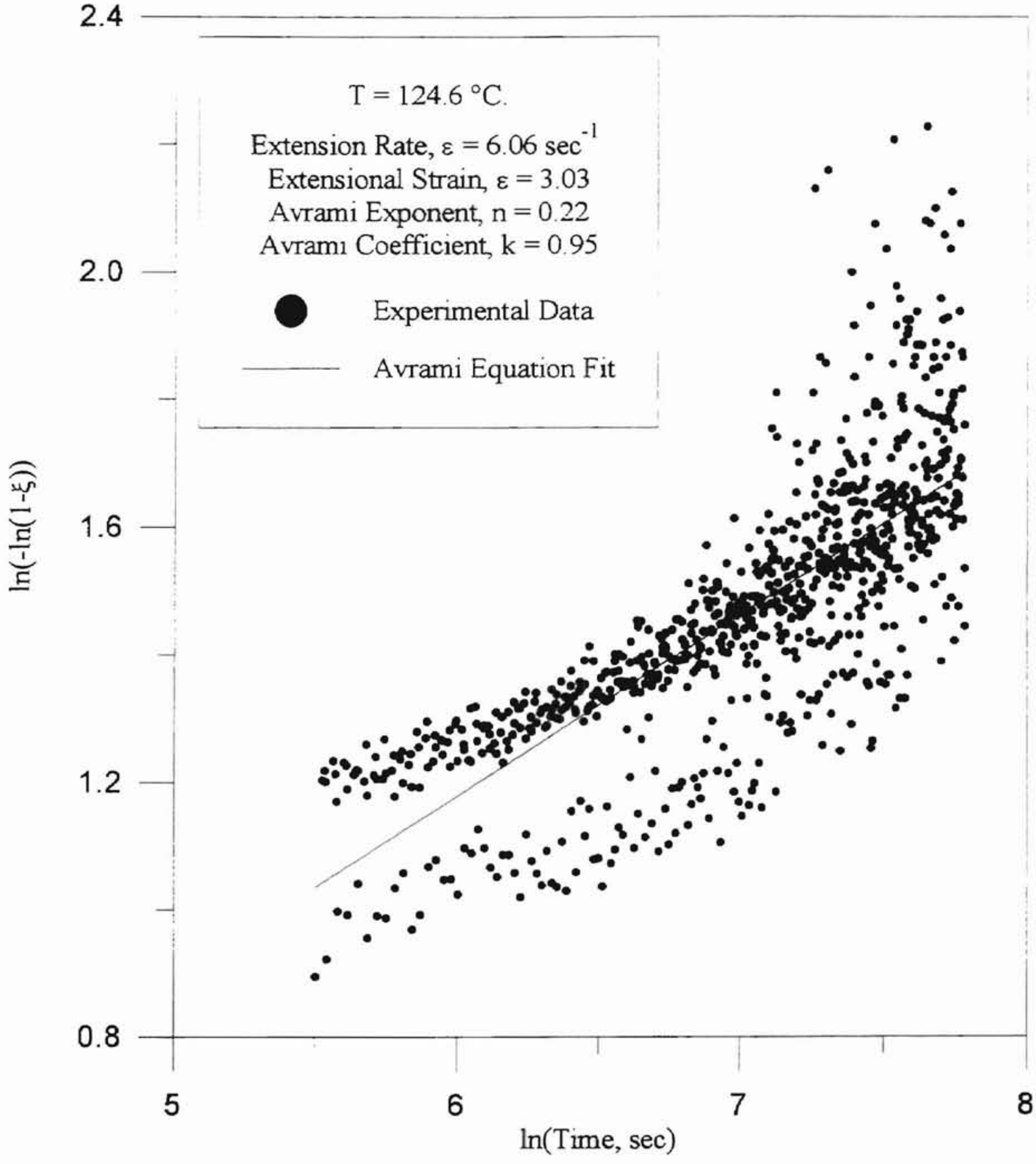

Figure D.18 (c) Correlation of Experimental Data With Avrami Equation for HDPE at Extension Rate = 6.06 sec^{-1}, Extensional Strain = 3.03

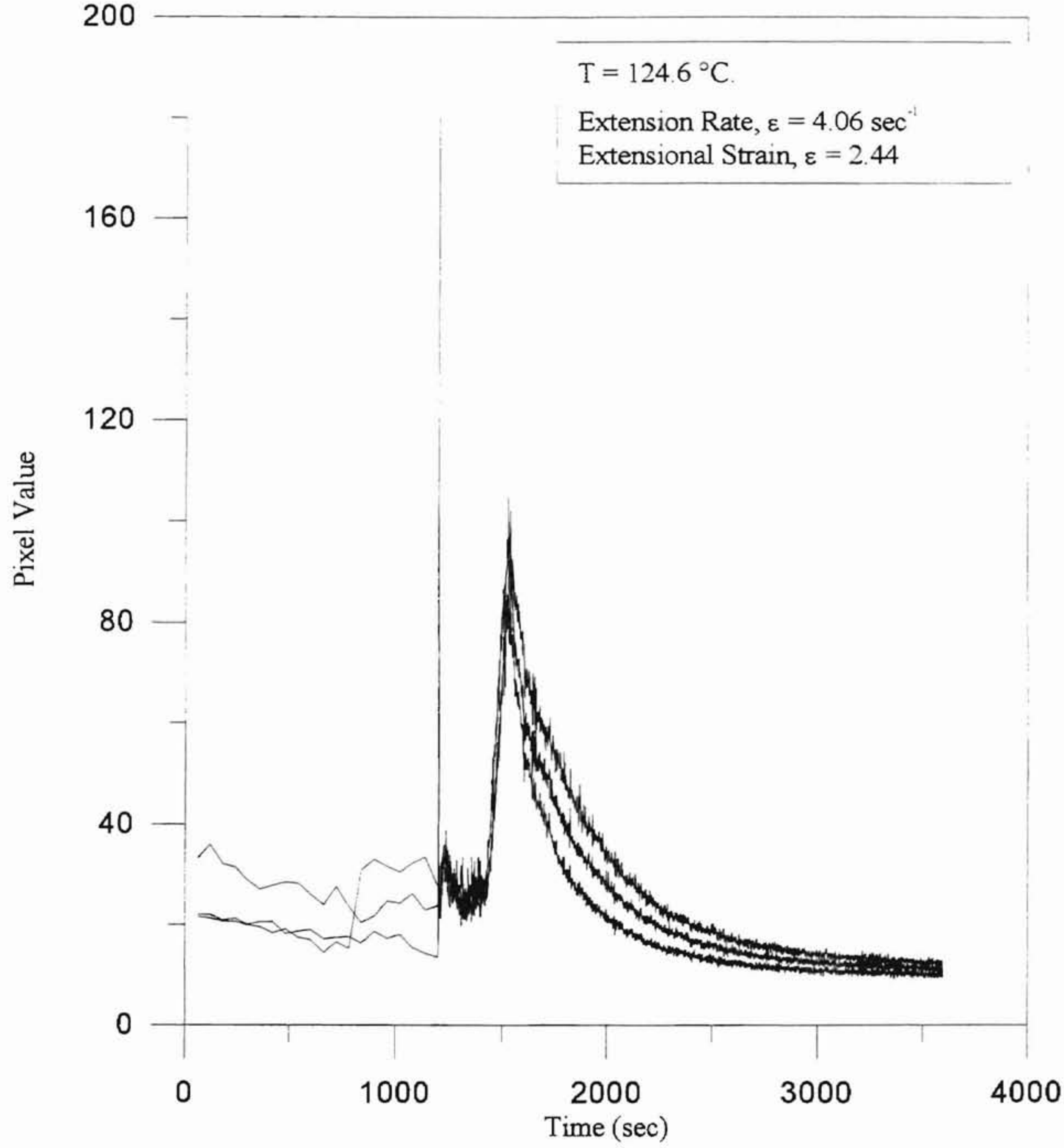

Figure D.19 (a) Pixel Value vs. Time for HDPE at Extension Rate = 4.06 sec^{-1}, Extensional Strain = 2.44

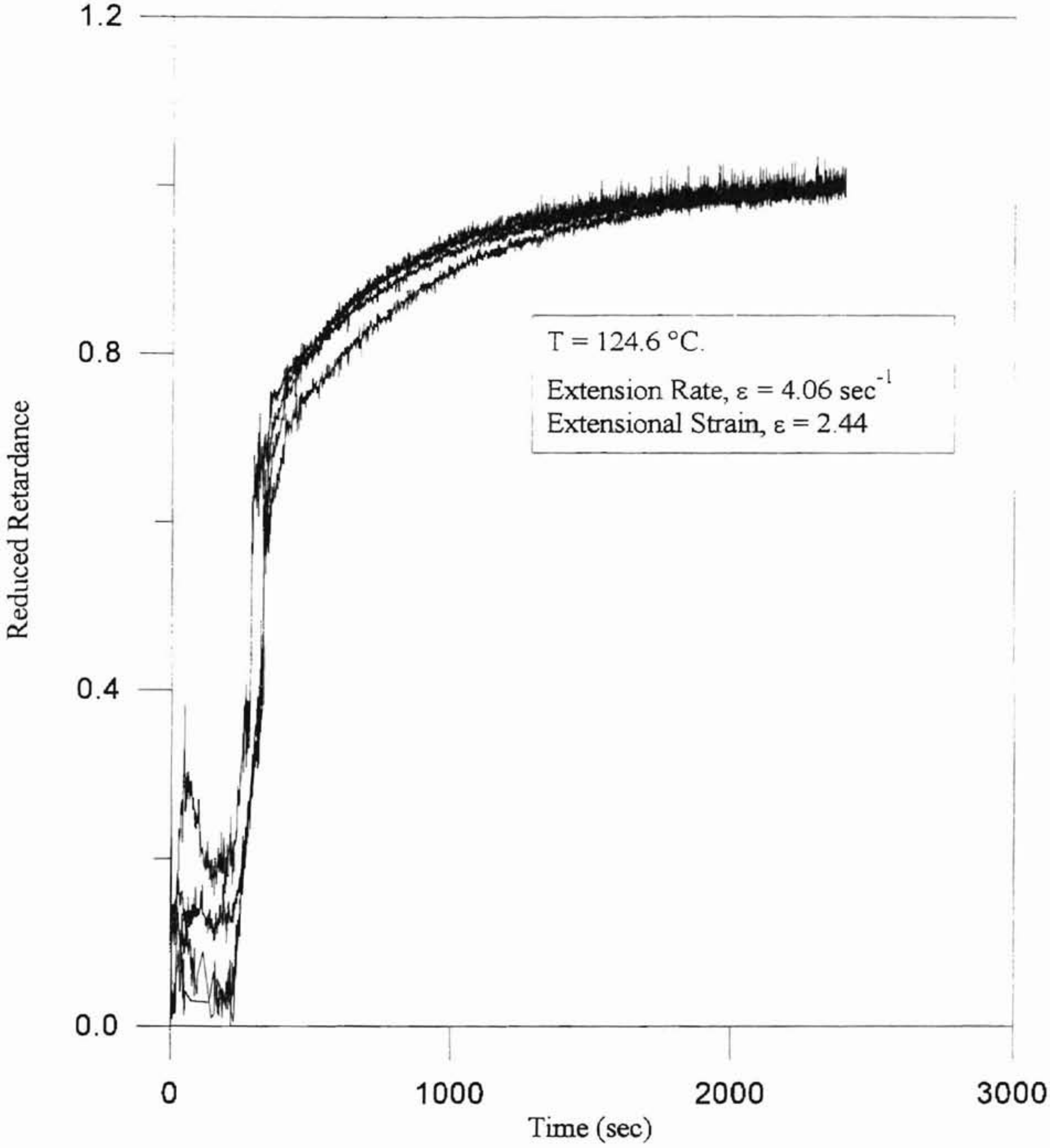

Figure D.19 (b) Reduced Retardance vs. Time for HDPE at Extension Rate = 4.06 sec^{-1}, Extensional Strain = 2.44

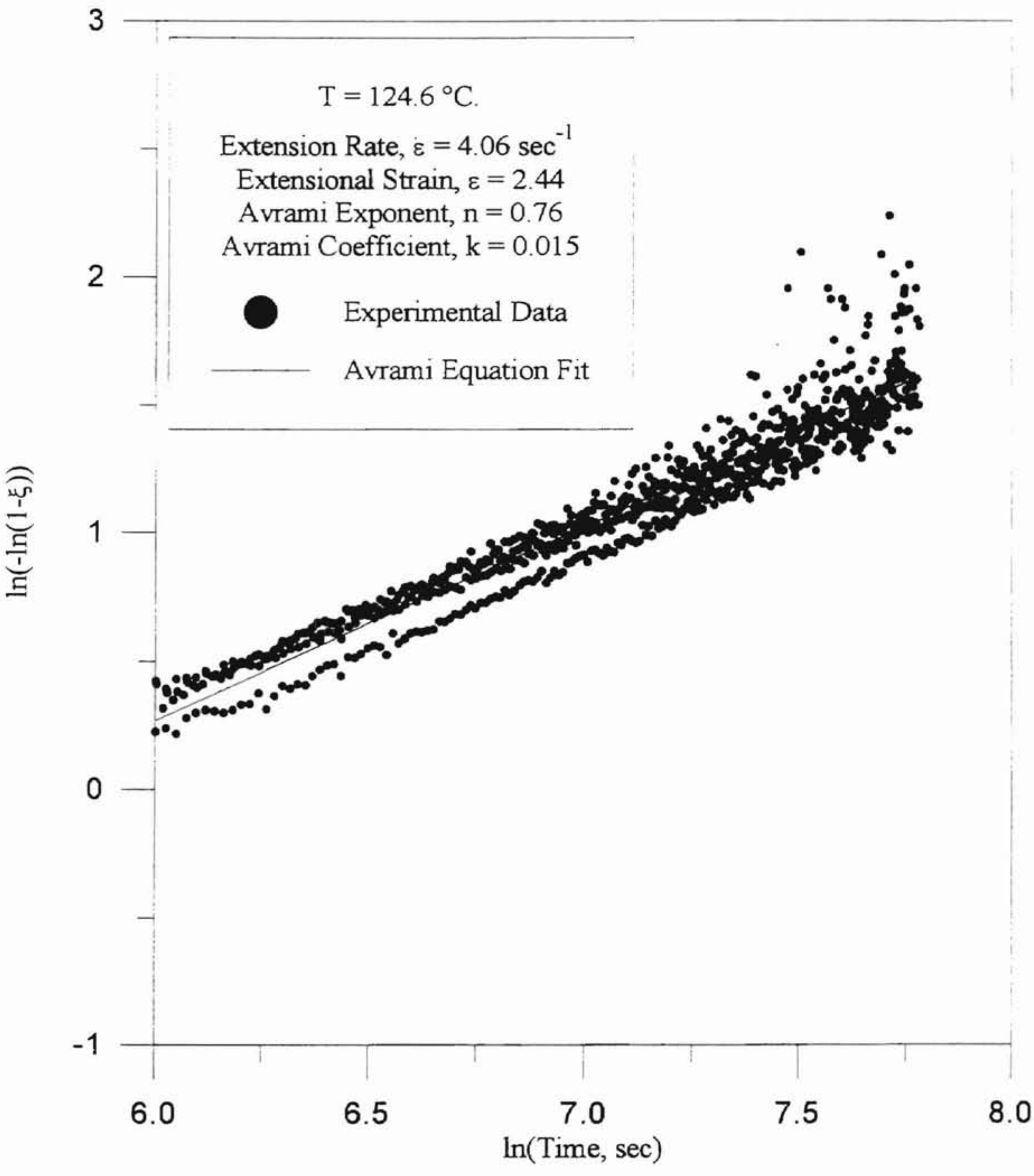

Figure D.19 (c) Correlation of Experimental Data With Avrami Equation for HDPE at Extension Rate = 4.06 sec $^{-1}$, Extensional Strain = 2.44

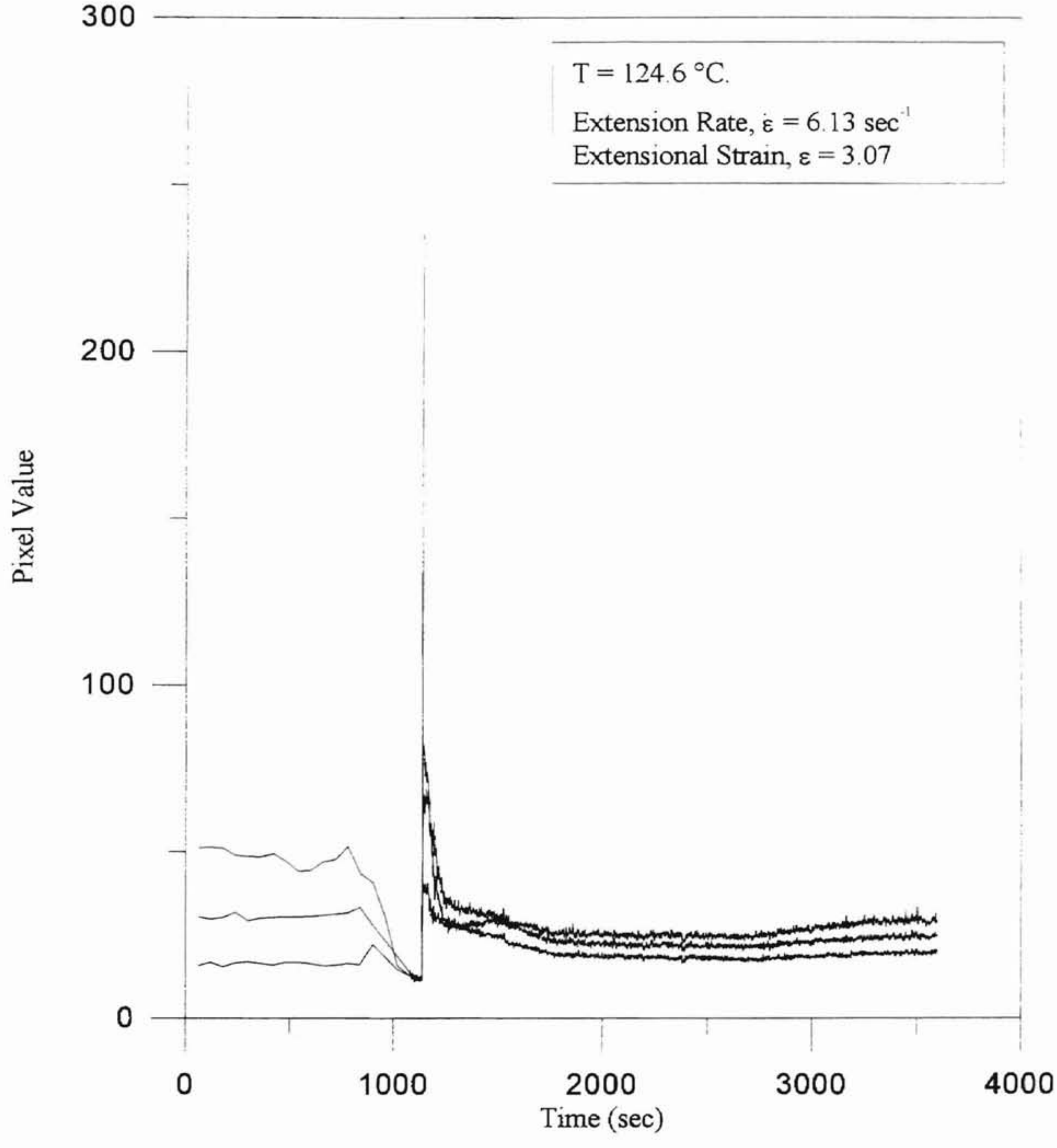

Figure D.20 (a) Pixel Value vs. Time for HDPE at Extension Rate = 6.13 sec^{-1}, Extensional Strain = 3.07

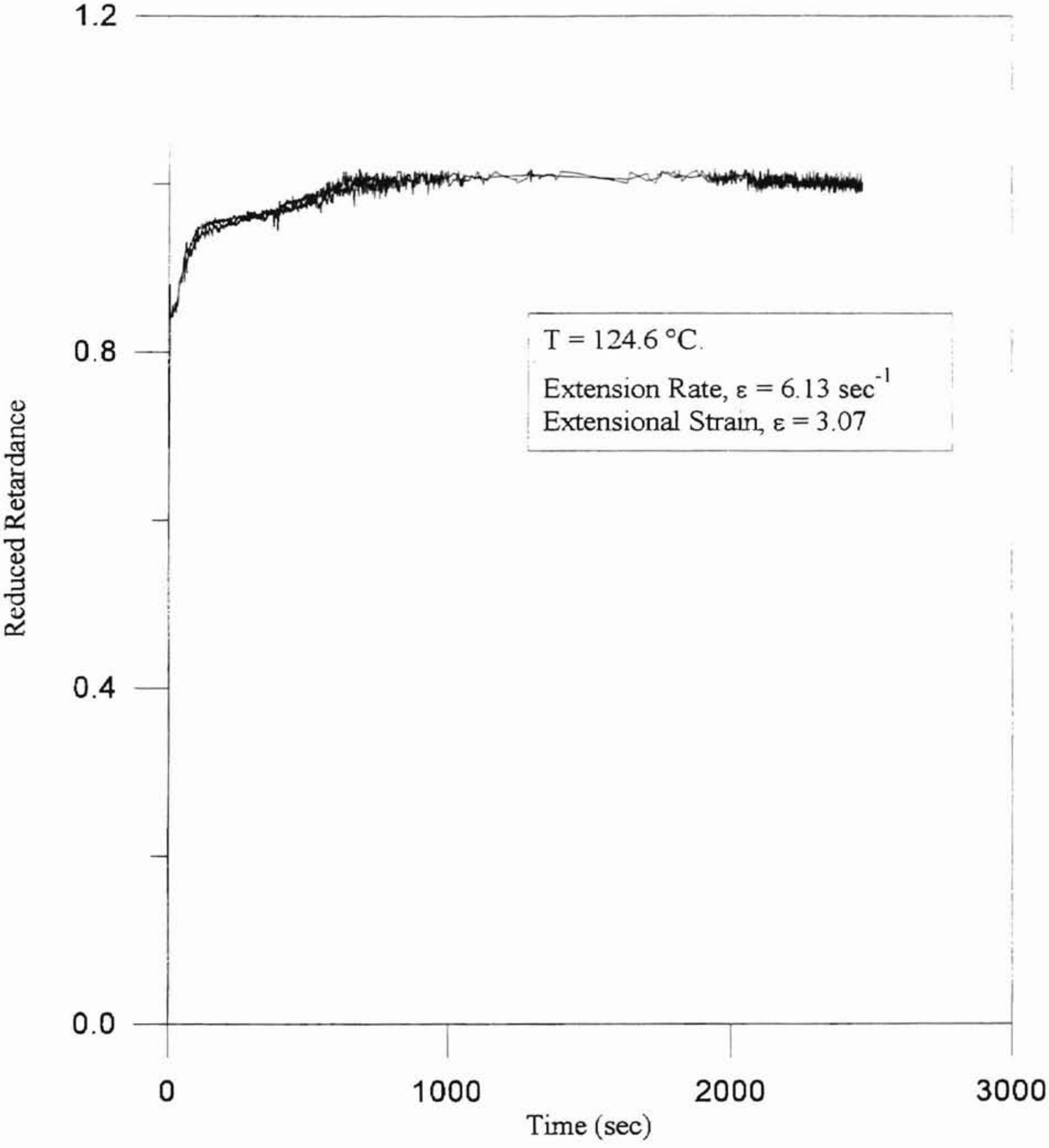

Figure D.20 (b) Reduced Retardance vs Time for HDPE at Extension Rate = 6.13 sec^{-1}, Extensional Strain = 3.07

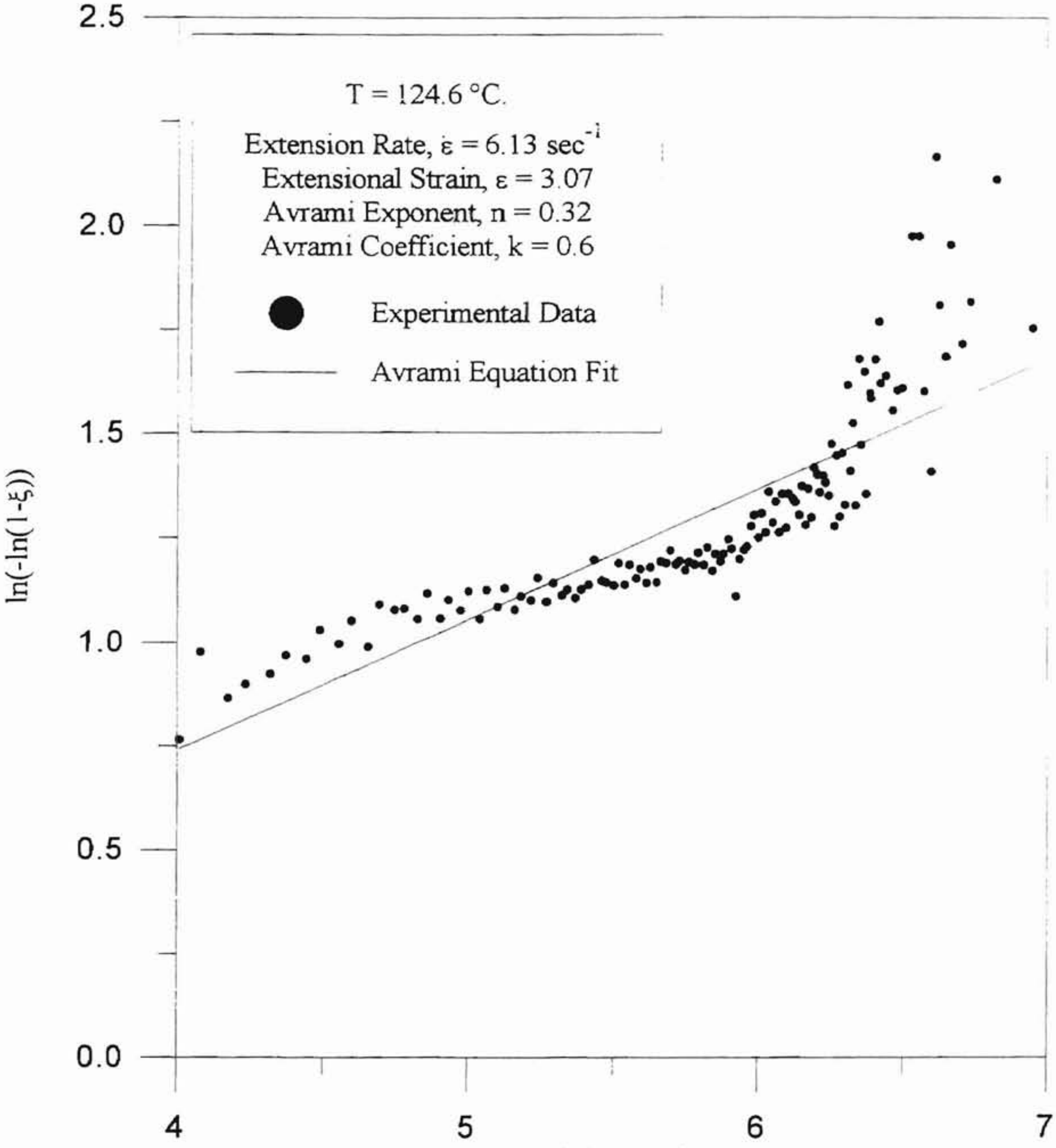

Figure D.20 (c) Correlation of Experimental Data With Avrami Equation for HDPE at Extension Rate = 6.13 sec $^{-1}$, Extensional Strain = 3.07

2

VITA

Madhav Kakani

Candidate for the Degree of

Master of Science

Thesis: AN EXPERIMENTAL STUDY OF FLOW-INDUCED CRYSTALLIZATION IN HIGH DENSITY POLYETHYLENE AND POLYPROPYLENE

Major Field: Chemical Engineering

Biographical:

Personal Data: Born in Guntur, Andhra Pradesh, India, March 14, 1970, the son of K. Sridhara Rao and K. Kamala.

Education: Graduated from Chaithanya Kalasala Junior College, Hyderabad, AP, India, in May 1988; received Bachelor of Technology with Honors degree in Chemical Engineering from Indian Institute of Technology, Kharagpur, India, in May 1992; completed requirements for the Master of Science degree at Oklahoma State University in December 1996.

Professional Experience: Research Engineer, Bharat Heavy Electricals Limited, Corporate R & D Division, Hyderabad, India, August 1992, to August 1994; Teaching Assistant, School of Chemical Engineering, Oklahoma State University, August 1994, to December 1994; Research Assistant, School of Chemical Engineering, Oklahoma State University, January 1995, to June 1996.